Materials Science and Engineering R 35 (2001) 1–138

R Reports: *A Review Journal*

www.elsevier.com/locate/mser

Recent advances in Schottky barrier concepts

Raymond T. Tung[1]

Research Center for Quantum Effect Electronics, Tokyo Institute of Technology, Ookayama, Tokyo, Japan

Accepted 25 July 2001

Abstract

Theoretical models of Schottky-barrier height formation are reviewed. A particular emphasis is placed on the examination of how these models agree with general physical principles. New concepts on the relationship between interface dipole and chemical bond formation are analyzed, and shown to offer a coherent explanation of a wide range of experimental data. © 2001 Published by Elsevier Science B.V.

Keywords: Schottky-barrier height; Interface dipole; Interface states; Heterojunction band offsets

1. Background and basics

1.1. Introduction

Metal–semiconductor (MS) interfaces are an essential part of virtually all semiconductor electronic and optoelectronic devices. One of the most interesting properties of a MS interface is its Schottky-barrier height (SBH), which is a measure of the mismatch of the energy levels for majority carriers across the MS interface. The SBH controls the electronic transport across MS interfaces and is, therefore, of vital importance to the successful operation of any semiconductor device. Despite the tremendous advances in solid state physics and semiconductor device physics in the past several decades, our knowledge on the basic formation mechanism of the SBH has not advanced much beyond a primitive level during the same period of time. Many textbooks, chapters, and review articles exist which describe the pervasive confusion and frustration with efforts to unravel the SBH mystery in the second half of the 20th century [1–4]. The writing of this review article would have been redundant if that dismal situation still persisted today. Fortunately, things have changed significantly. There are some surprising developments in the field of SBH research very recently, and with the surfacing of some new ideas, the need for a re-examination of the entire SBH literature immediately arises. Meeting that need is what this article hopes to accomplish.

The first-order theory of the formation of a Schottky barrier (SB) is the view attributed to the great Walter Schottky himself originally, and also to Sir Neville Mott [5,6]. The Schottky–Mott theory proposes that the SBH between a metal with a work function of ϕ_M and a semiconductor with an electron affinity of χ_S should be

$$\Phi_{B,n}^0 = \phi_M - \chi_S \tag{1.1.1}$$

[1] Formerly of Bell Labs, Lucent Technology

0927-796X/01/$ – see front matter © 2001 Published by Elsevier Science B.V.
PII: S0927-796X(01)00037-7

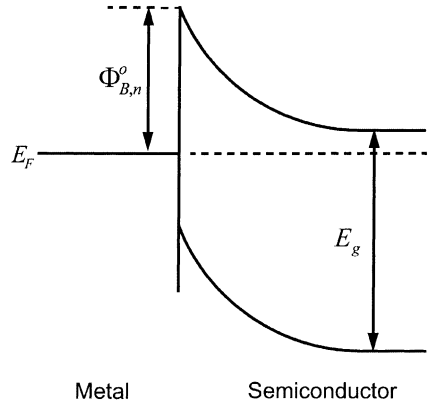

Fig. 1. Basic energy band diagram at a metal–semiconductor interface. The SBH to n-type semiconductor is indicated.

in the absence of interaction, where $\Phi^0_{\mathrm{B,n}}$ denotes the SBH measured on an n-type semiconductor, as shown in Fig. 1. Unfortunately, the strong dependence of the SBH on the metal work function, i.e. $\partial\Phi^0_{\mathrm{B,n}}/\partial\phi_{\mathrm{M}} = 1$, predicted by the Schottky–Mott relationship has received little support from experiment. The SBHs measured in actual experiments often showed some dependence on the preparation of the MS interface, which indicates that the SBH depends more than just the work function of the metal. Despite some scatters in the experimental data, by and large, metals with larger work functions have been found to have systematically higher SBHs than those with lower work functions. But the actual dependence observed is much weaker than that predicted by the Schottky–Mott theory, i.e.

$$S_\Phi \equiv \frac{\partial\Phi^0_{\mathrm{B,n}}}{\partial\phi_{\mathrm{M}}} \ll 1, \tag{1.1.2}$$

where S_Φ is known as the interface behavior parameter, or the S-parameter, of the semiconductor. A term, ''Fermi-level (FL) pinning'', has often been used to describe the insensitivity of the experimental SBH to the metal work function. ''FL-pinning'' is actually a term borrowed from the literature used to describe a seemingly similar phenomenon observed at semiconductor surfaces and semiconductor–insulator interfaces. However, as will be discussed explicitly, mechanisms responsible for these two phenomena, despite having the same name, are very different. Not distinguishing these cases, in the opinion of this author, has contributed to the confusion regarding the SBH formation mechanism. In this paper, we use the phrase ''FL-pinning'' to denote exclusively the experimental observation that the SBH is insensitive to the metal work function, with no intended reference to the underlying mechanism responsible for this phenomenon.

Because of the poignancy of the FL-pinning phenomenon, explanation of this effect alone had occupied the attention of most SBH studies conducted before the mid 1980s. Not surprisingly, most of the SBH theories proposed during that period of time contained some features or assumptions, which would automatically make the SBH insensitive to the interface structure. A well-known example is the common assumption that the distribution of interface states is a property of only the bulk semiconductor and not the metal. Although it clearly could explain the FL-pinning effect, such an ad hoc assumption is hard to rationalize from the standpoint of general physics and chemistry. When a metal and a semiconductor are joined to form an MS interface, a significant redistribution of charge is expected to take place due to the overlap of wave functions from the two sides. Old bonds are broke, and new bonds are formed. The electronic states that accommodate the charge transfer at

the interface should be characteristic of the MS interface and not just the semiconductor. So quantum mechanically, one expects the SBH to depend sensitively not only on the identity of the metal, but also on the interface structure, which would seem to be at odds with the experimentally observed FL-pinning phenomenon [2,3]. Since the mid 1980s, a few high-quality, single-crystal, MS interfaces were successfully fabricated and the SBH measured at these interfaces showed a rather dramatic dependence on the orientation/structure of the MS interface [7–9]. That the SBH depended on the interface structure was very much in line with the intuitive quantum mechanics picture of interface dipole and bonding, although it seemed to disagree with the FL-pinning phenomenon widely observed at polycrystalline MS interfaces. Some of the disagreement was settled when it was pointed out a few years later that the SBHs at polycrystalline MS interfaces were often inhomogeneous. The electrical data from polycrystalline SBs had always contained clear signs of SBH inhomogeneity [9]. However, the decipher of such evidence, as it turned out, would require some knowledge on the band bending of an inhomogeneous SB, which was lacking prior to the early 1990s [10]. Independently, direct evidence for SBH inhomogeneity also began to mount with the arrival of spatially-resolved SBH techniques, most notably the ballistic electron emission microscopy (BEEM) [11–13]. The general inhomogeneity in polycrystalline SBHs was in very good agreement with the structure-dependence observed at single-crystal MS interfaces. It, thus, appeared that a consistent view on the formation mechanism of the SBH was emerging, but there remained one more hurdle to overcome. One still had to answer the question ''how can a SBH mechanism which depends so sensitively on the interface structure lead to SBHs at polycrystalline interfaces that always average out to nearly constant values, irrespective of the metal?''. In other words, how does one explain the FL-pinning phenomenon with the bonding picture? This question was answered at the turn of the century/millennium when the interface dipole associated with chemical bonding at MS interfaces was modeled using established methods borrowed from molecular chemistry. It was shown that FL-pinning was a natural consequence of interfacial bonding [14]. Furthermore, a host of experimentally observed systematics which had hitherto been attributed to interface states could be directly derived within the bonding picture, through a minimization of the total energy. At the present moment, it seems that the major formation mechanism of the SBH has finally been clearly identified. It should surprise no one that the intuitive picture of the formation of the SBH should turn out to be the right one!

The ''recent advances'' advertised in the title of this review, of course refer mainly to the bond-polarization theory recently developed. Other closely-related key findings that gradually came to light in the past 10–15 years are also included here for completeness, although more focused reviews of these other findings already exist [4,9]. The present article is mostly concerned with the theoretical pictures of the SBH formation mechanism. Little effort will be spent on the application side of Schottky barriers and Ohmic contacts; although in illustrating the problems associated with the interpretation of experimental data, sometimes it is necessary to get into the details of current transport mechanisms a bit. In this article, we also critically examine all existing SBH models in detail, in order to put some long standing concepts and misconceptions about the SBH in their proper perspectives. The organization of this article is as follows. In the remainder of Section 1, we will provide some background of the SBH problem and, in particular, a discussion on the electrostatics of SBH formation will be included. Section 2 is concerned with SBH models that ignore the effect of metal–semiconductor interaction. Then we take a slight detour to look at the band offset problem at semiconductor heterojunctions in Section 3. The many shared ideas and parallel features between theories on band offsets and theories on SBH make this discussion relevant and vital for our main subject. In the following chapter, two different approaches to model the interface dipole due to metal–semiconductor interaction will be discussed in detail. These are, of course, the metal-induced

gap states model and the bond-polarization theory. Section 5 deals with the principles and techniques for the measurement of the SBH. Here, some effort will be devoted to the electronic transport at inhomogeneous SBs, which is essential to the understanding of a wide spectrum of experimental observations. Experimentally, observed SBH trends and phenomena are summarized in Sections 6–8. Included are the FL-pinning phenomenon, the SBH inhomogeneity issue at polycrystalline MS interfaces, and the structure-dependence of the SBH at single-crystal MS interfaces. Readers only interested in an overview of this field may wish to skip Sections 1, 3 and 5–7 on their first reading. Finally, in Section 9, some additional, brief comments are made concerning the future directions of SBH-related research and various ramifications for applications as a result of the new view on the formation mechanism of the SBH.

1.2. Charges, dipoles, potentials, bands, surfaces and model solids

To understand the band line-up at an MS interface, or at any other kind of interfaces for that matter, there are two seemingly trivial, yet very important, rules to remember. One is that the electronic and atomic structures are the result of some energy minimization process. Sometimes, due to the kinetic constraint on interface formation, metastable structures can be found at the interface. They still represent minima in the free energy diagram, being local minima rather than global minima. An optimized charge-density should be continuous and distributed smoothly throughout space. The other rule is that the electric potential must be continuous everywhere. When one thinks of the electric potential in a solid, it is often the long-range, slowly varying, ''average'' potential that comes to mind. However, the definition of a long-range potential is not unique. Some people prefer the muffin-tin zero potential as the slowly varying potential of a solid, and others prefer to use the per-cell average of the crystal potential, or the average interstitial potential to represent the long-range potential. Regardless of its definition, the long-range potential is, most likely, discontinuous across a MS interface, which does not violate any physical laws. However, the short-range, rapidly fluctuating, crystal potential has to be continuous everywhere, in order to satisfy Poisson's equation. The variation of the crystal potential across the MS interface directly impacts on the magnitude of the SBH, because the bulk band positions on either side of the interface are tied to the local distributions of the crystal potential. This is the most important message of this section: electrostatic potential decides how bands at different locations are referenced with respect to each other. The rest of this Section 1.2 and the next Section 1.3 merely quantify this simple message in mathematical terms. They may be omitted on first reading without loss of continuity.

To see the relationship between electronic states and crystal potential, one first turns to isolated bulk crystals. The one-electron eigenvalue of a solid crystal, in the Hartree–Fock approximation, can be written down as [15]

$$-\frac{\hbar^2}{2m}\nabla^2\psi_i(\vec{r}) - \sum_j \int \mathrm{d}\vec{r}' \frac{e^2}{4\pi\varepsilon_0|\vec{r}-\vec{r}'|}\psi_j^*(\vec{r}')\psi_i(\vec{r}')\psi_j(\vec{r}) + U(\vec{r})\psi_i(\vec{r}) = E_i\psi_i(\vec{r}), \tag{1.2.1}$$

where the first and the second terms of Eq. (1.2.1) are, respectively, the kinetic energy contribution and the exchange contribution. In the third term, $U(\vec{r})$ is the ''crystal potential'', which is the Coulombic interaction of an electron with all the ions and electrons in the solid, as well as charges external to the solid, namely

$$U(\vec{r}) = -eV(\vec{r}) = e^2\sum_j \int \mathrm{d}\vec{r}' \frac{|\psi_j(\vec{r}')|^2}{4\pi\varepsilon_0|\vec{r}-\vec{r}'|} - \sum_j^{\text{ion}} \frac{Z_j e^2}{4\pi\varepsilon_0|\vec{r}-\vec{R}_j|} - eV_{\text{ext}}(\vec{r}), \tag{1.2.2}$$

where $V(\vec{r})$ is the electrostatic potential and $-e$ is the electronic charge. Note that the charge distribution giving rise to $V(\vec{r})$ in Eq. (1.2.1) is assumed to include the time-averaged distribution of the ith electron itself. The self-energy term, in the time-averaged, frozen–charge-density, representation is not singular and is canceled by a corresponding term in the exchange-correlation sum. We can define a macroscopic electrostatic potential for any point $(\vec{r})$ inside the crystal as the average of $V(\vec{r})$ in a region surrounding $(\vec{r})$, in the shape of a Wigner–Seitz cell

$$\overline{V}(\vec{r}) = \frac{1}{\Omega_{\text{cell}}} \int^{\text{W-S}} V(\vec{r} + \vec{r}')\, \mathrm{d}\vec{r}', \tag{1.2.3}$$

where Ω_{cell} is the volume of the Wigner–Seitz cell. $\overline{V}(\vec{r})$ is ordinarily a very slowly varying function in a crystal.

For a perfect infinite crystal, the Hartree–Fock equation can be solved self-consistently, in theory if not always in practice. Because an infinite crystal has no exterior, its electric potential, $V_\infty(\vec{r})$, cannot be referenced to the potential at any external point, as shown in Fig. 2(a). So, the average potential for an infinite crystal can be assumed to be an arbitrary constant

$$\overline{V}(\vec{r}) = V_\infty^0 \quad (\text{infinite crystal}) \tag{1.2.4}$$

However, once V_∞^0 is specified, the energy bands of the infinite crystal are also uniquely defined, because the kinetic energy and the exchange-correlation energy in Eq. (1.2.1) are fixed bulk contributions. As a matter of fact, any characteristic energy level of the infinite crystal, $E_{i,\infty}$,

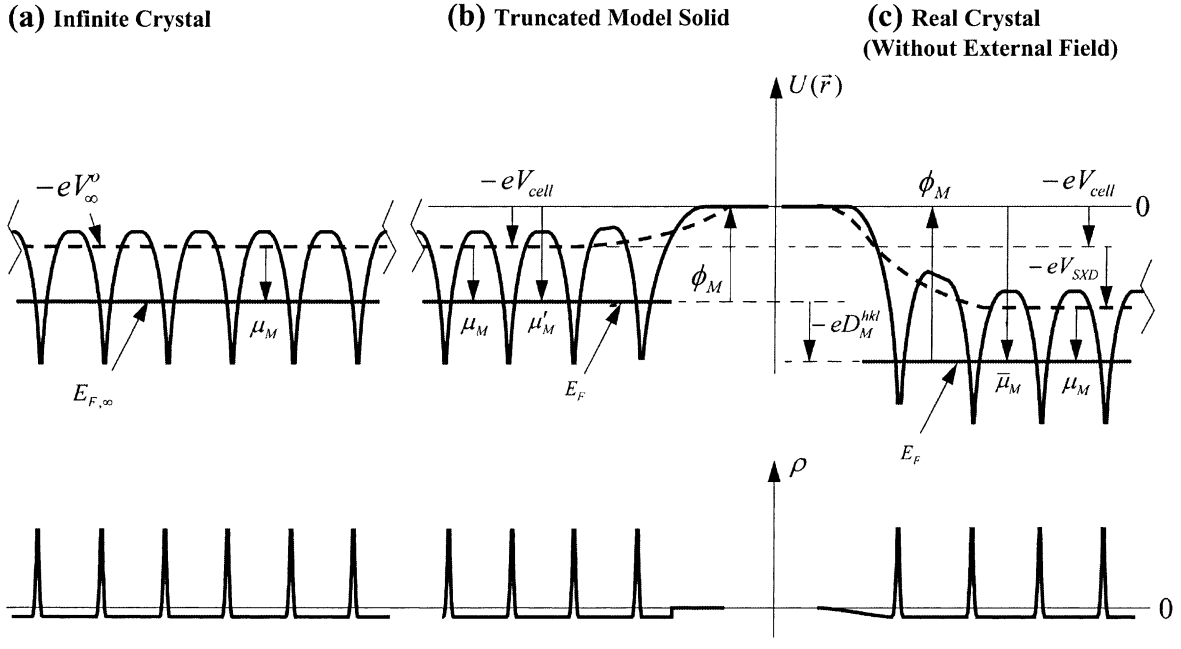

Fig. 2. The crystal potential $U(\vec{r})(= -eV(\vec{r}))$ (upper panel) and the charge density ρ (lower panel), plotted along a line of ions, of (a) an infinite crystal, (b) a surface terminated with frozen bulk charge density, and (c) a surface with relaxed charge density. The average crystal potential, i.e. $-e\overline{V}(\vec{r})$, is shown in dashed lines. Positive quantities are indicated by upward arrows, while down arrows indicate negative quantities.

can be divided into a bulk, or quantum–mechanical, contribution, $\hat{\varepsilon}_i$, plus a potential energy contribution, namely

$$E_{i,\infty} = \hat{\varepsilon}_i - eV^0_\infty. \tag{1.2.5}$$

For example, the Fermi energy of an infinite metal crystal, $E_{\mathrm{F},\infty}$, is

$$E_{\mathrm{F},\infty} = \mu_{\mathrm{M}} - eV^0_\infty, \tag{1.2.6}$$

where μ_{M} is the chemical potential of the metal. The relationship between energy levels and electrostatic potential is shown in Fig. 2(a). Even though Eqs. (1.2.5) and (1.2.6) can be expressed in explicit forms, they cannot be used to reference energy levels of an infinite crystal to an external scale, because V^0_∞ has no physical meaning.

When the crystal is of a finite yet macroscopic size, but is otherwise perfect in its crystal structure, the electron wave functions and the charge distribution in its interior should not be different from that of an infinite crystal. The crystal potential of the interior of a finite crystal differs from that of an infinite crystal by no more than a rigid-shift. Because the crystal is bounded, the electric potential can now be referenced with respect to $V(\infty) = 0$. Since the Coulomb interaction is notoriously long-ranged, the electric potential at any point seems to be influenced by the charge distribution of the entire crystal, as suggested by Eq. (1.2.2). However, the charge distribution can be first grouped into identical ''neutral-cells'', and the contributions from each cell to the potential are then summed up. This extra step is convenient because the potential due to the collection of charges in each neutral-cell can be made remarkably short-ranged. The electric potential, due to a neutral-cell centered at $\vec{r}'$, at an external point, $\vec{r}$, can be expressed in a multiple expansion:

$$V(\vec{r},\vec{r}') = \frac{Q}{4\pi\varepsilon_0|\vec{r}-\vec{r}'|} + \frac{\vec{P}(\vec{r}-\vec{r}')}{4\pi\varepsilon_0|\vec{r}-\vec{r}'|^3} + \sum_{i,j}\frac{\Omega_{ij}(r_i r_j - 3r^2\delta_{ij})}{4\pi\varepsilon_0|\vec{r}-\vec{r}'|^5} + \cdots \tag{1.2.7}$$

where Q, $\vec{P}$ and Ω_{ij} are, respectively, the net charge, dipole, and quadruple of the distribution of charge in the neutral-cell about the point $\vec{r}'$. It is often trivial to define space-filling neutral-cells in a crystal such that the net charge and dipole both vanish. A good example of such a neutral-cell is the Wigner–Seitz cell for a lattice. And for crystals with cubic and inversion symmetries, the total quadruple and r^{-4} contributions also vanish. So, if the neutral-cell of a periodic crystal is carefully chosen, the electric potential due to each neutral-cell is often very short-ranged, falling off more rapidly than r^{-5} [15]. This means that cells a few lattice spacings away will have little contribution to the local electric potential. The total contribution to the electric potential of a point, from a layer of neutral-cells at a distance between R and $R + \mathrm{d}R$ away from the point, decays faster than R^{-3}. Assuming that the finite crystal is placed near the origin, the electrostatic potential for any point in the interior of the crystal can be written as

$$V(\vec{r}) = \int_{\text{nearby\_n-cells}} \mathrm{d}\vec{r}'\,\frac{\rho_{\mathrm{perf}}(\vec{r}')}{|\vec{r}-\vec{r}'|} + V_{\mathrm{SXD}}(\vec{r}) \quad \text{for } |\vec{r}| \ll L, \tag{1.2.8}$$

where L is the characteristic dimension of the crystal, ρ_{perf} the charge distribution of a perfectly infinite lattice, and the integration is only over nearby cells which have non-negligible contributions. The term $V_{\mathrm{SXD}}(\vec{r})$ is the contribution from surfaces, external charges and any minor departure of the actual charge distribution from that of a perfect lattice (e.g. screening), as suggested by its subscript.

Inside a metal there can be no long-range electric field, so $V_{\mathrm{SXD}}(\vec{r})$ is a constant ($= V_{\mathrm{SXD}}^{\mathrm{M}}$) except very near the surface, i.e.

$$V_{\mathrm{SXD}}(\vec{r}) = V_{\mathrm{SXD}}^{\mathrm{M}} \quad (\text{inside a metal}) \tag{1.2.9}$$

It is also obvious that, except near the locations of free charges (e.g. defects, dopants, etc.) or under severe external fields, $V_{\mathrm{SXD}}(\vec{r})$ should be a very slowly varying function inside an insulator or a semiconductor. Because the average of the first term of Eq. (1.2.8) is a constant, V_{cell}, which is essentially the average potential of a cell due to charge distribution within the same cell, the macroscopic average of $V(\vec{r})$ is simply

$$\overline{V}(\vec{r}) = V_{\mathrm{cell}} + V_{\mathrm{SXD}}(\vec{r}). \tag{1.2.10}$$

Therefore, the energy bands of a finite crystal can be referenced to the ''vacuum level'' energy, $E_{\mathrm{VAC}}^{\infty} = 0$, of an electron at rest at infinity, as

$$E_i(\vec{r}) = \hat{\varepsilon}_i - eV_{\mathrm{cell}} - eV_{\mathrm{SXD}}(\vec{r}), \tag{1.2.11}$$

where $\hat{\varepsilon}_i$ is as defined before in Eq. (1.2.5). A drawing of the near surface region of a metal is shown in Fig. 2(c).

To understand the physical meaning of the surface term $V_{\mathrm{SXD}}(\vec{r})$, we note from Eq. (1.2.8) that, in the absence of external charge, $V_{\mathrm{SXD}}(\vec{r})$ is identically zero in the interior of a finite crystal that is made up of only neutral-cells. Such a crystal can be called a ''truncated model solid''. A ''model solid'' is an imaginary object with a charge distribution which mimics that of a real solid, with the exception that its surface charge distribution can be arbitrarily specified [16,17]. Such an object is not a real crystal because its charge distribution does not satisfy Schrodinger's equation. However, the electrostatic potential of a model solid is physically meaningful, because it satisfies Poisson's equation. A ''truncated'' model solid is one that is terminated on all sides abruptly on the boundaries of outermost neutral-cells, as schematically shown in Fig. 2(b). In the interior of a truncated model solid with a metal charge distribution, the potential is, obviously

$$V(\vec{r}) = \int_{\text{nearby\_n-cells}} \mathrm{d}\vec{r}' \, \frac{\rho_{\mathrm{perf}}(\vec{r}')}{|\vec{r} - \vec{r}'|} \quad (\text{inside a truncated model solid}) \tag{1.2.12}$$

A comparison with Eq. (1.2.8) shows that $V_{\mathrm{SXD}}(\vec{r})$ is the difference between the potential of a real solid and that of a truncated model solid. It is the electrostatic potential due to external charges and surface charge rearrangement. Eq. (1.2.10) perhaps gives the most straightforward definition of $V_{\mathrm{SXD}}(\vec{r})$: it is the average electrostatic potential without the bulk contribution. In the absence of external electric field, $V_{\mathrm{SXD}}(\vec{r})$ can be identified as the surface dipole

$$V_{\mathrm{SXD}}^{\mathrm{M}} = D_{\mathrm{M}}^{(h\,k\,l)} \quad (\text{polygon}) \tag{1.2.13}$$

where $(h\ k\ l)$ denotes the orientation and the structure of the surface, as schematically shown in Fig. 2(c). In order for the external field to vanish, not only must there not be any external charge, but the finite crystal itself must be uncharged. Furthermore, the surface structure of the finite crystal must be homogeneous. Therefore, Eq. (1.2.13) is valid only for a neutral metal crystal whose entire surface is made up of a unique kind of structure, e.g. a cube with $\{0\ 0\ 1\}$ surfaces or an octahedron

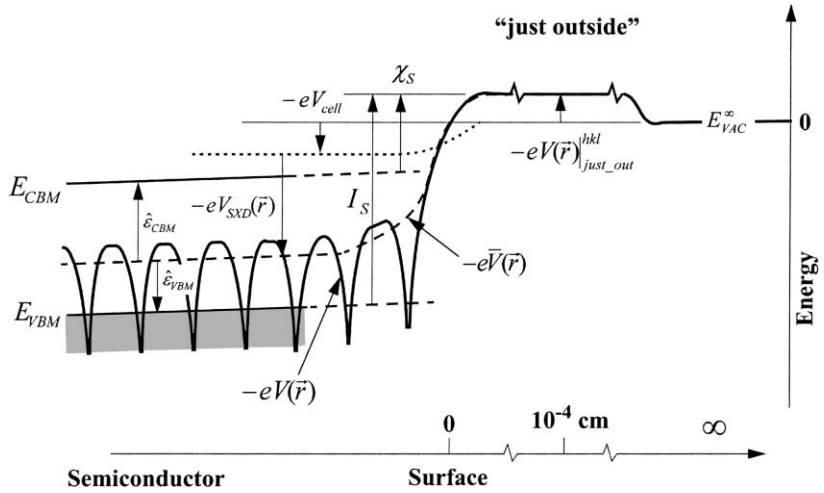

Fig. 3. The distribution of crystal potential, $-eV(\vec{r})$, near a semiconductor surface is shown in bold line. A slope is drawn inside the semiconductor to indicate the presence of an electric field in the space–charge region. Note that the electrostatic potential is defined with respect to vacuum level at infinity while measurable quantities such as χ_S and I_S are defined with respect to the potential just outside the semiconductor.

with {1 1 1} surfaces. For a metal with a random shape, external electric field is unavoidable and a more appropriate definition of the surface dipole has to be used

$$D_{\mathrm{M}}^{(h\,k\,l)} = V_{\mathrm{SXD}}^{\mathrm{M}} - V(\vec{r})|_{\mathrm{just\_out}}^{(h\,k\,l)} \tag{1.2.14}$$

where the second term is the electrostatic potential just outside the $(h\,k\,l)$ surface. Here "just outside" denotes a distance from the surface that is small compared with the sample dimension, but large compared with atomic dimensions. Typically, this distance is on the order of 100 nm–10 μm [18,19] as schematically indicated in Fig. 3. It should be noted that the definition of a surface dipole is more or less arbitrary. The present definition of the surface dipole has the advantages that it has effectively excluded the bulk contribution and that it allows a coherent definition of the interface dipole to be made later. The surface dipole is usually positive, as a spillover of electron density from the crystal into the vacuum increases the barrier for electrons to escape.

The most prominent characteristic energy level of a metal is its Fermi energy, $E_{\mathrm{F,M}}$. The energy required to move an electron from $E_{\mathrm{F,M}}$, and place it at rest just outside the metal is the work function of a metal, $\phi_{\mathrm{M}}^{(h\,k\,l)}$ [18,19]. One, thus, writes

$$\phi_{\mathrm{M}}^{(h\,k\,l)} = -E_{\mathrm{F,M}} - eV(\vec{r})|_{\mathrm{just\_out}}^{(h\,k\,l)} = eV_{\mathrm{SXD}}^{\mathrm{M}} + eV_{\mathrm{cell}} - \mu_{\mathrm{M}} - eV(\vec{r})|_{\mathrm{just\_out}}^{(h\,k\,l)} = eD_{\mathrm{M}}^{(h\,k\,l)} - \mu'_{\mathrm{M}} \tag{1.2.15}$$

where use has been made of Eqs. (1.2.11) and (1.2.14), and where

$$\mu'_{\mathrm{M}} = \mu_{\mathrm{M}} - eV_{\mathrm{cell}}^{\mathrm{M}}. \tag{1.2.16}$$

According to Eq. (1.2.15), the work function, which is the "band offset" between the FL of a metal and the lowest energy level of a vacuum, can be broken up into a surface term $eD_{\mathrm{M}}^{(h\,k\,l)}$ and a bulk term μ'_{M}. One notes from Fig. 2(b) that the bulk term is the electrochemical potential for the hypothetical truncated model solid, and can be regarded as an "effective chemical potential" for the bulk metal. The very unique feature about the present definition of surface dipole, Eq. (1.2.14), is

thus, revealed in Eq. (1.2.15), namely, the separation of a band offset into a surface term and a bulk term is independent of the definition of the long-range potential. In other words, any other definition of Eq. (1.2.3), such as by using the muffin-tin zero or the interstitial site potential, would render the same result, Eq. (1.2.15). Of course, both terms in Eq. (1.2.15) depend on the choice of the neutral-cell making up the model solid and, therefore, can still be argued as being model-dependent. The advantage in taking the extra step to define all the quantities through a comparison with the model solid may not be obvious for now. But, it should become clear when real examples of interface dipole are discussed.

The position of the FL at the surface of a semiconductor or insulator depends sensitively on the distribution of surface states, as discussed in Section 2. Since the bulk density of states is often zero at the FL, the concept of a work function is not particularly useful for semiconductors. Two other quantities are more often quoted for a semiconductor or insulator surface. The energy it takes to remove an electron from the highest occupied states of the semiconductor and place it ''just outside'' the semiconductor surface is the ionization energy, I_S; and the energy released when an electron is moved from just outside the surface to the lowest unoccupied state of the semiconductor is known as the electron affinity, χ_S. As before, the electric potential in a finite semiconductor crystal is distributed according to Eq. (1.2.8). And as before, a set of energy bands, characteristic of a perfect infinite semiconductor crystal, can be mapped onto the potential distribution

$$E_{n,\vec{k}}(\vec{r}) = \hat{\varepsilon}_{n,\vec{k}} - eV_{\text{cell}}^{\text{S}} - eV_{\text{SXD}}(\vec{r}), \tag{1.2.17}$$

where $\hat{\varepsilon}_{n,\vec{k}}$ is the energy level with quantum numbers n and $\vec{k}$ for the infinite and perfect crystal. It is clear from Eq. (1.2.17) that the rigid-shift of the bands, also known as band bending, originates from a variation of the long-range electric potential, which can be treated classically. This semi-classical approach of separating the energy into a classical component and a quantum mechanical part (the electronic states of the infinite crystal) is only valid when $V_{\text{SXD}}(\vec{r})$ varies slowly on the scale of the lattice parameter. Again, a surface dipole can be defined by a comparison with a model semiconductor crystal. However, because the bands are usually bent near the surface, in the so-called space–charge region of a semiconductor, the average potential of the semiconductor varies with position. The surface dipole to a semiconductor can be defined, similarly to Eq. (1.2.14) for a metal, as the difference between the asymptotic value of $V_{\text{SXD}}(\vec{r})$ as the surface is approached from inside the semiconductor and the electrostatic potential just outside the semiconductor:

$$eD_{\text{S}}^{(hkl)} = eV_{\text{SXD}}(\vec{r})|_{\vec{r}\to 0,\text{in}}^{(hkl)} - eV(\vec{r})|_{\text{just\_out}}^{(hkl)}. \tag{1.2.18}$$

The ionisation energy and the electron affinity are then defined as

$$I_{\text{S}}^{(hkl)} = eD_{\text{S}}^{(hkl)} + eV_{\text{cell}}^{\text{S}} - \mu_{\text{S}} = eD_{\text{cell}}^{(hkl)} - \mu'_{\text{S}}, \tag{1.2.19}$$

and

$$\chi_{\text{S}}^{(hkl)} = eD_{\text{S}}^{(hkl)} + eV_{\text{cell}}^{\text{S}} - \hat{\varepsilon}_{\text{CBM}} = I_{\text{S}}^{(hkl)} - E_{\text{g}}, \tag{1.2.20}$$

where $\hat{\varepsilon}_{\text{CBM}}$ and μ_{S} are, respectively, the internal contributions (with respect to the average potential energy of the solid, cf. Fig. 3) to the energies of the conduction band minimum (CBM) and the valence band maximum (VBM). Obviously, the CBM can also be defined, with respect to the truncated semiconductor solid

$$\mu'_{\text{S}} = \mu_{\text{S}} - eV_{\text{cell}}^{\text{S}}. \tag{1.2.21}$$

Note that all terms in Eqs. (1.2.19) and (1.2.20) are independent of the definition of the long-range electrostatic potential.

1.3. Interface-specific region

We now consider what happens to the electric potentials inside the respective crystals when a metal and a semiconductor are joined together. As before, we can start with an isolated crystal of metal and an isolated crystal of semiconductor, each with potential distribution given by Eq. (1.2.8). For simplicity, we assume that the metallurgical interface is intimate and sharp on an atomic scale, i.e. there is no compound formation or inter-diffusion at this MS interface. Furthermore, we assume that the interface has a homogeneous structure, so that the electronic property is also homogeneous for the entire MS interface. It is clear that the bulk band structure of either the metal or the semiconductor should be found deep in the interior of either crystal. It is also clear that, when the electronic structure evolves from purely metallic on one side of the MS interface to purely semiconducting on the other side, this change cannot occur abruptly and has to evolve over some finite distance. Theoretical calculations suggest that the recovery of the bulk electronic structure of either the metal or the semiconductor, from the metallurgical MS interface plane, requires at least the distance of a few lattice spacings [20–22]. Therefore, there exists an ''interface-specific region (ISR)'' with the width of a few lattice spacings (1–2 nm), whose electronic structure is unlike that of either the metal or the semiconductor. This region, schematically shown in Fig. 4, makes up the immediate surroundings of the MS interface, and its properties are dominated by the presence of the MS interface. Wave functions originating from the metal interact with those originating from the semiconductor in the ISR, resulting in interface-specific electronic states that are not found in either the bulk metal or the bulk semiconductor. We will leave the discussions on the electronic states in the interfacial region for a later section and will, for the time being, only be concerned with the net effect these interface states have on the match-up of bands on either side of the MS interface. We note,

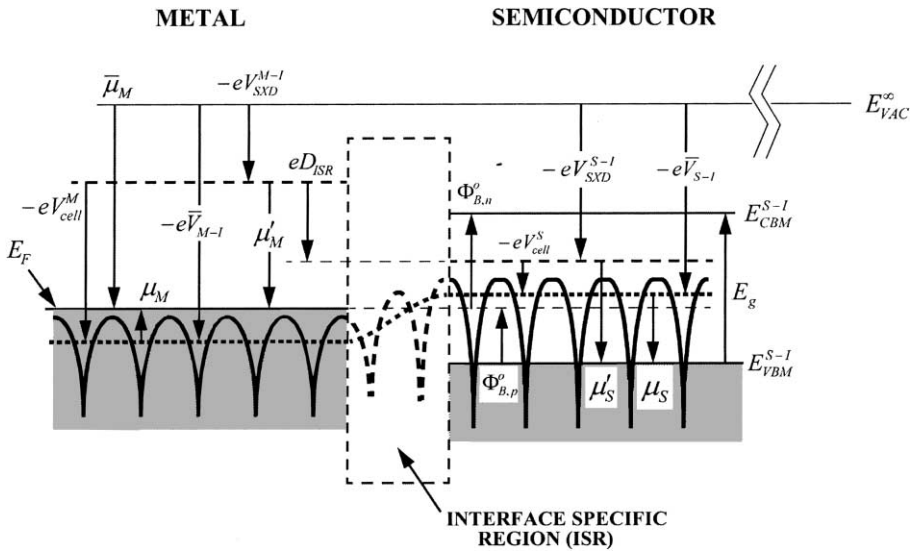

Fig. 4. The distributions of crystal potential, $-eV(\vec{r})$ (solid curve lines) and energy bands (solid straight lines) at a metal–semiconductor interface. The average crystal potential is drawn as thick dotted line, and $-eV_{\mathrm{SXD}}(\vec{r})$ is drawn as dashed lines.

nevertheless, that the two rules mentioned above for interfaces must also apply for the ISR, namely, that the electrostatic potential has to be continuous and that the electronic structure of the ISR is such that it minimizes the interface energy.

The ISR is assumed to be wide enough so that outside the ISR, the electronic properties, including the charge distribution and the band structure, etc. are again characteristic of the undisturbed bulk crystal. The average crystal potential on the metal side of the ISR-metal boundary, referenced to $E_{\mathrm{VAC}}^{\infty} = 0$, is

$$-e\overline{V}_{\mathrm{M-I}} = -eV_{\mathrm{cell}}^{\mathrm{M}} - eV_{\mathrm{SXD}}^{\mathrm{M-I}}. \tag{1.3.1}$$

The subscript/superscript M–I, which stands for ''metal–ISR'', signals the fact that the average electrostatic potential, although still a constant for the entire metal, may shift from the value for an isolated metal, expressed in Eq. (1.2.9). The average potential inside the semiconductor is given by

$$-e\overline{V}_{\mathrm{S}}(z) = -eV_{\mathrm{SXD}}^{\mathrm{S}}(z) - eV_{\mathrm{cell}}^{\mathrm{S}}. \tag{1.3.2}$$

The electrostatic potential is homogeneous in the *xy*-plane on our original assumption that the MS interface is laterally homogeneous. In reality, the average electrostatic potential could vary laterally, as discussed in Section 1.5. But for the present discussion, lateral inhomogeneity will be ignored. As will be discussed in detail in the next section, the variation of the V_{SXD} in the z-direction is due largely to the electric field in the depletion region, which is negligible on atomic scale. One can define asymptotically a $V_{\mathrm{SXD}}^{\mathrm{S-I}}$, which pertains to the semiconductor at the semiconductor–ISR interface, as

$$V_{\mathrm{SXD}}^{\mathrm{S-I}} = V_{\mathrm{SXD}}(z)|_{z\to 0}. \tag{1.3.3}$$

Other changes of notation in the quantities related to the electrostatic potential on the semiconductor side of the interface can be read off of Fig. 4.

The total potential shift across the ISR, $e\overline{V}_{\mathrm{M-I}} - e\overline{V}_{\mathrm{S-I}}$, is referred by some authors as the interface dipole. This definition is obviously arbitrary, because it depends on the definition of the average potential. Within the truncated model solid concept which we have been using, $V_{\mathrm{SXD}}(\vec{r})$ is the long-range potential and the interface dipole, D_{ISR}, is naturally defined as

$$D_{\mathrm{ISR}} = V_{\mathrm{SXD}}^{\mathrm{M-I}} - V_{\mathrm{SXD}}^{\mathrm{S-I}}. \tag{1.3.4}$$

It also has a very transparent physical meaning: D_{ISR} is the total dipole due to the rearrangement of charge, from their truncated bulk distribution, across the entire ISR region. Note that this definition is independent of the surface structure on the original isolated metal and semiconductor crystals. The SBH to a p-type semiconductor is defined as the difference between the semiconductor VBM and the Fermi-level at the interface. In thermal equilibrium, the FL is constant throughout the entire MS system, so the p-type SBH is

$$\Phi_{\mathrm{B,p}}^{0} = \mu_{\mathrm{M}}' - \mu_{\mathrm{S}}' - eD_{\mathrm{ISR}} \tag{1.3.5}$$

and the n-type SBH is

$$\Phi_{\mathrm{B,n}}^{0} = E_{\mathrm{g}} - \Phi_{\mathrm{B,p}}^{0} \tag{1.3.6}$$

$$\Phi_{\mathrm{B,n}}^{0} = \hat{\varepsilon}_{\mathrm{CBM}} - eV_{\mathrm{cell}}^{\mathrm{S}} - \mu_{\mathrm{M}}' + eD_{\mathrm{ISR}}. \tag{1.3.6a}$$

One notes that the sense of the interface dipole has been chosen such that the more positive D_{ISR} is, the larger is the n-type SBH. One also notes that none of the quantities in Eqs. (1.3.5) and (1.3.6) depend on the definition of the long-range potential, or the choice of the vacuum level. Since the first two terms on the right hand side of Eq. (1.3.5) are purely bulk properties, it is clear that the MS interface or, more precisely, the ISR influences the SBH only through the last term, i.e. the total interface dipole. In general, the net charge of the ISR does not affect the magnitude of the SBH; it only affects the long-range electric field in the semiconductor, i.e. through $[\partial V^{\mathrm{S}}_{\mathrm{SXD}}(z)/\partial z]_{z\to 0}$. One should also keep in mind that the SBH is likely inhomogeneous for real interfaces, which means that both the interface dipole and the net interface charge-density could vary laterally.

1.4. Space–charge region: homogeneous barrier

We assume that a semiconductor, occupying $z > 0$, has formed a uniform SB with a metal, as depicted in Fig. 5. The width of the ISR is usually negligible on the scale that band bending is considered, ~30 nm to 10 μm, so it has been neglected in this drawing. In thermal equilibrium, the Fermi-level is constant throughout the entire metal and semiconductor solids. However, the electric field need not vanish inside a semiconductor, because dielectric screening by bound electrons is incomplete. In comparison, the interior of a conductor has no static electric field because of perfect screening by mobile electrons. This difference in screening behaviors can be attributed to the presence of a band gap in the semiconductor, so the movement of the Fermi-level inside the band gap has little or only minor consequence on the local neutrality. The spatial variation of the long-range electric potential inside the semiconductor is governed by macroscopic Poisson's equation in a continuous dielectric medium

$$\left[\frac{\partial^2}{\partial x^2}+\frac{\partial^2}{\partial y^2}+\frac{\partial^2}{\partial z^2}\right] V^{\mathrm{S}}_{\mathrm{SXD}}(\vec{r}) = -\frac{\rho(\vec{r})}{\varepsilon_{\mathrm{S}}}, \tag{1.4.1}$$

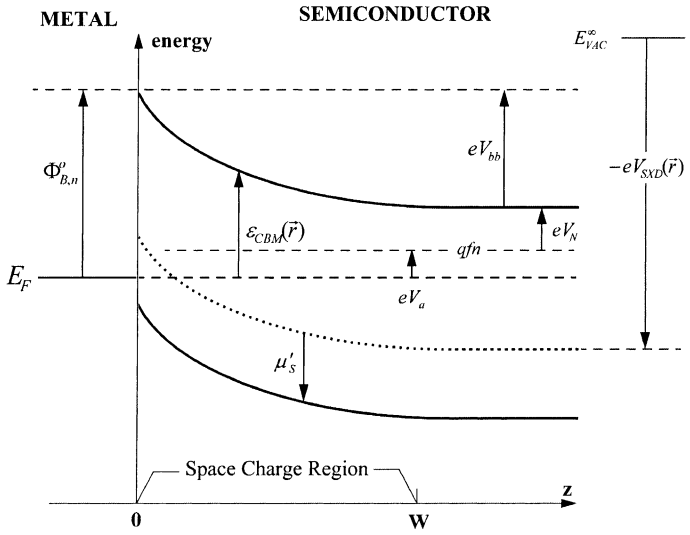

Fig. 5. Band diagram for a homogeneous SB with an applied bias.

where ε_S is the semiconductor permittivity and $\rho(\vec{r})$ the density of local free charge, which is determined by the local density of states $n(E,\vec{r})$ and the Fermi-level position

$$\rho(\vec{r}) = -e\int_{-\infty}^{\infty} \frac{n(E,\vec{r})}{1+\exp((E-E_F)/k_BT)}\,dE + \rho_+(\vec{r}), \tag{1.4.2}$$

where ρ_+ is the local charge-density due to positive ions. When the long-range electric potential varies spatially, there is an accompanying bending of the energy bands, as expressed in Eq. (1.2.17). Band bending is a semi-classical concept, as already mentioned. As the bands are bent from place to place, there is also a rigid-shift in the density of states, i.e.

$$n(E,\vec{r}) = n(E - eV_{SXD}^{S}(\vec{r})), \tag{1.4.3}$$

where $n(E)$ is the density of states of the semiconductor, referenced to the long-range crystal potential of the perfect crystal. Note that the density of states will depend on the presence of dopants and other imperfections in the semiconductor. Eqs. (1.4.1)–(1.4.3), thus, provide all the information to solve for the long-range potential in the semiconductor, when boundary conditions are specified. Since the energetic position of any semiconductor electronic state is only a rigid-shift away from the long-range electric potential, it also satisfies the Poisson's equation. So, one can use the conduction band minimum position with respect to the Fermi-level of the metal, $\varepsilon_{CBM}(\vec{r})$, to conveniently describe the band bending at an n-type Schottky barrier, as shown in Fig. 5. To generalize our discussion, we shall assume that a small external bias, V_a, has been applied to the semiconductor. The steady state current flow is assumed to be small and does not affect the thermal equilibrium of charge distribution, Eq. (1.4.2). Deep inside the semiconductor, the conduction band minimum is at

$$\varepsilon_{CBM}(z > W) = eV_N + eV_a, \tag{1.4.4}$$

where eV_N is the conduction band minimum with respect to the local Fermi-level in a neutral semiconductor and is determined by the charge neutrality condition. For a lightly doped semiconductor with a donor concentration of N_D, it is

$$eV_N = k_BT\ln\left(\frac{N_D}{N_C}\right), \tag{1.4.5}$$

where N_C is the effective density of states of the conduction band. In passing, we mention that an equivalent expression exists for a neutral p-type semiconductor with a doping concentration of N_A

$$eV_P = k_BT\ln\left(\frac{N_A}{N_V}\right), \tag{1.4.5a}$$

where N_V is the effective density of states of the semiconductor valence band. Here, only n-type SB is discussed. However, it is understood that descriptions for p-type Schottky barriers essentially mirror those given here.

At the MS interface, the conduction band is, by definition, $\Phi_{B,n}^0$ above the metal Fermi-level position

$$\varepsilon_{CBM}(z \to 0) = \Phi_{B,n}^0, \tag{1.4.6}$$

assuming that the SBH does not depend on the applied bias. The total band bending can be simply read off Fig. 5 as

$$eV_{bb} = \Phi^0_{B,n} - eV_N - eV_a. \tag{1.4.7}$$

In the absence of an applied bias, the band bending is known as the built-in potential

$$eV_{bi} = \Phi^0_{B,n} - eV_N. \tag{1.4.7a}$$

The V_{bi} can be viewed as the bias that is needed to render the ''flat band'' condition for a SB, and is a useful quantity particularly for capacitance measurements. With the boundary conditions, Eqs. (1.4.4) and (1.4.6), specified, the Poisson's equation can be solved numerically for a uniform SBH. However, at finite temperatures, the solution is not expressible in closed forms. Much insight about the band bending can be gained by an examination of the solution obtained within the ''depletion approximation'', which assumes that all electronic states below the FL to be occupied while those above the FL are empty. This is, in essence, a $T = 0$ approximation concerning the occupation of the electronic states. Within the depletion approximation, the density of charge is assumed to be a step function

$$\rho(z) = \begin{cases} eN_D, & 0 < z < W \\ 0, & z > W \end{cases} \tag{1.4.8}$$

where W is the depletion region width, is given by

$$W = \lambda_D \sqrt{\frac{2eV_{bb}}{k_B T}}, \tag{1.4.9}$$

and λ_D is the Debye length

$$\lambda_D = \sqrt{\frac{\varepsilon_S k_B T}{e^2 N_D}}. \tag{1.4.10}$$

The solution to the Poisson's equation is

$$\varepsilon_{CBM}(z) = \begin{cases} eV_{bb}\left(1 - \dfrac{z}{W}\right)^2 + eV_N + eV_a, & 0 < z < W \\ eV_N + eV_a, & z > W \end{cases} \tag{1.4.11}$$

One notes that the total charge per unit area in the space–charge region is

$$Q_{SC} = eN_D W = \sqrt{2\varepsilon_S N_D e V_{bb}}, \tag{1.4.12}$$

and that the maximum electric field near the MS interface is

$$E_{max} = \sqrt{\frac{2eN_D V_{bb}}{\varepsilon_S}}. \tag{1.4.13}$$

For moderately doped semiconductors, this field is only of the order of 10^4 to 10^5 V cm^{-1}, which leads to a potential change of 1 V in 50 nm or longer. This potential, is thus, varying very slowly and

the present semi-classical concept of band bending is thus justified. When the doping level of the semiconductor is low to moderate, the depletion approximation usually gives fairly accurate descriptions of the potential distribution at Schottky barriers or p–n junctions. Appreciable deviation only occurs when the band bending is small compared with the band gap and when the temperature is high. When the distribution of carriers at the edge of the depletion region is properly considered, analytic expressions can still be obtained approximately. The correction for finite temperature effect amounts to replacing V_{bb} in Eqs. (1.4.9), (1.4.12) and (1.4.13) with $(V_{bb} - k_B T/e)$.

1.5. Space–charge region: inhomogeneous barrier

When the SBH varies locally at a MS interface, the solutions obtained in Section 1.4 need to be modified to accommodate the lateral variation in the electrostatic potential. Whereas the boundary condition (1.4.4) has not changed, the condition (1.4.6) now reflects the lateral variation of the SBH:

$$\varepsilon_{CBM}(x, y, 0) = \Phi^0_{B,n}(x, y) = \Phi^{00}_{B,n} + e\delta(x, y), \tag{1.5.1}$$

where $e\delta(x, y)$ is the difference between the local SBH and a "mean" SBH, $\Phi^{00}_{B,n}$. For arbitrary distribution of the SBH, these boundary values can be used to solve for the band bending profile in the space–charge region [23]. However, as shown explicitly, a "dipole layer approximation" allows the potential to be accurately described with relative ease [10,24]. In this approach, the variation of the potential due to the presence of the SBH inhomogeneity is treated as a perturbation. It is obvious that the potential due to a dipole layer with a varying dipole moment per area, $2\varepsilon_S\delta(x, y)$, should be used as the perturbative term, since it satisfies the Laplace equation and reproduces the desired boundary condition at the MS interface. In other words, the potential in the depletion region of the semiconductor ($0 < z < W$) is approximately described by

$$\varepsilon_{CBM}(x, y, z) = eV_{bb}\left(1 - \frac{z}{W}\right)^2 + eV_N + eV_a + \iint dx_1\, dy_1 \frac{ze\delta(x_1, y_1)}{2\pi[z^2 + (x_1 - x)^2 + (y_1 - y)^2]^{3/2}}, \tag{1.5.2}$$

where eV_{bb} is the band bending corresponding to a MS junction with a uniform SBH of $\Phi^{00}_{B,n}$ ($eV_{bb} = \Phi^{00}_{B,n} - eV_N - eV_a$). The first three terms on the right hand side of Eq. (1.5.2) represent the potential, within the depletion approximation, due to a uniform SBH of $\Phi^{00}_{B,n}$. The last term is the variation of the potential due to the presence of SBH inhomogeneity. Strictly speaking, Eq. (1.5.2) is not an exact solution to Poisson's equation because the change in the charge distribution near the edge of the depletion region, due to the presence of the SBH inhomogeneity, has been ignored. However, for a rapidly fluctuating SBH or for any isolated variation of the SBH on a small lateral length scale, Eq. (1.5.2) gives a nearly perfect account of the potential close to the MS interface [25].

The most interesting form of SBH inhomogeneity is the presence of small regions with a low-SBH, $\Phi^{00}_{B,n} - e\Delta$, embedded in an interface with an, otherwise uniform, high SBH, $\Phi^{00}_{B,n}$. The most convenient geometries to consider for the low-SBH regions are small circular patches and narrow semi-infinite strips. For a low-SBH circular patch with a radius, R_0, which is small compared with W, the potential at any point (ρ, z), may be written down using Eq. (1.5.2). Along the z-axis ($\rho = 0$), the potential has an analytic form

$$\varepsilon_{CBM}(\rho = 0, z) = eV_{bb}\left(1 - \frac{z}{W}\right)^2 + eV_N + eV_a - e\Delta\left[1 - \frac{z}{(z^2 + R_0^2)^{1/2}}\right]. \tag{1.5.3}$$

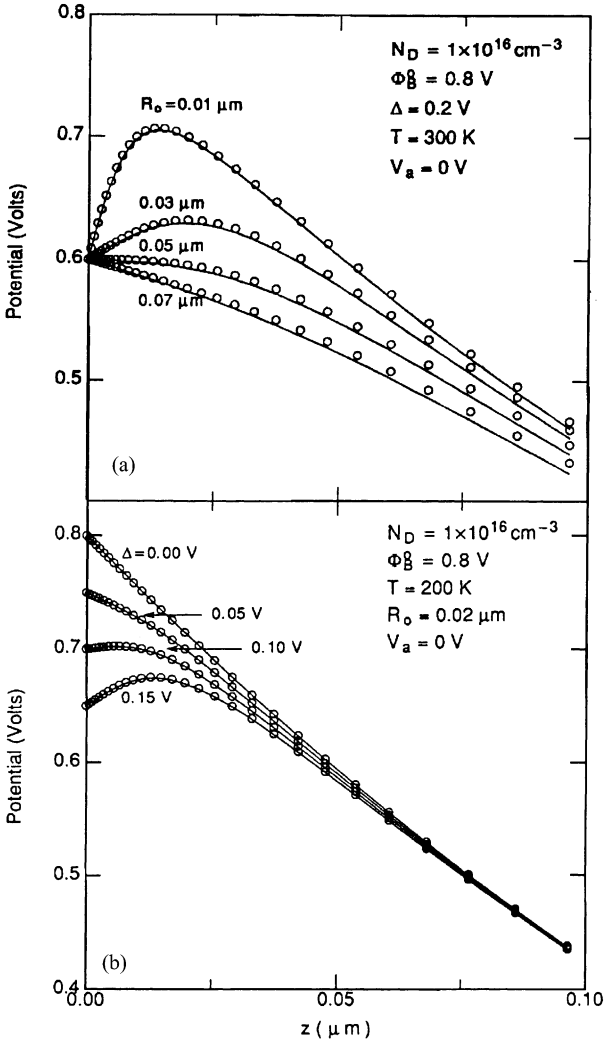

Fig. 6. Numerically determined potential distribution (shown as circles) along $\rho = 0$ of the low-SBH region. The potential based on the analytic theory is shown as the solid lines: (a) the radius of the low-SBH patch R_0 is varied; (b) the SBH difference Δ is varied (after Sullivan et al. [25]).

The excellent agreement between the potential obtained with the dipole layer approach and the numerical solutions obtained from solving Poisson's equation is shown in Figs. 6 and 7. Note that there are no fitting parameters for the curves drawn in these figures. For a large Δ, or a small R_0, the potential in front of the patch is obviously pinched-off. "Pinch-off" is a terminology often used to describe the operation of a field effect transistor. In the present context, an area is said to be pinched-off if majority carriers originating from outside the space–charge region need to go over a potential barrier, higher than the band-edge position at the MS interface, in order to reach the MS interface. One notes that if the potential has a positive slope at small z, then it will go through a maximum before descending at large z to the value for neutral semiconductor. Thus, the condition for pinch-off is obtained by differentiating Eq. (1.5.3) with respect to z and setting the derivative positive:

$$\frac{\Delta}{V_{bb}} > \frac{2R_0}{W}. \tag{1.5.4}$$

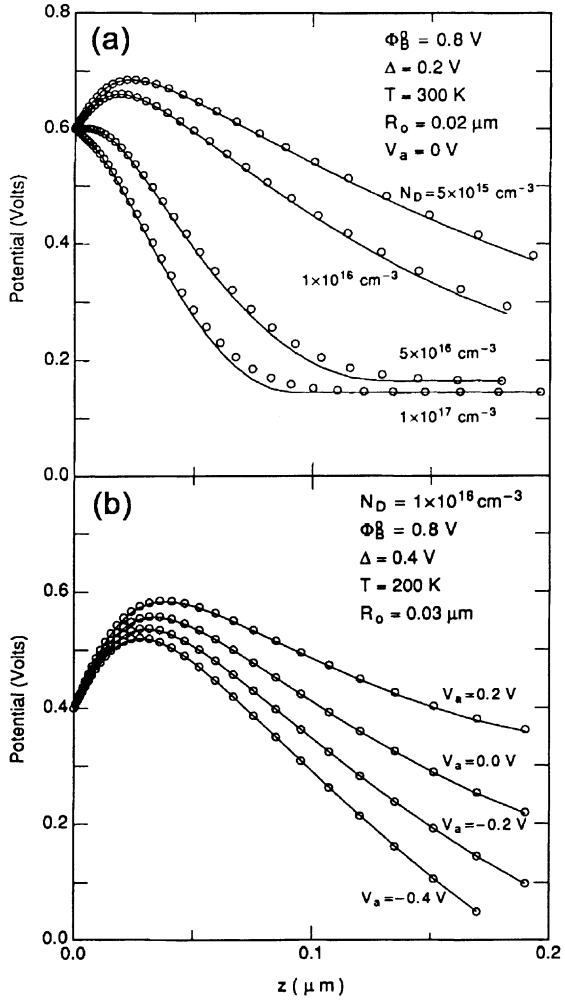

Fig. 7. Numerically simulated potential distribution (shown as circles) along $\rho = 0$ of the low-SBH patch for (a) various n-type doping levels, and (b) various applied bias voltages (after Sullivan et al. [25]).

The condition set by Eq. (1.5.4) shows that potential pinch-off is most prominent when the semiconductor doping level is low and the low-SBH patch is small. The dependence of the potential on the applied bias, illustrated in Fig. 7(b), has a very significant impact on transport properties at inhomogeneous SB junctions. The potential barrier between the semiconductor and the metal increases with forward bias. As will be discussed, this dependence of the potential on applied bias is the key to understanding a host of "anomalous" phenomena in *I–V* measurements. To first-order, the potential does not depend on temperature.

For a strip of low-SBH, which is semi-infinite along the *y*-axis and has a width of L_0 in the *x*-direction, the CBM potential in the space–charge region may be written down as

$$\varepsilon_{\mathrm{CBM}}(x,y,z) = eV_{\mathrm{bb}}\left(1-\frac{z}{W}\right)^2 + eV_{\mathrm{N}} + eV_{\mathrm{a}} + \frac{e\Delta}{\pi}\tan^{-1}\frac{|x|-L_0/2}{z} - \frac{e\Delta}{\pi}\tan^{-1}\frac{|x|+L_0/2}{z}. \tag{1.5.5}$$

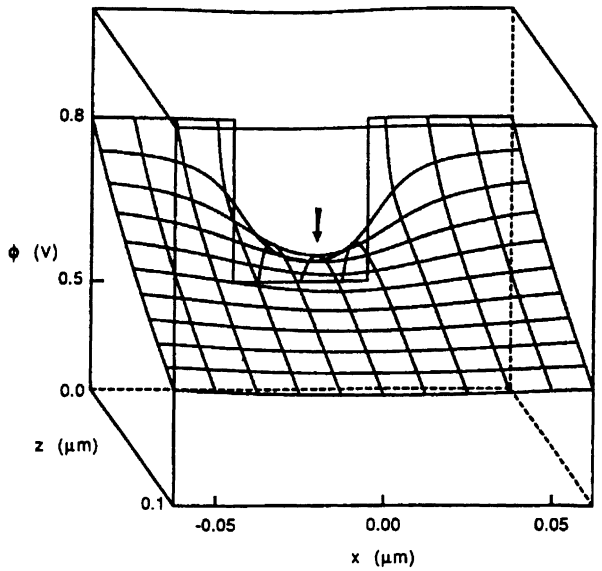

Fig. 8. Semiconductor conduction band diagram, showing the difference between the intrinsic or local SBH at the interface of a low barrier region and the actual potential barrier for electrical transport across the interface, i.e. the saddle-point potential (arrowed). In this particular example, a narrow semiconductor strip with a width of 0.04 μm and a local SBH of 0.5 eV is surrounded by a high barrier background with a SBH of 0.8 eV. The doping level is 5×10^{15} cm^{-3}. The z-axis is normal to the interface.

A 3-D view of this potential for a low-SBH strip which is pinched-off is shown in Fig. 8. As before, the condition for pinch-off may be obtained:

$$\frac{\Delta}{V_{bb}} > \frac{\pi L_0}{2W}. \tag{1.5.6}$$

The approach described above gives a very accurate account of the electric potential in the presence of SBH inhomogeneity, irrespective of the size of the inhomogeneity. When the dimension of low-SBH patches or strips is small compared with the depletion length, one may further simplify the potential by replacing the spatially extended dipole patch/strip with a point-dipole or a dipole line. Such a ''point-dipole approximation'' gives a good approximation to the potential except very close to the patch/strip [10]. This approach is quite adequate for an estimation of the expected *I–V* behavior from an inhomogeneous SBH distribution, because, as will be discussed, the most relevant potential for electron transport is that near the saddle-point, some distance away from the MS interface.

For a circular patch with radius R_0, the total dipole moment is $2\varepsilon_S \pi R_0^2 \Delta$. The potential around the patch, except near the core of the dipole, is given by

$$\varepsilon_{CBM}(\rho, z) = eV_{bb}\left(1 - \frac{z}{W}\right)^2 + eV_N + eV_a - \frac{eV_{bb}\Gamma^3 z W^2}{(\rho^2 + z^2)^{3/2}}, \tag{1.5.7}$$

where Γ is a dimensionless quantity which measures the ''strength'' of a given patch and is defined by

$$\Gamma^3 = \frac{R_0^2 \Delta}{2V_{bb}W^2} = \frac{R_0^2 \Delta}{4\eta V_{bb}^2}, \tag{1.5.8}$$

where $\eta = \varepsilon_S/eN_D$. Numerical simulations show that the point-dipole approximation adequately describes the potential around the saddle-point when $R_0 \ll W$ [25]. One notes that Eqs. (1.5.7) and (1.5.8) are not limited to low-SBH patches with a circular geometry, as Γ may be defined for any small patch with an irregular shape and/or a varying SBH by an integral:

$$\Gamma^3 = \frac{-1}{4\pi\eta V_{bb}^2} \int\int_{patch} dx_1\, dy_1 \delta(x_1 y_1). \tag{1.5.9}$$

Because the point-dipole approximation lumps the effect of a dipole patch with a finite size into a point source, it errs on slightly overestimating the depth of the potential "valley" at the saddle-point and slightly underestimating the valley width.When pinch-off occurs, the location of the saddle-point, at (0, z_0), may be obtained by differentiating Eq. (1.5.7) along the z-axis and setting the derivative to zero. When $\Gamma \ll 1$, z_0 is found to be, approximately

$$z_0 \approx \Gamma W, \tag{1.5.10}$$

and the saddle-point potential is

$$\varepsilon_{CBM}^{sad\text{-}p} = \varepsilon_{CBM}(0, z_0) \approx eV_{bb}(1 - 3\Gamma) + eV_N + eV_a. \tag{1.5.11}$$

This represents the minimum potential barrier separating the low-SBH patch from the neutral semiconductor.

The dipole layer due to a semi-infinite strip with a width L_0, may be approximated by a "dipole line" with an infinitesimal width. The dipole moment per unit length is $2\varepsilon_S L_0 \Delta$ and the potential may be written down as follows:

$$\frac{\varepsilon_{CBM}(x, y, z)}{e} = V_{bb}\left(1 - \frac{z}{W}\right)^2 + V_N + V_a - \frac{2V_{bb}\Omega^2 W_z}{x^2 + z^2}, \tag{1.5.12}$$

where Ω is a dimensionless quantity which measures the strength of the strip, defined in Table 1. Using procedures similar to those described above, the location and the potential of the saddle-point may also be found for the strip geometry (Table 1).

Table 1
Relevant parameters for an isolated low-SBH region with a local SBH of $\Phi_{B,n}^{00} - e\Delta$ surrounded by regions with a SBH of $\Phi_{B,n}^{00}$

Geometry	Circular	Semi-infinite strip
Dimension	Radius $= R_0$	Width $= L_0$, length $= L_{strip} \gg L_0$
Region parameter	$\gamma = \left(\frac{3R_0^2\Delta}{4}\right)^{1/3}$	$\varpi = 2\left(\frac{\sqrt{2}L_0\Delta}{\pi}\right)^{1/2}$
Space–charge parameter	$\Gamma = \left(\frac{R_0^2\Delta}{4W^2V_{bb}}\right)^{1/3}$	$\Omega = \left(\frac{L_0\Delta}{2\pi W V_{bb}}\right)^{1/2}$
Saddle-point position	$(\rho = 0, z = \Gamma W)$	$(x = 0, y, z = \Omega W)$
Effective area, A_{eff}	$\frac{4}{3}\pi\lambda_D^2\Gamma$	$\sqrt{\pi\Omega}\lambda_D L_{strip}$
Effective SBH, Φ_{eff}	$\Phi_{B,n}^{00} - 3e\Gamma V_{bb}$	$\Phi_{B,n}^{00} - e4\Omega V_{bb}$
Ideality factor, n	$\approx 1 + \Gamma$	$\approx 1 + \Omega$

2. Non-interacting Schottky-barrier height models

Theoretical models on the formation of the SBH can be roughly divided into two groups, based on whether the metal and the semiconductor are assumed to interact or not. The two major items discussed in this section, the Schottky–Mott model and various models based on the fixed-separation view of interface states, comprise the group of non-interacting SBH models. A common characteristic of these models is the absence of charge rearrangement at MS interfaces. Therefore, these models deal with the mechanics of SBH formation and ignore the thermodynamic aspect of interface formation. In other words, the continuity of the electrostatic potential can be explicitly shown to be satisfied in these models, but there is no attempt to minimize the interface energy. Interacting SBH models, which extend from the simple rules which govern the non-interacting models and attempt to estimate the interface dipole due to charge rearrangement, will be discussed in Section 4.

2.1. The Schottky–Mott relationship

The famous Schottky–Mott relationship, Eq. (1.1.1), can be viewed as a zeroth-order theory on the formation of the SBH. Even though the barrier now bears his name, the theory that Schottky advanced has not demonstrated much relevance for real Schottky barriers. Schottky's main contribution, instead, lies in correctly predicting the electric potential and field distribution in the space–charge region. A common perception of the Schottky–Mott relationship is that this rule predicts the barrier height in the absence of interface states. Perhaps the best way to see the rationale behind this perception is to derive the Schottky–Mott condition in a "Gedanken" experiment, as illustrated in Fig. 9. In this exercise, large flat surfaces of metal and semiconductor are assumed to be placed parallel to each other and with a small gap δ_{gap} separating them. An electrical connection is made externally, thus, equating the Fermi-level of the two crystals ($V_{\text{a}} = 0$). For a uniformly doped, non-degenerate semiconductor, the total charge per unit area arising from charges in the depletion region is still given by Eq. (1.4.12). If the semiconductor has no surface states, as assumed, the

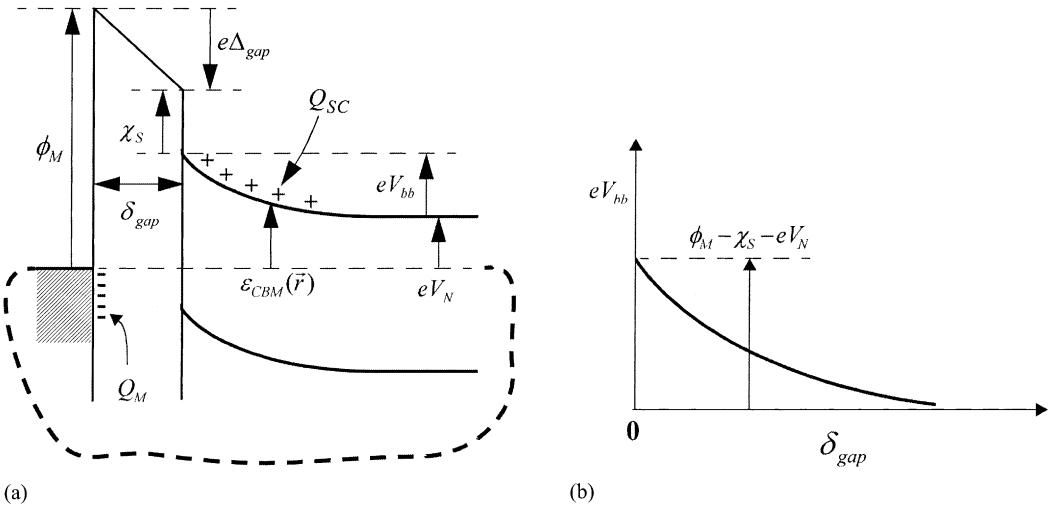

Fig. 9. (a) Band diagram of a semiconductor without surface states, held at a small distance, δ_{gap}, from a metal. An external connection has been made, so the Fermi-levels of the two crystals are unified. (b) The dependence of the semiconductor surface band bending as a function of δ_{gap}. The Schottky–Mott relationship is obtained at zero gap distance.

space–charge, Q_{SC}, is the only source of charge on the semiconductor surface. The charge on the semiconductor is balanced by a charge of equal magnitude, but of opposite sign, on the surface of the metal. These charges lead to a constant electric field in the gap between the semiconductor and the metal, much like that in a parallel plate capacitor, and a total potential drop of

$$\Delta_{gap} = -\frac{\delta_{gap} Q_{SC}}{\varepsilon_0}. \tag{2.1.1}$$

The sense of the potential drop has been chosen to be the same as that of the interface dipole, namely, the larger the potential drop, the larger the band bending of the n-type semiconductor. Since the electric potential is continuous everywhere, the electric field in the gap is also required to be. According to Fig. 9:

$$e\Delta_{gap} = \chi_S + eV_{bb} + eV_N - \phi_M. \tag{2.1.2}$$

Combining Eqs. (2.1.1) and (2.1.2) allows the total band bending to be determined as a function of the gap width

$$eV_{bb} = \phi_M - \chi_S - eV_N + \frac{e^2\varepsilon_S\delta_{gap}^2 N_D}{\varepsilon_0^2} - \left[\frac{e^2\varepsilon_S\delta_{gap}^2 N_D}{\varepsilon_0^2}\left(\frac{e^2\varepsilon_S\delta_{gap}^2 N_D}{\varepsilon_0^2} + 2\phi_M - 2\chi_S - 2eV_N\right)\right]^{1/2}, \tag{2.1.3}$$

as plotted in Fig. 9(b). As expected, Eq. (2.1.3) gives zero band bending when the separation is large ($\delta_{gap} \to \infty$). And when the gap collapses ($\delta_{gap} \to 0$), one gets

$$eV_{bb} = \delta_M - \chi_S - eV_N \quad \text{for } \delta_{gap} \to 0, \tag{2.1.4}$$

which is equivalent to the Schottky–Mott condition

$$\Phi_{B,n}^0 = \phi_M - \chi_S \quad \text{for } \delta_{gap} \to 0. \tag{2.1.5}$$

So, the Schottky–Mott relationship can be viewed as the asymptotic result of the band line-up when a semiconductor without surface states approaches a metal. There is thus some perceived connection between the Schottky–Mott relationship and the absence of surface states. This perception, even though expressed profusely in the literature, is incorrect.

Some may be quick to point out that the Schottky–Mott relationship is also trivially obtained if the vacuum level outside the metal is lined up with the vacuum level outside the semiconductor. What this entails is for the electric field to vanish in the gap between the metal and semiconductor, which can be accomplished by applying an external bias of $\phi_M - \chi_S - eV_{bb} - eV_N$ to the semiconductor, as illustrated in Fig. 10. With such a bias applied, the semiconductor band bending will be independent of the width of gap, δ_{gap}, and the semiconductor can approach the metal with its CBM already positioned at $\phi_M - \chi_S$ above the E_F of the metal. Again, the Schottky–Mott relationship can be inferred as the asymptotic result when $\delta_{gap} \to 0$. Note that this approach works independent of the density of surface states on the semiconductor. Actually, the Schottky–Mott relationship is simply related to the absence of a gap between the metal and the semiconductor. This somewhat disturbing result is of course just an artifact of the analysis model that has been used. The analysis model assumes that the interface dipole is made up of transferred charge between the metal and some pre-existing states on the semiconductor surface. So when the gap vanishes, there can be

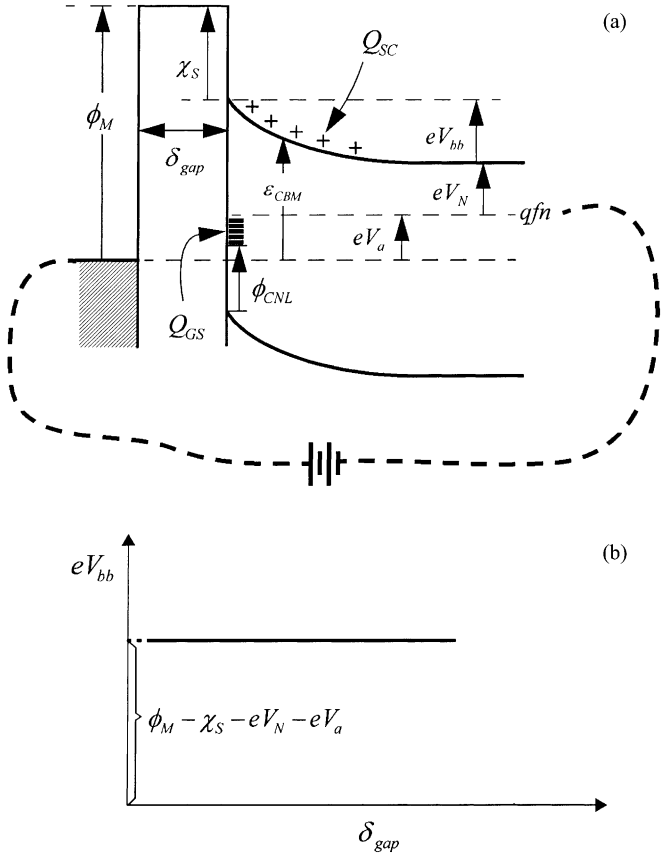

Fig. 10. (a) Band diagram of a semiconductor with surface states, held at a small distance, δ_{gap}, away from a metal. An external bias has been applied, so that the net charge on the metal surface vanishes. (b) The dependence of the semiconductor surface band bending as a function of δ_{gap}.

no interface dipole! In reality, when the semiconductor does come into contact with the metal, chemical bonds will form, new states will be created, charge will flow, and it really does not matter how the two materials were brought together in the first place, nor whether or not the semiconductor had surface states before.

Within the concept of the ISR (Section 1.3), it is plain to see what the Schottky–Mott relationship really implies about the charge distribution at such a MS interface. With the help of Eqs. (1.2.15) and (1.2.20), one writes

$$\phi_{\mathrm{M}} - \chi_{\mathrm{S}} = eD_{\mathrm{M}}^{(hkl)} - \mu'_{\mathrm{M}} + eD_{\mathrm{S}}^{(hkl)} + \hat{\varepsilon}_{\mathrm{CBM}}. \tag{2.1.6}$$

A comparison of Eq. (1.3.6a) with Eq. (2.1.6) shows that the Schottky–Mott relationship is equivalent to

$$D_{\mathrm{ISR}} = D_{\mathrm{M}}^{(hkl)} - D_{\mathrm{S}}^{(hkl)} \quad (\text{Schottky}-\text{Mott}) \tag{2.1.7}$$

Therefore, when the Schottky–Mott condition holds, the interface dipole is the difference between the surface dipole of the metal and that of the semiconductor. This condition is trivially satisfied if the charge distributions on the two original, isolated surfaces are maintained, or frozen-in, at the

eventual MS interface. In other words, the Schottky–Mott relationship results from an absence of charge rearrangement or interaction. Since significant charge redistribution at a MS interface usually occurs when new bonds are formed and/or when old bonds are broken, the Schottky–Mott relationship is not expected to give accurate predictions of the SBH at common MS interfaces where interface bonding is unavoidable.

2.2. Fermi-level pinning at semiconductor surfaces

When the periodic structure of a crystal lattice is terminated at a surface, electronic states particular to the surface are created. These are states that have no equivalent in the band structure of the bulk crystal. Surface-specific states can be true surface states with wave functions which are peaked near the surface plane and which decay in amplitude away from the surface, both toward vacuum and toward the bulk crystal. Surface-specific states can also be surface resonant states that have enhanced amplitudes at the surface, but are coupled to bulk states. Of course, the distribution of surface-specific states depends on the atomic structure of the surface, and conversely, the atomic structure of the surface is determined more or less as a result of the minimization of the surface energy, to which the surface-specific states are a major contribution. Surface-specific states are present at the surfaces of all matters. On metallic surfaces, they are known to lead to a surface dipole which contributes to the work function of the metal surface. On semiconductors, the presence of surface states in the band gap is known to ''pin'' the Fermi-level position of the semiconductor. Pinning does not happen on every semiconductor surface, however, because surface states are not positioned inside the band gap of some semiconductor surfaces, such as the non-polar (1 1 0) surfaces of some III–V semiconductors. So, on some cleaved non-polar surfaces, there is little band bending.

Central to the concept of Fermi-level pinning by gap states is the charge neutrality level (CNL) concept, which can be roughly defined as follows. At zero temperature, the surface states are populated from the lowest energy states up to the Fermi-level. If electrons are filled to a point short of the CNL, i.e. when the Fermi-level is lower than the CNL, the very surface region, meaning the first few atomic planes of the surface, has a positive net charge. If the Fermi-level is above the CNL, the surface has an excess of electrons and is negatively charged. Since the Fermi-level is a constant throughout all regions of a semiconductor, the CNL allows a unique correspondence to be made between the band bending at the semiconductor surface and the population of surface states. To calculate the exact pinning position of the surface Fermi-level, one can assume the density of surface states, D_{GS}, to be roughly constant near the CNL, i.e. $\partial D_{GS}/\partial E \approx 0$. As schematically shown in Fig. 11, the net charge per unit area of the surface is simply

$$Q_{GS} = eD_{GS}(\Phi^0_{B,n} + \phi_{CNL} - E_g), \tag{2.2.1}$$

where ϕ_{CNL} is the CNL position with respect to the valence band maximum, and $\Phi^0_{B,n}$ is the difference between the FL and the CBM at the surface. Note that D_{GS} has the unit of number of states per area per energy ($cm^{-2}\,eV^{-1}$). Here, the subscript ''GS'' (gap states) is used to represent surface states, to be consistent with later notations. As $\Phi^0_{B,n}$ is analogous to the n-type SBH at an MS interface, here it is allowed to retain its usual symbol even though there is no Schottky barrier at a semiconductor surface. One should also note that the definition of the CNL at a surface involves a tacit assumption: the energy levels of surface states are assumed to be referenceable to the bulk bands of the semiconductor. Since the bulk bands are considerably modified near a surface, strictly speaking there is no CBM right on the atomic plane of a semiconductor surface, as shown in Fig. 3.

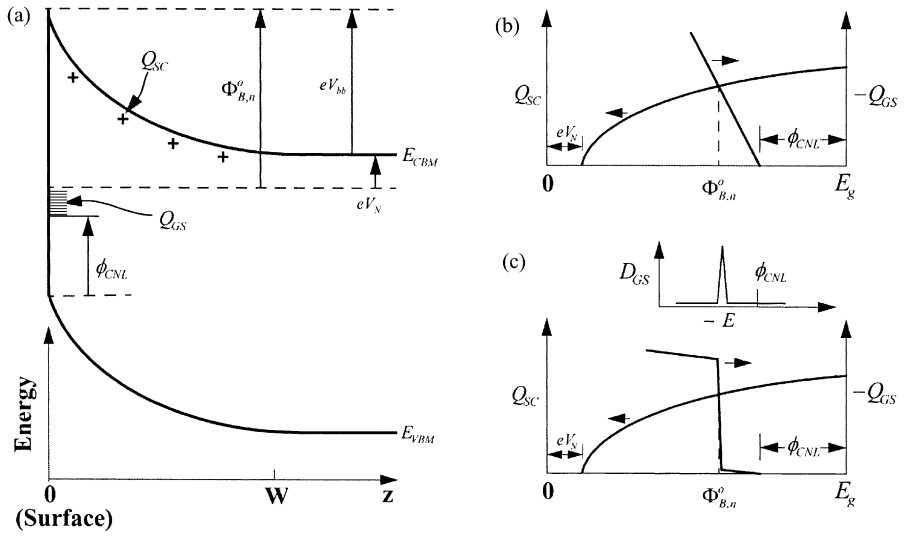

Fig. 11. (a) Band diagram of a semiconductor surface with surface states. (b) The determination of the surface Fermi-level position for a uniform distribution of surface gap states, by graphic method. (c) Same as (b) except that the gap states are assumed to have a peaked distribution as shown in the inset.

The location closest to the surface where bulk semiconductor bands can be identified is a few lattice spacings away and it is the CBM position at that location which provides the reference point. Since the definition of a CNL involves states that are spatially separated, it may be subject to variation due to changes in the relative electric potential (chemical shift). While this definition does not lead to any ambiguities on the determination of the FL position on a semiconductor surface, it can render the concept of CNL fuzzy for MS interfaces.

For an intrinsic semiconductor with homogeneous surfaces, the Fermi-level should coincide with the CNL of the surface states. For uniformly doped semiconductors, the surface Fermi-level position deviates slightly from the CNL to yield the necessary surface net charge which balances the charge due to exposed dopants in the space–charge region (Q_{SC} from Eq. (1.4.12))

$$eD_{GS}(\Phi^0_{B,n} + \phi_{CNL} - E_g) + \sqrt{2\varepsilon_S N_D(\Phi^0_{B,n} - eV_N)} = 0. \tag{2.2.2}$$

Eq. (2.2.2) can be solved to give the surface FL position

$$\Phi^0_{B,n} = E_g - \phi_{CNL} + \frac{\varepsilon_S N_D - \sqrt{\varepsilon_S^2 N_D^2 + 2\varepsilon_S N_D e^2 D_{GS}^2 (E_g - \phi_{CNL} - eV_N)}}{e^2 D_{GS}^2}. \tag{2.2.3}$$

Alternatively, one notes that $\Phi^0_{B,n}$ can be obtained graphically, as shown in Fig. 11(b), by plotting both terms of Eq. (2.2.2) on the same graph. The graphical method is of some value as its results can be more transparent than analytic expressions, especially when the system gets more complex. As shown by Eq. (2.2.2), even a relatively low density of surface states, say $1 \times 10^{13}\ \mathrm{cm}^{-2}\ \mathrm{eV}^{-1}$, can quite effectively fixate the surface Fermi-level to within 0.05 eV of the CNL independent of the doping type or the doping level of a moderately doped ($N_D < 1 \times 10^{17}\ \mathrm{cm}^{-3}$) semiconductor. The surface states are said to pin the Fermi-level near the CNL under these conditions. Often, the density of surface states is thought to have peaks at certain energetic positions, such as due to states

associated with defects or dangling bonds. With a non-uniform density of surface states, the net charge due to surface states, the first term of Eq. (2.2.2), is replaced by an integral

$$Q_{GS} = -e\int_{\Phi^0_{B,n}}^{E_g-\phi_{CNL}} D_{GS}(E)\,dE. \tag{2.2.1a}$$

For a distribution of gap states with discrete peak(s), as schematically illustrated in Fig. 11(c), the surface Fermi-level can be pinned tightly at the position of the peak. A review of Fig. 11 makes it clear that only those gap states with energy above the CNL, i.e. acceptors, affect the surface Fermi-level position on an uncharged, n-type semiconductor; and only gap states with energy below the CNL (donors) can affect the Fermi-level position on a p-type semiconductor surface.

Perhaps because the net surface charge is the only relevant parameter for the determination of surface Fermi-level, the surface pinning concept is clear and straightforward. An important consequence of the surface states is the formation of the surface dipole, cf. Eq. (1.2.18), and, accordingly, its influence on the electron affinity of the semiconductor, Eq. (1.2.20). The magnitude of a surface dipole has to do with the entire spatial distribution of charge. It is not difficult to imagine that patches of the surface that have the same net charge-density, or even the same density of surface states distribution, can turn out to have different surface dipoles. In writing down Eq. (2.2.2), one has obviously assumed the absence of external electric field. Only when the surface dipole is uniform across the entire surface is it possible for the external electric field to vanish everywhere. When the surface dipole of the semiconductor is inhomogeneous, Eq. (2.2.2) has to be modified to account for the non-zero, local electric field:

$$-e\int_{\Phi^0_{B,n}}^{E_g-\phi_{CNL}} D_{GS}(E)\,dE + \sqrt{2\varepsilon_S N_D(\Phi^0_{B,n} - eV_N)} = -\varepsilon_0 \vec{n}\cdot\nabla V(\vec{r})\big|_{just\_out}, \tag{2.2.4}$$

where $\vec{n}$ is a unit vector normal to the surface. In Eq. (2.2.4), parameters such as D_{GS}, $\Phi^0_{B,n}$, χ_S and eD_S (see Eq. (1.2.18)) are understood to vary laterally. When the total charge of semiconductor is zero, the application of the Gauss Theorem leads to

$$\oint_{just\_out} \nabla V(\vec{r})\,dS = 0. \tag{2.2.5}$$

One may wonder how the local external electric field is related to the magnitude of the local surface dipole. For example, a larger than average $V(\vec{r})_{just\_out}$ usually implies a positive local electric field, and a smaller than average potential should lead to a locally negative electric field. But this is only an expected average behavior. The electric field at any particular point of the surface is influenced by the distribution of the charge, dipole and band bending of the entire semiconductor surface. So, there is no simple rule that relates the local surface dipole to the local electric field. One may consider the example shown in Fig. 12 of the surface potential distribution on a sphere. The surface of the upper half of the sphere has assumed a potential of $+1$ V, with the exception of a small patch that has $V = 0$. The lower hemisphere has a potential of -1 V, with the exception of a small patch that has $V = 0$. The average potential of the sphere is zero, but the two small patches, even both with zero potential, would have different local electric fields. The small patch on the upper hemisphere has a positive electric field and a negative net charge, while the patch on the lower hemisphere has a negative electric field and a positive net charge. These can be viewed as results of potential pinch-off in vacuum!

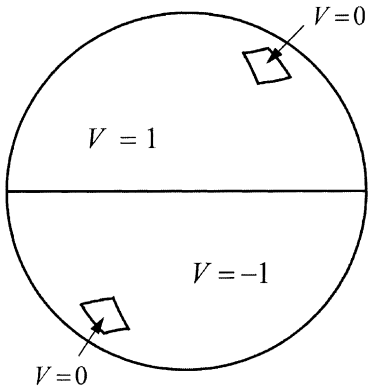

Fig. 12. An example of surface potential distribution on a sphere. The upper hemisphere has a positive surface potential, while the lower hemisphere has a negative surface potential. Small patches with zero surface potential are located on both hemispheres.

2.3. Surface states at MS interfaces: fixed-separation model

The concept of Fermi-level pinning by gap states at the free surface of semiconductors is a physically sound concept, because the surface charge, baring any external electric field, essentially determines the surface band bending. The SBH at a MS interface, on the other hand, is linked to the interface dipole, cf. Eq. (1.3.6a), and not the interface charge. In other words, the density of states at the metal Fermi-level is so high that a variation of the interface net charge brings negligible change to the Fermi-level position. So, it does not appear a priori that the CNL concept of surface states is of any importance at MS interfaces. Nevertheless, the CNL concept has often been used to explain the experimentally observed weak dependence of the SBH on the metal work function. Here, we examine the most popular model assumed to analyze the effect of surface/interface states on the electrostatics at a SB. From the discussion in Section 2.1, it is clear that in order to have an effect on the magnitude of the SBH, interface states need to be spatially separated from the immediate MS interface. Without a physical separation ($\delta_{\text{gap}} = 0$), there can be no additional interface dipole to steer the SBH away from the Schottky–Mott condition. So, SBH theories based on surface states invariably assume the presence of an interface dielectric layer, which separates the semiconductor and the metal. Vacuum technologies and surface preparation techniques were not very sophisticated in the early days of Schottky barrier studies, prompting wide, early speculations on the frequent presence of an oxide or dielectric layer on the semiconductor surface before a metal layer had a chance to be deposited. This argument provided some pretext to the inclusion of an interface dielectric layer in the analysis of SBH. To make the analysis simple, the assumption was usually made that the original surface states were still present at the dielectric–semiconductor interface. In other words, the interface dielectric layer was thought not to modify the characteristics of the semiconductor gap states. Instead, the interface dielectric layer plays only two passive roles: that of providing a separation between the charges due to surface states and those on the metal, and that of providing some dielectric screening of the electric field at the interface.

The energy bands at a MS interface with surface (or interface) states have often been analyzed with a diagram like Fig. 13(a). In such an analysis, the surface/interface states are assumed to be a property of only the semiconductor, so any influence the metal has on the SBH can only be exerted through a change in the metal work function. The metal and the semiconductor are assumed to be

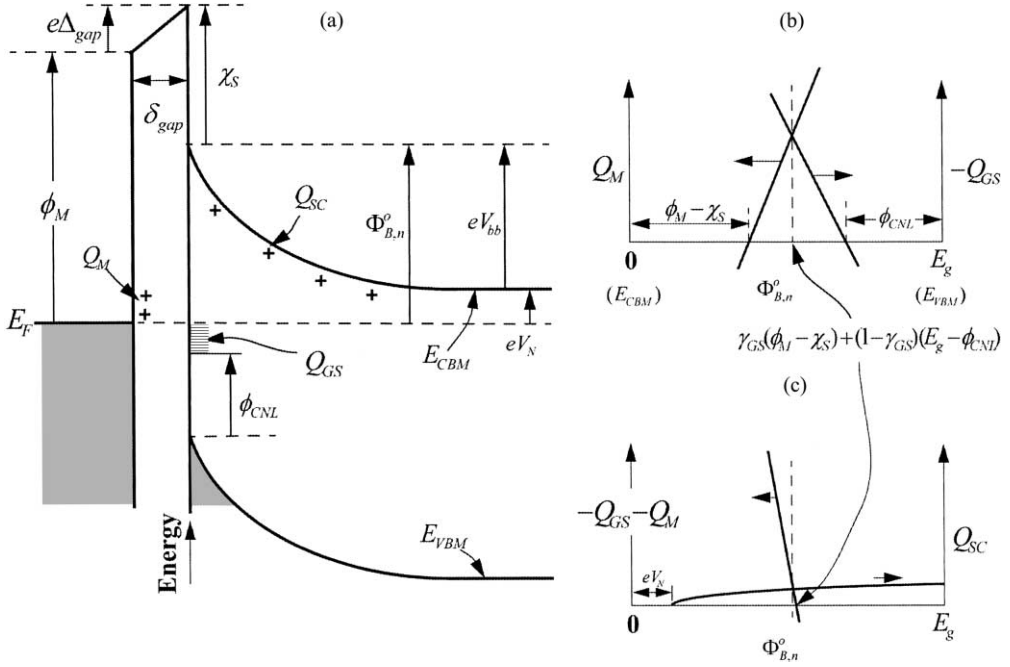

Fig. 13. The fixed separation model for a semiconductor surface with a uniformly distributed surface states and an interfacial dielectric layer: (a) band diagram; (b) graphic method to determine the SBH, neglecting the space–charge; (c) graphic method to determine the SBH with the space–charge considered, using result from (b).

separated by an interfacial dielectric layer with a thickness of δ_{gap} and a permittivity of $\varepsilon_{\mathrm{int}}$. The charges on the semiconductor side, Q_{SC} and Q_{GS}, have the same definitions as before (see Fig. 11), and are exactly balanced by the charge on the metal

$$Q_{\mathrm{SC}} + Q_{\mathrm{GS}} + Q_{\mathrm{M}} = 0. \tag{2.3.1}$$

At the same time, Q_{M} is related to the electric field in the dielectric layer through

$$Q_{\mathrm{M}} = \frac{\varepsilon_{\mathrm{int}} \Delta_{\mathrm{gap}}}{\delta_{\mathrm{gap}}} = \frac{\varepsilon_{\mathrm{int}}(\Phi^0_{\mathrm{B,n}} - \delta_{\mathrm{M}} + \chi_{\mathrm{S}})}{e\delta_{\mathrm{gap}}}. \tag{2.3.2}$$

Here, the quantity Δ_{gap} is some kind of a potential drop across the dielectric layer. Note that it is referenced to the Schottky–Mott condition

$$e\Delta_{\mathrm{gap}} = \Phi^0_{\mathrm{B,n}} - \phi_{\mathrm{M}} + \chi_{\mathrm{S}}, \tag{2.3.2a}$$

and can be considered as the difference in the vacuum levels immediately outside the metal and the semiconductor. Because Δ_{gap} represents a correction to the Schottky–Mott relationship, it is known as the ''Schottky dipole'' and should not be confused with the interface dipole defined earlier. Plugging Eqs. (1.4.12), (2.2.1) and (2.3.2) into Eq. (2.3.1), one gets

$$\frac{\varepsilon_{\mathrm{int}}(\Phi^0_{\mathrm{B,n}} - \phi_{\mathrm{M}} + \chi_{\mathrm{S}})}{e\delta_{\mathrm{gap}}} + eD_{\mathrm{GS}}(\Phi^0_{\mathrm{B,n}} + \phi_{\mathrm{CNL}} - E_{\mathrm{g}}) + \sqrt{2\varepsilon_{\mathrm{S}} N_{\mathrm{D}}(\Phi^0_{\mathrm{B,n}} - eV_{\mathrm{N}})} = 0. \tag{2.3.3}$$

Eq. (2.3.3) can be solved into closed forms [26]. However, much more insight can be gained through analysis by the graphic method. Rearranging the first two terms of Eq. (2.3.3), one gets

$$\frac{-\varepsilon_{\text{int}}}{e\delta_{\text{gap}}\gamma_{\text{GS}}}[\Phi^0_{\text{B,n}} - \gamma_{\text{GS}}(\phi_{\text{M}} - \chi_{\text{S}}) - (1-\gamma_{\text{GS}})(E_{\text{g}} - \phi_{\text{CNL}})] = \sqrt{2\varepsilon_{\text{S}}N_{\text{D}}(\Phi^0_{\text{B,n}} - eV_{\text{N}})}, \tag{2.3.4}$$

where γ_{GS} is a constant given by

$$\gamma_{\text{GS}} = \left(1 + \frac{e^2\delta_{\text{gap}}D_{\text{GS}}}{\varepsilon_{\text{int}}}\right)^{-1}. \tag{2.3.5}$$

The two sides of Eq. (2.3.4) can be used to solve for $\Phi^0_{\text{B,n}}$ by graphic method, as illustrated in Fig. 13(c). Since Q_{SC}, the right hand side of Eq. (2.3.4), is usually small compared to Q_{M} and Q_{GS}, it can be ignored here to arrive at the familiar expression

$$\Phi^0_{\text{B,n}} = \gamma_{\text{GS}}(\phi_{\text{M}} - \chi_{\text{S}}) + (1-\gamma_{\text{GS}})(E_{\text{g}} - \phi_{\text{CNL}}). \tag{2.3.6}$$

Eq. (2.3.6) itself can be obtained graphically as shown in Fig. 13(b). As Eq. (2.3.6) suggests, the dependence of SBH on ϕ_{M} is weakened, by a factor of γ_{GS}, from that predicted by Eq. (1.1.1). The γ_{GS} can be identified as the interface behavior parameter S_Φ defined in Eq. (1.1.2). In this paper, γ will be used to indicate theoretical predictions, while S-parameters are used to indicate experimental observations. For a high density of surface states ($\gamma_{\text{GS}} \ll 1$), the second term on the right hand side of Eq. (2.3.6) dominates, and the n-type SBH values will be pinned close to $E_{\text{g}} - \phi_{\text{CNL}}$.

Although Eq. (2.3.6) offers an explanation of the Fermi-level pinning effect, the many assumptions of the fixed-separation model should be noted. The presence of a dielectric layer is an essential part of this model. Without the dielectric layer ($\delta_{\text{gap}} = 0$), there can be no dipole, and the Schottky–Mott relationship is recovered, independent of the gap state density. Without the dielectric layer, it is also hard to rationalize why the distribution of the gap states does not depend on the metal. So, the fixed-separation model is not appropriate for intimate MS interfaces. Even when a dielectric layer is known to be present, the overall dipole through the entire metal–insulator–semiconductor (MIS) structure is not really given by $Q_{\text{M}}\delta_{\text{gap}}/\varepsilon_{\text{int}}$, as assumed in the fixed-separation model (the band bending in the dielectric layer in Fig. 14). There are two more microscopic interface dipoles, one at the metal–dielectric interface and the other at the semiconductor–dielectric interface, which have been left out of the present analysis, as shown in Fig. 14. Their absence reveals another tacit assumption of the fixed-separation model, which is that the Schottky–Mott relationship and the Anderson rule [27] are operative at the metal–dielectric and the dielectric–semiconductor interfaces, respectively. Whereas one already has a strong argument against the validity of Anderson rule at the dielectric–semiconductor interface (i.e. because surface states are present), one is certainly right in arguing that the Schottky–Mott relationship cannot hold for all metal–dielectric interfaces. After all, metal–dielectric interfaces are also known to be plagued by, oh yes, the Fermi-level pinning phenomenon. So, the validity of the fixed-separation model, with which one hopes to explain the Fermi-level pinning phenomenon, actually relies on the assumption that the Fermi-level is unpinned at both of its component interfaces! Because of these internal inconsistencies, the fixed-separation model is not expected to bear much relevance to any real Schottky barrier, regardless of whether a dielectric layer is actually present at its interface.

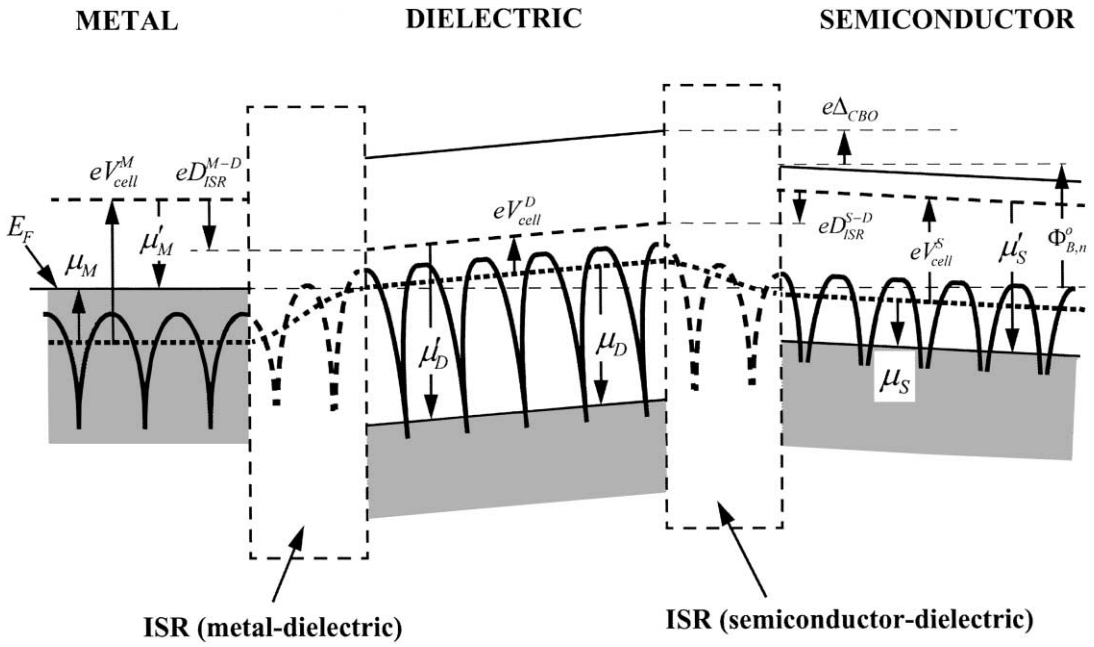

Fig. 14. Band diagram of a metal–semiconductor interface with a thin interfacial dielectric layer. A net positive charge is drawn for the ISR between the metal and the dielectric, while a negative net charge is drawn for the ISR between the dielectric and the semiconductor. The electrostatic potential is continuous throughout the entire MIS structure.

2.4. Defects and deep-levels: fixed-separation model

The phenomenon of Fermi-level pinning naturally led to the idea that the Fermi-level at the MS interface is predominantly a property of the semiconductor. A possible explanation of such a result is pinning by defects in the semiconductor [28,29]. Some structural defects in bulk semiconductors are known to have electric activities deep in the band gap of the semiconductor. Common deep traps in semiconductors have energy levels and capture cross sections that have been well characterized by deep-level transient spectroscopy (DLTS) and photoluminescence (PL) techniques. If a high density of electrically active defects is present anywhere in the semiconductor, the local FL can be pinned at close to the energetic position of the defects. Thus to explain the FL-pinning effect at an MS interface, it seems that one only need to invoke the presence of a high density of defects close to the MS interface. As before, deep-levels (gap states) cannot be assumed to be too close to the metal to still have a significant effect on the magnitude of the SBH. So, defects are usually assumed to be positioned at a fixed distance, δ_{gap}, away from the MS interface, as shown in Fig. 15. A comparison of Figs. 13 and 15 shows that the analysis model used to calculate the expected influence of defect states is very similar to that used for surface states. One difference is that the material separating the defects from the metal is the semiconductor itself, rather than a different, dielectric material. So, the dielectric screening in this region is still characteristic of the bulk semiconductor. Another difference is that the distribution of the deep-levels is assumed to be peaked at specific energetic positions in the present model (not so drawn in Fig. 15) than a uniform distribution in the case of surface states. This change means that the net charge residing on the deep-levels is no longer expressible in a simple formula, but, rather, is given by the integral of Eq. (2.2.1a). Neglecting the space–charge of the semiconductor, one uses

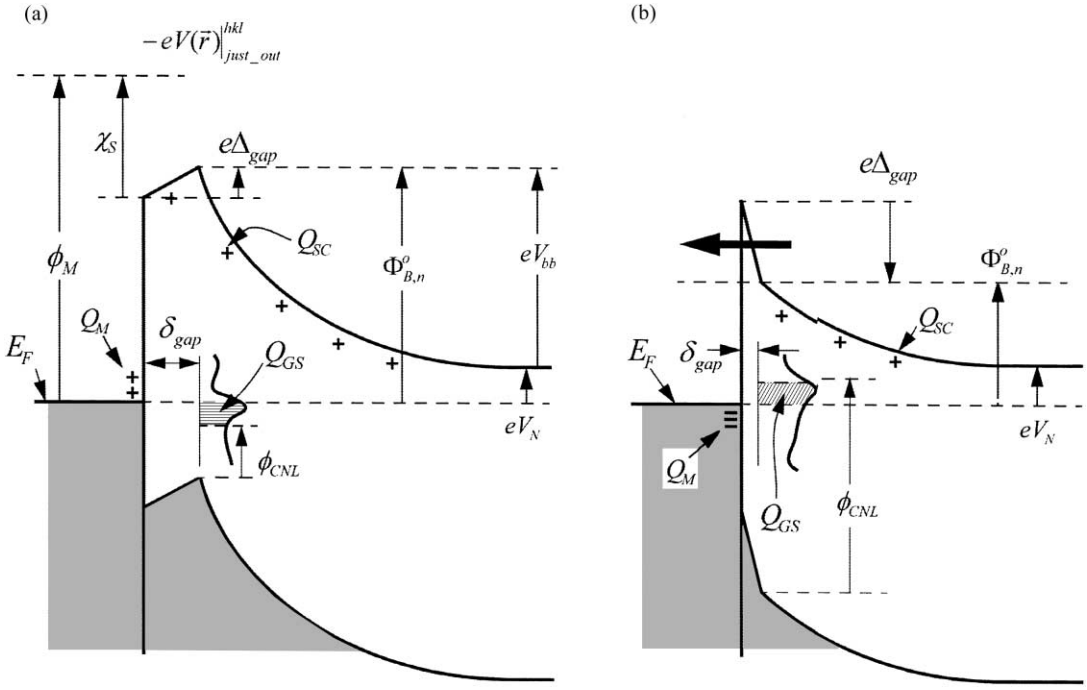

Fig. 15. Band diagrams at intimate metal–n-semiconductor interfaces, according to the fixed-separation model of interface gap states. Gap states are assumed to be positioned at a fixed distance away from the atomic MS interface. The two drawings are for (a) negatively charged gap states, and (b) positively charged gap states. In (b), the thin barrier between the metal and the gap states is assumed to be transparent to electrons by tunneling, and therefore, has no effect on the electrical transport properties of the Schottky barrier. This model is frequently used to analyze effects due to metal induced gap states or defect states.

a balance of charge, Eq. (2.3.1), to get

$$e\int_{\Phi^0_{B,n}}^{E_g-\phi_{CNL}} D_{GS}(E)\,dE = \frac{\varepsilon_S(\Phi^0_{B,n} - \phi_M + \chi_S)}{\phi_{gap}}. \tag{2.4.1}$$

When the distribution of defect states is known, or assumed, Eq. (2.4.1) can be used to determine, by graphical method, the dependence of the SBH on the metal work function, as illustrated in Fig. 16. A large density of deep acceptors, i.e. positioned at lower energy than the CNL, a smaller density of deep and discrete donors, and a uniform distribution of gap states are assumed to be present at the interface, as shown in Fig. 16(a). The expected dependence of the SBH on the work function of the metal is shown in Fig. 16(c). Generally speaking, plateau-like behavior is expected at SBH with energy corresponding to the energetic position of the discrete deep-levels. And the width of the plateau is proportional to the density of the discrete (defect) level. At the position of the continuum distribution of gap states, there is a change in the slope of the curve, as already discussed above and shown in Eq. (2.3.6). Schottky–Mott like behavior, i.e. with a slope of 1, is expected at energy ranges between regions of gap states. The expected dependencies of the SBH on the metal work function in the presence of defects, as shown in Fig. 16(c), have been used to analyze defect density in many studies. It is apparent that the model assumes that the Schottky–Mott relationship is obeyed at the intimate MS interface, in the absence of defects. Models which include the effects due to defects and other sources of interface states, such as MIGS, have also been utilized to analyze experimental data [30].

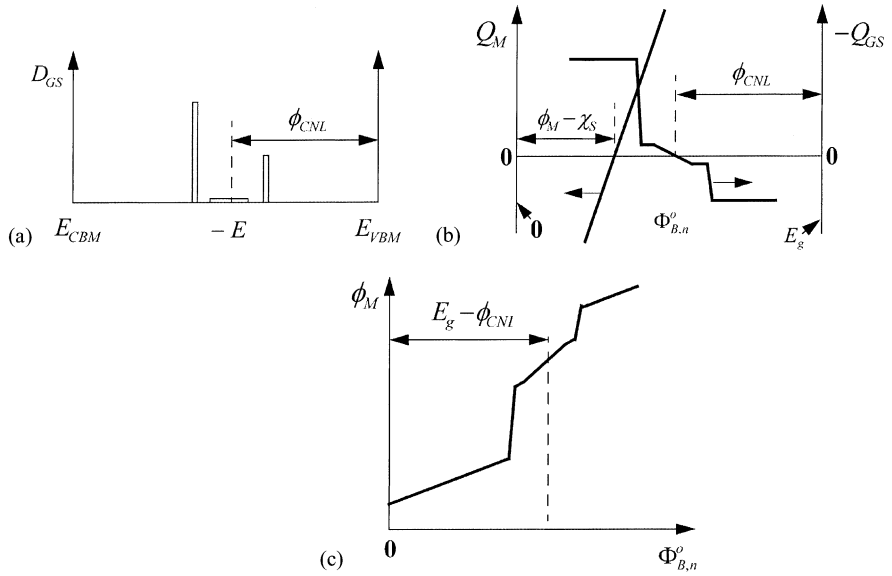

Fig. 16. An example of the influence of discrete levels of interface gap states on the SBH: (a) density of gap states; (b) graphic method, neglecting space–charge; (c) the dependence of the SBH on the metal work function.

2.5. Surface states and defects: variable–electron-affinity model

Even though the fixed-separation model has been the model most frequently used to evaluate the effects due to surface states, deep-levels, and MIGS, another analysis model of the gap states has also found its way into the literature [31]. This model, here referred to as the variable–electron-affinity model, is very different from the fixed-separation model and is illustrated in Fig. 17 under different bias conditions. There are two basic assumptions in this model: the population of the interface states is controlled by the Fermi-level of the metal; and that there is no net charge on the metal, i.e. $Q_{\mathrm{M}} = 0$ in Eqs. (2.3.1) and (2.3.2). Because the charge on the metal is zero, the voltage drop across the interface dielectric layer is also zero, which means that the band diagram is independent of the width of the gap, δ_{gap}. Therefore, it has been customary to draw the band diagram without an interface gap, as in Fig. 17. The charge stored in the interface gap states exactly

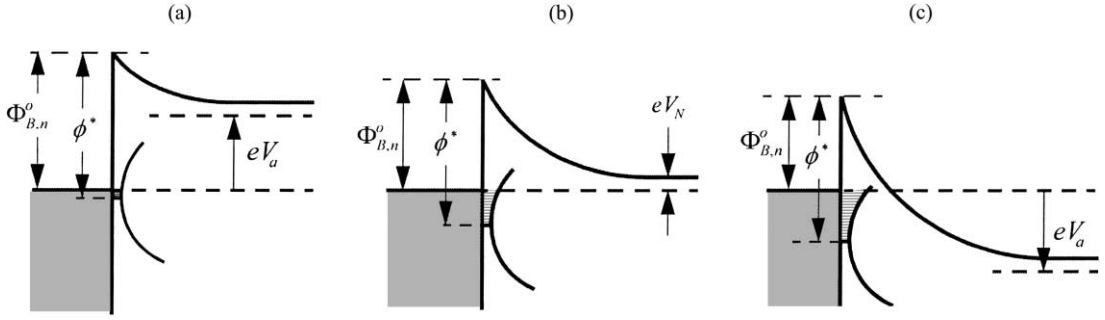

Fig. 17. Schematic relationship between SBH and change in the interface gap states for (a) forward-bias, (b) zero-bias, and (c) reverse-bias conditions, according to the variable–electron-affinity model [31]. Note that the charge neutrality level, ϕ^*, is referenced to the conduction band edge in these drawings.

balances the space–charge of the semiconductor, similar to Fermi-level pinning on a semiconductor surface. Eq. (2.2.2) holds under the present assumption. It is slightly modified to accommodate an applied bias

$$eD_{GS}(\Phi^0_{B,n} + \phi_{CNL} - E_g) + \sqrt{2\varepsilon_S N_D(\Phi^0_{B,n} - eV_N - eV_a)} = 0. \tag{2.5.1}$$

The solution is obviously similar to Eq. (2.2.3), but with V_N replaced by $V_N + V_a$, namely

$$\Phi^0_{B,n} = E_g - \phi_{CNL} + \frac{\varepsilon_S N_D - \sqrt{\varepsilon_S^2 N_D^2 + 2\varepsilon_S N_D e^2 D_{GS}^2 (E_g - \phi_{CNL} - eV_N - eV_a)}}{e^2 D_{GS}^2} \tag{2.5.2}$$

The bias dependence predicted by Eq. (2.5.2) has been used to explain the T_a anomaly [31].The variable–electron-affinity model is severely flawed, as it leads to a contradiction that one can immediately point out. The requirement that the electric potential remains continuous throughout the MS interface leads to the condition that the Schottky–Mott relationship must be followed in this model, because $Q_M = 0$ in Eq. (2.3.2). The only way for the Schottky–Mott relationship and Eq. (2.5.2) to simultaneously hold is for the semiconductor electron affinity to somehow vary with the bias, so that the semiconductor surface Fermi-level position, with respect to the vacuum level, always remains the same. This strange constraint has no basis and is just silly. The SBH is also rendered completely independent of the metal work function, as revealed in Eq. (2.5.2). This model is essentially the result of simply equating the Fermi-level of the semiconductor free surface with the Fermi-level of the metal, with no regards for the electron affinity of the semiconductor and the work function of the metal. The error arises because, in so doing, a discontinuity is created in the electric potential across the MS interface. The variable–electron-affinity model is obviously unphysical. Unfortunately, the basic concept of this model has been invoked in the analysis of interface gap states from electrical measurements [32] and further developed into a more sophisticated model to analyze defects and SBH inhomogeneity [33].

3. Heterojunction band offsets

3.1. The basics

The formation of valence band offset (BO) at semiconductor heterojunctions (HJ) share many similar issues with the formation of the SBH at MS interfaces. Many concepts and ideas on the BO are directly transferable to the SBH problems. It is therefore worthwhile to examine what has been known in the area of BO formation at semiconductor HJ. Using the same concept as discussed previously for the SBH, one can define an ISR for a semiconductor HJ, the width of which is presumably only one or two lattice spacings. Again, the electrostatic potential is required to be continuous across the interface, as shown in Fig. 18, which sets an important condition on the formation of the BO. Assuming lateral homogeneity, the valence band maximum on Semiconductor A side of the interface is

$$E_{VBM}^{S(A)-I} = -eV_{SXD}^{S(A)-I} + \mu'_{S(A)} \tag{3.1.1}$$

where reference has been made to the vacuum level $E_{VAC}^{\infty} = 0$. A similar equation can be written for semiconductor B. The valence-band BO (VBO), $e\Delta_{VBO}^{A-B}$, is the difference in the VBM levels across a

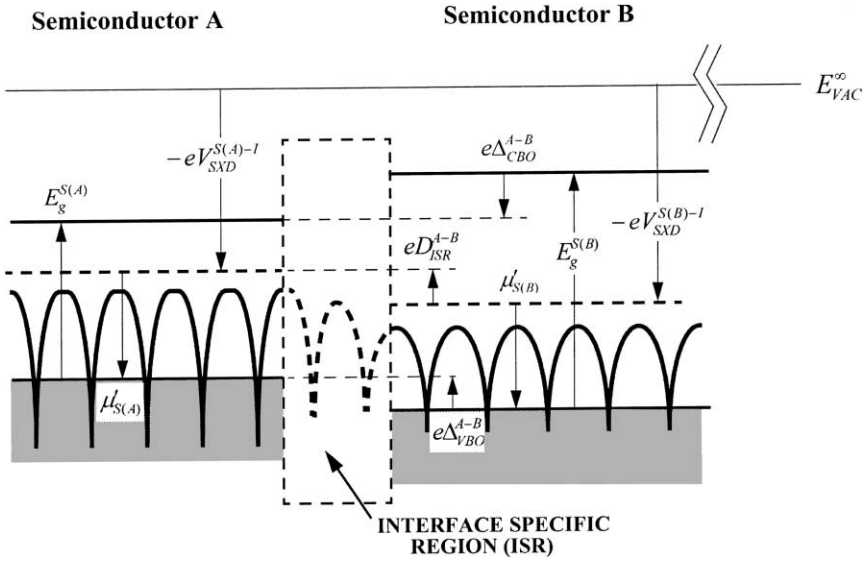

Fig. 18. The distributions of crystal potential, $-eV(\vec{r})$ (solid curve lines) and energy bands (solid straight lines) at a semiconductor heterojunction interface. Dashed lines represent $-eV_{\mathrm{SXD}}(\vec{r})$.

semiconductor HJ interface, and is directly related to the difference in the average crystal potential across the ISR as follows:

$$e\Delta^{\mathrm{A-B}}_{\mathrm{VBO}} = E^{\mathrm{S(A)-I}}_{\mathrm{VBM}} - E^{\mathrm{S(B)-I}}_{\mathrm{VBM}} = \mu'_{\mathrm{S(A)}} - \mu'_{\mathrm{S(B)}} + eD^{\mathrm{A-B}}_{\mathrm{ISR}} \tag{3.1.2}$$

where

$$D^{\mathrm{A-B}}_{\mathrm{ISR}} = V^{\mathrm{S(B)-I}}_{\mathrm{SXD}} - V^{\mathrm{S(A)-I}}_{\mathrm{SXD}}, \tag{3.1.3}$$

as schematically shown in Fig. 18. From Eq. (3.1.2), it is seen that the VBO, just like the SBH, consists of two bulk terms and one interface term. Again, the electronic structure of the ISR affects the BO only through the total net dipole across the ISR, without regard to the energetic positions of the electronic states inside the ISR. Clearly, the BO problem is an interface dipole problem, much like the SBH. But unlike the SBH, the BO problem has never been mistaken for a problem of the interface Fermi-level position. The Fermi-level position at a HJ depends primarily on the doping characteristics, and has little to do with the formation of BO. Another significant difference between the SBH and the BO is that semiconductor HJ interfaces are usually epitaxial and can be made with nearly perfect, known structures, contrasted with the essentially random structures seen at ordinary, polycrystalline MS interfaces. Typically, the bonds across a HJ interface plane are identical in density and strength to that across any other plane in the bulk semiconductor. The known atomic structures of the epitaxial interfaces are also amenable to ab initio calculations. So, at least on paper, the BO of semiconductor HJs should be an easier problem to understand than the SBH. Additionally, advanced epitaxial technologies now offer choices in the amount of strain, the kind of interface bonds, interface roughness, the orientation of the interface, etc. in a HJ interface, so the dependencies of various parameters can in principle be studied independently. Indeed, calculations have been carried out on a number of HJ interfaces, giving valuable information on the stability and the electronic properties associated with detailed structure of the interface. The BO values obtained

from these calculations are often in good agreement with experimental results. But ab initio calculations can provide only numerical solutions and not the physical reason for the formation of the BO. So the BO formation mechanism is still under considerable debate. Readers are strongly encouraged to consult a few excellent and extensive reviews [22,34,35] for detailed discussions on both the experimental and the theoretical aspects of the heterojunction band offset problem. In our discussion, attention will be placed only on concepts and theories that have direct implications on the SBH problem.

Experimentally measured BO has been recognized as largely dependent only on the bulk properties of the two semiconductors. In other words, the BO measured for a pair of semiconductors is usually insensitive to the interface orientation (whether it is the (1 1 0) or the (1 0 0) surface), the roughness of the interface (whether intermixing has taken place), and the interface bonding (e.g. whether a polar GaAs–InP interface has In–As bonds or Ga–P bonds, or, whether a heterovalent Ge–GaAs polar interface has Ge–As or Ge–Ga bonds). Variations in these interface-specifics, such as going from a heterovalent non-polar to a polar orientation or changing the interface bonds of a heterovalent HJ, do have a small effect, of the order of 0.1 eV, on the BO. But the overriding influence is exerted only by the identity of the two semiconductors. So, by and large, a ''transitivity'' rule is observed for any three semiconductors A, B, and C, such that

$$e\Delta_{\mathrm{VBO}}^{\mathrm{A-B}} + e\Delta_{\mathrm{VBO}}^{\mathrm{B-C}} + e\Delta_{\mathrm{VBO}}^{\mathrm{C-A}} = 0. \tag{3.1.4}$$

With these experimental results in mind, it is easy to understand why BO models have all looked for some characteristic reference energy level of the bulk semiconductor to help explain the line-up of bands across the interface when a HJ is formed. On the other hand, various ''interlayers'' were known to significantly change the overall VBO [36] and inhomogeneities were observed in the band offset of some heterovalent HJs [37]. So, these effects also need to be explained by a satisfactory model of the BO.

3.2. Charge-density-based models

Proposed models for the VBO can be roughly separated into two groups according to whether they are based on the charge-density of the bulk crystal, or whether they are based on some energy band feature. A conceptual view of the difference between these two groups of models is shown in Fig. 19. Basically, models based on the charge-density assume some distribution of the charge-density at the surface, which allows the energy band positions of the individual (isolated)

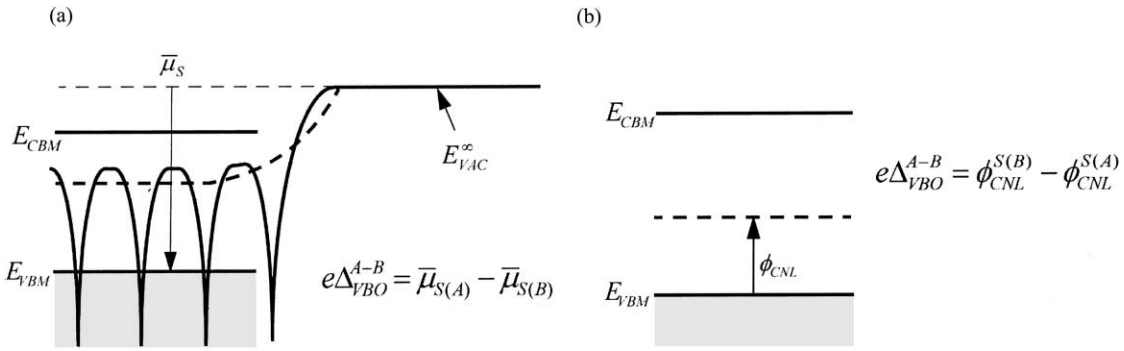

Fig. 19. Schematic illustration of the difference between (a) charge-density-based theories, and (b) CNL-based theories.

semiconductors to be referenced with respect to the vacuum level, as shown in Fig. 19(a). The difference in the band-edge positions of any two semiconductors, referenced to the vacuum level, is then assumed to be the band offset when a HJ is formed between these two semiconductors. The electron affinity rule [27], which is equivalent to the Schottky–Mott relationship for SBH, states that the conduction band offset is simply the difference between the experimentally obtained electron affinities of the two semiconductors. This condition, equivalent to a line-up of the experimental vacuum level, assumes that the charge distribution at the HJ interface remains ''frozen'' at the distribution on the original surfaces. Harrison [38] used a linear combination of atomic orbital (LCAO) method to calculate the band-edges of semiconductors based on the energy levels of the original atomic orbitals. These calculations thus put the band-edges of all the semiconductors on a single energy scale, which led to predictions of the band offsets [39,40]. Frensley and Kroemer [41] argued that the interstitial potential (half-way between cation and anion sites) in bulk electronic structure calculations could be expected to be close to the vacuum level. Therefore, the interstitial potentials should line-up across a HJ interface. Later, the effect due to charge transfer at the interface were included, by simply assuming that the charge transfer between any two neighbor atoms is related to their electronegativity difference [42]. The charge transfer between each pair of atoms is assumed to be one-fourth of the effective charge transfer found in the bulk, because of tetrahedral bonding in the bulk crystal. This approach represents a simple yet elegant way to account for the bond-polarization throughout the interface region. However, it is not expected to be very accurate, because of various simplifications. Van de Walle and Martin [16] and Van de Walle [43] analyzed charge distributions around a variety of semiconductor interfaces calculated using self-consistent ab initio methods and found that these can be reasonably approximated by a superposition of neutral atomic charge densities. They, thus, developed and used the ''model solid'' concept to calculate the bulk-related potential/energy levels of all the semiconductors on a common scale. One advantage of the model solid scheme is the ease with which it can be used to include the effect of strain in the calculations [43]. Absolute deformation potential, which governs the movement of the bands with strain, with respect to the average crystal potential, can be calculated. The strain-dependence of VBO has been shown, as a result of these studies, to be a bulk-related effect. Baldereschi et al. [17] calculated the average potential from a bulk crystal made up of atom-centered Wigner–Seitz cells, similar to the truncated model solid described in Section 1, and used it to explain BO observed at lattice-matched, isovalent HJ interfaces. Listed in Table 2 are the VBM positions of some semiconductors on the common scale proposed in some of these theories.

All the models described above share the common conviction that the vacuum level outside the semiconductor crystals, real or simulated, should line-up. One notes that in the case of the LCAO theory, it is actually the vacuum level outside of the isolated atoms that is assumed to line-up. The common rationale behind these charge-density-based, or electrostatic-potential-based, theories is the validity of the superposition principle of the electric potential. The charge distribution of a HJ is imagined to be dissected at an appropriate location and separated into two neutral ''half-crystals''. The band position of each half-crystal can be referenced to the vacuum level ''just outside''. When put back together, the relative position of the bands remains intact, because of the superposition principle of the electric potential. The accuracy of the models thus relies on the absence of significant charge rearrangement from the assumed charge distribution of the half-crystals. This is usually a good approximation at isovalent interfaces. For heterovalent, polar interfaces where some charge rearrangement seems unavoidable, there are known schemes to include the effect of extra dipole. The interface dipole correction described by Frensley and Kroemer [42] is one such scheme. Another is the interface-bond-polarity model [44], which puts the interface dipole concept in more formal terms. In addition, a ''linear response theory'' [22,45] treats the creation of a HJ interface as a

Table 2
Models of band offset formation at semiconductor heterojunctions[a]

Semi-conductor	Charge density-based theories $\overline{\mu}_S$ (eV)			CNL-based theories ϕ_{CNL} (eV)		
	Frensley and Kroemer	Van de Walle and Martin	Harrison	Tersoff	Cardona and Christensen	Harrison and Tersoff
Si	−3.16	−7.02	−9.35	0.36	0.23	−0.03
Ge	−3.25	−6.25	−8.97	0.18	0.03	−0.32
AlP		−8.09	−10.22	1.27	1.13	0.76
AlAs	−3.96	−7.4	−9.67	1.05	0.92	0.46
AlSb	−3.94	−6.44	−8.76	0.45	0.41	0.23
GaP	−4.12	−7.37	−10.21	0.81	0.73	0.66
GaAs	−3.96	−6.81	−9.64	0.5	0.55	0.34
GaSb	−3.89	−5.98	−8.67	0.07	0.06	0.14
InP	−4.58	−7	−10.03	0.76	0.87	0.77
InAs	−4.38	−6.54	−9.48	0.5	0.62	0.47
InSb		−5.82	−8.61	0.01	0.2	0.28
ZnS	−5.34	−9.13	−12			2.15
ZnSe	−5.07	−8.23	−11.06	1.7	1.44	1.69
ZnTe	−4.74	−6.87	−9.87	0.84	0.73	1.4
CdS	−5.42		−11.89			2.14
CdSe	−5.29		−10.97			1.71
CdTe	−4.9	−6.76	−9.8	0.85	0.83	1.43
HgTe		−6.53		0.34	0.16	

[a] Entries are the electrochemical potentials (negative of the ionization potential) for charge density-based theories, and the charge neutrality level for CNL-based theories. To calculate the predicted valence band offset between two semiconductors, simply take the difference in the entries for the two semiconductors. See Fig. 19 for schematic diagrams. For example, the VBM of GaAs is predicted to be higher than the VBM of InP by 0.62, 0.19, 0.39, 0.26, 0.32, and 0.43 eV, respectively, by the six theories in order. Theories: Frensley and Kroemer [42], Van de Walle and Martin [16], Harrison [479], Tersoff [49], Cardona and Christensen [69], and Harrison and Tersoff [50].

perturbation (involving the transfer of protons), whose effect on the electrostatic potential is simply screened by the dielectric response of the semiconductor, and comes up with BOs which are remarkably close to results obtained from full-fledged calculations. The success of the linear response theory clearly has its roots in the similarity in crystal bonding among most common semiconductors with zinc-blend structures. Such a perturbative, dielectric-responsive, treatment does not appear a priori to be transferable to metal–semiconductor interfaces, across which the bonding and the charge distribution are drastically different. But amazingly, reasonable agreement has been found between the experimental result and the result of such a calculation even for some MS interfaces [22]!

3.3. Energy level based models

3.3.1. The CNL concept

The other group of the BO models is largely based on the CNL concept, which was originally proposed for the MS interfaces [46]. Underlying the CNL concept is the belief that, even though a band gap exists for a bulk semiconductor, movement of the Fermi-level inside the band gap at the interface of a semiconductor still leads to local charging [47]. The net charge resides in some electronic states which are introduced into the gap when an interface is created. At an MS interface, these states are known as metal-induced gap states (MIGS) and are related to the tails of metal wave functions. The distribution of induced gap states, including the CNL of the induced gap states, has been argued to be an intrinsic property of the semiconductor and, thus, is independent of the nature

of the hetero-interface (i.e. they are the same for MS interfaces and HJ interfaces). The CNL of the induced gap states is argued to be similar to the equilibrium FL position of a neutral metal. So, when two semiconductors are joined, a simple line-up of the CNLs from the two sides is proposed. One, thus, imagine putting the band-edge positions of all the semiconductors, with respect to their individual CNLs, on a single chart. The difference in the band-edges of two semiconductors on that chart is then the BO of the HJ formed between these two semiconductors, as shown in Fig. 19(b). Significant charge rearrangement may be required at the interface in this case, as opposed to the frozen-charge condition envisioned in charge-density based models, Fig. 19(a). The first task of the CNL-based approach is to identify the CNL. States induced in the band gap are derived from conduction band states and valence band states of the semiconductor. So, there is a natural tendency for states in the upper half of the band gap to have conduction band character and those in the lower half to behave like valence band states. Tersoff argued that the CNL should be the energy level of the evanescent state with equal conduction and valence band character [48]. In one dimension, this is the branch point of the complex band structure. Arguments were also given as to why this level roughly corresponds to the midgap level of the indirect band gap [49]. Cardonna and Christensen proposed that the midgap state at the Penn gap, called the ''dielectric midgap energy'' (DME), is the intrinsic CNL of the semiconductor. Harrison and Tersoff drew from the tight-binding concept to propose that the average hybrid energy in the semiconductor, i.e. the dangling bond orbital energy, should act as the CNL [50,51]. The relationship of this level to the defect levels of transition metal impurities has also been pointed out [52–54]. Note that even though the same LCAO approach was used, this CNL model of Harrison and Tersoff's represented a significant departure from Harrison's original theory [38]. There is also an empirical rule on the CNL from a compilation of experimental data [55]. The VBMs of common semiconductors, relative to the CNL proposed in these theories, are listed in Table 2.

3.3.2. Band offset analysis: fixed-separation model

Even after the CNLs for two semiconductors have been identified, there is still the issue of how the line-up of the two CNLs actually takes place. Namely, how does the charge redistribute at the interface to create the $eD_{\mathrm{ISR}}^{\mathrm{A-B}}$ (cf. Eq. (3.1.2)) necessary for the line-up condition? One obvious way that this can happen is by assuming the negative charge on one semiconductor to be positioned at a fixed distance, δ_{gap}, away from the positive charge on the other semiconductor, as already illustrated for MS interfaces in Fig. 13. The amount of charge is dictated by the densities of gap states on the two semiconductors. A simple calculation within this fixed-separation model yields

$$e\Delta_{\mathrm{VBO}}^{\mathrm{A-B}} = \gamma_{\mathrm{HJ}}(I_{\mathrm{B}} - I_{\mathrm{A}}) + (1 + \gamma_{\mathrm{HJ}})[\phi_{\mathrm{CNL}}^{\mathrm{S(B)}} - \phi_{\mathrm{CNL}}^{\mathrm{S(A)}}], \tag{3.3.1}$$

where I is the ionization potential, ϕ_{CNL} the semiconductor CNL referenced to the VBM, and

$$\gamma_{\mathrm{HJ}} = \left[1 + \frac{e^2 D_{\mathrm{GS}}^{\mathrm{A}} D_{\mathrm{GS}}^{\mathrm{B}} \delta_{\mathrm{gap}}}{\varepsilon_{\mathrm{S}}(D_{\mathrm{GS}}^{\mathrm{A}} + D_{\mathrm{GS}}^{\mathrm{B}})}\right]^{-1}, \tag{3.3.2}$$

where $D_{\mathrm{GS}}^{\mathrm{A}}$ is the density of gap states, per unit area and unit energy, on Semiconductor A. It is well-known that there is always a continuum of induced gap states in the semiconductor when it makes contact with a metal. However, at the interface of high-quality isovalent semiconductor HJs, states deep in the common gap of the two semiconductors are usually of very low densities, $D_{\mathrm{GS}} \to 0$. Under this condition, $\gamma_{\mathrm{HJ}} = 1$ and Eq. (3.3.1) would not be able to force a line-up of the CNLs. A high density of gap states is required in the fixed-separation model to line-up the CNLs. With the

presence of the gap states, the Fermi-level would also be pinned near the CNL, in disagreement with experimental result. So, the fixed-separation model cannot be invoked to explain band offset formation at high-quality semiconductor HJs with the CNL concept. This difficulty has not derailed BO formation theories based on the CNL concept. Quite on the contrary, the CNL concept is among the best-known explanations of the band line-up at HJs. The way the problem with the lack of gap states was circumvented was to invoke a ''division-by-epsilon'' argument.

3.3.3. Band offset analysis: division-by-epsilon model

Since the CNL of a semiconductor is often compared to the Fermi-level of a metal, it has been argued that a CNL also behaves like a Fermi-level when two semiconductors are joined together [56]. When two metals come into contact, there is a perfect line-up of the two Fermi-levels. This results from perfect screening (infinite dielectric constant) in the metal, so it seems. An argument was therefore given that when semiconductors are joined, dielectric screening takes place much like at a bi-metallic contact. However, the dielectric constant of a semiconductor is finite, which means that the initial difference between the two CNLs, $\Delta\phi_{\mathrm{CNL}}$, is not eliminated entirely, but only reduced by a factor of the dielectric constant, i.e. to $\Delta\phi_{\mathrm{CNL}}(\varepsilon_0/\varepsilon_{\mathrm{S}})$ [50]. Here, the initial $\Delta\phi_{\mathrm{CNL}}$ is understood to be the difference seen when both CNLs are referenced to the vacuum level, i.e.

$$\Delta\phi_{\mathrm{CNL}}^{\mathrm{A-B}} = (I_{\mathrm{A}} - \phi_{\mathrm{CNL}}^{\mathrm{S(A)}}) - (I_{\mathrm{B}} - \phi_{\mathrm{CNL}}^{\mathrm{S(B)}}) \tag{3.3.3}$$

To reduce this to $(\varepsilon_0/\varepsilon_{\mathrm{S}})$ its original value, one needs a Schottky dipole at the interface with a magnitude of

$$e\Delta_{\mathrm{Sch}} = \frac{\varepsilon_{\mathrm{S}} - \varepsilon_0}{\varepsilon_{\mathrm{S}}}\,\Delta\phi_{\mathrm{CNL}}^{\mathrm{A-B}}. \tag{3.3.4}$$

The resulting VBO is

$$e\Delta_{\mathrm{VBO}}^{\mathrm{A-B}} = I_{\mathrm{B}} - I_{\mathrm{A}} + e\Delta_{\mathrm{Sch}} \tag{3.3.5}$$

$$e\Delta_{\mathrm{VBO}}^{\mathrm{A-B}} = \frac{\varepsilon_0}{\varepsilon_{\mathrm{S}}}(I_{\mathrm{B}} - I_{\mathrm{A}}) + \frac{\varepsilon_{\mathrm{S}} - \varepsilon_0}{\varepsilon_{\mathrm{S}}}[\phi_{\mathrm{CNL}}^{\mathrm{S(B)}} - \phi_{\mathrm{CNL}}^{\mathrm{S(A)}}]. \tag{3.3.6}$$

Since the dielectric constant of common semiconductors is large, $(\varepsilon_{\mathrm{S}}/\varepsilon_0) > 10$, the second term of Eq. (3.3.6) dominates. Therefore, the final line-up condition is largely independent of the initial mismatch in the CNLs and is very close to that predicted by equating the two CNLs. Note that the division-by-epsilon argument leads to stronger pinning with increasing ε_{S}, which is just the opposite to the prediction based on the fixed-separation model, Eqs. (3.3.1) and (3.3.2).

The dielectric response is known to screen electric potential due to free charges. When a discontinuity in electrostatic potential is introduced by a modification of charge distribution, as in the linear response theory [22,45] or the interface-bond-polarity model [42,44] described above, dielectric screening occurs, resulting in an $\varepsilon_{\mathrm{S}}/\varepsilon_0$-fold reduction of the initial potential rise. In these examples, however, the screening occurs in response to assumed change in the electric charge distribution. The proposed division-by-epsilon approach uses the dielectric response in a very different manner, i.e. to screen energy differences instead of potential differences. Under some special conditions, such as when the energy difference is the result of a rigid shift of the bands (band bending), an energy difference is completely equivalent to a potential difference. This is the reason why the band-edge position can be used as a solution to the Poisson's equation, and why the free charge in Eq. (1.4.1) is divided by the semiconductor dielectric constant. But not all energy

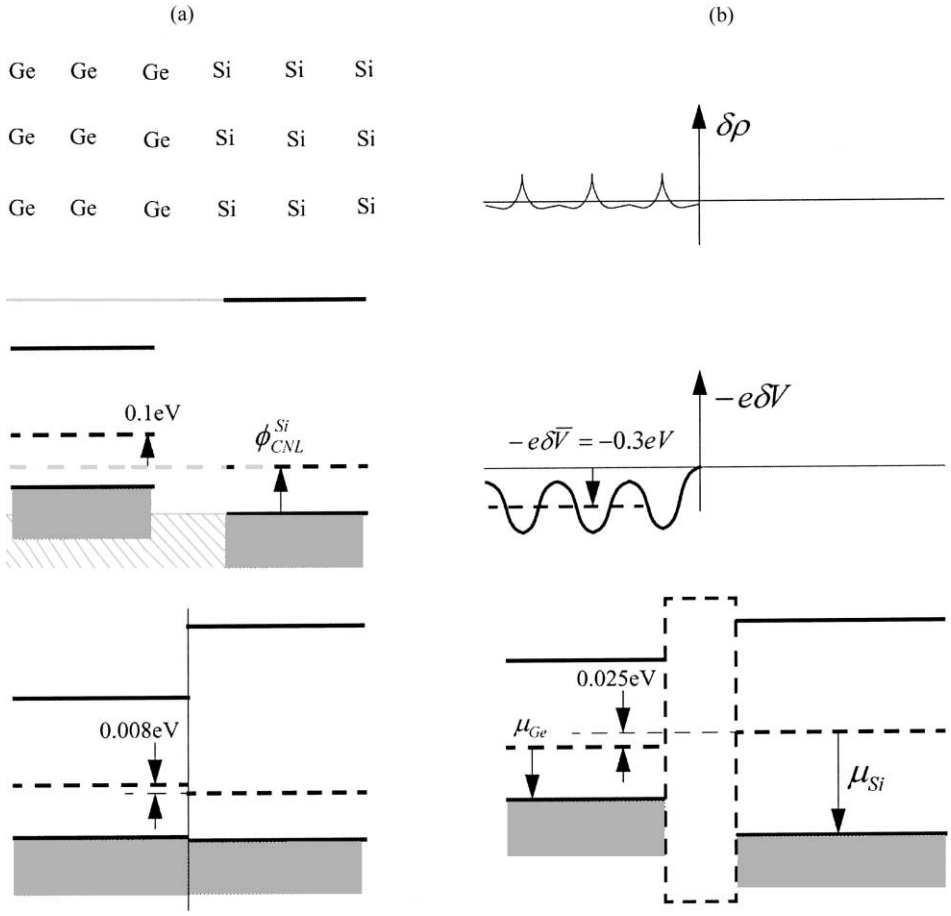

Fig. 20. (a) The division-by-epsilon concept of the formation of band offset. When half of a Si crystal is converted into Ge, the characteristic energy level increases by about 0.1 eV. This difference is screened by the Si dielectric response to 8 meV, leading to the final band offset. (b) The linear response approach of charge-density-based theories. The difference in the charge density between the Ge and the Si (upper panel) is used to compute an electrostatic potential energy difference in free space of, for example, −0.3 eV (middle panel). Dielectric screening of this electrostatic potential (0.3/12 = 0.025 eV) results in the final band offset. Band diagrams are not drawn to scale.

difference can be ‘‘screened’’ like this. Energy differences due to chemical changes cannot be simply screened by dielectric response. For example, if one-half of a Si crystal is converted into Ge in a conceptual exercise, as shown in Fig. 20, one notes that the energies of the atomic orbitals on the left half of the crystal have changed. Suppose the dangling bond energy of Ge is higher than that of Si by 0.1 eV, an argument has been given [50] that this difference should be simply screened and reduced to ∼0.008 eV, since the dielectric constant of Si is ∼12. And that will determine the band offset. This argument is dubious because, in this case, the Ge bands cannot be derived from the Si bands by a rigid-shift. Part of the difference between the orbital energies of Si and Ge is a kinetic energy contribution. There is no known way for a kinetic energy term to be ‘‘screened’’ by the dielectric response. If the morphing of Si into Ge is viewed in a different manner, as in Fig. 20(b), then the concept of dielectric screening may still be used. The change of a Si atom into a Ge atom can be viewed as the result of adding a few protons to its nucleus and a few electrons to its electron cloud. It is quite conceivable to treat these modifications in the charge distribution of the solid as a perturbation and then use the dielectric constant to partially screen out the step-wise voltage drop,

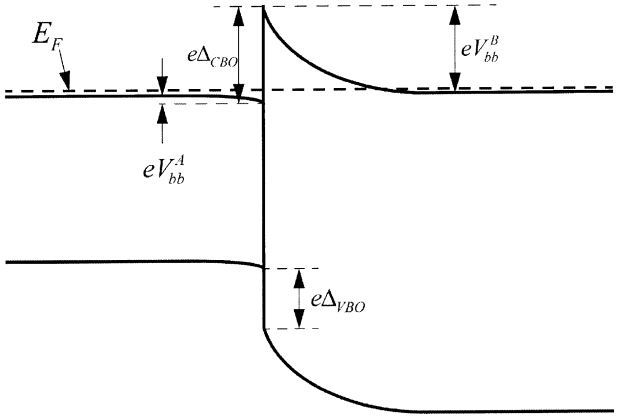

Fig. 21. Band diagram of a degenerately-doped n^+–n^+ semiconductor heterojunction.

to which this charge redistribution would have led in free space. The screening in this case is a response to the charge distribution, with no regard to the energetic levels of the charge. This latter approach, Fig. 20(b), is actually the basic procedure taken in the linear response theory, discussed above along with other charge-density-based theories. Some may find the addition of protons and electrons to be ''drastic'' enough to think that these modifications of the charge density must lie outside the linear response regime. However, experience has shown surprisingly good numerical agreement between the results of such simple exercises and results from full-fledged calculations.

One may also point out that the notion that Fermi-level simply lines up at a metal–metal interface is an oversimplified view of the actual situation. Take the example of a degenerately doped HJ, as shown in Fig. 21. There is metallic screening in a neutral degenerate semiconductor, whose Fermi-level lies slightly inside the conduction- or valence-band, because the presence of free carriers. The bulk Fermi-level positions of the two semiconductors line-up, as shown in Fig. 21. However, at the interface there is still band bending. It is revealing to compare the vastly different amounts of band bending on the two sides of the HJ. At the interface, the Fermi-level of the semiconductor with the smaller gap (left) is little moved from its bulk position, reminiscent of metallic screening. However, the interface Fermi-level position for the semiconductor with the large band gap (right) is far removed from its bulk position. The reason for the presence of band bending in the right semiconductor is a lack of carriers in the depletion region, whose screening thus becomes semiconductor like. The requirement on the continuity of the electric potential across the HJ tends to push the bands on the left downward, but the left semiconductor cannot budge because the density of states is high in the conduction band. The same force pushes the bands on the right semiconductor upward and meets little resistance, because the density of states below the Fermi-level is low in the gap. So, one of the two degenerate semiconductors acts like a metal and the other a semiconductor, because of the asymmetric distribution in the density of states above and below the bulk Fermi-level position. Therefore, the lack of ''band-bending'' at a bimetallic contact is more appropriately attributed to the high density of mobile states at the Fermi-level, rather than the large dielectric constant. One notes that ''nanoscopic'' band bending, as reflected in a shift in the core-level position, is still present at the interfaces of two metals with a large difference in their work functions [57,58]. One should also note the entirely different natures of metallic screening and dielectric screening. Metallic screening arises from movement, sometimes of long-range, of mobile carriers, and dielectric screening is due to the distortion of the wave functions of bound electrons. These two types of screening often work in opposite directions, as has been dramatically demonstrated on metal

surfaces [59]. Metallic screening can respond to chemical (electronegativity) and electric-field-related driving forces, whereas dielectric screening can only respond to external electric field.

3.4. Summary

The valence band maximum positions, in reference to either the CNL position for the CNL-based models, or the external vacuum level in charge-density-based models, are summarized in Table 2. Amazingly, theoretical models based on the CNL concept and those based on charge densities tend to give similar predictions on the BO [34], despite their completely different views on the BO formation process. Better agreement with the experimental result is more common for isovalent HJ interfaces. ''There is no single theory that yields band offset values that are substantially more accurate than those predicted by any other theory'' concluded Yu et al. after an extensive side-by-side comparison of 15 different theories on BO formation [34]. The selection process of the ''true'' mechanism of BO formation from experimental data, is thus, thwarted by an inability to discriminate between the predictions of the models. The similarity in the predictions of these two types of models indicates that the two diagrams drawn in Fig. 19 should in fact be very similar, at least for isovalent HJs. Even though the interface dipole is envisioned to be large in Fig. 19(b) without affecting the validity of the CNL models, it in fact may be quite small when actual data are analyzed for most HJs. Alternatively, the similarity in the predictions of various models suggests that when two semiconductors meet under a frozen-charge condition, Fig. 19(a), their CNLs are already closely matched. Therefore, formation of an additional dipole would be unnecessary. What all of this means is that the proposed CNLs for many semiconductors are at roughly the same position, when referenced to the external vacuum level. There may be some underlying reason for this ''coincidence'', as pointed by Harrison and Tersoff [50]. The connection is most transparent in a tight-binding formalism, as used in both the LCAO theory [38–40] and the hybrid energy model [50]. The average hybrid energies calculated from the Hartree–Fock term values [60] do not differ for semiconductors with similar bond length [50]. So, for semiconductors with similar lattice constants, between which the BOs are most accurately known, the CNLs are already naturally lined up. Even though the models based on the CNL concept are able to predict the BO with some degree of success, the problem associated with the lack of interface gap states near the CNL cannot be overlooked. Without gap states, there is no valid driving force for the CNL to line-up across a HJ. Actually, the CNL can be viewed as the energy of the atomic orbital involved in the bonding. So a difference between orbital energies should induce a polarization of the interface bonds, which tend to reduce the initial difference in orbital energies. After the bonds are formed these energy levels correspond to the average of the bonding (valence band) and anti-bonding orbitals (conduction band). So, there is a chemical force that drives the CNLs together, irrespective of the density of gap states. The exact relationship between the chemical driving force and the dielectric constant of the semiconductor is not immediately clear.

4. Models on bonds and dipoles at MS interfaces

When an intimate MS interface is formed in thermodynamic equilibrium, chemical bonds are established at the interface. All the electronic properties of the MS interface, including the formation of the electric dipole and the SBH, are naturally influenced by these interface bonds. The main drawback of the non-interacting models of the SBH is the neglect of this chemical effect. So, the departure of the experimentally observed SBH from the Schottky–Mott relationship is clearly related

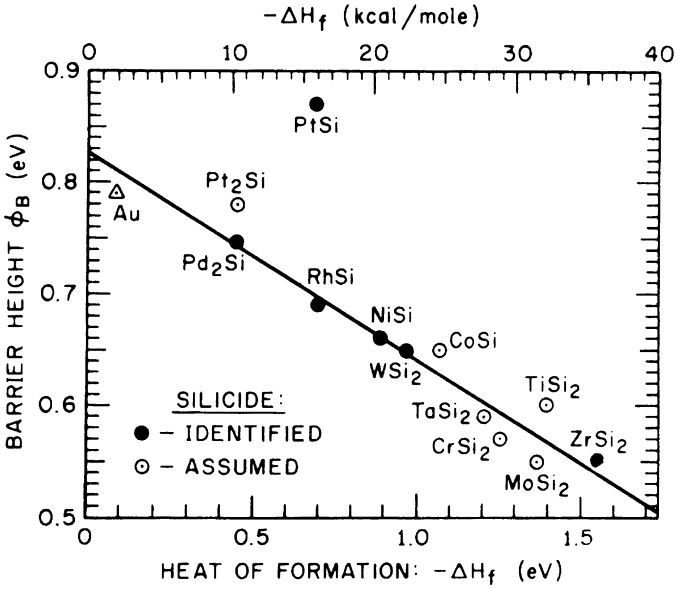

Fig. 22. Barrier heights of transition metal silicide–Si interfaces plotted against heats of formation ΔH_f of the identified (assumed) silicide compound. The correlation coefficient (excluding the PtSi datum) is 97%. $\Phi_{B,n} = 0.83 + 0.18\,\Delta H_f$ (from Andrews and Phillips [61]).

to this effect, which shows how important and significant interface bonds are. Here, we examine what numerical calculations have taught us about the formation of dipole at single-crystal MS interfaces. In addition, the well-known model based on MIGS, and a recently developed model, based on bond-polarization, have specific proposals on how to estimate the amount of charge transfer at MS interfaces. The principles and assumptions behind these models are also discussed in detail.

4.1. Empirical models

The relevance of bonding and structure of metal semiconductor interfaces to the formation of the SBH was pointed out by Andrews and Phillips [61] in their study of the heats of formation of silicides. These results are reproduced in Fig. 22. Silicides are crystalline metal–silicon compounds, which are usually electrical conductors. The SBH of silicide was shown to correlate linearly with the heat of formation of the silicide, $-\Delta H_f$, provided the heat of formation was normalized per metallic atom per formula unit. But as the authors pointed out, the charge transfer between the metal and Si, and therefore, the magnitude of the interface dipole, should have been proportional to the square-root of the heat of formation. So the linear dependence of the silicide SBH on $-\Delta H_f$ was rationalized as a result of longer metal–Si bonds and weaker interaction [61]. There are other interesting and perhaps accidental aspects about Fig. 22, which were pointed out by the authors, namely that the experimental data extrapolated to a SBH of 0.83 eV at zero heat of formation, which corresponded to the Si free surface Fermi-level position and that the extrapolated heat of formation at zero SBH was very close to the Si cohesive energy. The SBHs of silicides have also been shown to correlated with the shift, observed by XPS, in the core-level position of the metal upon silicide formation [62,63], as shown in Fig. 23. Again, the importance of chemical bonds to SBH formation was pointed out [62,63]. Apparently, the core-level shifts in these cases were interpreted only in terms of the initial state effect. Chemical bonds and interface structure are obviously of primary importance, as far as the formation of the SBH is concerned, because the potential drop across the ISR is obviously

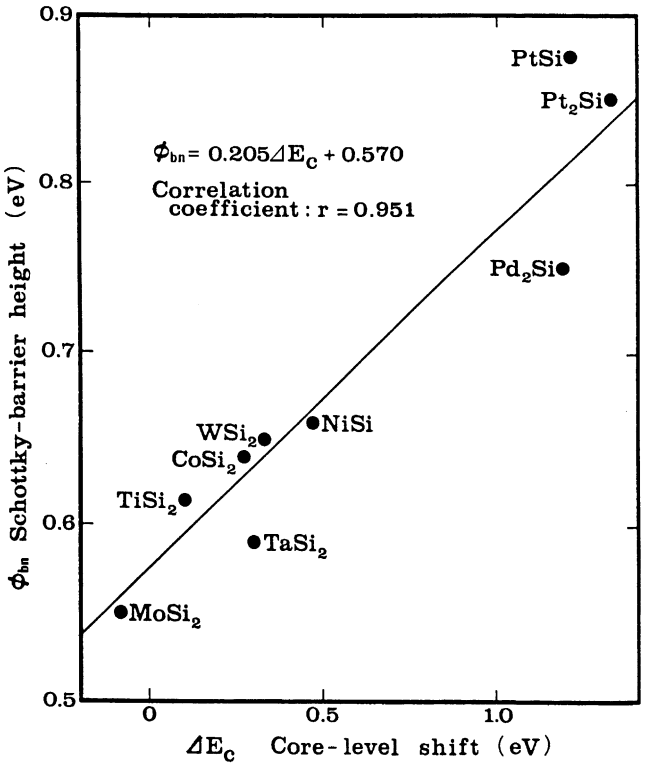

Fig. 23. Schottky-barrier height of silicide–n-Si interfaces plotted vs. core-level shifts of transition metals with silicide formation toward higher binding energy ΔE_C. Since ΔE_C is a bulk electronic parameter, this relation shows that the SBH has a correlation with bulk electronic structure (from Hara and Ohdomari, [62]).

dependent on these. So, the work of Andrews and Phillips and subsequent works along the same vein should get ample credit for calling attention to this aspect of SBH formation. However, these approaches have at least two problems. First, a direct comparison of the silicide SBH with the heat of formation of that silicide has no obvious physical basis. The heat of formation is a bulk property and its relationship with the interface dipole that forms at the silicide–Si interface is only to the extent that the individual bond could be similar. There is no reason to expect the density, geometry, bond length, chemical environment, etc. of the silicide–Si interface to be similar to that in a bulk silicide crystal. In other words, if an analysis of some form of energy were to be used to derive quantities relevant to the SBH formation, it should have been the interface energy of a silicide–Si system rather than the bulk heat of formation of the isolated silicide. In yet another way to put it, it makes more sense to view the charge transfer deduced from the heat of formation of a particular silicide, or the core-level shift of a particular silicide, as a relevant parameter to understand the SBH formation between the pure metal and the Si, rather than that between this silicide and Si. The second problem with the direct correlation of heat of formation with the SBH is the lack of a proper baseline condition. In general, the magnitude of the interface dipole should be superimposed onto a "baseline" SBH condition, to ensure the continuity of the electric potential across the MS interface. This baseline condition, as discussed, is simply the Schottky–Mott condition.

That a relationship existed between SBH and the heat of compound formation was the main point of another study, on metal–compound semiconductor interfaces [64]. It was pointed out that the data of Fig. 65 could also be plotted against the heat of formation of the semiconductor with

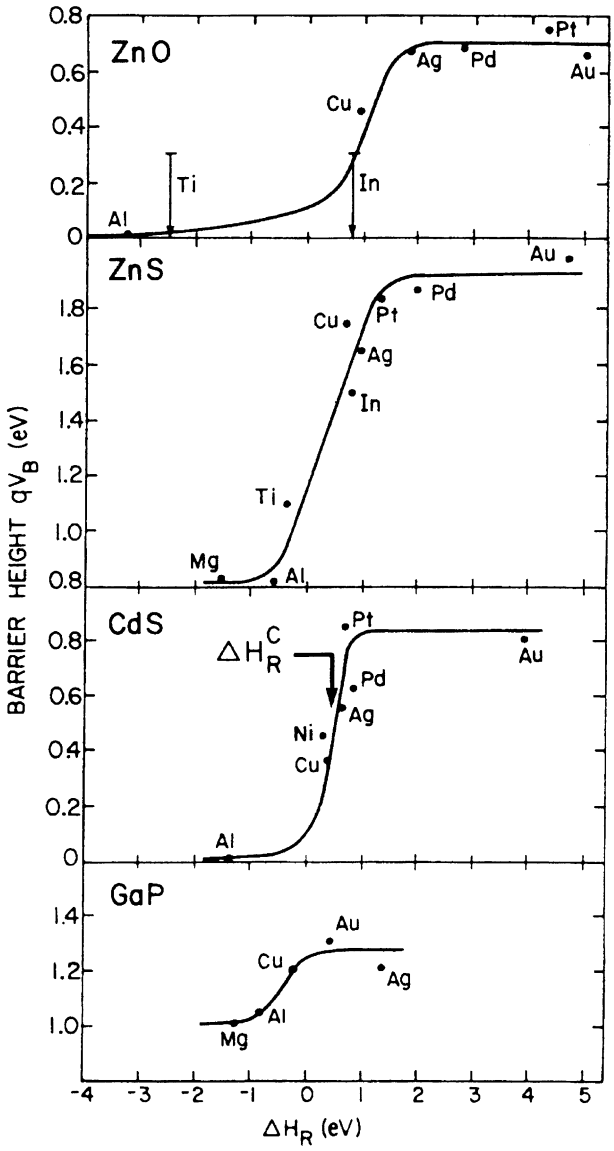

Fig. 24. Barrier heights correlated with heats of chemical reactivity for metals on ZnO, ZnS, CdS, and GaP (from Brillson [64]).

essentially the same dependence. Since it could be argued that semiconductors with smaller heats of formation (covalent semiconductors) were more likely to react with metal, this observed correlation was interpreted as an indication of the role played by the interface in determining the SBH. This same point was reemphasized through a study of the relationship between the SBH and the heat of formation of metal–anion compounds (e.g. Ti_2S, MgSe, etc.), as shown in Fig. 24. On each semiconductor, experimental SBHs seemed distinguishable into a group of non-reactive metals with higher SBH, a group of reactive metals with much smaller SBHs, and some metals between these two extremes [64]. This observation was interpreted as evidence for the role played by chemical reactivity in the formation of interface dipole. Even though the data of Fig. 24 could be, and probably should have been, fitted to straight lines with no less satisfaction than the actual fit to a bi-level dependence, and that the x-axis could probably have been replaced by the metal work function

without much change in the actual dependence, the presence of such a correlation between the SBH and the heat of formation is important nevertheless. One notes that here thermodynamic data on bulk compound phases were correlated with the interface property of nominally pure metal contacts. This angle is clearly much more in line with the bond-polarization picture [14] to be discussed later than the previous models on silicide heats of formation [61,62]. One notes however that, like the silicide models, this approach also suffered from a lack of proper baseline. Other empirical proposals on the interface dipole exist. For example, Tove [65] proposed an empirical rule on the interface dipole, although the specific reason behind such a rule is vague.

4.2. Metal-induced gap state models

The overlap of wave functions at a MS interface can significantly alter the electronic structure and the charge distribution in the ISR. Much effort has been devoted to investigate one particular aspect of the interface electronic property, namely the formation of MIGS, and the role played by MIGS in the formation of the SBH. This is a rather restricted focus, out of the full spectrum of events/processes that could affect the total potential drop across the ISR. But this simple approach has led to some interesting and attractive correlations with experimental data. As a result of some degree of success, models concentrated on the distribution of MIGS are the ones most frequently used to explain SBH formation. As discussed in the last section, the presence of a foreign entity in close proximity to a semiconductor can induce electronic states in the band gap of the semiconductor. These induced gap states are thought to arise from the tunneling of metal wave function into the semiconductor. It has been argued that even though metal is the thing that ''induces'' the formation of gap states, the actual distribution of the gap states is essentially a property of only the semiconductor itself. Early theoretical calculations, using ''jellium'' as the metal, seemed to support this view, as shown in Fig. 25. The density of states (DOS) of the semiconductor (Si) seemed only mildly disturbed from its bulk distribution, even at the MS interface. The effect of the jellium seemed to be to allow some states originally in the valence- and conduction-bands to be pulled into the band gap. The density of the MIGS decays from the MS interface with a characteristic length that correlates with the ionicity of the semiconductor. The range of MIGS is longer for covalent semiconductors and shorter for ionic semiconductors. At the time of these calculations, this dependence was used to explain the sharp transition in the *S*-parameter found by Kurtin et al. [66] shown in Fig. 65. However, this MIGS explanation was criticized [67] and later the experimental basis for the Kurtin transition was also shown to be in error [68].

The presence of a continuum of states in the gap makes the interface semiconductor effectively a ''metal''. The question naturally arises as to where the CNL, or the de facto Fermi-level, is for the interface semiconductor. It is obvious that, in thermal equilibrium, this CNL should roughly line-up with the Fermi-level of the metal. Thus, the most important aspect of MIGS formation, in connection with the formation of the SBH, seems to be the location of the CNL of the MIGS. Furthermore, if the formation of MIGS is independent of the metal as assumed, the CNL is an intrinsic property of the semiconductor, which means that a common reference frame can be established for all the semiconductors (cf. Section 3.3). This is the basis for the transitivity rule among any three semiconductors, or even among two semiconductors and a metal. Various theories and arguments exist concerning the location of the CNL, as already discussed in detail in the last section. The proposed CNLs include the branch point [48] the dielectric midgap energy [69] the energy of hybrid orbitals [50], etc. and their predictions vary only slightly, as shown in Table 2. Another important parameter, as far as the interface line-up condition is concerned, is the density of the MIGS, on which more comments will be made later.

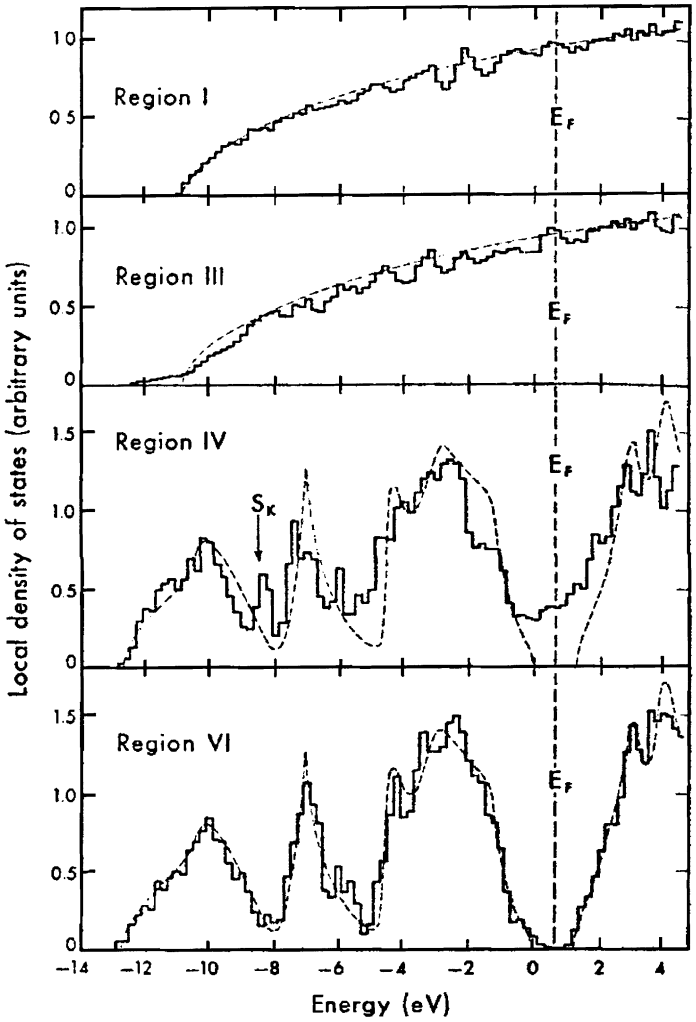

Fig. 25. Local density of states calculated by self-consistent pseudopotential method for a jellium–Si interface. Regions III and IV are close to the interface, while regions I and VI are away from the interface (from Louie and Cohen [480]).

4.2.1. Fixed-separation model of MIGS

In a simplified view of the MIGS, one can regard the entire energy and spatial distributions of the MIGS to be intrinsic properties of the semiconductor. Thus, the CNL, the density, and the decay length of the MIGS can all be assumed to be invariant for a semiconductor. However, one still need to construct a model to show how the SBH is determined for any given metal, based on these MIGS parameters. Similar to the determination of the BO at HJ interfaces, there are two analysis models, the ''division-by-epsilon'' model and the ''fixed-separation'' model, which allow the SBH to be deduced for a MS interface. In the division-by-epsilon model, the initial difference between the metal Fermi-level and the semiconductor CNL is proposed to be simply reduced by a factor of the dielectric constant. For a given metal, this model would predict a SBH of

$$\Phi^0_{B,p} = (I_S - \phi_M)\frac{\varepsilon_0}{\varepsilon_S} + \phi_{CNL}\frac{\varepsilon_S - \varepsilon_0}{\varepsilon_S}. \tag{4.2.1}$$

Note that Eq. (4.2.1) predicts an S-parameter of $\varepsilon_0/\varepsilon_S$, which is not directly related to either the density or the range of the MIGS. The many problems with the division-by-epsilon approach were already discussed in Section 3.

The second method, the fixed-separation model, is identical to the model used to analyze SBH in the presence of deep-levels, shown in Fig. 15, and the model based on surface states, shown in Fig. 13. This model assumes the charge due to MIGS to be positioned uniformly on a plane that is located at a fixed distance away from the metal. The interface dipole, established from the charge on this plane and its image charge on the metal, reduces the initial mismatch between the semiconductor CNL and the metal Fermi-level. It has been common to assume that the interface separation, δ_{gap}, is the decay length of MIGS. Equations previously obtained in Section 2.4 for deep-level states are still valid for the present MIGS model, with a change in the relevant symbols. For a uniform density of gap states, one gets

$$\Phi^0_{B,p} = \gamma_{GS}(I_S - \phi_M) + (1 - \gamma_{GS})\phi_{CNL}, \tag{4.2.2}$$

where γ_{GS}, the S-parameter predicted by the MIGS fixed-separation model, is

$$\gamma_{GS} = \left(1 + \frac{e^2\delta_{GS}D_{GS}}{\varepsilon_{int}}\right)^{-1}. \tag{4.2.3}$$

The permittivity here is generalized and expressed as ε_{int} to account for the likelihood that the interface region has a permittivity significantly different from that of the bulk semiconductor, ε_S. With the assumption of the same D_{GS}, ϕ_{CNL}, and δ_{gap} for different metals on the same semiconductor, Eqs. (4.2.2) and (4.2.3) have been used to analyze systematic dependence of the SBH on metal work function to infer D_{GS} and ϕ_{CNL} of the semiconductor. Such analyses usually led to reasonable estimated on the density of MIGS, which tended to support the relevance of the overall MIGS concept. Furthermore, Monch used properties of the complex 1-D band structure to estimate the density of states and the decay length near the branch point [70]. Carried over to three-dimension semiconductors, these results would predict that $(S_\Phi^{-1} - 1)$ should be proportional to $(\varepsilon_\infty/\varepsilon_0 - 1)^2$, where ε_∞ the optical dielectric constant of the semiconductor. As shown in Fig. 26, a fit of

$$S_\Phi^{-1} - 1 = 0.1\left(\frac{\varepsilon_\infty}{\varepsilon_0} - 1\right)^2 \tag{4.2.4}$$

was indeed found. This observation provided further support for the MIGS fixed-separation model. One notes that this correlation, shown in Fig. 26 as a log–log plot, would not have appeared impressive on a linear plot.

There are many advantages of the MIGS fixed-separation model. First of all, the fixed-separation model is a very easy model with which to analyze experimental SBH data. Like the Schottky–Mott theory, it has a clear proposal on the distribution of charge at the interface, from which the band line-up is deduced. In other words, the continuity of the electric potential is trivially satisfied in the fixed-separation model. Some form of the electric dipole, arising from the electronic interaction between the metal and the semiconductor, has been included, in general agreement with the expected quantum chemistry at the MS interface. The band line-up was clearly done in a fashion that equalizes the electrochemical potential, which, as discussed later, is a procedure that leads to a minimization of the total energy. So what is the problem with the MIGS fixed-separation model? The main problem is that the charge transfer here is done with the constraint that the distribution of

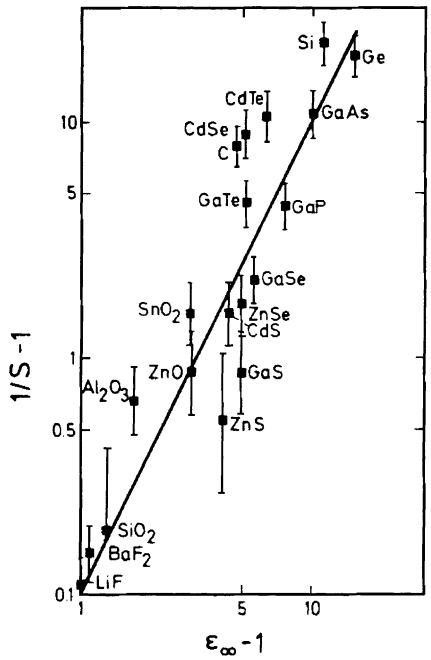

Fig. 26. Slopes $S_{\Phi}^{-1} - 1 (= A/S_{\chi} - 1)$, plotted vs. the electronic contribution to the dielectric constant of the semiconductor (from Monch [70]).

the MIGS does not depend on the metal. This assumption is in clear disagreement with the experimentally observed dependence of the SBH on epitaxial structures and the observed SBH inhomogeneity at polycrystalline MS interfaces. Furthermore, first-principles calculations, described in the next section, have generally found disagreement with various assumptions of the MIGS fixed-separation model. Actually, it should have been clear that the assumption must be false that the density of MIGS is an intrinsic property of the semiconductor. One can perform the Gedanken experiment described in Section 2.1 again, holding a flat metal surface extremely close and parallel to a GaAs(1 1 0) surface, which is known to have no gap states. Imagine closing the gap very slowly, and ask the question ''when do the semiconductor MIGS suddenly appear with a predetermined density''. Since the metal wave functions on the metal free surface usually decay exponentially toward vacuum, it can be viewed that the metal wave functions have no boundaries and therefore always tail into the semiconductor even from a distance, albeit extremely weakly. Therefore, by this line of reasoning, GaAs(1 1 0) surface should always have a full distribution of MIGS. The fact that MIGS is a response of the semiconductor to electronic disturbances of the metal is one feature that is amiss in the fixed-separation model. There is no reason to think that the response (MIGS) is independent of the stimulus (metal) and that the MIGS is only in thermal equilibrium with the semiconductor. Actually, any ''interaction'' has to go both ways almost by definition. Chemical bond formation and minimization of energy drive the change in the DOS in not only the semiconductor but also the metal at the interface. It seems easier to predict the net effect of interface charge distribution from a study of its driving force (bond formation) than from an empirical study of one aspect of the resultant charge distribution (MIGS). In other words, charge transfer between the metal and MIGS is an appropriate view of the chemistry that goes on at an MS interface. However, since the chemistry is usually different at different MS interfaces, MIGS parameters will also vary in general. So, for each new MS interface, a new set of ϕ_{CNL} and D_{GS} becomes operative. There is no sound

justification for involving Eqs. (4.2.2) and (4.2.3) in a study of the systematics of SBHs measured on different MS interfaces.

There is another problem with the MIGS theory of SBH formation, which has to do with the magnitude of δ_{gap} assumed between the metal and the MIGS. Jellium calculations show that the typical decay length (penetration depth) of MIGS is on the order of 0.1–0.3 nm for different semiconductors [20] i.e. around the distance of one lattice spacing of the semiconductor. Such a distance gives the impression that the transfer of charge between the metal and semiconductor is more or less limited to only across the interface atomic plane, and suggests that MIGSs are really closely-related to interface bonding. Therefore, MIGSs should be viewed as an integral part of the interface. Namely, MIGSs should be viewed as largely residing inside the ISR, as schematically shown in Fig. 4. However, in correlating experimentally observed Fermi-level pinning phenomenon and transport characteristics with the distribution of MIGS, it has been customary to assume a much longer range of the MIGS, typically 0.5–3 nm. These larger separations are more in line with the assumption that the distribution of MIGS is an innate property of the semiconductor. However, when a large δ_{gap} is assumed, the notion that MIGS is an inseparable part of the interface is lost. Instead, MIGS are viewed like ordinary deep-levels of the semiconductor, essentially independent of the metal. Thus, the MIGS model becomes open to meaningless speculations on whether MIGSs exchange charges mainly with the semiconductor or the metal. Much ambiguity arises concerning the behavior of MIGS under applied bias, as will be discussed.

4.2.2. Negative charge model of MIGS

The negative charge model of the MIGS assumes a spatially extended distribution of the MIGS charge [71–73], which leads to the kind of band bending as shown in Fig. 27. The density of the MIGS charge, ρ_{MIGS}, is assumed to decay exponentially into the semiconductor, i.e.

$$\rho_{\text{MIGS}}(z) = \frac{Q_{\text{MIGS}}}{\lambda} \exp\left(-\frac{z}{\lambda}\right), \tag{4.2.5}$$

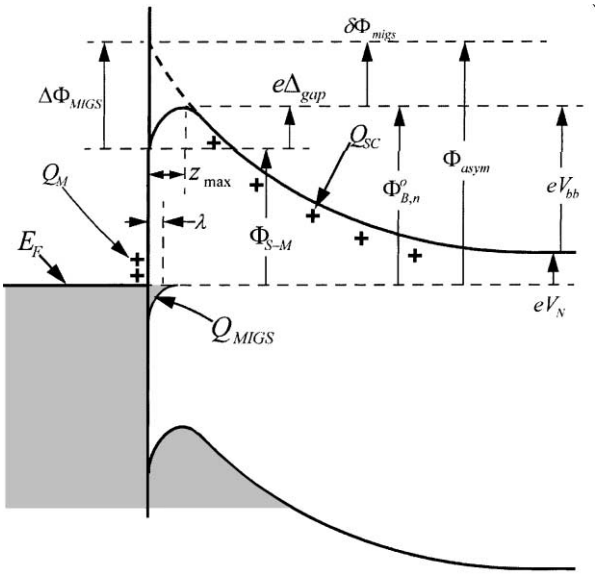

Fig. 27. Band diagram of the negative charge model [71,72], incorporating the effect of the exponential decay of a density of metal-induced gap states.

where Q_{MIGS} is the areal density of the net charge occupied by MIGS, and λ the penetration depth of MIGS into the semiconductor. An exponential distribution of the MIGS charge is certainly much more in line with the picture of the tunneling of metal wave function in MIGS formation [74], than the fixed-separation model. The charge-density of Eq. (4.2.5) can be added to the space–charge-density of Eq. (1.4.8) to solve for the band bending. However, since the range of MIGS is extremely short, only band bending within a short distance of the MS interface is influenced by the MIGS and need to be modified. As before, one assumes that the MIGS charge is much greater than the space–charge of the semiconductor. This allows the location of maximum band bending to be expressed analytically

$$z_{max} = \lambda \ln\left(\frac{-Q_{MIGS}}{\varepsilon_S E_{max}}\right) \tag{4.2.6}$$

$$z_{max} = \lambda \ln\left|\frac{Q_{MIGS}}{Q_{SC}}\right|, \tag{4.2.6a}$$

where E_{max} is the electric field due to the space–charge, given by Eq. (1.4.13). As can be seen from Fig. 27, there are now two more quantities Φ_{S-M} and Φ_{asym} of interest, in addition to the SBH, $\Phi^0_{B,n}$. The Φ_{S-M} is the barrier height at MS interface, so it can be identified with the Schottky–Mott SBH to preserve the continuity of the electrostatic potential

$$\Phi_{S-M} = \phi_M - \chi_S. \tag{4.2.7}$$

The asymptotic SBH, Φ_{asym}, which is characteristic of the true width of the space–charge region, is

$$\Phi_{asym} = \Phi_{S-M} + \Delta\Phi_{MIGS}, \tag{4.2.8}$$

where

$$\Delta\Phi_{MIGS} \approx -\frac{e\lambda Q_{MIGS}}{\varepsilon_S}. \tag{4.2.9}$$

The effective Schottky-barrier height, which actually controls the electronic transport, is

$$\Phi^0_{B,n} = \Phi_{asym} - \delta\Phi_{MIGS}, \tag{4.2.10}$$

where the ''SBH lowering'' due to MIGS is [71]

$$\delta\Phi_{MIGS} = e z_{max} E_{max}. \tag{4.2.11}$$

Because of its dependence on the electric field, this lowering mechanism of the SBH has been invoked to explain the large ideality factor [71,73] and the large reverse leakage current [72] observed at MS interfaces. One should note from Eq. (4.2.6a) that the apex of the conduction band is usually much farther from the MS interface than the penetration depth of MIGS. This has to do with the fact that the peak density of MIGS, Q_{MIGS}/λ, is usually orders of magnitude higher than the semiconductor doping level, N_D.

The negative charge model and the fixed-separation model share many similar features, but they also differ in a fundamental way. In the negative charge model, the MIGS charge has its maximum density right at the MS interface, which gives the impression that MIGS is an integral part of the

interface, or an extension of the metal states. Within such a scenario, it is difficult to argue how the distribution of MIGS could be an innate property of the semiconductor. The best way to distinguish the negative charge model from the fixed-separation model is perhaps the following. The fixed-separation model is used to analyze interface states which are in thermal equilibrium with the semiconductor, while the negative charge model is used to analyze interface states which are in thermal equilibrium with the metal. The negative charge model has been invoked almost exclusively to explain the bias-dependence of the SBH. It has not been applied in any significant way to explain the Fermi-level pinning effect. The key parameter here is the net MIGS charge, Q_{MIGS}, which is more or less an assumed quantity for an MS interface. There is no direct relationship between Q_{MIGS} and the work function of the metal, in the negative charge model. However, if one ignores the close relationship between the MIGS and the metal, and still assumes the interface charge to be controlled by some charge neutrality level, i.e.

$$Q_{\mathrm{MIGS}} = eD_{\mathrm{MIGS}}(\Phi_{\mathrm{S-M}} - E_{\mathrm{g}} + \phi_{\mathrm{CNL}}), \tag{4.2.12}$$

one can still arrive at expressions similar to that predicted by the fixed-separation model. Combining Eqs. (4.2.8) and (4.2.12), one gets

$$\Phi_{\mathrm{asym}} = \gamma_{\mathrm{MIGS}}(\phi_{\mathrm{M}} - \chi_{\mathrm{S}}) + (1 - \gamma_{\mathrm{MIGS}})(E_{\mathrm{g}} - \phi_{\mathrm{CNL}}), \tag{4.2.13}$$

However, γ_{MIGS} now takes on a slightly different form than that predicted by the fixed-separation model:

$$\gamma_{\mathrm{MIGS}} = 1 - \frac{e^2 D_{\mathrm{MIGS}}\lambda}{\varepsilon_{\mathrm{S}}}. \tag{4.2.14}$$

The intriguing difference in the functional forms displayed in Eqs. (4.2.3) and (4.2.14) can be traced to the physical separation, or the lack thereof, of the Fermi-levels controlling the metal and the semiconductor charges. The major difference is in the assumption of the interface charge. In the fixed-separation model, the interface charge, Eq. (2.2.1), depends explicitly on the final SBH itself. This leads to a negative feedback action on the SBH: the initial FL position of a metal always converges toward the CNL, but can never reach or go pass it. In the negative charge model however, the interface charge, Eq. (4.2.12), does not depend on the final SBH, Φ_{asym}. So Eq. (4.2.14) does not contain a negative feedback mechanism, and γ_{MIGS} can in principle become negative. One should keep in mind that when MIGSs are in thermal equilibrium with the metal, which they clearly are in the negative charge model, the concept of CNL (Eq. (4.2.14)) is extremely weak. Therefore, there is no reason to assume that a formula like Eq. (4.2.12) should hold for different metals. One should look for alternative guidelines on how MIGS charge varies with the metal work function, as the bond-polarization theory, discussed below, attempts to do. Our discussion on the Fermi-level pinning aspect of the negative charge model here is for exercise only. However, this exercise is not entirely futile, because the interface bond-polarization theory will prove to be amazingly similar, in its analysis model, to the approach used here.

4.3. Theoretical calculations of SBH

Compared with the overwhelming occurrences of HJ interfaces that are epitaxial, epitaxial MS interfaces that have been experimentally produced are relatively few in number. However, because of the good control over epitaxial MS interfaces, the electronic properties at these interfaces are thought

to provide the most direct clues to the SBH formation mechanism. Most notable among these interfaces are the type A and type B $NiSi_2$–Si(1 1 1) interfaces, where experiments showed a difference of 0.14 eV in SBH between the two interfaces [7]. Furthermore, the $NiSi_2$–Si(1 0 0) interface has a SBH which is about 0.25 eV lower than the type A $NiSi_2$–Si(1 1 1) interface [75]. Ab initio calculations [76,77], based on the experimentally determined structure, have yielded SBH results which are in excellent agreement with the (1 1 1) results. An n-type SBH for the type B $NiSi_2$ interface, which is 0.15–0.17 eV higher than the type A interface, was obtained in calculations involving large supercells. One should note that even though the SBH difference has been reproduced, the absolute values of the SBH from these calculations are not accurate, likely because of the problem with the local density approximation (LDA) assumed in these calculations. One also notes that the absolute SBH values were found to depend on the size of the chosen empty cells and that calculations involving smaller supercells, or non-self-consistent calculations, were generally incapable of explaining the experimental trends. The A–B comparison filtered out systematic errors in the calculations, because the same unit cell was used for both interfaces. The (1 1 1) to (1 0 0) comparison is a more difficult task because it is subject to errors in the absolute SBHs calculated in different unit cells. The experimentally observed $NiSi_2$–Si(1 0 0) SBH has not been reproduced in calculations. Even though the validity of even the most elaborate calculations is not beyond question, it is, nevertheless, informative to examine the calculated electronic structures for clues to the SBH mechanism. This is particularly true for the A- and B-type $NiSi_2$–Si(1 1 1) interfaces. Although the densities of MIGS were high at both interfaces [77], calculations found no easily identifiable feature in the energetic distribution of these states to suggest a "pinning" of the FL. Actually, the role played by MIGS in determining the FL position was not immediately revealed by these calculations [76,77]. One notes that there are significant differences in the distribution of MIGS at these two interfaces, suggesting a dependence of MIGS on the interface structure. An examination of the potential due to all charges at the two interfaces [77], as shown in Fig. 28, reveals several other surprising results. First of all, the charge due to MIGS is only a small part of the total redistributed charge at the interface. Furthermore, the local charge oscillates rapidly at the MS interface and extends roughly an equal distance, ~0.6–0.9 nm, into both the Si and the $NiSi_2$ sides of the interface. The potentials at these interfaces [77] shown in Fig. 28, bear no resemblance to the monotonic and smooth band diagram usually assumed in the negative charge model of the MIGS [71,74] shown in Figs. 15 and 27.

The electronic structures at the interfaces of other known epitaxial MS systems, such as $CoSi_2$–Si [78–80], Al–GaAs [81–83], and ErAs–GaAs [84], have also been calculated. Needs et al. found the

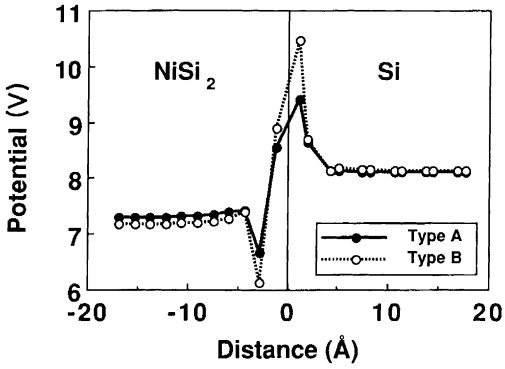

Fig. 28. Potential in each Si site for epitaxial type A and type B $NiSi_2$–Si(1 1 1) interfaces. This was calculated by Madelung constants and charges in other atomic spheres. The center line is the interface (from Fujitani and Asano [77]).

SBH at epitaxial Al–GaAs(1 1 0) interface to vary by as much as 0.7 eV with a change in the interface structure. A much smaller variation, ~0.1 eV, was found by Bardi et al. who mentioned the importance of interface relaxation [83]. In addition, experimentally observed dependence of the SBH of epitaxial Al–$Al_xGa_{1-x}As$(1 0 0) interface on the alloy composition has been reproduced by a linear response theory calculation [83]. For the epitaxial Al–GaAs(1 0 0) interface, Dandrea and Duke provided detailed analysis of the distribution of MIGSs as a function of interface structure [81]. The distribution and the spatial population of MIGS for the Ga-terminated (with Ga–Al interface bonds) and As-terminated interfaces (with As–Al interface bonds) are shown in Fig. 29. The density of MIGS is above the $1 \times 10^{14}\ cm^{-2}\ eV^{-1}$ level, usually considered high enough to pin the Fermi-level. However, the SBH varies by 0.23 eV for these two interfaces. The MIGS are incapable of pinning the Fermi-level because the electronic charge-density in the interface plane varies by as much as $6 \times 10^{14}\ cm^{-2}\ eV^{-1}$ and overwhelms MIGS screening. An examination of Fig. 29(b) and (c) reveals that the fraction of MIGS that are occupied is quite different: 0.38 for the Ga-terminated interface and 0.57 for the As-terminated interface. This usually implies that the semiconductor side of the interface is positively and negatively charged, respectively, for the two interfaces. Since the same metal, with only one work function, was used to contact GaAs, the CNL concept would predict either positive charge for both interfaces, or negative charge for both interfaces. But actually both interfaces are essentially neutral, due to the formation of MIGS at a different band gap (10 eV below the VBM). These results show a lack of direct connection between the Fermi-level in the gap and the neutrality of the semiconductor. Calculations have also been done

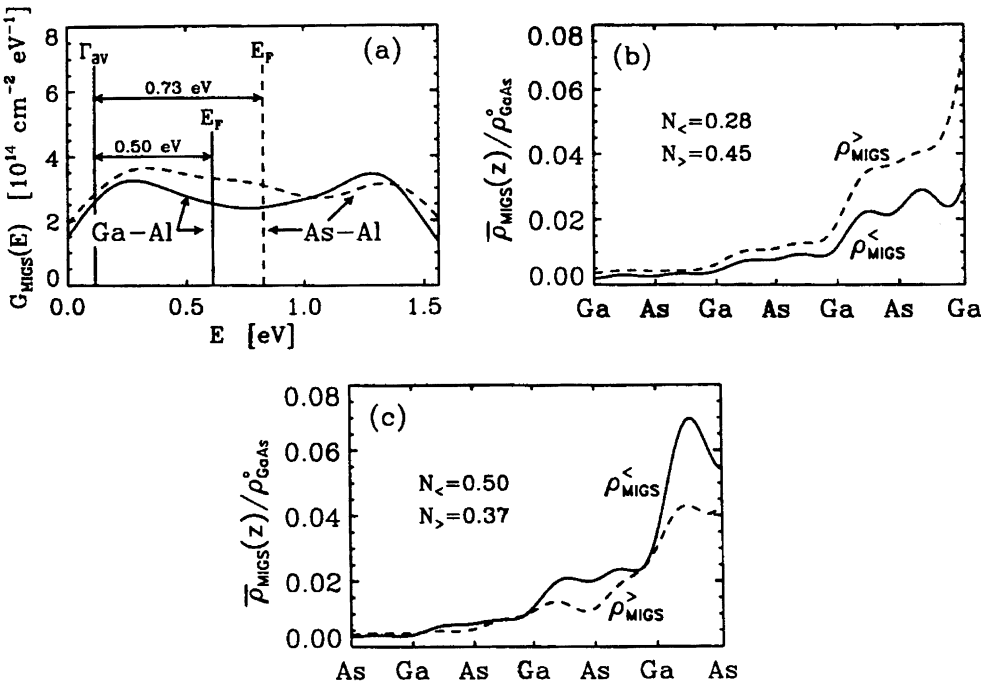

Fig. 29. (a) State density of the metal-induced states in the fundamental GaAs band gap. The solid line is for a structure with Ga–Al interface bonding, while the dashed line is for a structure with As–Al interface bonding. (b) Charge density in the MIGS (solid line filled MIGS, dashed line empty MIGS) for the structure with Ga–Al interface bonding, averaged over *xy*-planes. The leftmost Ga lies farthest from the Al interface; the rightmost Ga is bonded to Al. $N_<$ and $N_>$ are the number of electrons (per interface area $a^2_{GaAs}/2$) in the filled and empty MIGS, respectively. (c) Same as (b) for the structure with As–Al interface bonding (from Dandrea and Duke [81]).

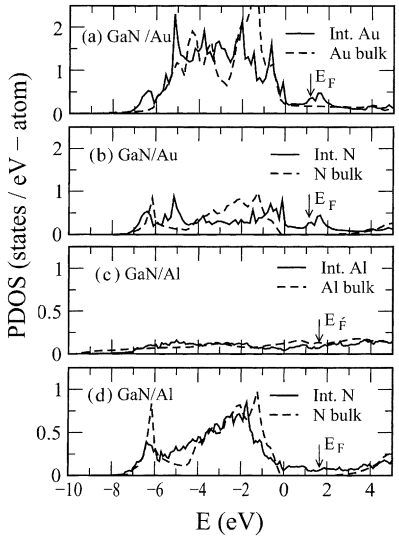

Fig. 30. Projected density of states for interface atoms in the GaN–Au and GaN–Al systems. In all panels, dashed lines indicate the corresponding atomic contribution in the bulk materials. The GaN VBM is taken as zero of the energy scale. Vertical arrows indicate E_F with respect to the semiconductor VBM (after Picozzi et al. [92]).

to study the modification of SBH by the insertion of an ultra-thin epitaxial Si or Ge layer between III and V compound semiconductors and the metal [85,86]. The epitaxial Al–GaAs(1 0 0) system has been used as a vehicle to explain this effect [87].

The SBHs of various ''assumed'' epitaxial MS structures, constructed by artificially placing metal atoms on the extended lattice sites of the semiconductor, have also been studied theoretically [21,88–92]. In good agreement with conclusions drawn from ''real'' epitaxial MS interfaces, the SBH and the distribution of MIGS were both found to depend on the identity of the metal, as well as on the detailed structure of the interface. Shown in Fig. 30, in solid lines, are the projected densities of states on atoms at the plane of a Au–GaN(0 0 1) and Al–GaN(1 0 0) interfaces [92]. The DOS distributions around both the Au and the N atoms are significantly altered from their bulk distributions, shown in dashed lines. Peaks in MIGS were found near E_F for nitrogen atoms at the Au–GaN interface. The interesting thing is that the same peaks were also found in the Au DOS. An analysis of the spatial distribution of the MIGS wave function in these peaks shows roughly equal weight on the interface N and Au sites [92]. In other words, MIGS states can peak inside the metal, and are not necessarily positioned inside the semiconductor as assumed in the fixed-separation model. These results indicate very active bonding between Au and N, which determines the distribution of all the interface states, including MIGS. This strong bonding is also in contrast to the passive role played by the metal in the fixed-separation model of MIGS pinning, where the valence band states of the semiconductor are assumed to be disturbed at an interface only to the extent that states near the band edges are pulled into the gap.

Very consistent results have been seen from all the first principles calculations on the SBH of epitaxial MS interfaces. They can be summarized as follows: (1) the SBH depends on the bonding structure of the interface; (2) the distribution of MIGS and the CNL are not intrinsic properties of the semiconductor, they depend on the interface structure; (3) the distribution of all charges, including MIGS, states below the VBM, and states in the metal, determines the interface dipole. From these findings, one can view the formation of SBH as a result of two mechanisms: the line-up of energy states according to the initial ''baseline'' charge densities, and the redistribution of charge due to

chemical bonding. The first mechanism is a bulk effect and it guarantees the continuity of the electric potential through the interface. The second mechanism is an interface effect, and is there to satisfy the requirement of energy minimization. These two requirements are the driving forces for the MIGS and other interface states to be created. Interface dipoles do not form as a result of passive charge transfer between the metal and some pre-existing MIGS. Instead, the formation of the interface dipole is much more active and complicated, i.e. MIGS are created because of bonding.

4.4. Bond-polarization theory

4.4.1. The need for a bond-based explanation of Fermi-level pinning

First principles calculations clearly demonstrated that the SBH of single crystal MS interfaces depends on the bonding and the structure of the interface. Such a picture is also in excellent agreement with the observation of SBH inhomogeneity at most polycrystalline MS interfaces, to be discussed. A polycrystalline interface is just a collection of many small, individual, differently structured, single crystal interfaces. Therefore, the SBH mechanism determined at single crystal interfaces should also govern the formation of interface dipole at polycrystalline interfaces. But any attempt to unify the diversified views on SBH mechanism at these two fronts soon faces two problems. One problem is that the structure of polycrystalline interfaces is essentially unknown. The other is that the structure and, hence, the SBH of a polycrystalline MS interface is inhomogeneous, which means that the macroscopic SBH measured from such an interface is a (weighed) statistical average of a range of SBHs. This line of reasoning makes the experimentally observed Fermi-level pinning phenomenon even more intriguing. After all, why should the SBH, which depends so sensitively on the structure of epitaxial interfaces, average out to nearly constant values for polycrystalline MS interfaces which are independent of even the metal? It was exactly the Fermi-level pinning effect that inspired the proposal of the many flavors of the fixed-separation model. These ad hoc mechanisms, by design, could explain the Fermi-level pinning phenomenon very well, but they involve unrealistic assumptions and they are not compatible with the single crystal SBH results. There is little doubt that the relevant physical laws are identical at all MS interfaces. So, the Fermi-level pinning phenomenon must have an explanation within the chemical bonding picture. And if indeed one can be found, a coherent explanation of all the SBH results may finally become within reach.

If one takes a moment to reflect upon exactly what the bonding-associated SBH mechanism is, which was revealed by first principles calculations [77,81], one realizes that there is little that one can pinpoint and make use of in a general model. The complicated numerical solutions of the electronic densities all but completely masked the simple physical and chemical reasons for the actual charge densities to take shape. Without identifiable rules, the numerical approach simply cannot be applied to polycrystalline interfaces. But actually the rules for charge distribution in any matter are already well known. The hybridization of orbitals and the creation of bonding and anti-bonding states are all familiar concepts that reduce the overall energy. This past decade has seen a clear movement toward studying the electronic structure of materials in real space [93,94]. The phase stability and the electronic and optical properties of solids and molecules have generally found qualitative, or even semi-quantitative, agreement with simple rules within the tight-binding picture of chemical bonds. The real-space approach is particularly important for polycrystalline MS interfaces where the structure is inhomogeneous. The ‘‘averaging’’ of bond configurations likely filters out the variations in the interface dipole due to changes in the fine details of the interface structure and leave behind the bare essence of interface charge distribution. In other words, the SBH average is expected to reflect the essential chemistry of the interface, which manifests itself most prominently

in individual (and isolated) MS bonds. Thus, the methodology and philosophy used by chemical physicists to analyze chemical bonds of small molecules are expected to shed light on the SBH problem at hand. This was the basic premise for the development of a bond-polarization theory of SBH formation. Our discussion in this section will essentially follow the approach adopted by Tung. Readers are referred to the original publications for details in the mathematical derivation [14,95].

4.5. Polarization of chemical bonds in molecules

There are a few methods of estimating the dipole moment of a molecule. In the simplest case of a heteronuclear diatomic molecule with s-valence orbitals, the most intuitive way to calculate the dipole moment is to approximate molecular orbitals by a linear combination of atomic orbitals (LCAO). Relevant to the relative weight of the bonding molecular orbital are the difference in the orbital energies for the individual atoms, ΔE, and the bond integral, φ, which is negative for s-electrons. It has been shown that [94], for a total bond order of one, the charge transferred from the atom with the higher energy level (atom A) to the atom with a lower energy level (atom B) is

$$n_{\mathrm{B}} = \frac{x^2 + x(1+x^2)^{1/2}}{1 + x^2 + x(1+x^2)^{1/2}} = x - x^3 + \cdots, \tag{4.5.1}$$

where x (i.e. $\Delta E/|\varphi|$) is the normalized atomic energy-level mismatch and n_{B} is the number of excess electrons on atom B. In the case of a small energy difference in the original atomic levels, the total charge transferred from A to B is simply $-ex$ and the dipole moment is exd_{AB}, where d_{AB} is the inter-atomic distance for the AB molecule.

A second method which allows all the atomic charges of a large molecule to be estimated simultaneously is the electrochemical potential equalization (or electronegativity equalization) method (ECPE) (CPEE) [14,96–100]. In this scheme, the molecular energy is approximated by a second order Taylor expansion about the neutral atoms. The energy of the ith atom in a molecule is [98]

$$E_i(n_i) = E_i^0 + U_i n_i + \tfrac{1}{2} Y_i n_i^2 + \cdots, \tag{4.5.2}$$

where E_i^0 is the ground state energy for the neutral atom, $-en_i$ is the net charge, and U_i and Y_i are the first and second derivative of the energy of the atom with respect to n_i, respectively i.e. $U_i = (\partial E_i/\partial n_i)_{n_i=0}$ and $Y_i = (\partial^2 E_i/\partial n_i^2)_{n_i=0}$. For an isolated atom, U_i and Y_i are ill-defined because strictly speaking, the energy is only defined for integral n_i and is not differentiable around $n_i = 0$. However, within the spirit of the density functional theory [100,101], and using an ensemble average of the various configurations [102], these quantities have been argued to be meaningful. Analyses show that U_i is the Mulliken electronegativity ($U_i = \chi_i/2 + I_i/2$, where χ_i and I_i are the electron affinity and the ionization potential of the atom, respectively) and Y_i is the idempotential, or the hardness [98,103], of the isolated atom ($Y_i = I_i - \chi_i$). The total energy of a molecule is then the sum of the energies of the individual atoms and the interactions between them. Representing the off-diagonal elements of the hardness matrix with only Coulombic interactions, one writes

$$E_{\mathrm{tot}}(n_1, n_2, \ldots, n_N) = \sum_i^N \left(E_i^0 + U_i n_i + \frac{1}{2} Y_i n_i^2 \right) + \sum_{i \neq j}^N \frac{n_i n_j J_{ij}}{2}, \tag{4.5.3}$$

where J_{ij} is the Coulombic interaction between one electron located at atomic positions i and another at the position of the jth atom, i.e. $J_{ij} = e^2/\varepsilon_0 d_{ij}$, where d_{ij} is the distance between these two atoms.

The task now is to minimize E_{tot}, subject to the constraint that the net charge of the molecule is zero. Mathematically, this sort of problems is most conveniently solved by the method of Lagrangian multipliers. Here, Lagrange's undetermined multiplier is obviously the electrochemical potential, $\partial E_{tot}/\partial n_i$, for each atomic site. In thermal equilibrium, the requirement that the electrochemical potential is constant throughout the molecule then allows the charge transfer between atoms to be estimated. This method predicts the correct trend, if not always numerically accurate values, of the observed electric dipoles in molecules. Since the included interaction contains no dipolar or higher-order terms, this method obviously applies only to the situation where the charge on each individual atom is centered on its nucleus. In reality, the electric dipole in molecules can be much more complicated [99,100,104,105]. In addition, the division of molecular charge distribution into individual atomic charges can be ambiguous [105]. Its faults notwithstanding, this method is simple and has a sound basis. Its use in the study of MS interfaces seems adequate, since one is only interested in explaining the systematic trend of the SBH, rather than determining accurate numerical values for individual SB systems.

4.5.1. Bonds and dipoles at metal–semiconductor interfaces

To account for the chemical effect which takes place at a MS interface, one assumes that the Schottky dipole can be identified with the polarization of the chemical bonds. Within the simple picture of charge transfer, Eq. (4.5.1), one can assume a uniform density, N_B, of chemical bonds, each with a dipole of exd_{MS}, to be present at a MS interface. Here d_{MS} is the distance between metal and semiconductor atoms at the interface. The SBH from such a dipole layer is given by

$$\Phi_{B,p}^0 = I_S - \phi_M + \frac{e^2 x N_B d_{MS}}{\varepsilon_{int}}. \tag{4.5.4}$$

From Eq. (4.5.1), x is related to the difference in atomic orbital energies. This definition of x does not seem appropriate for an MS interface, considering the fact that the atoms involved in the interface bonds are already bonded in their respective crystals. Thus, one can conceivably substitute ΔE with some other parameter that reflects more appropriately the energy mismatch across the MS interface. In that respect, the difference between the Fermi-level of the metal and the CNL of the semiconductor might take the place of ΔE. Making the switch $x \to (\phi_M - I_S + \phi_{CNL})/|\varphi|$, one sees that interface bond-polarization leads to the expected Fermi-level pinning effect:

$$\Phi_{B,p}^0 = \gamma_B(I_S - \phi_M) + (1 - \gamma_B)\phi_{CNL}, \tag{4.5.5}$$

where

$$\gamma_B = 1 - \frac{e^2 N_B d_{MS}}{\varepsilon_{int}|\varphi|}. \tag{4.5.6}$$

Eq. (4.5.5) has the same functional form as that predicted by models of interface gap states, Eq. (2.3.6). However, it is not very useful for comparisons with experimental results, because the bond integral φ is specific to each MS system. Furthermore, the assumptions on s-valence electrons and non-interacting dipoles in this approach are obviously not very realistic. Despite these shortcomings, the chemical trend suggested by Eq. (4.5.6) is still a valid one. It is interesting to note that here the Fermi-level pinning would be weakened if the dielectric screening, ε_{int}, were to increase. Such a dependency is in good agreement with the general concept of screening, namely, screening acts in the direction opposite to that of charge transfer. The charge transfer itself is driven by chemistry, not screening.

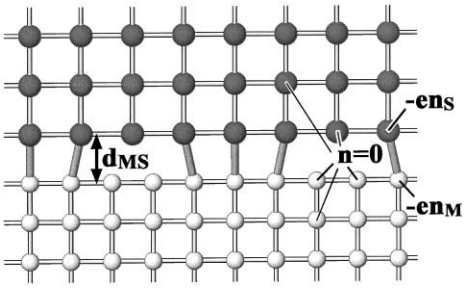

Fig. 31. A cross-sectional view of the model of a metal–semiconductor interface, used in the chemical bonding theory. A number of bonds, drawn as thick bars, are assumed to form between the semiconductor (upper half) and the metal (lower half). Charge transfer is assumed to occur only between atoms directly involved in the interface bonds.

To apply the chemical potential equalization method to estimate the charge transfer and electric dipole at an MS interface, one can regard the entire metal–semiconductor region (ISR) as a giant "molecule" [14]. A few planes of atoms each from the semiconductor and metal lattices are included in this molecule, consisting a total of N_B metal atoms and N_S semiconductor atoms. The MS interface is assumed to be atomically abrupt and the two truncated lattices are assumed to form a density of chemical bonds, N_B, on an atomically flat interface plane, as schematically shown in Fig. 31. In general, N_B need not equal, and is likely less than, the total number of semiconductor (or metal) atoms per unit area of the interface. Lattice mismatch, structure incompatibility, the formation of tilted bonds, etc. all tend to reduce the number of effective bonds formed across an MS interface. To simplify the problem, one assumes that the semiconductor is either an elemental semiconductor or, in the case of a compound semiconductor, consists of hybrid atoms, i.e. atoms which possess the traits of the compound rather than the individual (anion and cation) atoms. Without loss of generality, one assumes chemical bonds to form in a square array with a lateral dimension of d_B (i.e. $N_B^{-1/2}$). The total energy for the ISR can be written down as

$$\begin{aligned} &E_{\mathrm{ISR}}(n_{\mathrm{M}_1},\ldots,n_{\mathrm{M}_{N_\mathrm{M}}},n_{\mathrm{S}_1},\ldots,n_{\mathrm{S}_{N_\mathrm{S}}}) \\ &\quad=\sum_i^{N_\mathrm{M}}\left(E_\mathrm{M}^0+U_\mathrm{M}n_{\mathrm{M}_i}+\frac{1}{2}Y_\mathrm{S}n_{\mathrm{M}_i}^2\right)+\sum_i^{N_\mathrm{S}}\left(E_\mathrm{S}^0+U_\mathrm{S}n_{\mathrm{S}_i}+\frac{1}{2}Y_\mathrm{S}n_{\mathrm{S}_i}^2\right) \\ &\qquad+\sum_{i\neq j}^{N_\mathrm{M}}\frac{n_{\mathrm{M}_i}n_{\mathrm{M}_j}J_{\mathrm{M}_i\mathrm{M}_j}}{2}+\sum_{i\neq j}^{N_\mathrm{S}}\frac{n_{\mathrm{S}_i}n_{\mathrm{S}_j}J_{\mathrm{S}_i\mathrm{S}_j}}{2}+\sum_{i,j}^{N_\mathrm{M},N_\mathrm{S}}n_{\mathrm{M}_i}n_{\mathrm{S}_j}J_{\mathrm{M}_i\mathrm{S}_j}. \end{aligned} \tag{4.5.7}$$

The boundary condition for the ISR naturally requires all n_{M_i} and n_{S_j} to be zero on the extreme outside atomic planes of the ISR. Taking that condition to the limit, we shall assume n to be non-zero only for those metal and semiconductor atoms on the immediate interface planes which are directly involved in the bonding (see Fig. 31). Then, from symmetry, each metal atom involved in the bonding contains the same net charge of $-en_\mathrm{M}$, and every semiconductor atom involved in the bonding contains a net charge of $-en_\mathrm{S}$ (i.e. $+en_\mathrm{M}$). As will be discussed, this approximation turns out to be necessary for the use of the ECPE method at MS interfaces. One now minimizes the total energy by equating the electrochemical potentials for interface atoms. Setting $n_\mathrm{M}=n_\mathrm{S}$, one obtains

$$n_\mathrm{S}=\frac{U_\mathrm{M}-U_\mathrm{S}}{Y_\mathrm{S}+Y_\mathrm{M}-2J_{\mathrm{MS}}+4J_{\mathrm{MM}}+4J_{\mathrm{SS}}}. \tag{4.5.8}$$

In the spirit of analyzing charge transfer between two crystals, rather than between atoms, one can let the atoms acquire bulk characteristics. For a bulk metal, the ionization potential and the electron affinity are both identified as the work function of the metal, ϕ_M. Thus, $U_M = \phi_M$ and $Y_M = 0$. For a semiconductor, the ionization potential, I_S, and the electron affinity, χ_S, differ by its band gap, E_g. Therefore, $U_S = I_S - E_g/2$ and $Y_S = E_g$. Also, to account for the fact that the Coulombic interactions take place inside a solid rather than in free space, screening by the respective dielectric medium is also assumed. Eq. (4.5.8) becomes

$$n_S = \frac{I_S - \phi_M - E_g/2}{E_g + \kappa} \tag{4.5.9}$$

where κ is the sum of all the hopping interactions, i.e.

$$\kappa = 4J_{SS} + 4J_{MM} - 2J_{MS}, \tag{4.5.10}$$

which is expected to be small, compared with the band gap of typical semiconductors, because of dielectric screening. The Schottky dipole across the MS interface, which is equivalent to $e\Delta_{gap}$ drawn in Figs. 13 and 15, as a result of the charge transfer, is

$$e\Delta_{Sch} = -\frac{e^2 N_B d_{MS}(\phi_M - I_S + E_g/2)}{\varepsilon_{int}(E_g + \kappa)}, \tag{4.5.11}$$

and the SBH is

$$\Phi^0_{B,p} = \gamma_B(I_S - \phi_M) + (1 - \gamma_B)\frac{E_g}{2}, \tag{4.5.12}$$

where

$$\gamma_B = 1 - \frac{e^2 N_B d_{MS}}{\varepsilon_{int}(E_g + \kappa)}. \tag{4.5.13}$$

Obviously, Eq. (4.5.12) predicts a dependence of the SBH on the metal work function which is similar to that predicted by gap state models, Eq. (4.2.2), with $E_g/2$ taking the place of the CNL. However, the ''interface parameter'', γ_B, according to the equilibration of chemical potential method is quite different from that predicted by the gap state models, Eq. (4.2.3). Experimentally observed S_Φ [68] is plotted in the format $\varepsilon_0/\varepsilon_\infty(1 - S_\Phi)^{-1}$ against the band gap of the semiconductor in Fig. 32. A linear relationship is observed in Fig. 32, in good agreement with the prediction of the bond-polarization theory of SBH formation. The deduced slope of this plot gives an estimate of N_B of $\sim 3 \times 10^{14}$ cm^{-2}, which is a very reasonable estimate of the number of available bonds on a typical semiconductor surface. The intercept with the x-axis yields a value to -0.68 eV for κ, which also compares very favorably with the numerically calculated value of -0.76 eV, based on values of N_B and d_{MS} deduced/assumed earlier [95]. These agreements lend strong support for the validity of the bond–polarization view of the formation of the Schottky dipole at MS interfaces.

4.5.2. Limitations of electrochemical potential equalization approach

The bond-polarization theory arbitrarily imposes the constraint that the charge transfer at the interface is limited to those atoms on the immediate interface planes. This condition seems to capture the essence of the problem while still keeping the problem tractable at the intended level of

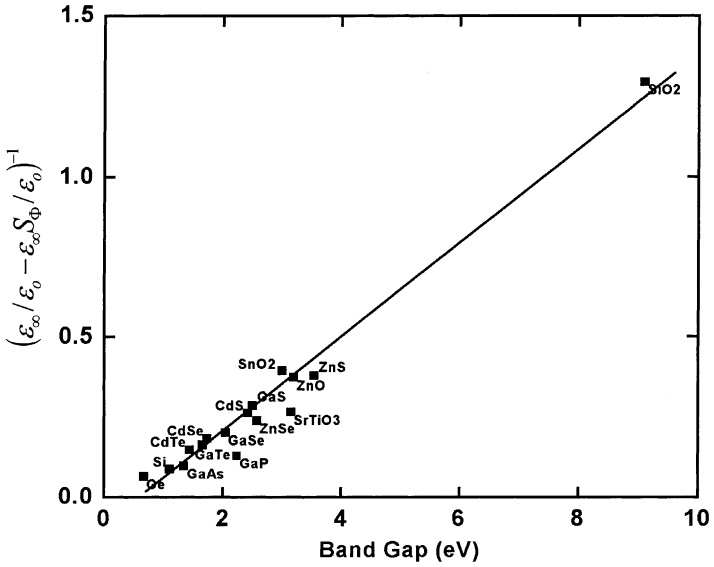

Fig. 32. Experimentally observed interface behavior parameter [68], plotted as $(\varepsilon_\infty/\varepsilon_0 - \varepsilon_\infty s_\Phi/\varepsilon_0)^{-1}$ against the band gap of the semiconductor.

sophistication. But its value lies deeper than its superficial advantages. Without this assumption, the electrochemical potential equalization approach would not be appropriate for the MS interfaces. To see the consequence in the absence of this assumption, one can write down the electrochemical potential for a semiconductor atom in the ISR, but not directly involved in the interface bonding. An attempt to equate the electrochemical potentials across the interface, of atoms not directly involved in the bonding, leads to the following expression:

$$I_S - \phi_M - \frac{E_g}{2} = \frac{e^2 N_B d_{MS} n_S}{\varepsilon_{int}}, \tag{4.5.14}$$

which simply states that the SBH should be one-half of the band gap:

$$\Phi^0_{B,p} = \frac{E_g}{2}. \tag{4.5.15}$$

This result apparently contradicts Eq. (4.5.12) obtained earlier. This discrepancy actually has little to do with the approximation that was made on the limited range of the charge transfer, but is related to the presence of an energy gap in the semiconductor. One notes that even if the charge transfer were not limited to the immediate planes of the interface, Eq. (4.5.15) would still be obtained by equating the chemical potentials of atoms far from the interface.

To understand the crux of the problem, we take a closer look at the ECPE technique. An inherent assumption of this method is that the energy at each atomic site is analytical near zero net charge [101]. This assumption breaks down when a band gap is present. One notes that a semiconductor at low temperatures will remain essentially uncharged irrespective of the exact position of the Fermi-level, so long as the Fermi-level is positioned inside the band gap. Because Y_S, the hardness of an atom, is proportional to the inverse of the density of states near the CNL of the atom, it becomes indefinable when the hardness concept is applied to a semiconductor. Inside a band gap, the density of states is zero, resulting in a singularity in Y_S at $n_S = 0$. Therefore, strictly

speaking, the ECPE method cannot be used for a semiconductor or any other material with zero density of states at its CNL position. What saves this method and still makes it a valuable technique to estimate the interface dipole semi-quantitatively, if not with great precision, is the fact that MIGSs are present at the semiconductor atoms immediately in contact with the metal. In other words, the electrochemical potential for the semiconductor atoms involved in the interfacial bonding is well defined and, therefore, can be used to analyze the transfer of charge between this layer of atoms and the metal. The chemical shift between the first layer of semiconductor atoms and the second or third layer of semiconductor atoms, which is expected to be small anyway, cannot be deduced using the ECPE method. Therefore, the assumption that only the first layer of semiconductor atoms is involved in the charge transfer is an important condition for the use of the ECPE method at MS interfaces.

In the transition of Eqs. (4.5.8) and (4.5.9), U_S has been identified as $I_S - E_g/2$ in analogy with the corresponding quantity for the individual atom ($[I + \chi]/2$). The later term is the de facto CNL of the individual atom. Because of the significant differences between atomic levels and semiconductor band structures, U_S need not be immediately identified with the midgap energy. Various proposals for the CNL [50,69,106] are all reasonable candidates for this characteristic energy level. Some thought could also go into the choice of the bulk-equivalent of Y_S, the atomic ''hardness'' which is a measure of the repulsion between electrons in the same atom. A direct translation identifies the band gap of the semiconductor as Y_S. As already mentioned, Y_S is actually ill-defined for an unperturbed semiconductor because of the presence of its band gap. At the interface, the singularity is removed because of MIGS, but the question remains as to whether E_g best represents the hardness of interfacial semiconductor. A possible replacement of this term is the square-root of the second moment of atomic bonds in the moments theory [94,107]. These issues still remain unsettled for the application of the chemical potential equalization method at MS interfaces. Actually, its use in molecules has also not been without debate. Under scrutiny, these uncertainties represent the most serious problem of the bond-polarization theory of SBH formation, although they do not affect the validity of the overall view on the bonding-related charge-transfer at the interface.

The interface parameter, γ_B, can become negative according to the bond-polarization picture, for semiconductors with small band gaps [14]. The MIGS on narrow-gap semiconductors have long decay lengths, which means that the limitation of charge transfer to one atomic plane is inappropriate for narrow-gap semiconductors. Charge transfer involving two or more layers of atoms needs to be considered to estimate the interface dipole under these circumstances, invalidating the necessary condition of the present method. It should also be kept in mind that the higher order terms ignored in the bond-polarization theory may bear heavily on the interface dipole for narrow-gap semiconductors. This suggests that the ECPE approach is only valid for semiconductors with large band gaps. Even though the bond-polarization theory is not applicable to narrow-gap semiconductors, the suggestion that γ_B can become negative is not necessarily preposterous. This is because, unlike the MIGS picture which requires smeared-out, pancake-shaped orbitals, the Coulomb interaction for three-dimensional orbitals, assumed in the bond–polarization picture, does not amount to a monotonous negative feedback mechanism for metal work function change [95]. As a matter of fact, a negative S_Φ has been reported experimentally on MoS_2, a narrow-gap semiconductor [108].

4.6. Comparison of the bond-polarization and the MIGS approaches

According to the bond-polarization theory, the polarization of interfacial bonds can quantitatively account for the Fermi-level pinning phenomenon experimentally observed at polycrystalline MS

interfaces. Traditionally, the Fermi-level pinning effect has been attributed to the presence of MIGS. Since the dependence of the SBH on the metal work function is predicted in very similar fashions by the bond-polarization theory and the fixed-separation model of MIGS, it is worthwhile to explore possible connections between these two theories. We will first examine the similarities. Both theories recognize that, due to the requirement of the minimization of total energy, the charge density at a MS interface needs to relax from the frozen distributions assumed in the Schottky–Mott model. This charge relaxation is assumed by both theories to be the source of the additional interface dipole, the Schottky dipole, and the origin of the Fermi-level pinning effect. So, both theories try to estimate the optimum amount of charge transfer that minimizes the energy. That the interface energy is minimized is ensured in the bond-polarization theory through the use of the Lagrange's multipliers method. Since the fixed-separation model of MIGS specifically works with the Fermi-level, it also should lead to a minimized interface energy, albeit only implicitly. The fact that the fixed-separation model of MIGS is also based on the ECPE method has been explicitly demonstrated [95]. Therefore, the MIGS fixed-separation theory and the bond-polarization theory deal with the same phenomenon, charge transfer at MS interface; the two theories are also based on the same principle, the minimization of interface energy. However, there are significant differences in the assumptions and methodologies used in these theories.

The biggest difference between these two theories is probably the ''basis set'' used in the analysis. As an example of the significance of the basis set, we first look at the analogous case of molecular states versus atomic states in molecules. In the analysis of molecular dipoles, the basis set used in the ECPE method, Eq. (4.5.3), is the isolated atomic levels prior to the formation of molecules. The eventual charge distribution in the molecule is expanded in the basis set of atomic states, whose spherical distribution around each nucleus validates the use of point charges to represent atomic charges and the neglect of off-diagonal terms [96,98]. This approach rightfully ignores the details of how molecular orbitals are actually formed. Even though the ''density of states'' projected onto each atom will change upon the formation of molecules, this change is a derivative of, and can be predicted from, the distribution of the initial energy levels. Therefore, the energy levels of an oxygen atom can be used to analyze dipoles of all small molecules containing oxygen, e.g. CO and N_2O. Alternatively, one can use the molecular states as the basis set to analyze the molecular dipole. This involves first solving for the molecular orbitals, with, for example, the LCAO approach, and then calculating the dipole moment from the sum of charge densities of all the occupied molecular orbitals. Irrespective of which basis set (atomic or molecular) is used, similar dipole moment should be obtained for the molecule. For systematic studies, however, the use of the molecular states as the basis set is inconvenient because the basis set changes with molecules and needs to be solved for different molecules. In other words, one cannot use the orbitals of a CO molecule to analyze the dipole moment of an N_2O molecule. The bond-polarization theory is, in spirit, similar to the analysis of molecular dipoles in terms of atomic states, while the MIGS fixed-separation theory is similar to the approach based on molecular states. The use of the bulk band structure of the isolated semiconductor and metal crystals, as done in the bond-polarization theory, naturally allows the analysis of the SBHs observed for different metals with similar N_B and d_{MS}, because these are only geometrical parameters. In the MIGS theory, however, the basis set is the MIGS. In an attempt to perform systematic analysis, the MIGS theory has to assume that the distribution of MIGS is independent of the metal. This is inappropriate, since calculations already showed that the actual distribution of MIGS depends on the metal [76,77,81].

Another difference between the two theories is the discreteness of the individual bonds in the bond-polarization theory versus the smeared-out charge distribution in the MIGS theory. This difference reduces the interface electrostatics from a three-dimensional problem for the

bond-polarization theory, to a one-dimensional problem for the fixed-separation model of MIGS. The one-dimensionality of the fixed-separation model allows the Coulomb interaction to be expressed in a closed form, which leads to a Schottky dipole, Eq. (2.3.2a), that is proportional to the *final* difference between the characteristic energy levels of the metal and the semiconductor. Therefore, this term works like a negative feedback in a unity-gain amplifier, with the resulting overall gain quite predictably given by Eq. (2.3.5), in a form of $(1+F)^{-1}$, where F is the transmission factor of the feedback circuit [95]. In contrast, the Schottky dipole in the bond-polarization theory, Eq. (4.5.11), is proportional to the *initial* energy difference, indicating an absence of feedback mechanism. So the difference in the functional forms of γ for the two theories, i.e. Eqs. (4.2.3) and (4.5.13), can be attributed to the different dimensionalities of the two theories. However, since both theories are linear, their distinction exists only in the range of achievable γ-values.

The third difference between the bond-polarization theory and the MIGS fixed-separation theory concerns the length of charge transfer at the interface. In the bond-polarization theory, the charge transfer is associated with bond formation and, therefore, d_{MS} is assumed to be the length of one atomic plane, $\sim$0.25 nm. In the MIGS picture, the density of interface charge decays exponentially with some ''penetration depth''. In the original jellium calculations [20] the penetration depth was found to be as short as 0.1 nm for ionic semiconductors and $\sim$0.3 nm for covalent semiconductors. Such a length for the charge transfer is obviously characteristic of bond formation at the interface, which involves interactions between the metal and the semiconductor. However, the capability of the MIGS model to analyze SBH systematics relies on the assumption that the distribution of MIGS is independent of the metal. To be consistent with that assumption, the scenario is usually created in the MIGS model that the MIGS charge resides at the tail end of metal wave functions which tunnel into the semiconductor. Typically, δ_{int} in the fixed-separation model of MIGS is assumed to be $\sim$0.5–2 nm [70]. With the spatial extension of their exponential tails into the semiconductor, MIGSs were often assumed to lead to band bending in the semiconductor as far as 5–10 nm away from the MS interface [71,72]. As a result of such large distances, the charge transfer in the MIGS theory is envisioned to take place passively, between the metal and some pre-existing MIGSs in the semiconductor. Conversely, the bond-polarization theory views the creation of all interface states (including the MIGS) as a result of active interaction involving both the metal and the semiconductor.

5. Measurement of Schottky-barrier height

5.1. Current–voltage behavior: homogeneous SB

One of the most widely used techniques to measure the SBH is the current–voltage (*I–V*) technique. In particular, the forward-bias portion of the *I–V* characteristics has often been used to deduce the magnitude of an SBH. The transport of carriers across a MS interface is very sensitively dependent on the magnitude of the energy barrier, SBH. So, the measurement of the SBH figures to be a relatively straightforward task. This is in principle correct. However, the interpretation of experimental results of SBH measurements, in particular *I–V* data, has not been without controversies and debates. Some of the confusion is clearly linked to a failure to recognize the many different looks an inhomogeneous SBH can give to the measured *I–V* characteristics. Discussions of current transport at SBs, thus, need to distinguish between the behavior expected of homogeneous SBH and that expected of inhomogeneous SBH. For the present discussion, a homogeneous SBH can be roughly defined as one whose SBH varies on a lateral length scale much

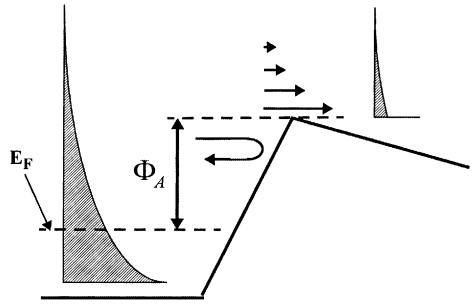

Fig. 33. Schematic of the thermionic emission process of electrons from a reservoir (left) over a barrier with a barrier height of Φ_A. Note that this process is independent of the shape of the barrier and that the barrier height is measured from the Fermi-level.

longer than the depletion region length. As will be shown, this condition corresponds to the case where the current transports across different regions behave independently. The principal mechanism responsible for the current flow at the majority of Schottky diodes on non-degenerate semiconductors has been shown by various studies to be the thermionic emission process. According to theory, the thermionic emission of electrical carriers from a region in thermal equilibrium, over a neighboring energy barrier, with a maximum height of Φ_A above the (quasi-) Fermi-level of that region, is

$$I_{\text{uni-directional}} = AA^*T^2 \exp\left(-\frac{\Phi_A}{k_B T}\right), \tag{5.1.1}$$

where A is the cross-sectional area of the barrier, A^* the Richardson's constant, k_B the Boltzmann constant, and T is the absolute temperature. This current, as schematically shown in Fig. 33, represents carrier transport away from the region of interest, which is in thermal equilibrium. Applying this theory to a uniform Schottky barrier under an applied bias, V_a, as shown in Fig. 34, one writes down the current flowing in the forward direction, i.e. from the n-type semiconductor to the metal, as

$$I_{\text{forward}} = AA^*T^2 \exp\left(-\frac{\Phi_{B,n} - eV_a}{k_B T}\right), \tag{5.1.2}$$

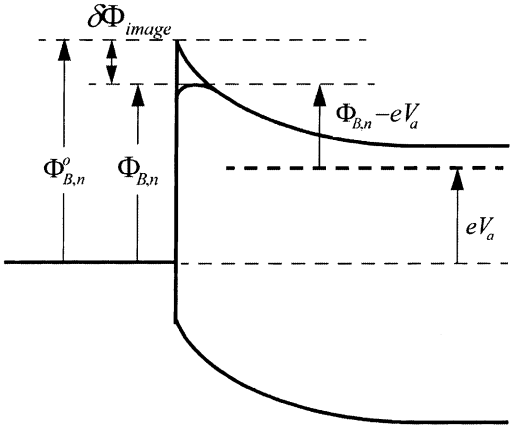

Fig. 34. Schematic of the image-force lowering (Schottky lowering) at a Schottky barrier. A forward bias is drawn.

since $\Phi_{B,n} - eV_a$ is the barrier for electrons traveling in that direction. One notices that a current of electrons originating from the metal also flows over the barrier in the reverse direction and its magnitude is independent of the applied bias:

$$I_{reverse} = I_{Sat} = AA^*T^2 \exp\left(-\frac{\Phi_{B,n}}{k_B T}\right). \tag{5.1.3}$$

So, the net current flow at the MS interface is the difference of the two:

$$I_{SB}(V_a) = AA^*T^2 \exp\left(-\frac{\Phi_{B,n}}{k_B T}\right)\left[\exp\left(\frac{eV_a}{k_B T}\right) - 1\right] \tag{5.1.4}$$

$$I_{SB}(V_a) = I_{Sat}\left[\exp\left(\frac{eV_a}{k_B T}\right) - 1\right] \tag{5.1.4a}$$

At large forward bias, $eV_a > 3k_BT$, the numeral 1 in the square bracket can be ignored, and the current should display an exponential dependence on the applied bias.

Although the prediction of the thermionic emission theory, namely Eq. (5.1.4), is familiar to most people, it is less clear exactly what the thermionic emission process is. For example, it has often been stated that the validity of the thermionic emission theory depends on the emission process at the MS interface being the rate-controlling step of electronic transmission. In other words, the transmission probability of carriers across the MS interface need to be small in order for the transport mechanism to be called thermionic emission. Alternatively, it has been shown that even if the quantum mechanical transmission probability were large, i.e. 1, the prediction of the thermionic emission theory would still be correct [109,110]. Another basic assumption usually attributed to the thermionic theory is that electrical carriers suffer a negligible number of scattering events in the space–charge region so their velocity distribution (corrected for electric potential difference) is still largely characteristic of the electrochemical potential of their origin. In other words, the distribution of carriers flowing in the forward direction in the space–charge region is controlled by the electrochemical potential of the neutral region of the semiconductor where the carriers are in local thermal equilibrium. However, more careful analyses show that such an assumption is unnecessary. For example, in Bethe's original derivation of the thermionic emission theory [111] which was largely based on intuitive arguments, a very loose definition of the condition for thermionic emission was given: that the average number of scattering must be negligible over a distance where the band bending changes by k_BT. Some of the perceived conditions for thermionic emission undoubtedly stem from the desire to draw a quasi-Fermi-level in the space–charge region under an applied bias. In reality, however, under an applied bias, carriers near the MS interface moving in one direction have a velocity distribution that is different from carriers traveling in the opposite direction. A unique quasi-Fermi-level cannot and should not be defined for the semiconductor region very close to the metal. Without the compulsion to define a unique quasi-Fermi-level, the thermionic emission process is valid irrespective of whether the quantum mechanical emission process at the top of the barrier is the rate-limiting step. In actual simulations, the emission process at the top of the barrier has not been found to be rate-limiting.

The thermionic emission process is independent of the longitudinal shape of the energy barrier, i.e. how the bands bend in the direction perpendicular to the MS interface. However, these results are only valid for barrier heights that are laterally homogeneous. The barrier height controlling thermionic emission of carriers, $\Phi_{B,n}$, actually is slightly less than the SBH, $\Phi^0_{B,n}$, because of the

effect of image-force lowering:

$$\Phi_{B,n} = \Phi^0_{B,n} - \delta\Phi_{image} = \Phi^0_{B,n} - \left[\frac{e^3 N_D V_{bb}}{8\pi^2 \varepsilon_S^3}\right]^{1/4} \tag{5.1.5}$$

As shown in Fig. 34, the maximum of the energy barrier for thermionic emission is actually inside the semiconductor, at a small distance away from the MS interface. The image-force concept, sometimes referred to as the ''Schottky lowering'' effect, is easily described in classical terms. However, it has a quantum mechanical equivalent in the form of the energy lowering due to the interaction of carriers with their exchange holes. When a carrier leaves the metal, the exchange hole left behind flattens and acts similarly to the classical image charge. The long range behavior of image-force effect has been demonstrated by ab initio calculations of the quasi-particle spectrum at MS interfaces [112]. Because of the image-force, $\Phi_{B,n}$ has a weak dependence on the interface electric field. Therefore, it depends slightly on the applied bias.

In writing down Eq. (5.1.4), it has been implicitly assumed that the entirety of the applied bias has fallen across the MS interface. In real devices, the applied bias can dissipate in voltage drops across the Ohmic contact and the bulk semiconductor. If the effect of series resistance is taken into consideration, an Ohmic drop of $I_{SB}R_S$ should be subtracted from the applied bias to render the actual voltage drop across the MS interface. One gets

$$I_{SB}(V_a) = AA^*T^2 \exp\left(-\frac{\Phi_{B,n}}{k_B T}\right)\left[\exp\left\{\frac{eV_a - eI_{SB}(V_a)R_S}{k_B T}\right\} - 1\right], \tag{5.1.6}$$

where the series resistance R_S has been assumed to be independent of the applied bias. Under this condition, the effect of series resistance can be easily deconvolved from the experimental *I–V* curves by the use of various ingeniously designed plots, as discussed in the following sections.

On heavily doped semiconductors, tunneling of carriers at energies lower than the full barrier height can lead to current that is comparable to, or even far exceeds, thermally activated transport of carriers over the barrier. Since the tunneling probability for a potential barrier increases sharply with electron energy, and the carrier density decreases exponentially with electron energy, the energy distribution of carriers that tunnel through the barrier is narrowly peaked, as schematically shown in Fig. 35. Therefore, the tunneling process can be viewed as effectively reducing the Schottky barrier for thermionic emitted carriers by a specific amount, which depends on the shape of the energy barrier and the temperature. The combined mechanism of partially thermally activation and tunneling is known as thermionic-field-emission (TFE) [113,114]. The total TFE current has been calculated within the WKB approximation to be

$$I = I_{S-TFE}\left[\exp\left(\frac{eV_a}{E_0}\right) - 1\right], \tag{5.1.7}$$

where I_{S-TFE} is the saturation current for the TFE process, and E_0 is given by

$$E_0 = E_{00}\coth\left(\frac{E_{00}}{k_B T}\right). \tag{5.1.8}$$

The parameter E_{00} is a property of the bulk semiconductor:

$$E_{00} = \frac{e\hbar}{2}\left(\frac{N_D}{\varepsilon_S m^*}\right)^{1/2}, \tag{5.1.9}$$

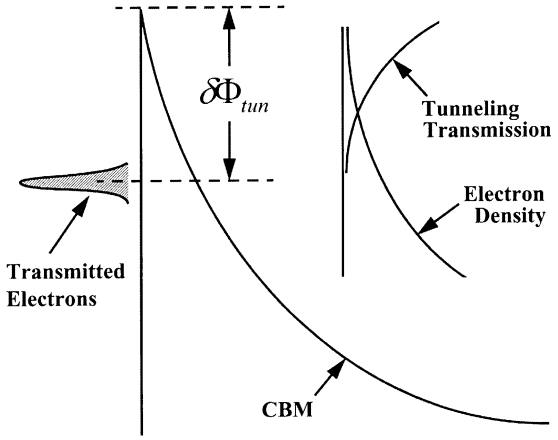

Fig. 35. Schematic of the thermionic field emission (TFE) process. The product of the electron density and the transmission coefficient leads to a sharply peaked energy profile of electrons tunneling through the tip of the potential barrier. The tunneling process leads to a reduction in the effective barrier height by $\delta\Phi_{\text{tun}}$.

and it is an indicator of how efficient tunneling is in a semiconductor. E_0 can be thought of as the amount of band bending for a semiconductor that would yield a tunneling probability of $\exp\{-1\}$ ($\sim$37%) at the base of the barrier. Since the actual band bending is usually much larger than E_{00}, some degree of thermal activation is always more efficient than direct tunneling. A comparison of E_{00} with $k_{\text{B}}T$ determines whether thermionic emission or tunneling will be more efficient near the very top of the energy barrier, i.e. whether to go over or go through the last few E_{00} (or $k_{\text{B}}T$) of the Schottky barrier. Obviously, when $E_{00} > k_{\text{B}}T$, tunneling will dominate because the Boltzmann distribution tail of thermionic emission drops off by a factor of $\exp\{-1\}$ every $k_{\text{B}}T$, which is much faster than the decrease rate of the tunneling probability. Conversely, thermionic emission will dominate whenever $k_{\text{B}}T \gg E_{00}$, because the tunneling probability drops off faster than thermionic emission in that case. As a rule of thumb, the effect due to tunneling is small at room temperature for common semiconductors with a doping level of $1 \times 10^{17}\,\text{cm}^{-3}$ or less ($E_{00} \sim 3$ meV), whereas tunneling will be very significant for semiconductors with a doping level higher than $1 \times 10^{18}\,\text{cm}^{-3}$ ($E_{00} \sim 10$ meV). As the temperature is lowered, the relative importance of tunneling naturally increases.

On semiconductors with low mobilities, electrical carriers from the semiconductor likely suffer frequent collisions and can be thermally equilibrated within a short distance of the MS interface, where the band bending has changed by less than $k_{\text{B}}T$. Under such circumstances, the local quasi-Fermi-level is well defined and has to be assumed to be close to the metal Fermi-level. Carrier diffusion become important under these circumstances and its effect on the current flow has been described in standard textbooks [3,26]. On lightly doped semiconductors and/or for large SBHs, the effects of minority carriers cannot be ignored. We will mention some interesting effects due to minority carriers to illustrate the kind of complications that could arise in a seemingly simple task of interpreting *I–V* behavior at SBs. At large forward biases, the minority carrier injection ratio increases, and the amount of stored minority carriers in the semiconductor depends sensitively on the quality of the back Ohmic contact [115–117]. Stored minority carriers can significantly affect the bulk resistivity of the semiconductor. The series resistance of the SB device thus can change with bias, leading to spurious features in the *I–V* traces [118,119]. The small signal ac response of the SB could show negative capacitance (inductance) or large excess capacitance, depending on the exact situation with minority injection [116,120]. Unfortunately, some of these spurious variations have

made it into the literature and been interpreted as real signals from interface states. At MS interfaces of large SBH (small minority carrier barrier height), the minority carrier density could approach the doping concentration, significantly increasing the electric field at the interface and causing other related effects.

5.1.1. Analysis of real I–V curves

In an *I–V* experiment, the main purpose is usually to determine the magnitude of the SBH. As the different current transport mechanisms predict slightly different functional forms of the *I–V* curves, one is often also interested in determining the transport mechanism responsible for the observed *I–V* curves. One of the most prominent parameters that can be extracted from an *I–V* trace, which seemingly reveals the transport mechanism directly is the ideality factor of that *I–V* trace. The ideality factor, n, of an *I–V* curve is defined as the inverse of the slope of the *I–V* curve, normalized by that expected of the perfect thermionic emission process. Mathematically, it is defined as

$$n = \frac{e}{k_B T}\left[\frac{\partial(\ln I_{SB})}{\partial V_a}\right]^{-1}, \tag{5.1.10}$$

$$n = \left[1 - \left(\frac{\partial \Phi_{B,n}}{e\,\partial V_a}\right)\right]^{-1}. \tag{5.1.10a}$$

Even though n is known as the ''ideality'' factor, its numerical value actually reflects the departure from ideality; namely, the larger n is, the less ''ideal'' is said of the SB. Most *I–V* curves can be fitted with a single n and expressed as (with the inclusion of the series resistance effect)

$$I_{SB} = I_{Sat}\left[\exp\left(\frac{eV_a - eI_{SB}R_S}{nk_B T}\right) - 1\right], \tag{5.1.11}$$

where I_{Sat} is the saturation current, which can be used through Eq. (5.1.4) to deduce the magnitude of the SBH. When the effect of series resistance is small, a logarithmic current versus voltage plot, at any fixed temperature, usually contains a wide enough linear section which can be used to deduce an ideality factor as well as extrapolate to zero bias to yield the saturation current. When the series resistance is significant, it is not always possible to discern a linear region from the *I–V* plot, especially for elevated temperature measurements. Various schemes have been proposed which greatly facilitate the analysis of *I–V* traces. The use of the small bias portion of the *I–V* trace [121], the use of a special function of the current and the bias [122], and the use of two temperature measurements [123] have all demonstrated some value. If incremental conductance can be calculated, such as from digitized data, then there are a few plots which allow n and R_S to be determined graphically, as illustrated in Fig. 36 [124]. In these plots, I_d is the diode current, G the small signal conductance ($G = \partial I_d/\partial V_a$), and R_{dr} is the differential resistance ($R_{dr} = G^{-1}$). It is important to remember the two assumptions one has made in writing down Eq. (5.1.11), namely, that the SBH is homogeneous and that the series resistance is independent of bias. As will be discussed below, series resistance can affect the *I–V* characteristics in many different and dramatic ways when the SBH is inhomogeneous. Also, minority carriers can leads to bias-dependent Ohmic effect. A failure to account for either of these effects could lead to erroneous conclusions of hilarious proportions [119,125].

Generally speaking, the ideality factor is an indicator of the bias dependence of the SBH. With increasing forward bias, there is a tendency for the effective SBH which controls the current

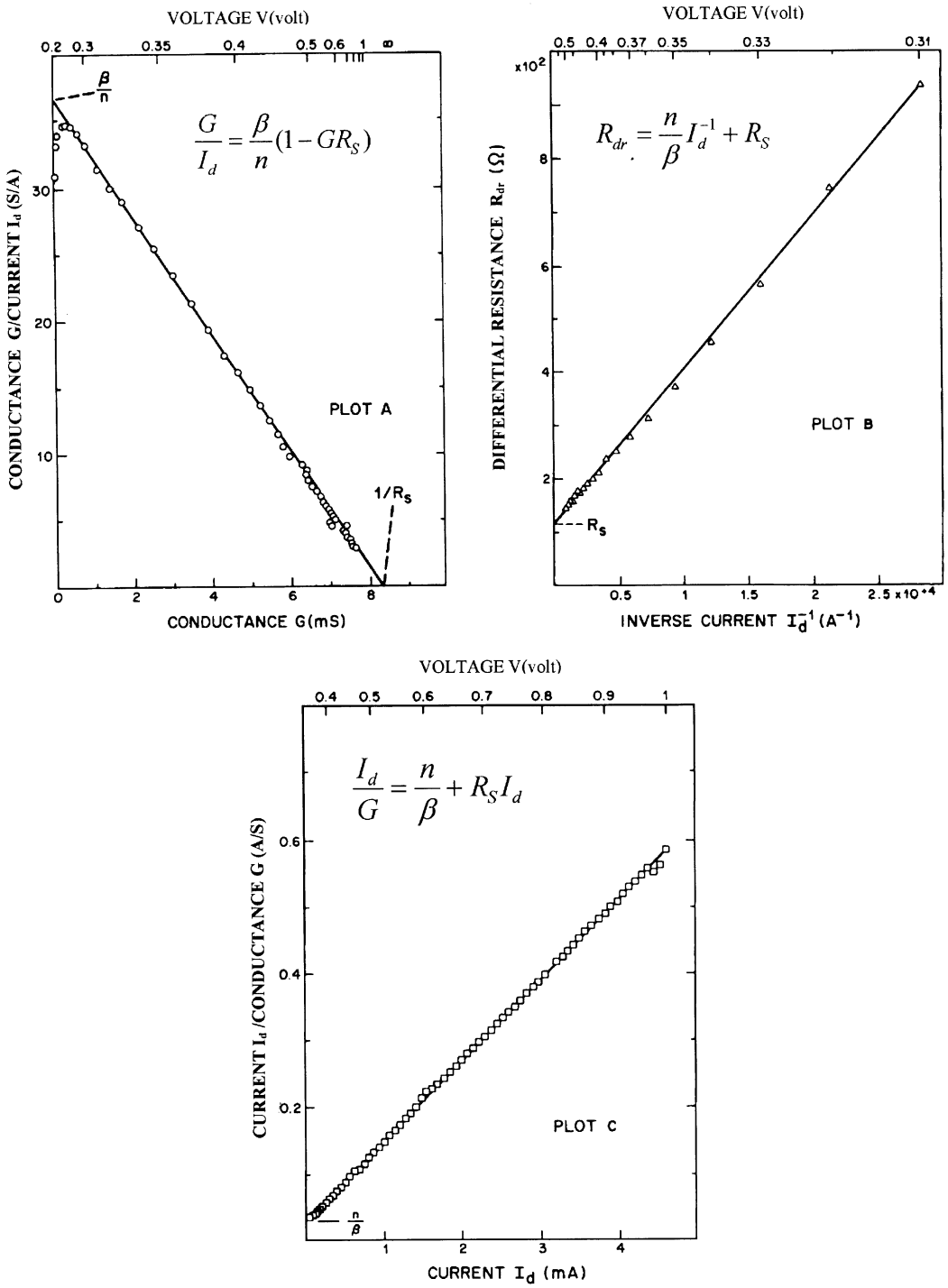

Fig. 36. The same set of experimental *I–V* data from a PtSi–Si Schottky diode, corrected for shunt resistance, is used to three different plots. The series resistance and the ideality factor of the diode can be deduced in each of these plots (after Werner [124]).

transport to also increase, giving rise to $n > 1$. Even for pure thermionic transmission, effect due to image-force lowering alone could lead to an ideality factor in excess of 1. From Eq. (5.1.5), one can derive an expression for the ideality factor:

$$n \approx 1 + \frac{1}{4}\left[\frac{e^3 N_D}{8\pi^2 \varepsilon_S^3 V_{bb}^3}\right]^{1/4} \qquad \text{(TE)} \tag{5.1.12}$$

However, this typically gives an ideality factor of only around 1.01–1.02 for non-degenerate semiconductors. With TFE, the characteristic energy at which the distribution of the transmitted electrons is peaked increases with applied bias, leading to an ideality factor that can significantly exceed unity:

$$n = \frac{E_{00}}{k_B T} \coth\left(\frac{E_{00}}{k_B T}\right) \qquad \text{(TFE)} \tag{5.1.13}$$

The ideality factor expected from TFE increases sharply at low temperature, such that the actual slope can become independent of temperature at low temperatures. As illustrated in Fig. 37, Saxena [126] has divided the temperature dependence of the ideality factor into different categories, each supposedly due to different conduction mechanisms. Beside the behaviors attributed to TFE and thermionic emission, there is also a category called "T_0" reserved for a class of diodes which, for some reasons, display this particular and striking temperature dependence. Because different transport mechanisms predict different dependence of the ideality factor on temperature, there is thus some expectation that a study of this dependency can allow a definitive determination of the transport mechanism. At least that was the accepted point of view for a long time. What has been neglected in this line of reasoning is the fact that all of these theories assume that the SBH under study is homogeneous. As will be described later, one fact that has been brought more into the

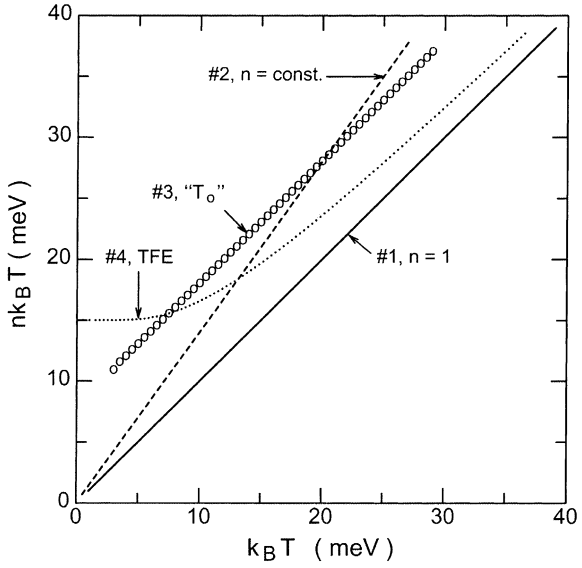

Fig. 37. Experimentally observed temperature dependence of the ideality factor from Schottky barriers. Line #1 is an ideal SB which follows the prediction of thermionic emission theory. Line #2 shows a temperature independent, greater-than-unity, ideality factor. Line #3 displays the T_0 effect. The behavior of Line #4 is usually attributed to thermionic field emission. The numbering of these lines is according to Saxena [126].

light by recent experiments is that all SBs, except those made of high quality epitaxial interfaces, contain some degree of inhomogeneity. Another fact is that most of the seemingly widely varying dependencies of the ideality factor can originate from the same transport mechanism, e.g. thermionic emission, when the SBH is inhomogeneous. These facts do not imply that the conduction mechanism at SBs is exclusively thermionic emission, but rather that the ideality factor dependency cannot be used as the only criterion for the determination of conduction mechanism.

5.2. Current–voltage behavior: inhomogeneous SB

5.2.1. Non-interacting models of inhomogeneous SB

The junction current of an inhomogeneous SB has been proposed to be described by a parallel conduction model [127,128]. In such a model, the junction current is a linear sum of the contribution from every individual area, namely:

$$I(V_a) = A^* T^2 \left[\exp\left(\frac{eV_a}{k_B T}\right) - 1\right] \sum_i A_i \exp\left(-\frac{\Phi_i}{k_B T}\right), \tag{5.2.1}$$

where A_i and Φ_i are the area and the SBH of the ith "patch", respectively. Here, the overall transport mechanism has been assumed to be thermionic emission, as evidenced by the unity ideality factor assumed in the equation. In general, the transport mechanism can be assumed to be any other mechanism with only minor modifications. The main assumption behind the parallel conduction model is the independence, as far as the electrical conduction is concerned, of the different segments of an interface of each other. Under this condition, transport theories for homogeneous SBH can be simply extended to cover inhomogeneous SBs. Such a model has been applied to describe mixed-phase diodes [129–132] and also to analyze SB diodes with an assumed continuous range of SBH [133–135]. In a randomly produced SB diode, some degree of SBH inhomogeneity can always be expected. By assuming the distribution of the SBH to follow some standard statistical distribution, the diode current can be integrated into closed forms and conveniently analyzed [133,135]. Specifically, if the probability that any patch of the interface is found to have a SBH between Φ and $\Phi + d\Phi$ is assumed to follow a Gaussian distribution, i.e.

$$P(\Phi)\, d\Phi = \frac{d\Phi}{\sqrt{2\pi}\sigma_{SBH}} \exp\left\{-\frac{(\Phi - \Phi_{B,n}^{00})^2}{2\sigma_{SBH}^2}\right\}, \tag{5.2.2}$$

where the constants $\Phi_{B,n}^{00}$, and σ_{SBH} are the mean and the standard deviation of the distribution, respectively. The integral of Eq. (2.2.1) can be carried out to yield an effective SBH, which controls the current flow as a whole, at the inhomogeneous MS junction as [135]:

$$\Phi_{I-V}^{inh} = \Phi_{B,n}^{00} - \frac{e\sigma_{SBH}^2}{2k_B T}. \tag{5.2.3}$$

Namely, the total current of the inhomogeneous SB is given by

$$I_{SB}^{inh}(V_a) = AA^* T^2 \exp\left(-\frac{e\Phi_{I-V}^{inh}}{k_B T}\right)\left[\exp\left(\frac{eV_a}{nk_B T}\right) - 1\right], \tag{5.2.4}$$

It is seen that the SBH deduced from I–V measurement is always smaller than the arithmetic average of the SBH. Furthermore, this departure is more pronounced at lower temperatures. Since the

SBH measured by the C–V technique is exactly the mean SBH, $\Phi_{B,n}^{00}$, as has been demonstrated [25,135], the SBH measured from an inhomogeneous SB diode will depend on the measurement technique.

The inhomogeneity of SBH has been speculated to be a primary reason for the common observation of large ideality factors ($n > 1.1$) even under band bending conditions which are not conducive to tunneling [135]. Within the statistical model of inhomogeneous SBH, there is a parameter, σ_{SBH}, at one's disposal, in addition to the regular SBH parameter, $\Phi_{B,n}^{00}$. Analyses have been made of the experimentally observed temperature dependence of the SBH and the ideality factor of common SB diode, and the results have been used to infer how $\Phi_{B,n}^{00}$ and σ_{SBH} must depend on the applied bias in order for certain experimental phenomena, including the T_0 effect, to be observed [135]. These empirical assumptions are commendable, as they correctly link the large ideality factors to SBH inhomogeneity. However, the physical reason for the variation of these parameters with bias is unknown in these analyses. Without an understanding of the fundamental processes responsible for the changes in these parameters, there is little hope to generalize the concept or to extend experimental results between systems. Such an understanding is not possible without taking a proper account of the band bending at inhomogeneous MS interfaces.

5.2.2. Interactions at inhomogeneous SBs

What has been missing from all models based on the parallel conduction concept is the interaction between neighboring sections of the same interface. When the actual band bending is considered, not only the probabilistic distribution of the magnitude of the SBH, e.g. Eq. (5.2.2), is found to be important, but also the length scale with which the SBH varies is found to be very important. As first revealed by numerical simulations at MS interfaces [23,136,137] and semiconductor–liquid interfaces [138], the parallel conduction model is in significant error when the SBH varies spatially on a scale less than, or comparable to, the width of the space–charge region. The error arises because Eq. (5.2.1) fails to take into account the potential "pinch-off" effect, as described in Section 1.5 [10,25]. From earlier discussion, it is clear that the shape of the inhomogeneous SBH has a strong effect on the current transport. For example, small-amplitude variation of the SBH and isolated high-SBH patches lead to a junction current which obeys the parallel conduction model. However, when the SBH varies with large amplitudes on a small lateral length scale (cf. conditions (1.5.4) and (1.5.6)), potential pinch-off occurs and the current transport deviates considerably from the parallel conduction model. Numerical simulations gave excellent support to expressing the total current as a modified sum of currents flowing in each patch:

$$I(V_a) = A^* T^2 \left[\exp\left(\frac{eV_a}{k_B T}\right) - 1\right] \sum_i A_{i,\text{eff}} \exp\left(-\frac{\Phi_{i,\text{eff}}}{k_B T}\right), \tag{5.3.1}$$

where the effective SBH, $\Phi_{i,\text{eff}}$, is simply the local SBH for patches which are not pinched off, but $\Phi_{i,\text{eff}}$ assumes the value of the saddle-point potential (see Table 1) in front of the ith low-SBH patch when pinch-off occurs. Likewise, the effective area of a patch, $A_{i,\text{eff}}$, is given by Table 1 for pinched-off patches, but reverts to the size of the patch, A_i, in the absence of pinch-off. The most important difference between Eqs. (5.3.1) and (5.2.1) is that the $A_{i,\text{eff}}$ and the $\Phi_{i,\text{eff}}$ depend on bias, temperature, doping level, geometry, etc., while the A_i and the Φ_i do not. It is the various dependencies of the parameters in Eq. (5.3.1) which leads to a wealth of interesting I–V characteristics. For example, the increase of the saddle point potential with forward bias, expressed in Eq. (1.5.11) and shown in Fig. 7(b), leads to an ideality factor greater than 1 for the component of current which flows through

this saddle-point. Specifically, for the current flowing to a low-SBH patch:

$$n \approx 1 + \Gamma = 1 + \frac{\gamma}{3\eta^{1/3} V_{bb}^{2/3}} \tag{5.3.2}$$

where $\eta = \varepsilon_S / eN_D$. So, if the current transport is dominated by current flowing to pinched-off low-SBH patches, the ideality factor measured will be greater than 1.

At a real MS interface, SBH variations may occur at a variety of shapes and spatial frequencies. The observed *I–V* behavior from an inhomogeneous diode depends very much on the characteristics of SBH variation. A random variation of the SBH at a MS interface may be simulated by a statistical distribution of the patch/strip characteristics. For instance, one may assume a Gaussian distribution of the patches:

$$P(\gamma) = \frac{c_1}{\sigma_{SBH}} \exp\left[-\frac{\gamma^2}{2\sigma_{SBH}^2}\right] \qquad \gamma > 0, \tag{5.3.3}$$

where $P(\gamma)\,d\gamma$ is the density of circular patches with a characteristic γ between γ and $\gamma + d\gamma$. In Eq. (5.3.3), σ_{SBH} is the standard deviation of the normal distribution. It has been shown that the current flowing in such a composite inhomogeneous SB diode is made up of two components. One component is the current over the entire diode, which is governed by a uniform SBH of $\Phi_{B,n}^{00}$, and the other is an additional current due to the presence of the low-SBH patches. The combined effect of all the low-SBH patches is as if there were a big low-SBH region in the diode with an effective SBH of

$$\Phi_{EFF} = \Phi_{B,n}^{00} - \frac{e\sigma_{SBH}^2 V_{bb}^{2/3}}{2\eta^{2/3} k_B T} \tag{5.3.4}$$

and with an "overall ideality factor" of

$$n_{EFF} \approx 1 + \frac{e\sigma_{SBH}^2}{3\eta^{2/3} V_{bb}^{1/3} k_B T}. \tag{5.3.5}$$

Eqs. (5.3.4) and (5.3.5) are fascinating. They show that, even though the effective SBH and the ideality factor of each individual patch are roughly temperature-independent, put together in the same diode, they may be represented by a temperature-dependent effective SBH and a temperature-dependent ideality factor. Analytic expressions qualitatively similar to those derived in Eqs. (5.3.2)–(5.3.5) have also been obtained for the strip geometry. The main difference between the two geometries is in the dependence of the effective SBHs on bias: $\Phi_{B,n}^{00} - \Phi_{eff}$ is proportional to $V_{bb}^{1/3}$ for the patch geometry and proportional to $V_{bb}^{1/4}$ for the strip geometry. Hence, the currents for both patch and strip geometries may be expressed in a generalized functional form:

$$I_{total} = A^* A T^2 f(\beta, V_d)[\exp(\beta V_a) - 1] \exp(-\beta \Phi_{B,n,0}^{mean} + \beta\kappa_1 V_d^{\xi/2} + \beta\kappa_2 V_d^{\xi}), \tag{5.3.6}$$

where β is $(k_B T/e)^{-1}$, f is a slowly varying function in comparison to the exponential function, and the exponent ξ is 2/3 and 1/2, respectively, for the patch and strip geometry. The constants, κ_1 and κ_2, depend on the doping level and the distribution of SBHs.

In the above discussion, the effect of series resistance has not been included to simplify the mathematical expressions. The effect of Ohmic drop is significantly magnified and considerably

more complicated for inhomogeneous SB diodes than for uniform diodes. Because the current density is laterally inhomogeneous, the usual approach of simply replacing $\exp(\beta V_a)$ in Eq. (5.3.1) with $\exp(\beta V_a - \beta I R_S)$ is no longer valid. In general, the Ohmic drop relevant to each patch may be different. This effect is particularly pronounced for low-SBH patches that have been pinched-off. As has been suggested [10], the spreading resistance associated with the spatial confinement of current flow should be used for each individual patch. And, furthermore, since the current flow is most congested near the saddle-point, the characteristic area for each patch used in the calculation of the spreading resistance should be $A_{i,\mathrm{eff}}$, rather than the actual size, A_i. The spreading resistance of a circular disc with a diameter, d, is

$$R_{sp} = \frac{\rho}{2d}, \tag{5.3.7}$$

in the limit that d is much smaller than the sample thickness [139]. In (5.3.7), ρ is the resistivity of the semiconductor. So, taking into consideration effects due to series resistance, the current of an inhomogeneous SB can be approximately expressed as

$$I(V_a) = \sum_i I_i(V_a) = A^* T^2 \sum_i^{\text{``not\_p-o''}} A_i \exp(-\beta\Phi_i)\left[\exp\left(\beta V_a - \beta I_i \frac{\rho t}{A_i}\right) - 1\right] + A^* T^2 \sum_i^{\text{``p-o''}} A_{i,\mathrm{eff}} \exp(-\beta\Phi_{i,\mathrm{eff}})\left[\exp\left(\beta V_a - \beta I_i \frac{\rho}{4\sqrt{A_{i,\mathrm{eff}}/\pi}}\right) - 1\right], \tag{5.3.8}$$

where the patches which are not pinched-off (first term) are assumed to act independently. One should note that since $A_{i,\mathrm{eff}}$, and $\Phi_{i,\mathrm{eff}}$, have explicit dependence on the applied bias, a change of variable of from V_a to $(V_a - I_i\rho/4\sqrt{A_{i,\mathrm{eff}}/\pi})$ is necessary for these parameters. Eq. (5.3.8) has been used to numerically model current flow in inhomogeneous SB diodes [10] and has been shown to give results nearly identical to the true numerical solutions of Poisson's equation and the continuity equation [25].

5.2.3. Numerical simulations of inhomogeneous SBH

Numerical simulations of the potential distribution and current transport associated with spatially varying SBHs had been in existence [23,137] even before the phenomenon of potential pinch-off was formally discussed in the analytic theory of inhomogeneous SBH [10]. The modest computational capabilities of tools used in the early days limited the amount of details which could be specified regarding SBH distribution. Even though potential pinch-off was evident in earlier numerical solutions, the connection between pinch-off and the bias-dependent SBH was not made until the concept of the ''saddle-point potential'' [10,75] was developed. Detailed and systematic simulations were then carried out to test the validity of the saddle-point concept and the various predictions associated with this concept [25]. As shown in Fig. 38, numerically calculated ideality factor and effective SBH agree with theoretical predictions, Eq. (5.3.2) and Table 1. The importance of having a small enough mesh size was found crucial in the success of these numerical simulations. Failure to heed this potential problem is known to lead to unphysical results [140,141]. Numerical results from simulations using fine-grids were in excellent agreement with the predictions of the analytic theory. As a matter of fact, the overall conclusion of the numerical studies was essentially that numerical simulations of majority carrier effects were largely unnecessary since they invariably

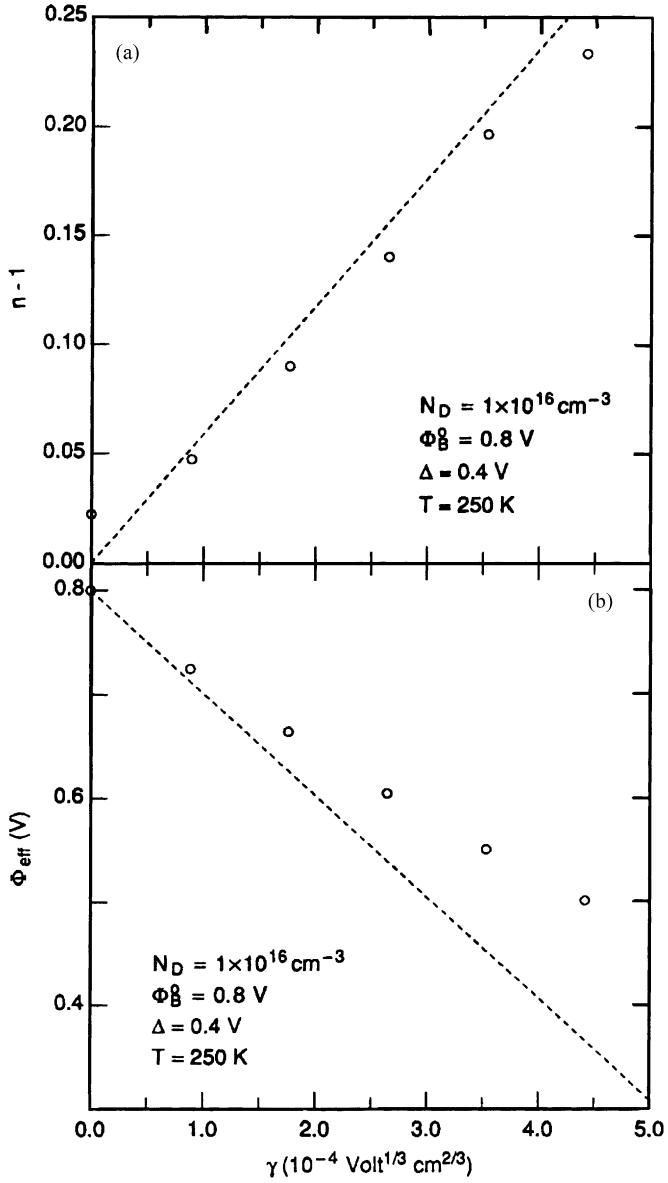

Fig. 38. Computer simulated (○) ideality factor (a), and effective SBH (b) for the current flowing to a circular patch with a local SBH of 0.4 eV at 250 K, against the γ parameter. This low-SBH patch is embedded in a background of 0.8 eV SBH on n-type Si with a 1×10^{16} cm^{-3} doping level (from Sullivan et al. [25]). Dashed lines are predictions of the analytic theory, Table 1.

duplicated the predictions of the analytic expressions. Widely varying and striking *I–V* behaviors have been numerically simulated [25], as well as calculated from analytic expressions [10], using only the thermionic emission theory. These include the T_0 effect, the reverse T_0 effect, the TFE look-alike behavior, bumps in the *I–V* traces, modified Richardson plot, etc. These results showed clearly that inhomogeneous SBs do not behave in any particular pattern. While the observation of certain phenomena is a clear indicator of SBH inhomogeneity, the absence of certain phenomenon does not guarantee SBH homogeneity. The inappropriateness of using the experimental *I–V* traces to

determine the conduction mechanism or to calculate the interface state density is also clearly illustrated in these numerical simulations.

5.3. Other measurement techniques of the SBH

5.3.1. Capacitance–voltage relationship

An often-used and convenient technique to measure the SBH is the capacitance–voltage (C–V) technique. According to Eq. (1.4.12), the charge per unit area due to uncompensated dopants is given by

$$Q_{SC} = eN_D W = \sqrt{2\varepsilon_S N_D (eV_{bb} - k_B T)}, \tag{6.1.1}$$

for a homogeneous SBH, and the small signal capacitance for the Schottky diode is

$$C = -\frac{\partial Q_{SC}}{\partial V_a} = \sqrt{\frac{e^2 \varepsilon_S N_D}{2(eV_{bb} - k_B T)}}. \tag{6.1.2}$$

Eq. (6.1.2) shows that a plot of C^{-2} as a function of the applied bias, known as a Mott–Schottky plot, is a convenient method to deduce the doping profile of the semiconductor. In the case that the doping profile is homogeneous throughout the space–charge region, a C–V plot should yield a straight line in the reverse bias region with a slope of $-2/e\varepsilon_S N_D$ and with an intercept with the bias voltage axis of $\Phi^0_{B,n} - V_n - k_B T/e$, as shown in Fig. 39. The value of this intercept, known as the built-in potential (see Eq. (1.4.7a)), can be used to deduce the SBH through the following relationship

$$\Phi^0_{B,n} = eV_{bi} + eV_n + k_B T. \tag{6.1.3}$$

The C–V technique gives a convenient measure of the average SBH when the SBH is inhomogeneous. The capacitance signal comes from the modulation of the total space–charge as a function of bias. For an inhomogeneous SB, the total space–charge is equal to that for a uniform SB with a height equal to the mathematical average of the inhomogeneous SBH. To see how this comes about, one notes that the total space–charge is equal to the charge in the metal, which can be integrated using Eq. (1.5.2)

$$\begin{aligned} Q_{SC} &= \frac{1}{A}\int\int \mathrm{d}x\,\mathrm{d}y \left(\frac{\varepsilon_S}{e}\right)\left[\frac{\partial \varepsilon_{CBM}(x,y,z)}{\partial z}\right]_{z\to 0} \\ &= \frac{1}{A}\int\int \mathrm{d}x\,\mathrm{d}y \sqrt{2\varepsilon_S N_D(\Phi^{00}_{B,n} - eV_N - eV_a)} \\ &\quad + \frac{1}{A}\int\int \mathrm{d}x\,\mathrm{d}y \int\int \mathrm{d}x_1\,\mathrm{d}y_1 \frac{\delta(x_1,y_1)}{2\pi[(x_1-x)^2 + (y_1-y)^2]^{3/2}} \\ &= \sqrt{2\varepsilon_S N_D(\Phi^{00}_{B,n} - eV_N - eV_a)}. \end{aligned} \tag{6.1.4}$$

The term on the third line can be seen to vanish, neglecting some edge effect, by reversing the integration sequence and making use of the fact that $\int \delta(x,y)\,\mathrm{d}x\,\mathrm{d}y = 0$ Thus the total space–charge of an inhomogeneous SB is controlled only by its average SBH.

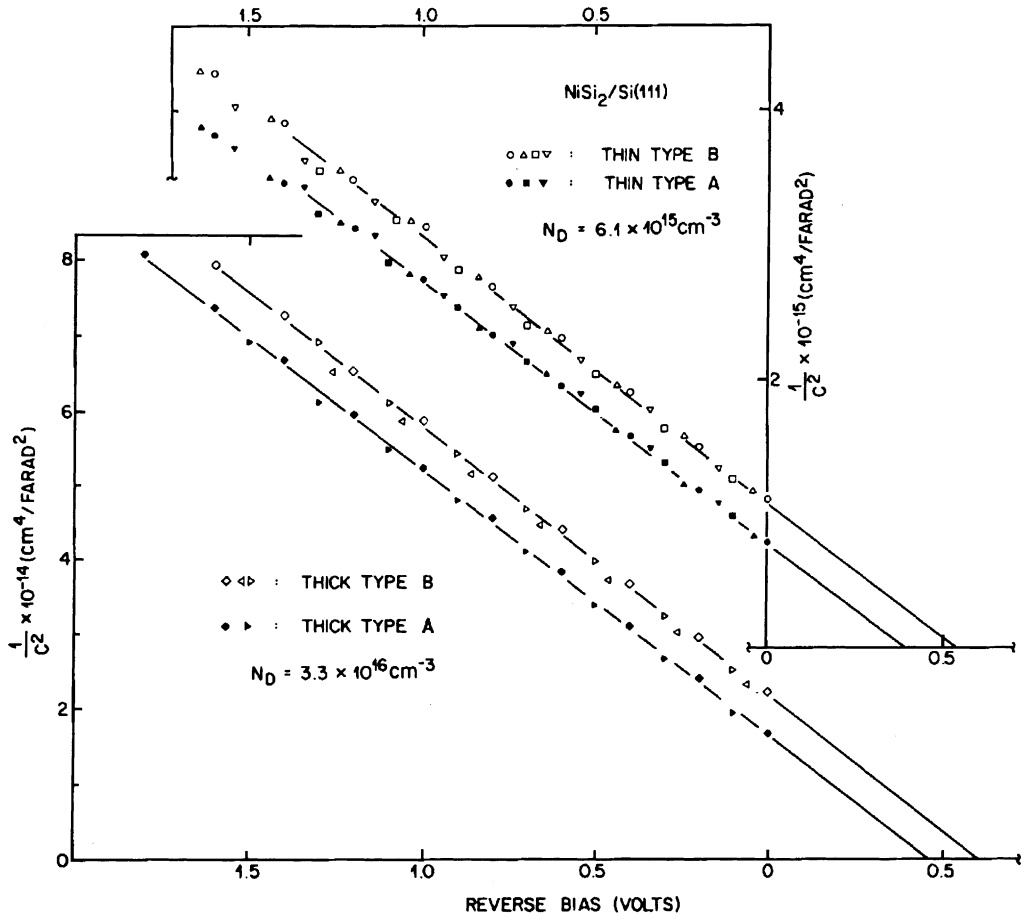

Fig. 39. Capacitance per unit area of $NiSi_2$–Si(1 1 1) junctions, as a function of reverse bias, measured at 1 MHz (from Tung [7]).

When there are deep levels in the semiconductor, the capture and emission of charge from these states can also contribute to the measured capacitance. This phenomenon can be utilized to characterize the density and the energetic position of deep levels in the temperature domain, as demonstrated in the technique of deep level transient spectroscopy (DLTS). For doping profile determination, the direct contribution to the capacitance from deep levels can be avoided by using higher frequency probe signals, although the capture and emission action of deep levels with the slower bias sweep is difficult to avoid. Therefore, *C–V* determination of the SBH is only accurate when the density of deep traps is low. There are other problems that can affect *C–V* measurements. For example, series resistance, leakage current, and minority carriers can all seriously hinder experimenter's ability to accurately determine the true capacitance due to the modulation of the width of the space–charge region. Influence by one or several of these effects, combined with the presence of SBH inhomogeneity, can lead to a plethora of spurious *C–V* results. Many abnormal or non-ideal *C–V* behaviors are known to happen in some SB diodes. For example, a constant excess capacitance has often been determined from *C–V* analysis [142–145]. Even though they have very reasonable explanations in effects described above, the excess capacitance and other non-ideal capacitance behaviors of Schottky barriers were often attributed to the presence of interfaces states. More discussion about interface states and capacitance measurements will be given below.

5.3.2. Photoemission techniques

A technique which has been used to measure the SBH since the beginning of SBH studies is the photoresponse (PR) technique, also known as internal photoemission [3,146]. Monochromatic light, with photon energies greater than the SBH, is used to illuminate the MS interface. Carriers in the metal are excited from near the Fermi-level and some are sent over the SBH as in the operation of a solar cell. The short-circuit current flowing in the SB diode depends on the photon energy, as governed by the Fowler equation. For photons with energies at least a few k_BT larger than the SBH, the photoelectric current can be shown to roughly scale with the square of the excess energy:

$$I_{ph} \propto (h\nu - \Phi_{B,n})^2. \tag{6.2.1}$$

So a plot of the square-root of the photoelectric current against the photon energy should give a straight line with an intercept with the energy axis at the SBH, as shown in Fig. 40 for diodes fabricated on p-type GaAs [147]. Since current flow is being monitored, the SBH measured is subject to the Schottky lowering effect. To reduce effects due to noise and leakage, PR is usually conducted in ac mode with a chopped light source and a lock-in amplifier. More often radiation enters from the semiconductor side of the sample. However, for thin layers of metal (<30 nm), light can also incident from the front side with enough intensity to reach the MS interface. The range of photon energy of interest is between the SBH and the band gap, which dictates the kind of light source and gratings to use, and which also explains why PR cannot be used to measure large SBHs which approach the band gap. In cases where the SBH is inhomogeneous yet with peaked distributions at only a small number of values, the PR signal may contain linear segments which may be used to identify each of these individual barrier heights [148,149]. For more complicated

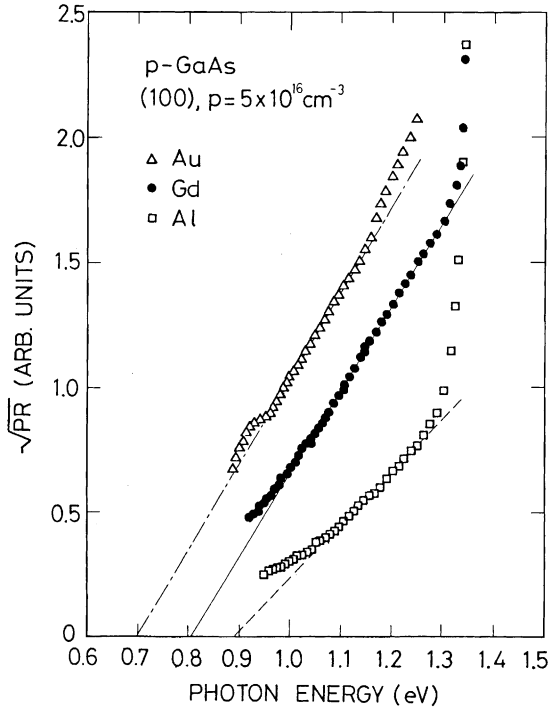

Fig. 40. Internal photoresponse plots for Au, Gd and Al diodes on p-type GaAs (from Okumura and Tu [147]).

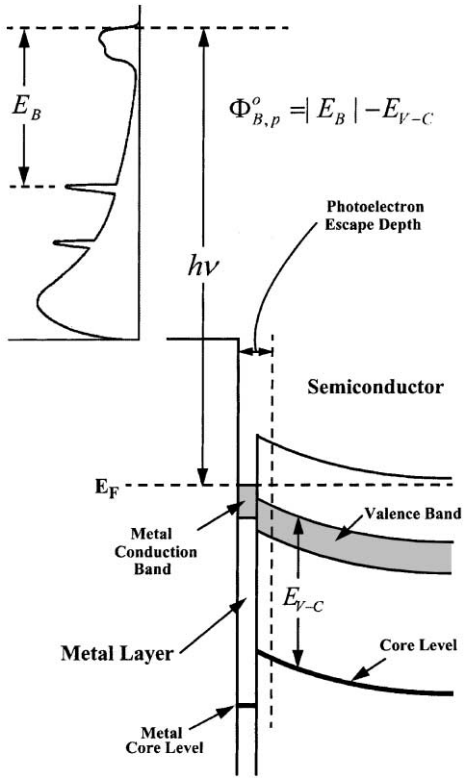

Fig. 41. Schematic of the principle of SBH measurement by photoemission spectroscopy. The binding energy of a core level of the semiconductor is measured at the MS interface. This, along with the E_{V-C} measured from a bulk semiconductor sample, can be used to determine the SBH.

distribution of inhomogeneous SBH, the PR signal is non-linear and, hence, unreliable for SBH determination.

Ever since the mid 1970s, core-level photoemission spectroscopy (PES) has been a popular technique surface scientists use to study SBH formation at semiconductor surfaces. From Eq. (1.3.4), it is clear that core levels are ''bent'' in exactly the same way as the edges of the conduction or valence bands. Therefore, any observed movement of the core level with respect to the Fermi-level also reflects an identical movement in the band bending. PES offers a unique ability to study the development of the band bending as a function of the coverage of metal deposited on the semiconductor surface, all under UHV conditions. Monochromatic X-ray or soft X-ray, usually from a synchrotron radiation source, excites core electrons to states high enough in energy to traverse the metal and escape into the vacuum. A schematic drawing of the surface photoemission process is shown in Fig. 41. The thickness of the metal layer has to be kept thin. The escape depth of electrons from a surface is essentially material independent, reaching a minimum of $\sim$2 nm at $\sim$50–100 eV where the photoemission process is at its most surface-sensitive condition. For band bending and SBH formation studies, it is desirable to operate under conditions that are not surface sensitive, so that the main signal can come from the semiconductor space–charge region, rather than the ISR. The chemical reaction at the MS interface, which is an interesting subject in its own right, can also be studied by the PES technique but with the photon energy tuned to emphasize the interface region. Because the change in the band bending is usually a few hundred meV, that is the sort of the energy resolution that is needed to study the formation of the SBH. Therefore, the kinetic energy of core

electrons of interest is usually kept low to achieve bulk sensitivity and good energy resolution at the same time. A few serious problems with the measurement of band bending with monolayers of metal have emerged in the course of these studies. The tendency for a submonolayer or monolayers of metal to cluster on the surface may lead to lateral inhomogeneity in the band bending for which the PES results need to be corrected [150,151]. Furthermore, intense light radiation generates electron–hole pairs that locally charge the isolated metal clusters and induce significant changes in the measured band bending. This surface photovoltage effect is most prominent for wide-gap semiconductors and/or at low temperatures [152], and has led to much confusion in the literature about the presence of a temperature-dependent SBH formation mechanism.

5.3.3. Spatially resolved techniques for SBH measurement

The lateral uniformity of SBH has long been of much interest to researchers, because it has been regarded as an important test of various SB theories. The desire to correlate SBH variation with defects, structure, etc. has stimulated the development of a few techniques that allow spatially resolved determination of the SBH. Since the signal from the photoemission process comes from the illuminated region of the sample, a reduction in the spot size directly lead to lateral resolution in the spectroscopies. Spatially resolved internal photoemission [153–155] and surface photoemission [156,157] can both be performed with focused light and an *xy*-scan stage. Spatial resolution in surface band bending has also been achieved by blanket illumination in a photoemission electron microscopy [158]. A focused electron beam has also been used as the local ''probe'' of the SBH. Electron-hole pairs generated in the space–charge region of the SBH, in a scanning electron microscopy (SEM), are swept by the electric field to opposite ends of the sample, thus setting up an electron beam induced conduction (EBIC) [159] or voltage (EBIV) [160]. Electron holography in a scanning transmission electron microscopy (STEM) has been used to probe the band bending at semiconductor interface with good spatial resolution; [161] symmetry-forbidden LO Raman scattering has been used to probe the electric field at MS interfaces [162]. Both of these techniques can potentially be used for spatially resolved determination of the SBH.

By far, the most powerful technique, and the one which has had the most impact on our present view of the lateral distribution of the SBH, is the ballistic electron emission microscopy (BEEM) [11], employing a scanning tunneling microscope (STM). Electrons (or holes) are injected into the metal side of an MS interface, at energies considerably above (below) the Fermi-level of the metal. A fraction of the hot electrons (holes) can traverse the thin metal layer without scattering and clear the SBH to enter the semiconductor. This BEEM current is then used to map out a microscopic profile of the MS interface. Alternatively, the energy dependence of the ballistic current at any specific point of the interface can be used to deduce the onset of the emission and thereby determine the local SBH, in the ballistic electron emission spectroscopy (BEES) mode [163]. A schematic of the operation of the BEEM technique is shown in Fig. 42. The thickness of the metal layer is usually kept much shorter than the electron mean free path to minimize scattering in the metal film. BEEM is frequently conducted in air, which prompted the use of noble metal (Au, Pt, etc.) to avoid oxidation. The emission process in a BEEM has been described by a simple theory, based on free electron band in the metal, which seems to fit some experimental data [163]. The injected hot electrons have a large forward momentum, which limits their lateral spread to a cone of a certain angle, in what has been called the ''search light'' effect. It has been speculated that the conservation of the lateral momentum at the MS interface, along with the search light effect, should forbid the emission into low-lying band minima which have large transverse momentum, such as the Si conduction band when probed along the (1 1 1) direction [164]. But actual BEEM results show that these conservation laws are not of primary importance. A well known example is that the BEEM current and spectroscopy for

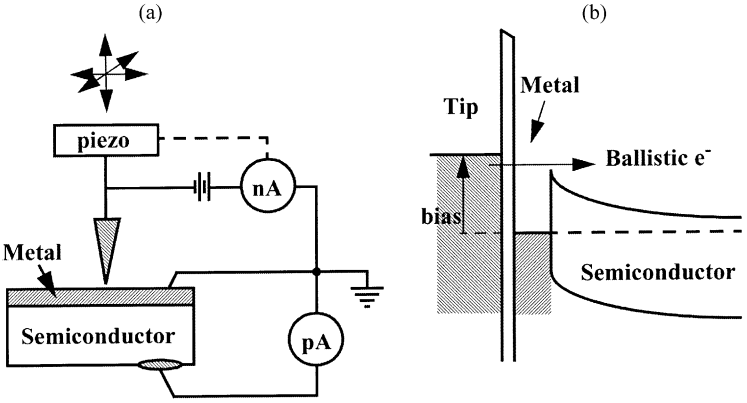

Fig. 42. (a) Circuit diagram of the BEEM experimental configuration. The Schottky barrier is formed at the interface between the metallic base and semiconducting collector. The tunnel current is measured by the nanoammeter and held constant by the STM feedback loop and the vertical piezo drive. The collector current is measured by the picoammeter. (b) Band diagram.

Au (or Pd) on Si(1 1 1) interface is very similar to that on Si(1 0 0) surface [165,166]. This seemed to suggest that some scattering and broadening has to take place, which would be inconsistent with the amazing spatial resolution, ~1 nm, of features experimentally imaged with the BEEM technique [167,168]. This puzzle seemed to be resolved recently, when it was pointed out [169–171] that the electron focusing effect [172], which has to do with the band structure of the metal, could lead to a coherent explanation of both of these observations. Therefore, the interpretation of BEEM signal appears to be much more complicated than originally anticipated. The electron focusing effect also makes BEEM a more useful technique, with much better spatial resolution than can be predicted from free electron model [163]. Even though all the steps leading to the transport of ballistic electrons into the semiconductor have excellent spatial resolutions, the potential pinch-off effect in the semiconductor can still have a devastating effect on the energy resolution of the BEEM technique. The SBH profile obtained by BEEM may be severely limited by the formation of saddle-points and, as a result, fails to reflect the SBH profile at the MS interface. In that respect, semiconductors with high doping levels should be preferred for a more realistic map of the SBH profile. The STM tip has also been used to probe SBH inhomogeneity as a nanoscopic contact, and also operated in the scanning capacitance microscopy mode [173].

5.4. Measurement of interface states

5.4.1. Fixed-separation model with applied bias

Interface states have long been thought to be the culprit responsible for the Fermi-level pinning phenomenon. Interest in directly measuring the density of interface states has always been high. The fixed-separation model, shown in Fig. 15, frequently invoked to analyze the SBH lineup in the presence of interface gap states, also has implications on the transport behavior at Schottky barriers. This connection has been exploited to study the distribution of interface states in numerous studies. The main vehicle through which interface states can influence the transport properties is the dependence of the interface dipole on the applied bias, as shown in Fig. 43. A common assumption associated with measurements of interface state density is that the population (and depopulation) of interface gap states is controlled by the local (quasi-) Fermi-level, shown as ‘‘qfn’’ in Fig. 43. The quasi-Fermi-level is usually assumed to be flat in the space–charge region of the semiconductor

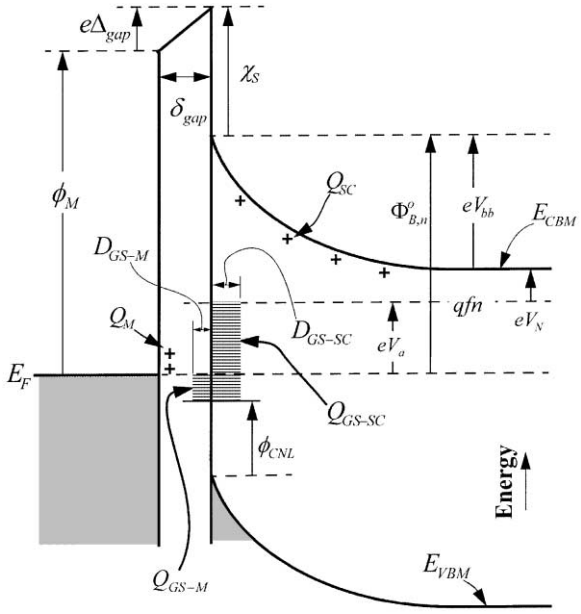

Fig. 43. The fixed-separation model of interface gap states under an applied bias. The interface states are distinguished into those in thermal equilibrium with the semiconductor, with a density of D_{GS-SC} and those in thermal equilibrium with the metal, D_{GS-M}. Note that under an applied bias, the population of states in equilibrium with the semiconductor is controlled by the quasi-Fermi-level of the semiconductor, whereas the population of gap states in thermal equilibrium with the metal is controlled by the Fermi-level of the metal.

under forward bias, due largely to the success of the thermionic emission theory. Since interface state models assume that the distribution of these gap states depends on only the semiconductor, it seems fitting to consider these states to be in thermal equilibrium with the semiconductor, as has been assumed so far in this paper. Some authors have included the possibility that a fraction of the gap states may be in thermal equilibrium with the metal and are controlled by the metal Fermi-level [174,175]. Assuming the density of gap states which are controlled by the semiconductor to be D_{GS-SC} and the density of gap states controlled by the metal to be D_{GS-M}, one can write down the charges stored in these two groups of gap states separately:

$$Q_{GS-SC} = eD_{GS-SC}(eV_{bb} + eV_N - E_g + \phi_{CNL}), \tag{7.1.1}$$

and

$$Q_{GS-M} = eD_{GS-M}(eV_{bb} + eV_N + eV_a - E_g + \phi_{CNL}). \tag{7.1.2}$$

One should mention, in passing, that Q_{GS-M} here is modeled differently than the MIGS distribution assumed in the negative charge model. So, no reference to the negative charge model should be drawn from the present discussion. Eqs. (7.1.1) and (7.1.2) are more easily envisioned for the forward bias, but will be assumed to be valid for all bias conditions. The SBH can be solved by requesting that

$$Q_M + Q_{SC} + Q_{GS-M} + Q_{GS-SC} = 0 \tag{7.1.3}$$

while making use of Eqs. (1.4.7), (1.4.12) and (2.3.2). Assuming uniform distributions of the gap states, and ignoring the space–charge as before, one arrives at

$$\Phi^0_{B,n} = \gamma_{GS}(\phi_M - \chi_S) + (1 - \gamma_{GS})(E_g - \phi_{CNL} + eV_a) - \gamma_{GS}\alpha'' eV_a, \tag{7.1.4}$$

where γ_{GS} is still given by Eq. (2.3.5), but with the total interface state density given by

$$D_{GS} = D_{GS-SC} + D_{GS-M}, \tag{7.1.5}$$

namely,

$$\gamma_{GS} = (1 + \alpha' + \alpha'')^{-1}, \tag{7.1.6}$$

where

$$\alpha' = \frac{e^2\delta_{gap}D_{GS-SC}}{\varepsilon_{int}}, \quad \text{and} \quad \alpha'' = \frac{e^2\delta_{gap}D_{GS-M}}{\varepsilon_{int}}. \tag{7.1.7}$$

To see the bias dependence of the SBH, one can differentiate Eq. (7.1.4) to get

$$\frac{\partial V_{bb}}{\partial V_a} = -\frac{1 + \alpha''}{1 + \alpha' + \alpha''}. \tag{7.1.8}$$

From this expression, it is clear that only gap states in thermal equilibrium with the semiconductor can lead to a dependence of the SBH on the applied bias. Gap states that are in thermal equilibrium with the metal are specific to the metal–semiconductor system, e.g. the dipole resulting from these states could be viewed as that arising from interface bonds (see Section 1.1). The population of these states is not affected by the bias and these states have traditionally been ignored in systematic studies of SBH, because they are obviously not properties of only the semiconductor. This neglect is a major fault of existing gap state models, as already discussed. Following this common practice ($\alpha'' = 0$), one is led to a more familiarexpression

$$\Phi^0_{B,n} = \gamma_{GS}(\phi_M - \chi_S) + (1 - \gamma_{GS})(E_g - \phi_{CNL} + eV_a) \tag{7.1.9}$$

The effective SBH has an explicit dependence on the applied bias when interface states are present. If the current transport mechanism across an MIS interface is similar to that at MS interfaces, the bias dependence, expressed in Eq. (7.1.9), can lead to an ideality factor much greater-than-unity. From Eq. (7.1.10), the ideality factor is

$$n = \left[1 - \frac{\partial\Phi_{B,n}}{e\partial V_a}\right]^{-1} = \gamma_{GS}^{-1}. \tag{7.1.10}$$

When the density of gap states is not uniform, the charge stored on the gap states, Eq. (7.1.1), need to be expressed as an integral:

$$Q_{GS-SC} = e\int_{\Phi^0_{B,n} - eV_a}^{E_g - \phi_{CNL}} D_{GS-SC}(E)\,dE, \tag{7.1.11}$$

which can then be used, along with the rest of the equations, to deduce a dependence of the apparent SBH on the applied bias. For very non-uniform distributions of the gap states, e.g. discrete deep levels due to defects, non-linear features can be expected from the logarithmic *I–V* traces.

The above derivation seems straightforward and uses some sound concepts. However, one should be aware of the severe limitations on the validity of the above approach. First of all, the many unrealistic assumptions and inconsistencies associated with a band diagram like Fig. 13, have already been mentioned at the end of Section 2.3. They will not be repeated here, but the readers are encouraged to get re-familiarized with what these faults are. As far as the *I–V* characteristics of the MIS structure is concerned, there are additional issues that need to be brought up. The model in this section relies upon the homogeneity of the effective SBH. If the SBH were inhomogeneous, various non-ideal and non-linear features would also be present, cf. Eq. (5.3.6), which would mar any additional dependence on the interface states. For the SBH to be homogeneous in the present MIS structure, as shown in Fig. 14, the microscopic SBH/BO at both the metal–dielectric and the dielectric–semiconductor interfaces would have to be uniform. The distribution of the interface states also need to be homogeneous. Then there is the issue of how the quasi-Fermi-level should be drawn through the MIS region under forward and reverse bias conditions. The example shown in Fig. 43 is the most commonly used assumption in the analysis. However, there is some arbitrariness in the choice of the quasi-Fermi-level and there are no clear guidelines.

5.4.2. Capacitance due to gap states

The *C–V* technique has been used to measure interface state densities much more frequently than the *I–V* method [176–178]. In some early experiments, the capture and emission of charge by the interface states were modeled as if they had no influence on the magnitude of the SBH, namely, the variation of the total band bending with bias was thought to be unchanged; only the shape of the band bending was thought to be modified by the interface states [179,180]. In such a scheme, interface states behave like ordinary deep levels and their spatial position with respect to the MS interface is not of primary concern. But, more often, interface gap states were viewed as having a direct influence on the interface dipole and analyzed with the model shown in Fig. 43. To analyze the capacitance in the presence of gap states, the space–charge which has been largely ignored up to this point, need to be re-included [175]. Eq. (7.1.8) now becomes

$$\frac{\partial V_{\rm bb}}{\partial V_{\rm a}} = -\frac{1+\alpha''}{1+\alpha'+\alpha''+(\delta_{\rm gap}/\varepsilon_{\rm int})(e\varepsilon_{\rm S}N_{\rm D}/2V_{\rm bb})^{1/2}}, \tag{7.2.1}$$

which is understood to be valid under static, or low-frequency conditions. To actually model the capacitance, one has to make assumptions on the capture and emission velocities of the gap states, as they decide whether the interface charge can keep up with the ac signal at the testing frequency. At low frequencies, all charges can follow the ac voltage, and the capacitance is given by

$$\begin{aligned} C &= -\frac{{\rm d}(Q_{\rm SC}+Q_{\rm GS-SC})}{{\rm d}V_{\rm a}} \quad (\text{at low-frequency}) \\ &= -\frac{\partial(Q_{\rm SC}+Q_{\rm GS-SC})}{\partial V_{\rm bb}}\frac{\partial V_{\rm bb}}{\partial V_{\rm a}}. \end{aligned} \tag{7.2.2}$$

At high testing frequencies, only $Q_{\rm SC}$ and $Q_{\rm M}$ can follow the ac signal. So,

$$\frac{\partial V_{\rm bb}}{\partial V_{\rm a}} = -1 \quad (\text{at high-frequency}) \tag{7.2.3}$$

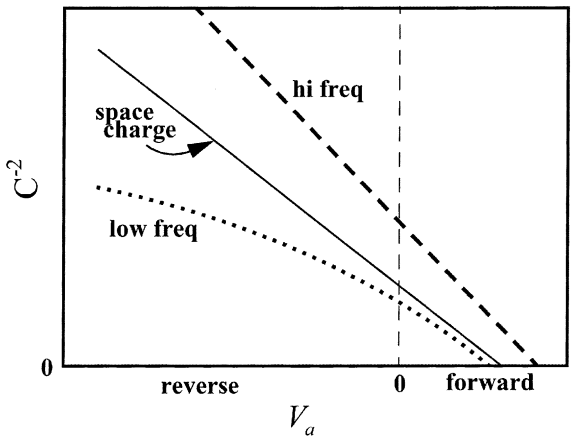

Fig. 44. Calculated C–V plot of a Schottky barrier without interface states (solid line). When gap states are present (here assumed that $\alpha' \neq 0$ and $\alpha'' = 0$), the C–V behavior depends on the testing frequency.

and the capacitance is still governed by Eq. (6.1.2). Non-linear C^{-2}–V curve should usually be observed when gap states are present, although linear dependences can also be expected under some conditions [175]. The expected influence of gap states on C–V characteristics is demonstrated by some examples in Fig. 44. Obviously, capacitance method cannot be used to deduce the magnitude of the SBH when gap states are present. It is also obvious that any experimental C–V data can be fitted to some distributions of the gaps states, given that the number of fitting parameters at one's disposal is virtually unlimited. Experimentally observed downward curvature in C^{-2}–V plots, similar to that shown in Fig. 44, has been explained in terms of an "excess capacitance" and attributed to the presence of interface states [32,143,144]. Excess capacitances observed at intimate SB diodes have also been attributed to interface states and analyzed with the fixed-separation model [125,181,182]. For intimate SBs, fixed-separation model has little physical basis, and one expects a negative capacitance (inductance) contribution from interface states [183]. It is likely that the observed excess capacitance may be dominated by minority carriers [120].

The validity of any measurement of the interface gap states relies on the validity of the analysis model used. The many unreasonable assumptions of the MIS model, Fig. 43, seem to make this model unreliable for interface states measurement, as has already been discussed. As far as capacitance measurements are concerned, there are additional artifacts and spurious effects that can plague both the experiment and the analysis [120]. Most interface states measurements are done in forward bias, where the in-phase component of the ac current can overwhelm the measuring instrument. Even when the out-of-phase current can be accurately determined, one still has to separate out the effect due to series resistance and other parasitics in the measuring circuit. Namely, an equivalent circuit diagram needs to be drawn to deconvolve the true junction capacitance from the measured capacitance. For this purpose, one need to know precisely the series resistance. For homogeneous SBH, the effect of series resistance is usually predictable and can be accounted for, except for high biases when the effect of minority carriers become significant. In actual diodes, the SBH usually has some degree of inhomogeneity and the series resistance effect is virtually unmanageable, cf. Eq. (5.3.8). Since the series resistance is not a fixed parameter for an inhomogeneous diode, an appropriate equivalent circuit diagram cannot be drawn. It is difficult to deduction the junction capacitance from experiments, under such conditions. Furthermore, minority carriers injected into the bulk semiconductor can alter the resistivity of the semiconductor and have very dramatic effect on the admittances measured at a SB diode [120,184–186]. Positive and

negative capacitances of large magnitudes have both been observed at MS interfaces, which have been traced to minority carriers. Due to all of these problems associated with the capacitance measurement technique in the forward bias, and the known faults of the analysis model, one must view the *C–V* deduction of interface gap states from MS interfaces with skepticism.

5.4.3. Variable electron affinity model

The variable electron affinity model of the interface gap states has been invoked to deduce the density of interface states from *I–V* to *C–V* measurements [32]. This model, shown in Fig. 17, assumes that the charge on the metal vanishes [31]. So, the total charge of the space–charge region is exactly offset by the gap state charge. Differentiating Eq. (2.5.2), one gets the ideality factor expected in this model as

$$n = \frac{X}{X-1}, \tag{7.3.1}$$

where

$$X = \left[1 + \frac{2e^2 D_{GS}^2}{\varepsilon_S N_D}(E_g - \phi_{CNL} - k_B T - eV_N - eV_a)\right]^{1/2}, \tag{7.3.2}$$

The small-signal capacitance is

$$C(V_a) = \frac{X-1}{X}\sqrt{\frac{e^2 \varepsilon_S N_D}{2(eV_{bb} - k_B T)}}. \tag{7.3.3}$$

The effect of isolated defects at the MS interface on the local SBH has been considered in an extension of the variable–electron-affinity model [33]. Isolated charges arising from defects are assumed to induce additional gap states charge of the MS interface in close proximity to the defects, as shown in Fig. 45. This effect leads to local lowering of the SBH, assuming positively charged

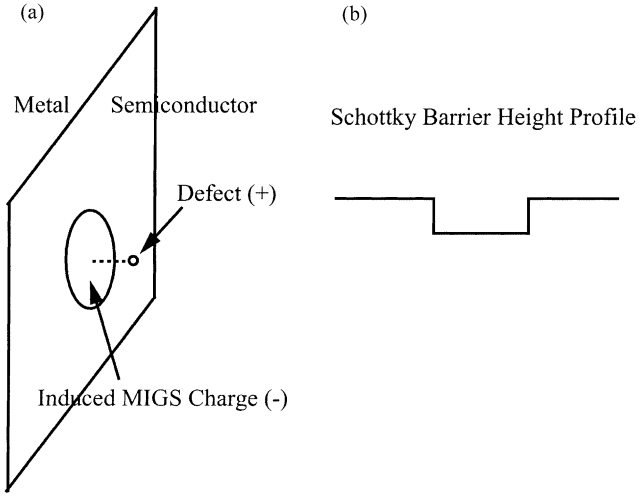

Fig. 45. (a) Model proposed by Maeda [33] to explain the origin of SBH inhomogeneity. An isolated defect induces image charge in the MIGS which lowers the local SBH, as shown in (b). The basic approach of this model is the variable–electron-affinity model of interface gap states.

defects, and SBH inhomogeneity. A statistical distribution of the interface defects has been used to explain the T_0 anomaly [33]. As already discussed, the variable–electron-affinity model has no physical basis. Therefore, schemes to infer interface state density from this basic approach are also meaningless.

6. Barrier heights of epitaxial interfaces

Epitaxially fabricated MS systems offer the best opportunity to understand the dependence of the electronic properties on the structure of a MS interface. The SBH at an epitaxial MS interface is frequently homogeneous and, therefore, can be directly correlated with the interface atomic structure. In addition, the atomic structure at single crystal MS interfaces can be determined by experimental means and then used to calculate the expected SBH. A comparison of the experimental and theoretical SBH allows a test of the validity of theories of the SB. Therefore, even though the formation mechanism of the SBH at ordinary MS interfaces is of the most technological interest, its deduction almost certainly has to come from the simpler, epitaxial, ''model'' MS systems.

6.1. Epitaxial silicide–silicon interfaces

Silicides are ordered metal–Si compound phases and have wide applications in Si integrated circuits as contacts and gate electrodes. Silicide thin films are usually formed by the deposition of metal on a Si substrate, followed by a high temperature treatment to induce solid-phase reactions. Because part of the substrate participates in the reaction of silicide thin films, the location of the final silicide–Si interface is usually well inside the original Si surface. This ensures intimate contact between the silicide and the Si, with transport behavior essentially independent of the initial conditions of the Si surface. A few silicides, most notably $NiSi_2$ and $CoSi_2$, have lattice structures similar to that of Si and close lattice matches with Si. As a result of these favorable conditions, these silicides can form epitaxially on silicon and the quality of these silicide–Si interfaces has been the best among MS interfaces ever fabricated. The SBH measured from single crystal silicide interfaces shows a remarkable dependence on the interface structure. The best known of these results is the dependence of the SBH on silicide orientation at the $NiSi_2$–Si(1 1 1) interfaces. High quality single crystals of $NiSi_2$ may be grown on Si(1 1 1) with either type A or type B orientation by a proper choice of template growth condition [187,188]. These two orientations differ only by an azimuthal rotation: the type A silicide has the same orientation as the silicon substrate, and the type B silicide shares the surface normal $\langle 1\ 1\ 1\rangle$ axis with Si, but is rotated 180° about this axis with respect to the Si. The atomic structure of both type A and type B $NiSi_2$–Si(1 1 1) interfaces have been studied by various experimental techniques and found to have the seven-fold structure [189–192]. Intriguingly, types A and B $NiSi_2$ have been found to have distinctively different SBHs [7], as illustrated in Fig. 46. This dependence of SBH on the epitaxial orientation was briefly challenged [193]. However, very extensive studies by various groups [194–196] have subsequently confirmed the original findings that type B $NiSi_2$ has a SBH about 0.14 eV higher than type A $NiSi_2$ on n-type Si(1 1 1). The reason for the misinterpretation of data [193] was also understood and shown to be due to surface contamination [197].

The study of the SBH of another epitaxial silicide system, $NiSi_2$–Si(1 0 0), has produced another interesting story which is intriguing in a totally different way. Layer uniformity is the main issue at this interface. Layers routinely prepared usually contain a density of interface imperfections, called ''facet bars'', which are slender and straight $NiSi_2$ protrusions bound by two inclined $\langle 1\ 1\ 1\rangle$

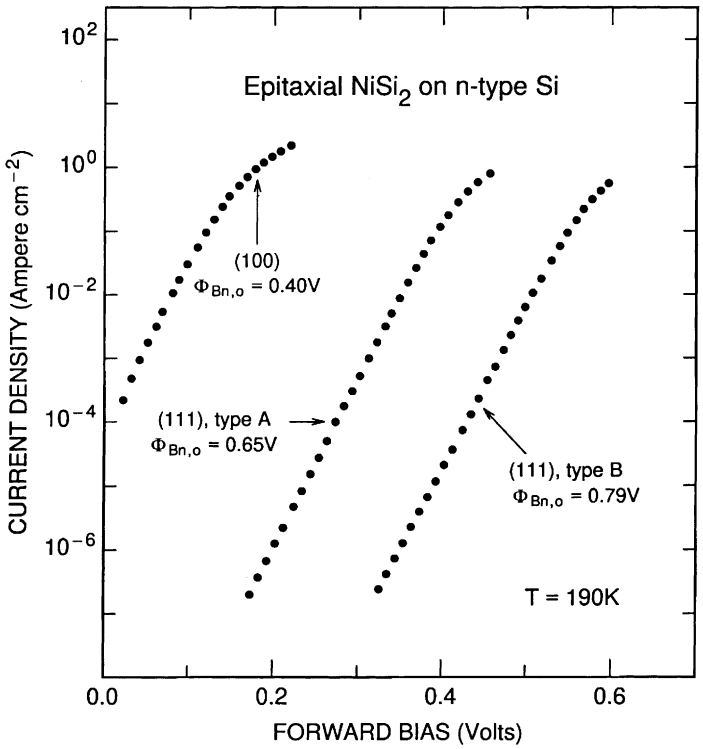

Fig. 46. *I–V* characteristics of single crystal $NiSi_2$ Schottky diodes on n-type Si, recorded at 190 K (from Tung [481]).

facets, usually ~10 nm in their depth and height and a few hundred nanometers in length [198,199]. The density and dimensions of facet bars can be conveniently studied by plan-view TEM, where under (0 2 0)-type dark field, these facet bars appear as short, bright streaks, as shown in Fig. 47(b). It was discovered that, with well chosen high temperature (>700 °C) anneals, facet bars in $NiSi_2$ layers could be completely suppressed [199], as shown in Fig. 47(c). It was also discovered that the deposition of a layer (~1 nm) of Ni on a thin $NiSi_2$ layer and the subsequent annealing at ~400–600 °C reproducibly lead to the fabrication of almost completely faceted interfaces [199], as shown in Fig. 47(a). An examination of the three micrographs shown in Fig. 47 reveals that the morphology of the epitaxial $NiSi_2$–Si(1 0 0) interface may be controlled. The atomic structure of the planar $NiSi_2$–Si(1 0 0) interface has been studied experimentally by HREM and shown to be consistent with having either six- or eight-fold coordination [200]. Theoretical calculations tend to favor the eight-fold model over the six-fold model [201,202]. Because extra streaks at the <1/2, 1/2, 0> related positions have been observed at flat $NiSi_2$–Si(1 0 0) interface by TED, it is clear that the atomic structure at this interface is more complicated than these basic models. Its exact details notwithstanding, the flat $NiSi_2$–Si(1 0 0) interface obviously has an atomic structure which is entirely different from either of the two $NiSi_2$–Si(1 1 1) interfaces. One thus expects to find the flat $NiSi_2$–Si(10 0) interface with an SBH of its own. Indeed, uniform $NiSi_2$–Si(1 0 0) interfaces show a SBH which is much lower on n-type Si than either of the two $NiSi_2$–Si(1 1 1) interfaces [75], as shown in Fig. 46. One notes that the low SBH of 0.4 eV measured from uniform $NiSi_2$ layers is also very different from the value of 0.6–0.7 eV usually observed for polycrystalline $NiSi_2$ on Si [203].

What is intriguing about the SBH of an $NiSi_2$–Si(1 0 0) interface is its critical dependence on the morphology of the silicide layer. Interfaces which are almost completely ⟨1 1 1⟩ faceted were

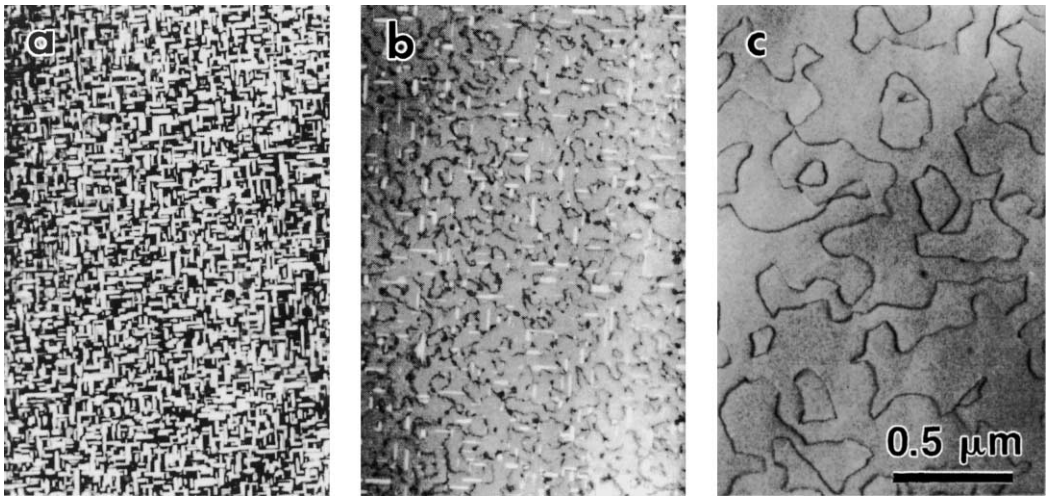

Fig. 47. Plan-view (0 0 2) dark-field, transmission electron microscopy images of ~8 nm thick $NiSi_2$ layers grown on Si(1 0 0). A fact bar show up as a bright streak under this imaging condition. Dark lines are defects with 1/4 (1 1 1) character, which decorate steps with an odd number of atomic planes at the interface: (a) a layer which is nearly completely faceted; (b) a layer with mixed morphology; (c) a uniform layer (from Tung et al. [75]).

shown to have SBHs similar to that found at a type A $NiSi_2$–Si(1 1 1) interface [75]. Since inclined facets at the $NiSi_2$–Si(1 0 0) interface are simply sections of type A, seven-fold, $NiSi_2$–Si(1 1 1) interface, it is not surprising that the SBH found for a $NiSi_2$–Si(1 0 0) interface made up entirely of facets is identical to that found at a planar type A $NiSi_2$–Si(1 1 1) interface. This result suggests that the local SBH is determined by the local atomic structure, irrespective of the orientation or symmetry of the overall interface. It also suggests that the SBH at a ''mixed'' interface, such as the one shown in Fig. 47(b), could be inhomogeneous. Specifically, facet bars are expected to have a locally higher SBH (0.65 eV) than that for the flat portion of the interface (0.40 eV) on n-type Si(1 0 0). However, they should have a lower SBH (0.47 eV) than the flat portion of the interface (0.72 eV) on p-type Si. Therefore, the presence of a few ''facet bars'' at $NiSi_2$–Si(1 0 0) interfaces, which are otherwise flat, should have a strong influence on the measured SBH on p-type Si, yet it should have little effect on n-type Si. This is exactly what has been observed in actual experiments. A low density of facet bars was found to have little effect on the SBH of $NiSi_2$ on n-type Si(1 0 0). Yet on p-type Si(1 0 0), the *I–V* deduced SBH decreased rapidly as the density of facet bars increased, while the decrease in the *C–V* SBH was much slower. As a result, the *C–V* measured SBH for any specific diode significantly exceeded that deduced from *I–V*. Mixed-morphology p-type diodes were ''leaky'', having poor ideality factors, $n > 1.1$, in forward bias and displaying reverse currents which did not saturate. There was also a clear dependence of the electron transport on the substrate doping level: $NiSi_2$ layers with similar densities of facet bars, but grown on p-type Si with different doping levels, showed almost identical SBHs as determined by *C–V*, but a sharp decrease of the SBHs determined by *I–V* with doping level [75]. As discussed, the experimental results observed on p-type Si are all symptoms of SBH inhomogeneity. Saddle point potentials estimated from the actual dimension of the facet bars have been shown to provide a semi-quantitative explanation of the experimental results observed on p-type Si. This example clearly demonstrated one of the tremendous advantages of epitaxial MS systems. Different parts of a complicated system can be studied individually, and the individual results can be pieced together to explain the combined effects observed at complicated systems. Such an analysis is not possible without the ability to isolate the interface structure and SBH at epitaxial interfaces.

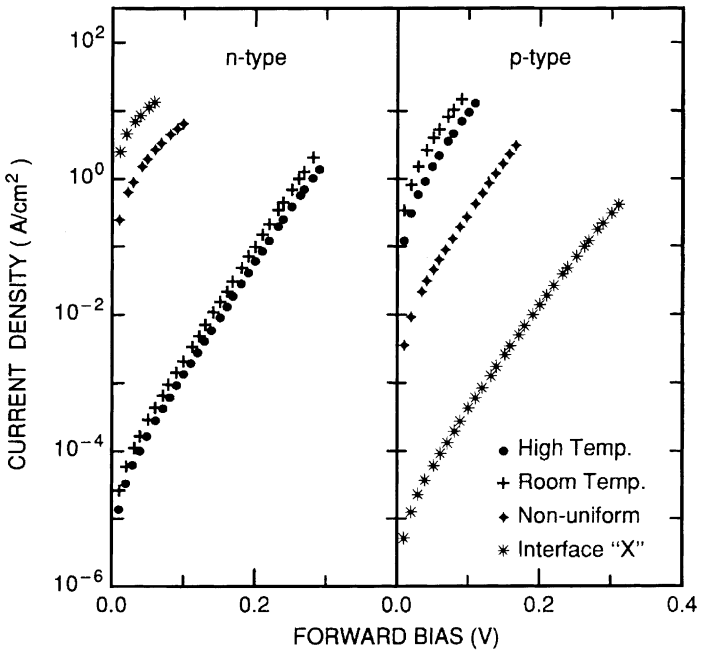

Fig. 48. *I–V* plots for room temperature measurements of high temperature, room temperature, *X*, and non-uniform $CoSi_2$ interfaces on n- and p-type Si(1 1 1) substrates (from Sullivan et al. [204]).

$CoSi_2$ has the same lattice structure as $NiSi_2$, but the details of the epitaxial growth are quite different for these two silicides. For example, type B is the dominant epitaxial orientation observed for $CoSi_2$ layers grown on Si(1 1 1). So, a comparison of the type A and type B SBH is not readily available for $CoSi_2$. The most commonly observed atomic structure of the type B $CoSi_2$–Si(1 1 1) interface also appears to be different from that found at the $NiSi_2$–Si(1 1 1) interfaces. Experimental and theoretical studies have indicated that the eight-fold model is most likely the structure for well annealed, type B $CoSi_2$–Si(1 1 1) interface. However, it is also known that the interfacial structure of type B $CoSi_2$–Si(1 1 1) may vary according to preparation. Evidence for seven-fold coordinated structure has been obtained from layers that have only been annealed to low temperatures, <500 °C. The SBH of type B $CoSi_2$ layers grown at ~600 °C by SPE is usually in the range 0.65–0.70 eV on n-type Si. It seems reasonable to attribute this SBH to an interface that has the eight-fold structure. On the other hand, $CoSi_2$ layers grown at lower temperatures, which have a low density of dislocations, show considerable variation in their SBH [204], as shown in Fig. 48. An SBH of ~0.27 eV has been observed from a specific interface, called "X" interface, fabricated on n-type Si(1 1 1), while a correspondingly high SBH, >0.7 eV, has been observed on p-type Si for the same interface. There is a high density of structural defects associated with the formation of the "X" interface, where both the structure and the SBH are apparently not homogeneous. The atomic structure of the "X" interface has not been determined, although the procedures for the fabrication of this interface would lead one to believe that this interface is more "Co-rich" than the well-annealed eight-fold interface. It seems reasonable to attribute, if only tentatively, the huge range (>0.4 eV) of SBHs observed at the type B $CoSi_2$–Si(1 1 1) interfaces to a variation in the interface atomic structure.

The SBH of epitaxial $CoSi_2$–Si(1 0 0) interface is usually found not to differ much from that observed for polycrystalline $CoSi_2$. The energies of various epitaxial structures of the $CoSi_2$–Si(1 0 0) interface have been studied theoretically [80]. A 2×1 reconstruction is often observed at

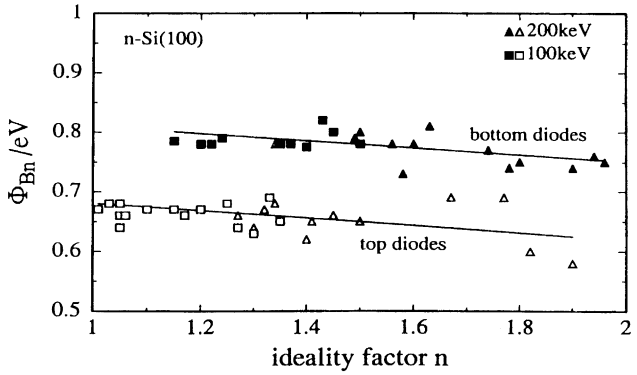

Fig. 49. Average Schottky-barrier heights vs. ideality factor n for various buried, epitaxial $CoSi_2$ layers fabricated by high energy Co ion implantation. Implantation energies are indicated (from Werner et al. [207]).

the interfaces of epitaxial $CoSi_2$, although its structure has not been definitively determined [205,206]. The existence of more than one stable structures has been suggested by HREM studies of the $CoSi_2$–Si(1 0 0) interface [207,208]. For example, the structures of the two interfaces of buried, epitaxial Si–$CoSi_2$–Si(1 0 0) structures have been found to be different, as shown in Fig. 49. The upper interface, between $CoSi_2$ and the Si overlayer, consists mostly of segments with six- and four-fold structures, while the lower interface, i.e. between $CoSi_2$ and the Si substrate, is made up of six- and eight-fold segments. Interestingly, the SBH of the upper interface has been measured to be ∼0.1 eV lower than the lower interface, on n-type Si [208]. This dependence has been attributed to the difference in the observed interface structures.

6.2. Other epitaxial metal–semiconductor interfaces

Experimentally observed SBH of the epitaxial Pb–Si(1 1 1) system has been observed to depend on the structure of the initial monolayer-covered Si(1 1 1) surface [209], as shown in Fig. 50. A SBH of ∼0.7 eV was measured when the surface had a starting (7 × 7)-Pb structure, and 0.93 eV was measured when the $(\sqrt{3} \times \sqrt{3})$ R30°-Pb structure was present [209]. This dependence has been attributed to the difference in the Pb–Si interface structures, carried over from the starting surfaces. A difference of this magnitude has also been observed for the FL positions of the two interfaces by photoemission [210]. However, the preservation of these surface reconstructions at the eventual Pb–Si interface was called into question [211,212]. In any event, the structures of the two Pb–Si interfaces, albeit possibly changed from those on the original surfaces, are still expected to be different. Hence, the observed difference in SBH is most likely still attributable to a structural difference. One notices that the high ideality factors (Fig. 50) and the difference between *I–V* and *C–V* measurements may be suggestive of some SBH inhomogeneity at these interfaces [209].

Epitaxial (1 0 0)-oriented, Al layers have been grown, with a 45° azimuthal rotation, on GaAs(1 0 0) [213]. However (1 1 0) oriented Al has also been observed [214]. It has been pointed out that the reconstruction of the initial GaAs surface structure may influence the epitaxial orientation of the Al films [215]. The interfaces between epitaxial Al and GaAs(1 0 0) have been studied by a number of techniques [216,217]. MBE prepared GaAs(1 0 0) surfaces may have a variety of reconstructions which are associated with different surface stoichiometry. The periodicities of some of these superstructures are found to be preserved at the Al–GaAs interface [218]. It has been discovered that the Schottky-barrier height between epitaxial Al or Ag layers and GaAs is a function of the original GaAs surface reconstruction/stoichiometry [219], which is

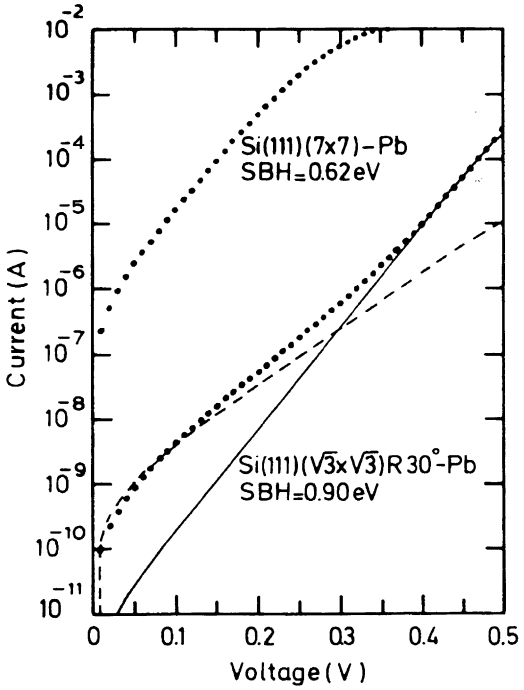

Fig. 50. Forward-current characteristics of 7×7 and $(\sqrt{3} \times \sqrt{3})$ R30° epitaxial Pb–Si(1 1 1) contacts. Contact area is 1.6×10^{-3} cm^2. For the $(\sqrt{3} \times \sqrt{3})$ R30° curve, the fitted thermionic emission current (solid line) and the generation–recombination current (dashed line) are shown (from Heslinga et al. [209]).

suggestive of a possible correlation of the interface structure and SBH. However, this correlation was found to be absent in other studies [220,221]. Recently, a direct correlation of the SBH with the experimentally observed superstructures, 1×6 and 1×4, at the Sb–GaAs(1 0 0) interface has been demonstrated [222], where the difference in the atomic structure has been offered as a likely explanation of the difference, ~0.1 eV, between the observed SBHs.

Except for refractory metals, most elemental metal/III–V compound semiconductor structures are thermodynamically unstable. Annealing, even at moderate temperatures, often leads to interdiffusion and formation of other compound phases. Two groups of intermetallic compounds are found to have stable interfaces with III–V compound semiconductors with good lattice matching conditions [223]. Hence, these are good candidates for the formation of stable, single crystal, MS interfaces with GaAs. NiAl [224] and related compounds [225] form one group. They have the cubic CsCl crystal structure and lattice parameters ~1–2% larger than one-half the lattice parameter of GaAs. Rare-earth (RE) monopnictides, mostly with the NaCl structure, form the other group of intermetallic compounds suitable for epitaxial growth on III–V semiconductors [226]. The usual (1 0 0) epitaxial orientation is found for these epitaxial systems. The interfaces between GaAs(AlAs) and a number of epitaxial intermetallic compounds have been examined by HREM [227,228]. However, the atomic structure of these interfaces have not been properly modeled. Evidence for a reconstruction has been observed at the interface between NiAl and overgrown GaAs. The SBH of various structures involving epitaxial metallic compounds has been studied in detail. It was found that buried NiAl has a different SBH with respect to the overgrown (AlAs)GaAs than that on an (AlAs)GaAs substrate [229]. The observed SBH also seems to depend on the thickness of the NiAl and CoAl layers [230]. Furthermore, the ideality factors of the *I–V* measurements are noticeably

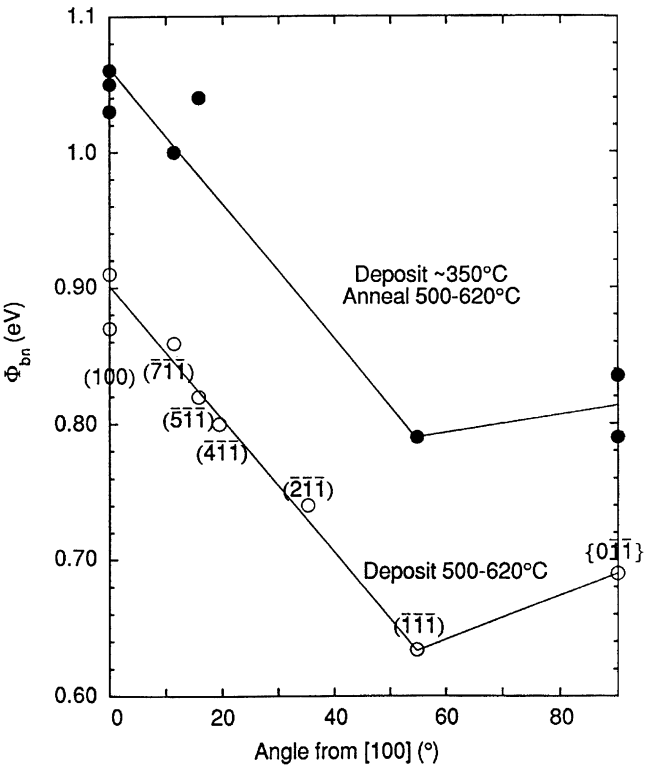

Fig. 51. Schottky-barrier height vs. substrate orientation for lattice matched $Sc_{1-x}Er_xAs$/GaAs{h 1 1} diodes (from Palmstrom et al. [8]).

higher than unity, and the measured SBHs depend on the measurement technique. From the previous discussion of such behaviors, a non-uniformity of the various SBHs is suggested. The most spectacular result from these epitaxial metallic compound interfaces is the observation of a dependence of the SBH on epitaxial orientation, observed at the lattice-matched $Sc_{1-x}Er_xAs$–GaAs systems [8,231], and shown in Fig. 51. It shows that annealing may lead to significant changes in the observed SBH. The SBH of the ternary compound $Sc_{0.32}Er_{0.68}$ As varies by as much as 0.4 eV when the n-type GaAs orientation is changed from (1 0 0) to (1 1 1) [8]. It is possible that this significant variation of the SBH is related to the different atomic structures at these MS interfaces.

6.3. BEEM study of epitaxial MS interfaces

The spatial resolution offered by BEEM has been used to study the SBH variation at epitaxial MS interfaces consisting of mixed orientations. A study on the mixed type A and type B $NiSi_2$–Si(11 1) failed to show an appreciable difference between these two orientations [232]. This apparent disagreement with regular diode measurements was likely the result of the pinch-off effect, as pointed out [232]. When the effect of pinch-off was specifically avoided, a dependence of the SBH on the epitaxial orientation has been observed at the $CoSi_2$–Si(1 0 0) interface [233]. Silicide grains with (1 1 0) orientation were found to have a lower SBH, 0.58 eV, than that for (1 0 0) oriented grains, 0.74 eV, on n-type Si(1 0 0). Because epitaxial MS interfaces are expected to have homogeneous SBH, BEEM images within a single epitaxial grain may appear to be uninteresting at first thought. However, a series of careful studies of epitaxial $CoSi_2$ interfaces has produced some of

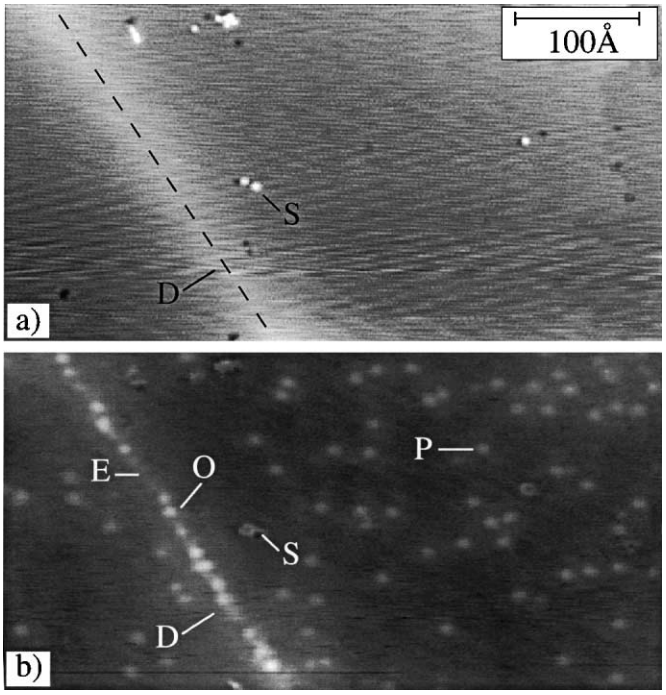

Fig. 52. (a) STM topography image of a 2.8 nm thick $CoSi_2$ film taken at $V_t = -1.2$ V, $I_t = 20$ nA. The bright line (D) is a 0.06 nm high protrusion caused by the strain field of a dislocation. Some surface point defects (S) are present. The gray scales range from 0 to 0.2 nm. (b) Corresponding BEEM image: interfacial point defects like the one labeled (P) have been trapped in the core of a dislocation (D). There are empty (E) and occupied (O) regions in the dislocation. The gray scales vary within a range of $\Delta I_C = 263$ pA (from Meyer and von Kaenel [482]).

the most spectacular images and has considerably improved our understanding of the SBH formation mechanism as well as our understanding of the BEEM technique itself. Shown in Fig. 52 are surface morphology and BEEM images obtained at cryogenic temperatures of ultra-thin epitaxial $CoSi_2$ layers grown in situ on Si(1 1 1). Because of the cleanliness of these experiments, surface structures and interface properties were meaningfully compared [168]. The uniformity of the SBH over the vast majority of the interface was very keenly noted, in good quantitative agreement with results obtained by macroscopic techniques. But the most striking result is the behavior of local SBH around structural defects. Because the dislocations at epitaxial interfaces are well understood, their electrical characterization by BEEM served as a testing ground for calculations and theories. Different types of defects behave quite differently in terms of their influence on the local SBH. The variation of the BEEM current around misfit dislocations for the type B $CoSi_2$–Si(1 1 1) interface, most likely with Burgers vector of $a_0/6[11\bar{2}]$ type, was found to be confined to within <1 nm of the dislocation [234]. The increased (decreased) BEEM current for hot electrons (hot holes) was likely due to increased scattering, because there was no measurable change in the local SBH. Dislocations and line defects at the $CoSi_2$–Si(1 0 0) interface also influence the BEEM current of their surrounding area. However, this time the affected regions had a width of ~4 nm and the local SBH within these regions decreased by about 0.04–0.08 eV for $a_0/4[11\bar{1}]$ dislocations, and about 0.1 eV for an unidentified type of line defect [13]. Because of the pinch-off effect, a drop of the apparent local SBH with this magnitude required a decrease in the interface SBH of at least ~0.3–0.7 eV [13]. It is worth commenting that the apparent difference (1 nm versus 4 nm) in the lateral dimensions of the BEEM current variation between the $CoSi_2$–Si(1 1 1) and the $CoSi_2$–Si(1 0 0) interfaces may in fact be

insignificant, because of the electron focusing effect which is known to take place along the ⟨1 1 1⟩ directions of the $CoSi_2$ crystal [170,171]. In any event, the energetic and spatial implications of the SBH mechanism responsible for this local decrease of SBH is difficult to reconcile with a deep-level-based concept of defect pinning, although one must recognize the invalidity of classical concepts at quantum mechanical dimensions. On the other hand, the very large energetic influence and very confined spatial influence of defects on the local interface dipole is in good agreement with the picture of individual bonds in the bond-polarization theory of SBH formation.

6.4. Comparison with theoretical calculations and discussions

The overall picture of the formation of the SBH at single crystal MS interfaces, presented by experimental investigations, is identical to that described earlier from theoretical studies. In the few cases where theoretical calculations have enough accuracy for a meaningful comparison with experimental SBHs, most notably on the difference of SBHs between the type A and type B $NiSi_2$–Si(1 1 1) interfaces, good numerical agreement was found. The message is unmistakable: the SBH depends on the atomic structure of epitaxial MS interfaces. This dependence is inconsistent with SBH models that ignore interaction between the metal and the semiconductor. It also disagrees with the basic notion of CNL-based models that the distribution of interface states is independent of the metal. It is in good agreement with the spirit of the bond-polarization theory. However, one notes that the tight-binding picture of the bond-polarization theory would not be able to explain the A–B dependence of the $NiSi_2$ SBH either. Before one rules out any SBH model based on the experimental data observed from epitaxial MS interfaces, however, one needs to appreciate the complexity of the SBH problem. Even after the entire interface electronic structures are known for a number of epitaxial MS interfaces from calculations, researchers are still at a loss as to the single most important feature or parameter that determines the SBH. There is none, other than the ''charge density distribution of the entire interface''. The formation of the SBH has always contained a bulk term and an interface term, as revealed by Eq. (1.3.5). Results described in this section give strong indication that the interface term depends on the interaction between the metal and the semiconductor. This should be regarded as the most important message from these studies. If we were to ask ourselves the question ''given all the information one now knows about the electronic properties of epitaxial MS interfaces, what is the most convenient way to view the formation of the interface dipole (at any MS interface)''? The answer cannot be anything other than ''bonding''.

7. Inhomogeneous barrier height

The uniformity of the SBH is an issue with important implications on the theory of SBH formation and important ramifications for the operation of SB diodes and contacts. Unfortunately, serious attention was not paid to this particular issue until the late 1980s, when various models and concepts on SBH formation, based on homogeneous MS interface, were already widely disseminated and adopted by many researchers in the field of SBH. Direct evidence for the presence of inhomogeneity in the SBHs was recognized and reported only sporadically [148,149,235]. Then two events occurred within the span of a few years, which changed our views on the subject: the introduction of the BEEM technique and the development of the analytic theory on electron transport at inhomogeneous MS interfaces. The former provided direct evidence for SBH variation at select MS interfaces, while the latter offered an insight into how severe and widespread the SBH inhomogeneity problem really was in polycrystalline Schottky diodes.

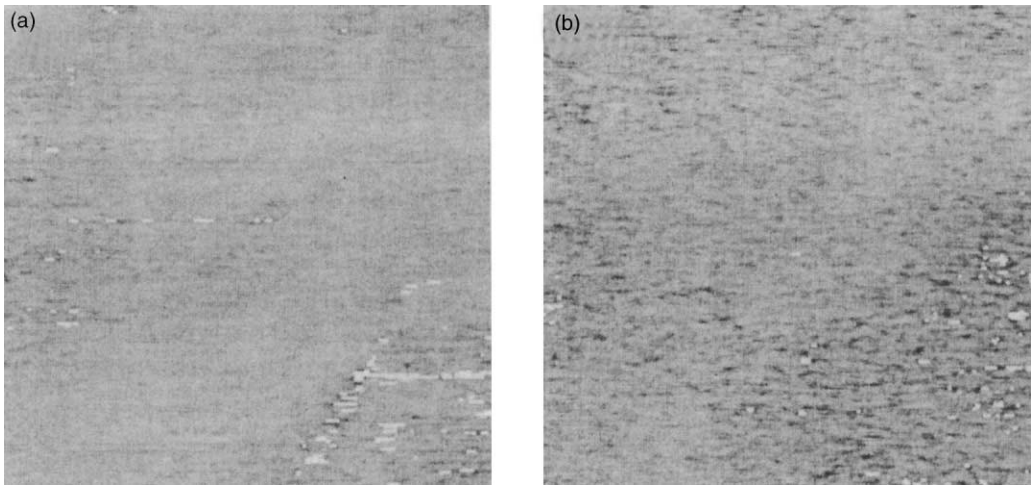

Fig. 53. (a and b) Spatial distribution of the effective Schottky-barrier height of a Au–n-Si(1 0 0) diode, as obtained by ballistic electron emission microscopy and spectroscopy. The image area is 60 nm × 60 nm and the image contrast window is 0.6 eV (black) to 1.0 eV (white). Dead pixels are depicted white. The doping level of the Si is 8×10^{16} cm^{-3} (from Palm et al. [12]).

7.1. BEEM studies of polycrystalline MS interfaces

The most direct evidence for barrier height variation in common SB diodes naturally came from spatially resolved SBH studies with the BEEM technique. The overall uniformity of a SB diode is easily revealed by BEEM images. Occasionally, large scale variations (0.7–1.1 eV) of the SBH have been observed at compound semiconductor [236]. But on lightly doped semiconductors, only slight modulation of the barrier height (∼0.1–0.2 eV) is more frequently observed. The barrier height of Au films was found to be exceptionally uniform on a number of semiconductors [12,165,237], as shown in Fig. 53(a). However, the amplitude of SBH modulations was found to depend on the doping level of the semiconductor, in good agreement with the potential pinch-off effect [12]. As shown in Fig. 53(b), a much wider range of the SBH is observed when more heavily doped semiconductor is used. BEEM has also been used as a quantitative tool to study the statistics of SBH distributions. BEES scans are carried out for a large number of spatial locations of the same diode to get a profile of the SBH distribution, which is then used to calculate the expected *I–V, C–V* and PR characteristics from the same diode in macroscopic measurements [12,238,239]. Generally, the SBHs calculated from BEEM distributions compare very closely with those measured with macroscopic techniques. This agreement is to be expected, since the SBH distribution measured by BEEM reflects the effective SBH after the potential pinch-off phenomenon has taken effect. Direct evidence for the potential pinch-off effect has been observed by BEEM in artificially generated inhomogeneous SBs [240,241]. A continuous Au films was deposited over small Co islands, of variable sizes, which were pre-deposited on GaAsP. Such ‘‘mixed’’ diodes are expected to have a background of high SBH decorated with small patches of low-SBHs, because the Co–GaAsP interface has a SBH that is lower than that of the Au–GaAs interface by about 0.15 eV. Such an overall BEEM pattern was indeed observed, as shown in Fig. 54(a). Because the sizes of the Co islands, 5–10 nm, are smaller than the depletion region width of GaAs, most of the low-SBH patches should be pinched-off. Furthermore, the smaller patches should be more severely pinched-off than the larger ones. Line scans taken across low-SBH regions of different dimensions, shown in Fig. 54(b), indeed show this size dependency clearly. Saddle-point potentials calculated according to

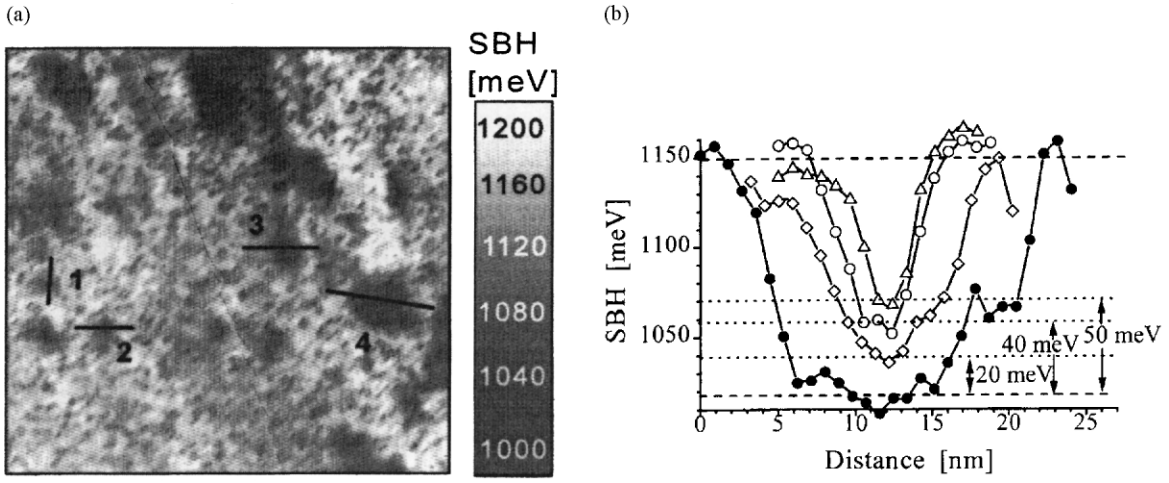

Fig. 54. (a) Schottky barrier map of an inhomogeneous 6 nm Au/0.5 nm Co/$GaAs_{0.67}P_{0.33}$ Schottky diode (size: 114 nm × 114 nm), dark areas correspond to Co clusters at the MS interface. The black lines (1–4) indicate the linescans through Co patches of different sizes. (b) SBH profiles along the linescans in (a). The diameters for the four Co patches are 5, 7, 10, and 18 nm, respectively (from Olbrich et al. [240]).

the analytic theory (Table 1), using the actual island sizes were found to be in good quantitative agreement with the ''valleys'' measured by BEEM. This example lends strong support for the potential pinch-off effect. In passing, it is worth mentioning that the bias dependence of the saddle point potential, which is the underlying reason for the existence of non-ideal diodes, has not been studied by BEEM. There are some experimental difficulties with such a study, particularly with the background diode current. However, a low-temperature study of smaller diodes may still succeed. It is also worth mentioning that, along the same vein as these results, the effect of potential pinch-off has also been observed at semiconductor–liquid interfaces [138,242]. Semiconductor electrodes pre-coated with isolated metal islands of precisely controlled sizes exhibited *I–V* behaviors which depended sensitively on the size of the metal particles [243], in good agreement with the prediction of the analytic theory of inhomogeneous SBH. In these cases, the ''barrier height'' of bare semiconductor surfaces, between the metal clusters, in direct contact with the liquid, can be controlled by the redox potential of the solution. The semiconductor–liquid interface provided the high barrier height background that was used to pinch-off the conduction patch in front of the metal clusters.

7.2. Leakages and edge-related currents

Experimentally observed *I–V* curves have frequently been analyzed and shown to be comprised of two or more components of current [124,244], as illustrated in Fig. 55(a). At small biases, the forward current is sometimes dominated by a ''soft'', or ''leaky'', component that leads to both a curvature in the *I–V* curve and a tangential slope that corresponds to an ideality factor much in excess of 1. As the bias increases, the *I–V* relationship becomes semi-logarithmic with an ideality factor not far from unity, before at very large biases, when the current turns over due to series resistance. The presence of a leaky component is particularly easy to detect at lower temperatures. It has been customary to attribute the linear portion of the *I–V* curve to the main conduction mechanism, e.g. thermionic emission over the SB, and the leakage current at low biases to a different mechanism. Generation and recombination in the space–charge region [245] and edge-related conduction [130,246,247] are the mechanisms most frequently thought to lead to the leakage

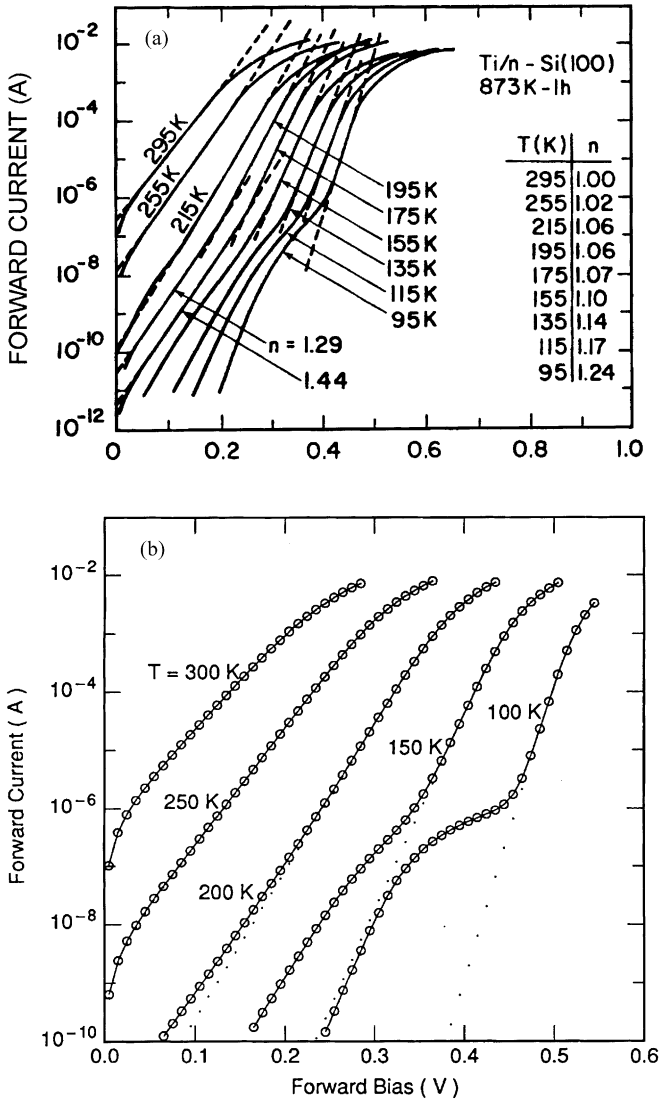

Fig. 55. (a) Forward *I–V* characteristics of Ti on n-type Si(1 0 0) as a function of temperature for samples annealed at 873 K for 1 h. Diode area is 4×10^{-4} cm^2 (from Aboelfotoh [244]). (b) Calculated *I–V* characteristics of an inhomogeneous SB (from Tung [10]).

currents. Because edge-related currents scale with the peripheral length of the diode, and not with the area of the diode as would be expected from common junction conduction mechanisms, they may be unambiguously identified by using diodes with different sizes [130,248]. Before the effect of SBH inhomogeneity was recognized, the additional current component associated with edges was thought to be due to a larger electric field at the diode edges which leads to increased tunneling and/or increased generation–recombination [245]. Because the oxide–silicon interface is usually unpinned, it has never been clearly demonstrated, at least for Si, what this large electric field could have originated from. Some experimental analyses showed that edge-related currents had ideality factors similar to [130], or smaller than [248,249], the ideality factor associated with the center portions of the diodes, as illustrated by the example of Fig. 56. Also, analyses of the leaky current often showed the activation energy to be far from one-half the semiconductor band gap [244,250], in disagreement

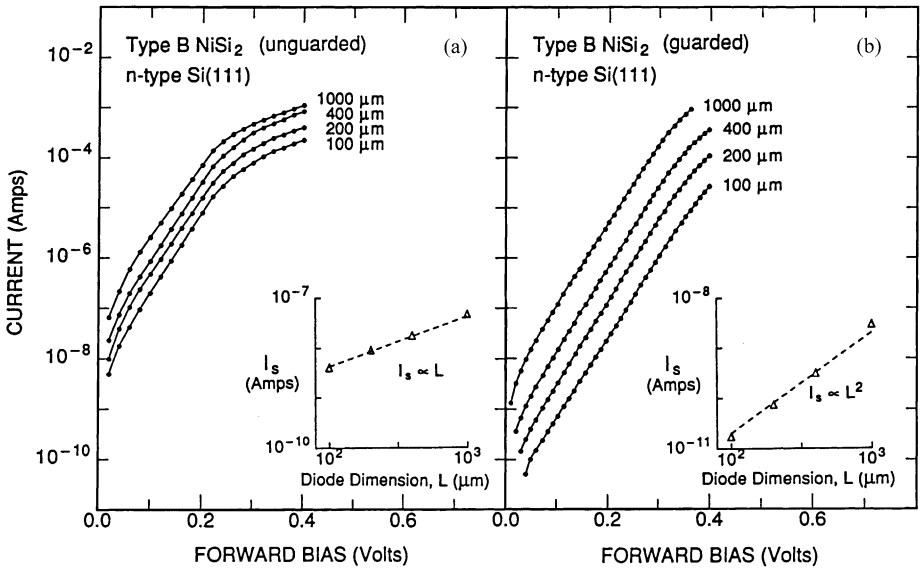

Fig. 56. *I–V* characteristics of epitaxial type B $NiSi_2$–Si(1 1 1), n-type Schottky circular diodes with varied diameter: (a) edges unprotected, showing edge-related current that is linearly proportional to the diode diameter, but with excellent ideality factors, ~1.01; (b) diode edges are protected by guard-rings. The current is proportional to the area of the diode (square of the diameter) (from Sullivan et al. [248]).

with the generation–recombination mechanism. All these observations indicate that edge-related currents should not be indiscriminately attributed to the generation–recombination process. When the leakage current is not clearly related to edges, generation–recombination was still the explanation most commonly invoked. However, the fact that leakage currents were observed to be clearly dominating in some diodes and completely missing in others, among diodes on the same sample [248], seems inconsistent with a uniform distribution of generation–recombination centers. Occasionally, the leakage current at low bias has been attributed to the presence of interface states and analyzed with the fixed-separation model [125]. This is unfounded, as comments in Section 6.3 will explain.

Experimentally observed leakage currents and edge-related currents are both consistent with SBH inhomogeneity. The presence of a few large low-SBH regions (with their large γ and, hence, large ideality factors) in the SB diode can certainly lead to the observation of a leaky component in the junction current, as shown in Fig. 55(b). The small slope of this current (high ideality factor) and effects due to series resistance limit the predominance of this leakage component to small forward biases. Because of a lower effective SBH, the presence of even a single low-SBH region can lead to the observation of leakage current. Experimentally observed diode-to-diode variations of the leakage current are in much better agreement with isolated "leakage spots" due to low local SBH rather than with a distribution of recombination centers in the space–charge region. The existence of a current component that is proportional to the perimeter of the diode is also in good agreement with SBH inhomogeneity. A low-SBH patch is less effectively pinched-off when it is situated in close proximity (on the order of the depletion width) to the edge than when it is at the central proportion of a diode, as has been clearly demonstrated by computer simulations [25]. To see the reason behind this effect, one only need to be reminded that a low-SBH patch, positioned right on the edge of a diode, is not pinched-off at all. When a SB diode contains a uniform distribution of low-SBH patches, the number of patches that are found near the edges is proportional to the peripheral length.

Therefore, most edge-related currents observed in experiments are consistent with the presence of SBH inhomogeneity. The fact that edge-related currents sometimes have low ideality factors is also consistent with SBH inhomogeneity [248], because low-SBH patches near the edges are less pinched-off. Finally, the structure of the MS interface near the edges may be different from that at the central portion of the diode, resulting in a locally different SBH and an edge-related current.

7.3. Greater-than-unity ideality factors

Even though the forward *I–V* plots experimentally observed from SBs are almost always semi-logarithmic, the slopes of such traces often differ from the prediction of the thermionic emission theory. An ideality factor greater than 1.03, has no direct explanation in the thermionic emission theory, and is generally attributed to a SBH that is bias-dependent. Image-force lowering [251], generation–recombination, interface states (negative charge) [174,178] and tunneling [113,252] have all been discussed as possible mechanisms which could lead to a greater-than-unity ideality factor. Since the image-force lowering and TFE may be calculated and the generation–recombination contribution can be distinguished experimentally, the maximum ideality factor due to these mechanisms may be accurately estimated. Observed ideality factors often far exceed these estimates, prompting the proposal that interface states are a main origin of greater-than-unity ideality factors.

Two slightly different mechanisms have been proposed to explain the ideality factor on interface states: the fixed-separation model and the negative charge model. With the fixed-separation model, the ideality factor can be predicted from an assumption of interface states, as shown in Eq. (7.1.3). However, because the charge of the interface states is controlled by both the applied bias and the metal work function, as shown in Eq. (7.1.1), a dilemma is reached in this analysis, as first noted by Freeouf [253]. This dilemma is clearly illustrated by Eq. (7.1.3), which states that the ideality factor for a semiconductor should be the inverse of the interface behavior parameter S_Φ observed for the same semiconductor. So, for semiconductors like Si and GaAs, where the Fermi-level is tightly pinned ($S_\Phi < 0.2$), the ideality factor should be greater than 5 (S_Φ^{-1}), in clear conflict with the experimental data. The band bending near the MS interface in the presence of MIGS has also been modeled with the negative charge model [71–73] as shown in Fig. 27. In contrast to the fixed-separation model, the negative charge model assumes that the population of the MIGS is independent of the applied bias. With this assumption, the effective SBH (the highest point of the potential in Fig. 27) varies linearly with the electric field, giving rise to the desired bias dependence that is consistent with large ideality factors. However, the decay length of the MIGS is often assumed to be unreasonably long, 2–5 nm, to be consistent with experimental observations. Furthermore, the negative charge model is inconsistent with experimental results observed on both n- and p-type semiconductors. The short-range band bending at the MS interface is generally regarded to be independent of the semiconductor doping type. In other words, the net charge of the MIGSs is either positive or negative (or vanishes), for a particular MS system. MIGS with a net negative (positive) charge can lead to large ideality factors only on n-type (p-type) semiconductors. Experimental results show large ideality factors on both n- and p-type semiconductors, in disagreement with the negative charge proposal. There are other experimental observations that are not consistent with interface gap states in general. For instance, the ideality factors are often found to vary significantly with processing, or from diode to diode on the same sample, while the SBHs are essentially the same. These results are hard to explain with interface gap states, because the gap states are usually assumed to have implications for both the magnitude of the SBH and the ideality factor of a SB diode. Occasionally, the ideality factor seems to correlate mysteriously with the

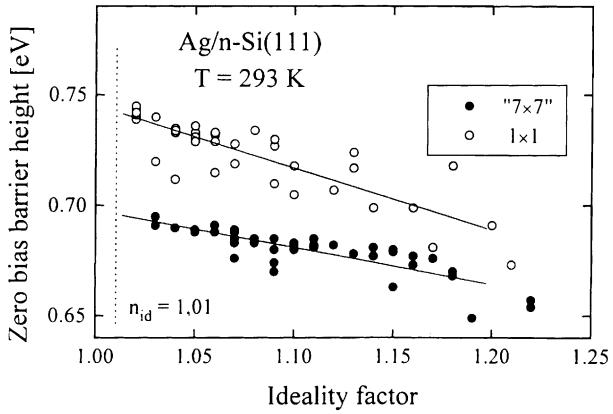

Fig. 57. Zero-bias barrier heights of Ag–n-Si(1 1 1) — "7 × 7" and Ag–n-Si(1 1 1) — 1 × 1 diodes as a function of the ideality factor (from Schmitsdorf et al. [483]).

magnitude of the observed SBH: among identically prepared diodes, higher ideality factors were often found to accompany lower observed SBHs [129,203] as shown in Figs. 49 and 57.

The bias dependence of the saddle-point potential of an inhomogeneous SB can explain the observed behavior of the ideality factors. Since the ideality factor depends on the characteristics of the low-SBH patches, the slope of the *I–V* curves can vary when the saturation current remains relatively unchanged. When the doping level increases (η decreases), the $\Phi_{\rm eff}$ of a low-SBH patch with a fixed γ decreases and its ideality factor increases, in good agreement with some experimental observations. The diode-to-diode variation of the ideality factor and the dependence on processing are also consistent with variations in the distribution of local SBH in the diodes under study. The observation of large ideality factors when the diode is in a state of maximum confusion [254,255] is also in good agreement with the interpretation of ideality factors based on SBH inhomogeneity. The correlation between the SBH and the ideality factor [129,203] shown in Figs. 49 and 57, can be trivially explained by the analytic theory on inhomogeneous SBH. Plugging Eq. (5.3.5) into Eq. (5.3.4), one gets

$$\Phi_{\rm eff} = \Phi^{00}_{\rm B,n} - (n_{\rm eff} - 1)V_{\rm bb}\xi^{-1}. \tag{9.3.1}$$

So, a linear dependence of the SBH on the ideality factor is expected whenever the local SBH varies about the same mean SBH, but with different amplitudes and/or periods. Recently, much has been made of this correlation in a series of publications [256,257], where the asymptotic SBH value extrapolated to $n = 1$ on such a plot has been proclaimed as the "homogeneous" SBH, or the "true" SBH, of the system. Some systematic analysis of these homogeneous SBH then ensued, culminating in a declaration of the success of the MIGS model [257]. Such a view is puzzling, since the SBH value extrapolated to $n = 1$ is still only a statistical average of the SBH of the MS system, albeit a simple mathematical average, as shown in Eq. (9.3.1). Furthermore, these systems have inhomogeneous SBHs, as the analysis showed, so the alleged state of homogeneous SBH does not exist for these systems in any real diodes.

A large ideality factor indicates a dependence of the apparent SBH on the applied bias. Rewriting Eq. (5.1.4) for a uniform SBH, but with a bias-dependent SBH:

$$I_{\rm SB}(V_{\rm a}) = AA^*T^2 \exp\left\{-\frac{\Phi_{\rm B,n}(V_{\rm a})}{k_{\rm B}T}\right\}\left[\exp\left(\frac{eV_{\rm a}}{k_{\rm B}T}\right) - 1\right], \tag{9.3.2}$$

and integrating Eq. (5.1.10a), one gets

$$\Phi_{B,n}(V_a) = \Phi_{B,n}(0) + \left(\frac{n-1}{n}\right)V_a. \tag{9.3.3}$$

Here, $\Phi_{B,n}(0)$ is the SBH measured by extrapolation to zero bias, as in a conventional *I–V* analysis. It has been argued that the origin of the bias-dependence of the SBH is the electric field at the MS interface. With this notion is mind, it seems reasonable to assume that the SBH corresponding to zero electric field, i.e. under flat-band condition, rather than $\Phi_{B,n}(0)$, should be the "fundamental SBH" of the system [258]. The flat-band SBH can be calculated as

$$\Phi_{F\text{-}B} = n\Phi_{B,n}(0) - \left(\frac{n-1}{n}\right)eV_N. \tag{9.3.4}$$

$$\Phi_{F\text{-}B} \approx n\Phi_{B,n}(0). \tag{9.3.4a}$$

So occasionally, $n\Phi_{B,n}(0)$, the alleged flat-band SBH, is quoted as the SBH from *I–V* measurements in the literature [259,260]. One notes that the flat-band SBH concept relies on the uniformity of the SBH under study, which is internally inconsistent with the known fact that the main reason for the observation of large ideality factors is SBH inhomogeneity. When the SBH is inhomogeneous, the band cannot be made flat near the MS interface at any applied bias. There is no "fundamental SBH" per se for an inhomogeneous MS system. An artificially created quantity $n\Phi_{B,n}(0)$ is not as meaningful as $\Phi_{B,n}(0)$, which, at least, is based on a sound physical model, the thermionic emission theory.

7.4. T_0 anomaly and other dependencies of ideality factor

Many different temperature dependencies of the ideality factor have been experimentally observed. Most frequently, the ideality factor of a diode increases when the sample temperature is lowered. At many MS interfaces, the deduced SBH and ideality factors are found to vary with the measurement temperature in a fashion generally known as the "T_0 anomaly" [126,261–263]. Such a phenomenon has been observed from many types of SBs, on elemental semiconductors and compound semiconductors [264] alike. A diode is said to display the T_0 effect if its junction current may be expressed as

$$I_{T_0} = A^{**}AT^2 \exp\left(\frac{-e\Phi_{T_0}}{k_B[T+T_0]}\right)\left[\exp\left(\frac{eV_a}{k_B[T+T_0]}\right) - 1\right], \tag{9.4.1}$$

where T_0, typically 10–60 K, and Φ_{T_0} are both constants. Demonstration of the T_0 effect is usually accomplished by plotting nk_BT (the inverse slope of an *I–V* curve) against k_BT and observing a straight line, parallel but offset from the $n = 1$ line [126] as illustrated by Line #3 of Fig. 37. In addition, by changing the abscissa of the Richardson plot from $1/T$ to $1/nT$, a straight line should be observed in cases displaying the T_0 anomaly. It has been proposed that the T_0 anomaly was due to an exponential distribution of the density of gap states [31]. However, such an analysis is not valid because it utilizes the unphysical variable–electron-affinity model, shown in Fig. 17. The fact that the measured T_0 varies significantly among similarly fabricated diodes [265] and the proposal that T_0 varies locally in a large diode [266] are suggestive that the T_0 anomaly is not directly related to the formation mechanism of the SBH. Crowell [267] pointed out that the T_0 anomaly was consistent

with band bending such as that arising from opposite-type doping at the interface [268] (see Fig. 27 and also Fig. 68). However, deliberate doping modifications brought out changes [269] in the apparent T_0 which were opposite to that expected from Crowell's proposal. The suggestion that the T_0 anomaly is a result of the temperature dependence of the work function [126] seems numerically off by at least an order of magnitude.

It is usually assumed that a study of the dependence of ideality factor on temperature can reveal the conduction mechanism of a particular SB diode. The T_0 phenomenon is only one of the distinctive temperature dependences according to the original categorization by Saxena [126], as schematically shown in Fig. 37. A temperature-independent, large ideality factor, Line #2 in Fig. 37, has often been observed experimentally. So has a dependence similar to Line #4 in Fig. 37, which is usually attributed to a domination of the conduction mechanism by TFE [113,252]. Good quantitative agreements of experimental data with the TFE theory have been observed. However, the occasional observations of data similar to Line #4 in Fig. 37, under experimental conditions where tunneling should be negligible [262] suggests that the interpretation of the conduction mechanism based on the temperature dependence of the ideality factor may not be unique. Frequently, the ideality factor of a SB diode is shown to follow different behaviors at different temperature ranges. For instance, a diode may exhibit a high (low) ideality at high temperature and yet a low (high) ideality at low temperatures. Furthermore, just like the magnitude of the ideality factor, the temperature dependence of the ideality factor of a diode also varies with processing.

With the assumption of homogeneous SBH, different transport mechanisms would have to be invoked to explain apparently different characteristics. This leads to all sorts of contradictions and inconsistencies. When SBH inhomogeneity is considered, however, a wide range of different *I–V* characteristics can be coherently explained with just one transport mechanism, thermionic emission. Shown in Fig. 58 is the temperature-dependence of the ideality factor, numerically simulated for inhomogeneous SBs with different SBH distributions [25]. A temperature-independent, greater-than-unity, ideality factor, often observed experimentally [263,270] is consistent with a SB diode whose current transport is dominated by low-SBH regions with narrowly distributed γ, as shown in Fig. 58(a). An increase of the ideality factor with decreasing temperature, as is the case for the majority of SB diodes, is consistent with the presence of many low-SBH regions with a distribution in their low-SBH characteristics (γ). The current of a random, inhomogeneous, SB diode is described by Eq. (5.3.6), which, as shown explicitly [10] may be expressed phenomenologically in a form identical to Eq. (9.4.1). Therefore, SBH inhomogeneity offers the only valid explanation of the T_0 anomaly: as the temperature is lowered, the junction current is dominated by fewer low-SBH regions with lower effective SBHs and larger ideality factors. As an example, the inverse slope, in an *I–V* simulation, of a SB diode with low-SBH patches of just two distinct γ is plotted in Fig. 58(b) as a function of temperature, to illustrate the origin of the T_0 mystery. The empirical constant T_0, which depends on how the ideality factor is evaluated experimentally, is related to σ_{SBH} and the doping level [10]. Since the fluctuation of SBH likely varies for different diodes, the inconsistency of the measured T_0 [265,266] and the doping dependence [269] are all naturally explained. A decrease of the ideality factor with cooling, occasionally observed, e.g. Fig. 7 of Aboelfotoh and Tu [271], is consistent with effects due to series resistance [272]. However, this inverse T_0 effect is also consistent with the presence of general SBH inhomogeneity about some mean SBH and, in addition, a small number of low-SBH regions which are large enough that they are not pinched-off, as shown in Fig. 58(d). The apparent switchovers, between different ideality factor categories (switching between lines shown in Fig. 37), observed at different temperature ranges, e.g. Fig. 13(a) of Aboelfotoh [270], and Fig. 3 of Aboelfotoh et al. [263], is also consistent with SBH inhomogeneity, as shown in Fig. 58(c). Since ideality factors are simply a manifestation of the SBH uniformity, it is

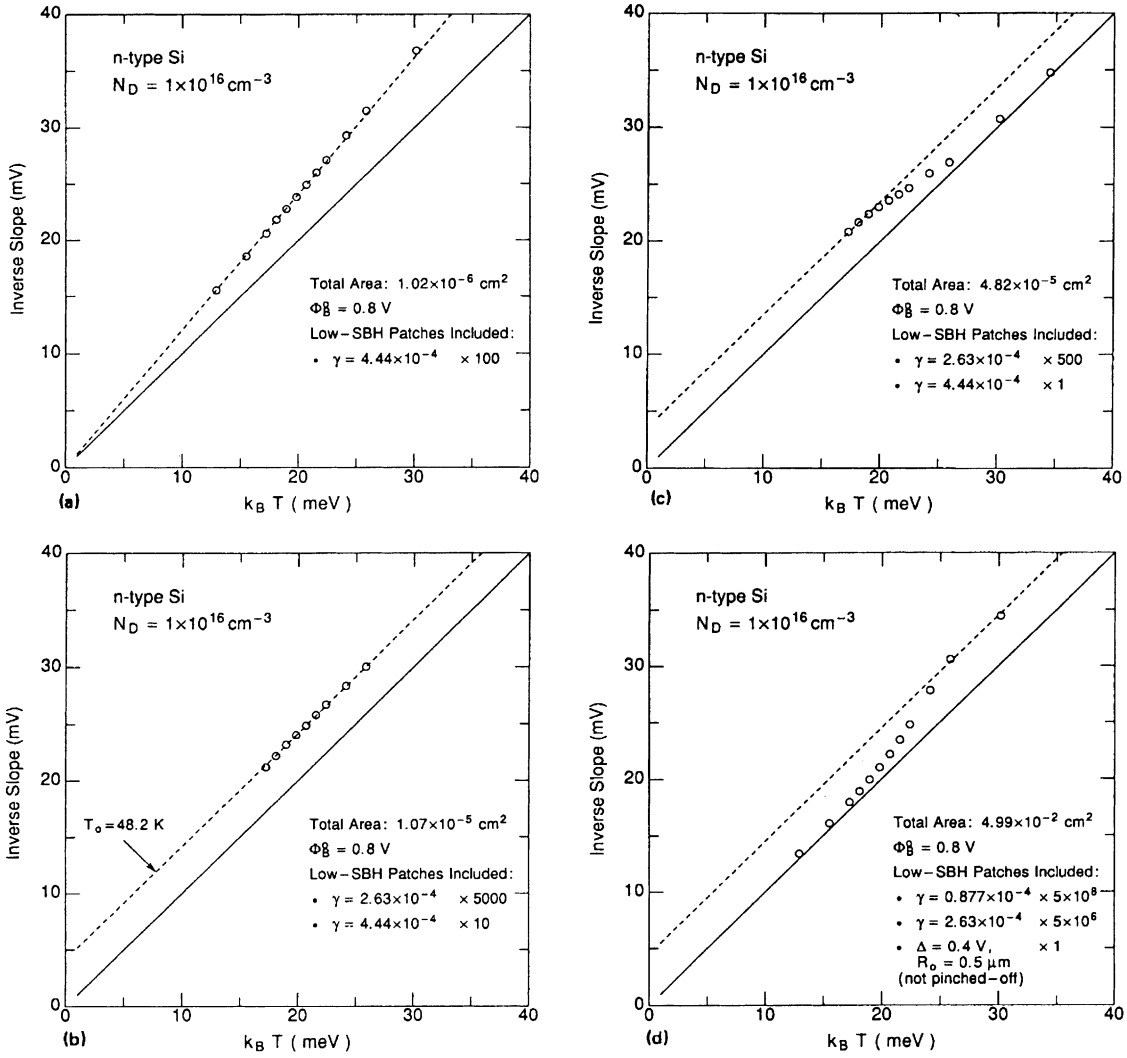

Fig. 58. Plots of the inverse slope of the *I–V* plot as a function of k_BT for inhomogeneous MS contacts composed of a distribution of low-SBH patches as described in the figures (γ is in units of $V^{1/3}$ $cm^{2/3}$): (a) plot showing a constant ideality factor in excess of unity; (b) plot showing the T_0 anomaly; (c) plot showing $n \approx 1 + T_0/T$ behavior at low temperature and ideal behavior at high temperature; and (d) plot showing ideal behavior at low temperature and $n \approx 1 + T_0/T$ behavior at high temperature (from Sullivan et al. [25]).

not surprising that it may be improved by improving the uniformity of the layer, which presumably leads to more uniform interface structures [273,274]. Nor should one find it odd that the ideality factor is the largest when the layer is the most non-uniform [255]. The excellent explanation of almost the entire spectrum of the observed temperature-dependences of the ideality factor by SBH inhomogeneity rules out interface states as being of any real significance to the ideality factor.

7.5. "Soft" reverse characteristic

It is a universal observation that the current from any SB diode never truly saturates at large reverse bias. These "soft" reverse characteristics are observed even when the utmost care is taken to

eliminate possible effects due to edges of the diode [246]. Image-force lowering is capable of explaining the reverse currents at some SB diodes [251,275]. However, the majority of SB diodes show reverse currents which far exceed that predicted by the image-force mechanism alone [245,276,277]. Andrews and Lepselter [72] who did an extensive investigation of the reverse characteristics of SBs, proposed that, in addition to SBH lowering due to image-force, $\delta\Phi_{\text{image}}$ in Eq. (5.1.5), there is a SBH lowering mechanism due to interface states, $\delta\Phi_{\text{MIGS}}$ in Eq. (4.2.11), which is proportional to the electric field, i.e.

$$\delta\Phi_{\text{total}} = \delta\Phi_{\text{image}} + \delta\Phi_{\text{MIGS}} = \frac{1}{2}\left(\frac{eE_{\max}}{\pi\varepsilon_{\text{S}}}\right)^{1/2} + ez_{\max}E_{\max}. \tag{9.5.1}$$

Experimental results in agreement with the prediction of this model have been observed in many studies [72,278–281]. However, even though the functional form of the experimental reverse current may be explained by this model, other consequences of this model, due to interface states, have not been born out by experiments. For instance, it is not clear why very different $z_{\max}$ are found for similar MS interfaces. Also, the proposed mechanism of SBH lowering is completely absent in some diodes [251,275]. But, as before, the most severe problem with the negative charge model is that the proposed SBH lowering is operative only on n-type semiconductors. Experimental results [280–282] including those shown by Andrews and Lepselter in their original paper [72], indicated that the soft SB characteristics for many metals–silicides occurred with similar magnitudes on both types of Si substrate. This contradiction suggests that interface states are not the main reason for the observed bias dependence of the reverse currents.

Due to the limited range of available reverse bias, a reliable determination of the functional form of the current of any particular SB diode is difficult enough. In addition, the reverse currents of different diodes often show different behaviors. Therefore, even though Eq. (9.5.1) may account for the observed reverse currents of some diodes, it is by no means the only lowering mechanism which is capable of explaining the experimental data, nor is it able to explain all the experimental observations. Any SBH lowering mechanism which varies with the electric field more rapidly than $E_{\max}^{1/2}$, could lead to a very satisfactory fit with the experimentally observed reverse currents. As discussed, the reverse characteristic of an inhomogeneous SB depends critically on the actual variation of the SBH. A variety of SBH lowering dependencies on the reverse bias, such as proportional to the 1/2 and 2/3 powers of V_{bb}, are possible in inhomogeneous SB diodes with a random distribution of low-SBH patches. SBH inhomogeneities are perfectly capable of explaining the bias dependence of experimentally observed reverse characteristics. Andrews and Lepselter's theory [72] tends to slightly overestimates the current at very-large reverse biases at high temperatures and underestimates it at low temperatures. The experimental results are actually in better agreement with the behavior expected of inhomogeneous SBs, shown in Fig. 59. The wide range of behaviors of reverse currents experimentally observed from various SBs suggests that each specific diode may have its own individuality. Such a scenario is in complete accord with SBH inhomogeneity and is not easily reconciled with the negative charge model [72].

7.6. Dependence of SBH on measurement technique

The SBH measured by the *I–V* technique, $\Phi_{I\text{–}V}$, often decreases with increasing doping level, while the SBH measured by the *C–V* method, $\Phi_{C\text{–}V}$, remains constant. Frequently, the SBHs depend on the technique of measurement, namely, $\Phi_{C\text{–}V}$ sometimes significantly exceeds $\Phi_{I\text{–}V}$ and the SBH derived from PR techniques, Φ_{PR} [283–285]. Identical to the proposed explanations of the ideality

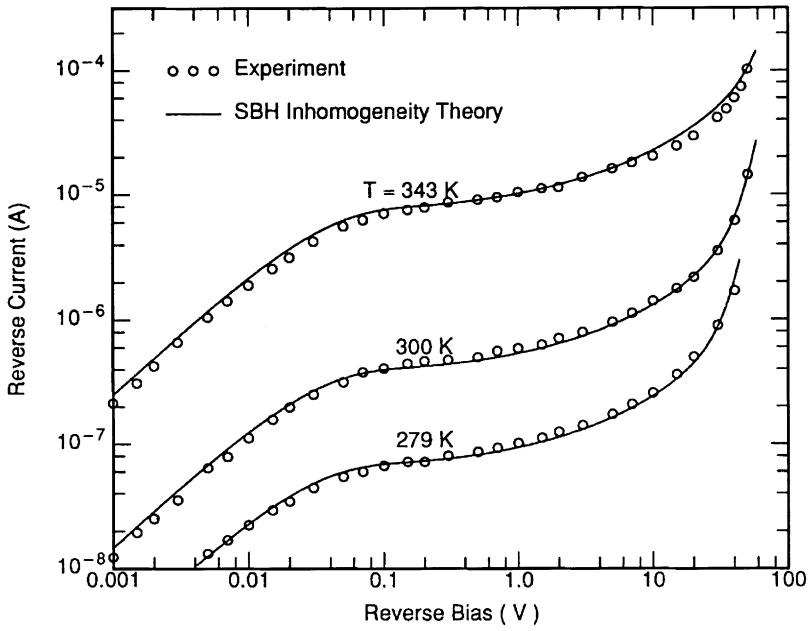

Fig. 59. Reverse characteristics (circles) of a $ZrSi_2$ Schottky diode experimentally observed by Andrews and Lepselter [72]. Solid lines are calculated currents of an inhomogeneous SB diode, which has a $\Phi^0_{B,n}$ of 0.56 eV and contains low-SBH patches with γ of 5.6×10^{-5} and 4×10^{-5} $V^{1/3}$ $cm^{2/3}$ (from Tung [10]).

factor, lowering of the SBH by image-force, interface states, and TFE have been frequently invoked to explain the doping-level-dependence of Φ_{I-V} [286–288], While SBH investigations, especially those where the doping-dependence of the SBH have been studied, have generally concentrated on n-type semiconductors, it is known that SBH difference on p-type semiconductors also routinely exceed that predicted by image-force alone. So, it is clear that the observed doping-dependence of moderately-doped, intimate, SB contacts may not be attributed to the negative charge model as previously thought. As already pointed out [23,128,289], a dependence of SBH on the measurement technique is in agreement with the presence of SBH inhomogeneities. Current transport at inhomogeneous SBs is dominated by low-SBH patches, leading to the deduction by *I–V* and PR techniques of apparent SBHs which are lower than the arithmetic average of the entire diode. Since under usual circumstances, the *C–V* technique yields an average SBH for the whole diode [10], the experimentally observed dependence of SBH on the technique of measurement is likely due to SBH inhomogeneity.

A common occurrence in *C–V* experiments is the deduction of an apparent SBH which is even higher than the true arithmetic average. This phenomenon is often associated with experimentation problems, namely, how to determine the true space–charge capacitance from raw *C–V* data. There are many well-known phenomena which may lead to the measurement of apparent capacitances which are not the true junction capacitances, as previously discussed [176]. Besides possible explanations from deep levels [145] doping variations [290,291] interface states [177], etc. one notes that a large series resistance may lead to such an observation [176,292]. The effect due to series resistance is particularly noticeable at high modulation frequencies and when the magnitude of *C* is large [176]. Non-linearity in C^{-2}–*V* plots has frequently been attributed to interface states. The problems with such an interpretation have already been discussed. One notes that in the presence of SBH inhomogeneity, effects due to minority carriers are greatly enhanced [120]. In many respects,

a fluctuation in the stored minority carrier charge is indistinguishable from capture and emission processes due to interface states. It is interesting to note that much higher excess capacitances are observed from interfaces which display higher ideality factors in *I–V* measurements [182] in good agreement with the behavior expected of inhomogeneous SBHs.

8. Polycrystalline SBH: correlations and dependencies

8.1. Surface Fermi-level pinning with (sub)monolayers of metal

The development of the surface Fermi-level position of semiconductors upon the deposition of metal was extensively studied in the late 1970s and the 1980s, in the hope of gaining information on the formation mechanism of the SBH [293–296]. Synchrotron radiation was a powerful technique with which to monitor the movement of the core level position of photoelectrons from the semiconductor surface and study, at the same time, the chemistry between the metal and the substrate [297,298]. Because the clean (1 1 0) surfaces of III–V compound semiconductors were easy to prepare in situ (by cleaving) and because a few of these surfaces, notably the cleaved GaAs and InP surfaces, contained no states in the band gap, these surfaces were frequently the favorite ''substrate'' for photoemission studies. One common focus of these experiments was to follow the development of the band bending as a function of the coverage of metal. A somewhat surprising result was that the equilibrium Fermi-level position, observed for thick metal overlayers, was actually established with the deposition of less than a monolayer of metal. As shown in Fig. 60, a rapid shift was observed in the Fermi-level position from their respective flat-band positions for the n- and p-type clean surfaces toward the middle of the gap, upon the deposition of less than one-half monolayer of metal [299]. Little change was observed for the Fermi-level position after the initial monolayer of metal. The FL position seemed to be essentially independent of the identity of the metal and it also corresponded to

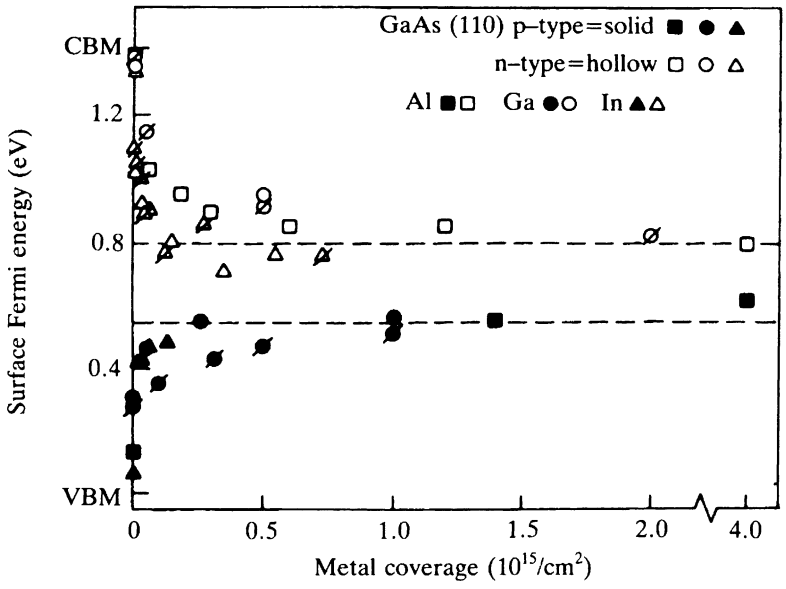

Fig. 60. The surface Fermi-level pinning position for p- and n-type GaAs as a function of metal coverage (from Spicer et al. [484]).

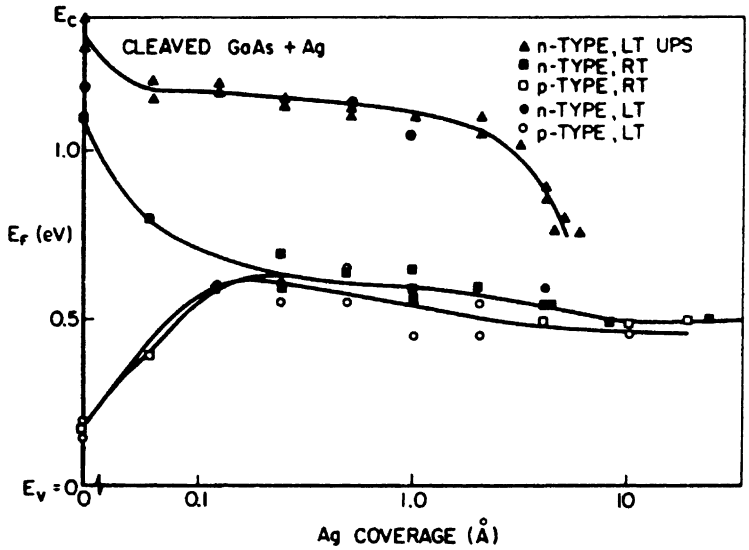

Fig. 61. Position of E_F at the (1 1 0) surface of n- and p-type GaAs as a function of Ag coverage at RT and LT, 70–100 K (from Stiles and Kahn [485]).

the FL position observed in oxygen and cesium adsorption experiment. Furthermore, there was a clear difference in the FL position on n-type GaAs and that on p-type GaAs, as shown in Fig. 60. These findings made popular the theory that extrinsic factors, such as defect generation upon the condensation or clustering of metal, determined the FL of semiconductor surface. It was further speculated that the SBH at thick-film MS interfaces was also determined by these defects. It should be pointed out that the deposition of some metals led to gradual change in the band bending [297] while the FL-pinning effect was found to be completely missing on some semiconductor surfaces [300,301].

An intriguing temperature-dependence of the Fermi-level movement of semiconductor surfaces was discovered in the mid 1980s, which triggered a flurry of investigations aimed at understanding the band bending behavior at monolayer coverages of metal deposited at cryogenic temperatures. At low temperatures (LT), the band bending on n-type GaAs and InP with the deposition of metal appeared to be delayed, while an "overshoot" was observed for band bending on p-type substrate [302–304] as shown in Fig. 61. Also, in sharp contrast to room-temperature results, the surface FL of LT deposited samples appeared to depend sensitively on the metal. The LT Fermi-level position was called "unpinned" by some authors. Within the defect pinning picture, these results were speculated to imply that the defect generation mechanism, or the formation of MIGS, was significantly inhibited at low temperature [305]. MS interfaces formed at LT, were thus, thought to be "ideal", whatever the word means. The use of MBE grown buffer layer, with a smaller defect density than bulk grown crystals, was thought important for the unpinning of the FL [306]. Following this line of reasoning based on defects, there were attempts to deposit the metal in a way which was even less invasive to the semiconductor surface. A thin layer of inert gas (Xe) was first condensed on the semiconductor surface at LT to buffer the metal deposition process. Metal clusters formed on top of the Xe layer was then left/transferred onto the semiconductor surface when the Xe layer was thermally desorbed [307]. Very different pinning position was apparently observed for cluster deposited at LT, compared with direct atom-by-atom deposition at any temperature.

An often-discussed issue concerning SBH formation at monolayer metal coverages was how the FL position was affected by the "metallicity" of the deposited metal layer [162,308,309]. The metal

character here refers to the in-plane conductivity of the metal layer. The central issue was whether a significant FL movement occurs when isolated metal islands become continuous. And the answer to this question supposedly revealed whether defects or MIGS was responsible for the band bending. But actually the metallicity issue cannot be used to infer SBH mechanisms. Instead, it only serves to put the spotlight on two serious problems with SBH studies in the monolayer coverage range: lateral uniformity and the surface photo-voltage effect. A layer of submonolayer or monolayers of non-epitaxial material on a foreign host surface is usually non-uniform for thermodynamic and kinetic reasons. Most of the monolayer MS systems studied fell into this category and displayed Volmer–Weber type of agglomerated island growth of the metal. This left the majority of semiconductor surface uncovered even after several monolayers of metal were deposited. The lateral inhomogeneity in the surface potential broadened and shifted the core level peak measured by an averaging technique such as the PES away from the true core level position underneath the metal-covered interface regions. This surface inhomogeneity issue is particularly severe on heavily doped semiconductors. Numerical simulations [150,151] of the potential distribution at heterogeneous surfaces, as shown in Fig. 62, could reproduce the difference between the FL positions on n- and p-type semiconductor observed in actual experiments. This suggested that the actual pinning position was the same for n- and p-type substrates and that there was no need to propose different mechanisms to account for the apparent core level positions. Furthermore, the pinning position for the areas of the semiconductor in contact with the metal clusters is independent of the metal coverage. This is not surprising since the each individual metal islands, even in the submonolayer (average) coverage range, was already characteristic of a thick layer of metal. So, the issue over the metallicity of monolayer of metal appears to be a moot point. Electron–hole pair generation due to light and electron beam is a well-known effect and, in fact, has been used to measure the SBH and other surface properties with techniques such as electron beam induced voltage (EBIV) [160] and surface photovoltage (SPV) [310]. The SPV due to photoemission light source is usually negligible for continuous metal layer or for semiconductors with high recombination velocities. On semiconductor surfaces covered with isolated metal islands, very large SPV could be induced at LT under typical photoemission experimental conditions [152,311]. Correction for the SPV effect has

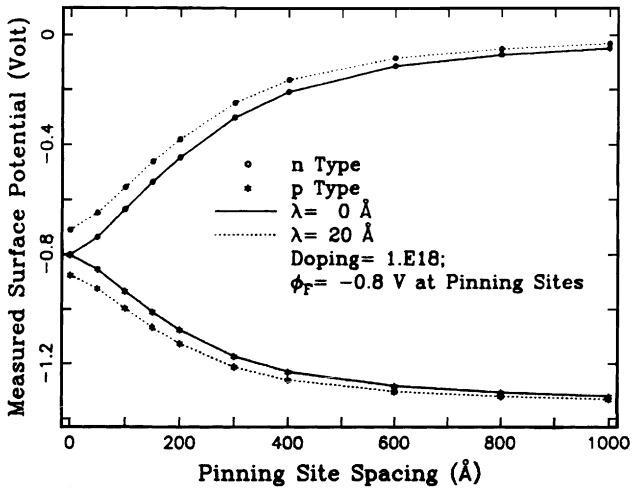

Fig. 62. Measured surface potentials vs. pinning site spacings for two different probe depths. Pinning potentials are assumed to be −0.8 eV at pinning sites. The measured surface potential is the weighed average over the entire surface (from Tang and Freeouf [150]).

been shown to modify the monolayer PES results obtained at LT to essentially conform to those obtained at RT. Thus, the temperature dependence alleged for both the FL-pinning and the interface chemistry could no longer be supported by experiment [312,313].

The full extent to which lateral inhomogeneity and SPV have affected the experimental SBH results concerning monolayers of metal is difficult to assess. But one should assume that some, if not most, of the conclusions drawn from earlier PES studies were likely influenced by these effects, if these effects had not been specifically looked for and ruled out under the exactly experimental conditions. This left us with the realization that experiments on submonolayer of metal have not unambiguously told us things which are different from experiments with thick-films of metals. The apparent rapid movement of band bending with metal coverage, shown in Figs. 60 and 61, cannot be used to infer the saturation of a SBH mechanism at submonolayer of metal coverage. With the experimental evidence for a pre-metallicity pinning of the Fermi-level position now removed by the discovery of the lateral inhomogeneity and the SPV effects, the proposal of FL-pinning by surface defects also lost its most attractive argument.

8.2. Thick-film SBHs: Fermi-level pinning systematics

Large-scale and systematic SBH studies were not possible in the first half of the 20th century because technologies to produce good-quality semiconductors were largely unavailable. But almost as soon as semiconductor technology advanced to the point where reliable SBH data began to appear, it was clear that the rule of Schottky and Mott was not obeyed in most MS systems. From the very beginning, the phenomenon of Fermi-level pinning was keenly noted. The SBHs found for a wide range of metals on a particular semiconductor seemed to fall within a narrow range [314,315]. The range of SBH was so narrow that an empirical ''one-third'' rule was noted which stated that the SBH always appeared at a constant fraction of the band gap: on p-type semiconductor the SBH was roughly 1/3 of the band gap (and the SBH on n-type semiconductor would be $\sim$2/3 of the band gap). Thus, the Fermi-level appeared to be fixed, or ''pinned'', at $E_g/3$ from the VBM. These early publications [314,315] marked the beginning of the expression ''Fermi-level pinning''. Naturally, surface states in that part of the band gap were speculated to be the source of this pinning effect. However, subsequent experiments showed that this empirical one-third rule was not obeyed by the majority of metal–semiconductor systems. So, this rule was only part of a larger picture, as far as the formation mechanism of the SBH is concerned. Another trend which was noticed from SBHs experimentally observed from compound semiconductor systems was the ''common anion rule'', which stated that the p-type SBH of electronegative metals depended only on the identity of the anion in the semiconductor [316,317]. For example, Au was observed to have the same SBH on CdSe and ZnSe. Moreover, the magnitude of the SBH decreases with the electronegativity of the anion. Although specific reasons for the common anion rule were not known, it was thought that the fact that the valence band of a compound semiconductor had strong anion character had something to do with this rule [317]. Gap states near the VBM were derived from the valence band and were expected to have strong anion character. So, it was recognized that the common anion rule was consistent with the spirit of interface gap states models. One notes now that since the interface bonds (between the metal and the compound semiconductor) are largely a result of the interaction between the conduction band of the metal and the valence band of the semiconductor, one would expect the interface bond-polarization and, therefore, the interface dipole to be influenced strongly by the anion. So, the common anion rule has a very logical explanation within the bond-polarization picture as well. Another SBH proposal that was related to the common anion rule was the effective work function model, which speculated on the presence of anion precipitates at metal–compound semiconductor

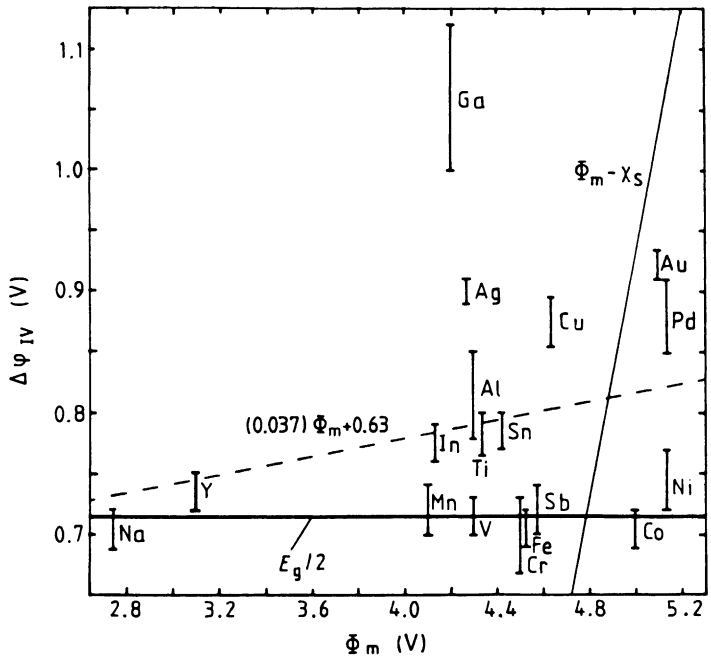

Fig. 63. Average experimentally observed SBH from four separate studies of n-type GaAs(1 1 0), $\Delta\varphi_{IV}$, vs. (polycrystalline) metal work function ϕ_M. The Schottky prediction is presented together with the best fit of the prediction from interface gap states model. The regression coefficient corresponding to this fit is 0.237 (from McLean and Williams [285]).

interfaces [318]. Thermodynamic arguments were given for the conversion of surface oxides into cation oxides, leaving anion precipitates at the interface, for certain semiconductors, including GaAs. Interfaces of these semiconductors would then consist of different phases and the local SBH for each different patch was assumed to obey the Schottky–Mott relationship according to the work function of that local phase [318]. An obvious problem with this proposal is the lack of experimental evidence for anion precipitates at common semiconductor interfaces. Of course, the Schottky–Mott relationship assumed in this model is also inconsistent with the Fermi-level pinning effect observed at MS interfaces where precipitates are known not to be present, such as at Si interfaces.

The SBH data of a group of metals on a semiconductor usually showed rather significant scatter, at times with no apparent correlation with metal work function [319,320] as shown in Fig. 63. But more often, a systematic trend can be found for any given semiconductor, such that metals with larger work functions tend to have larger (n-type) SBHs than metals with smaller work functions. As shown in Fig. 64, the SBH displays a systematic increase with the metal work function, but the rate of increase is far less than that predicted by the Schottky–Mott relationship. For example, least square fits of the data points in Figs. 63 and 64 against the metal work function yield interface parameter, S_Φ, of 0.04 and 0.13, respectively, for GaAs and Si. The thick metal films in these cases were simply evaporated onto semiconductor surfaces that had gone through some "standard" cleaning procedures. Even without intentional annealing, MS interfaces prepared in this fashion are not necessarily "abrupt" or "intimate". Lots of subtle dependencies of the SBH on processing conditions of the SB diode have been observed. It was recognized that a distinction needed to be made between reacted and abrupt interfaces to make better sense of the experimental systematics [64,319]. These finer details notwithstanding, the overall picture from randomly prepared SBH remained clearly that the Fermi-level was "strongly pinned" for these semiconductors. On the other

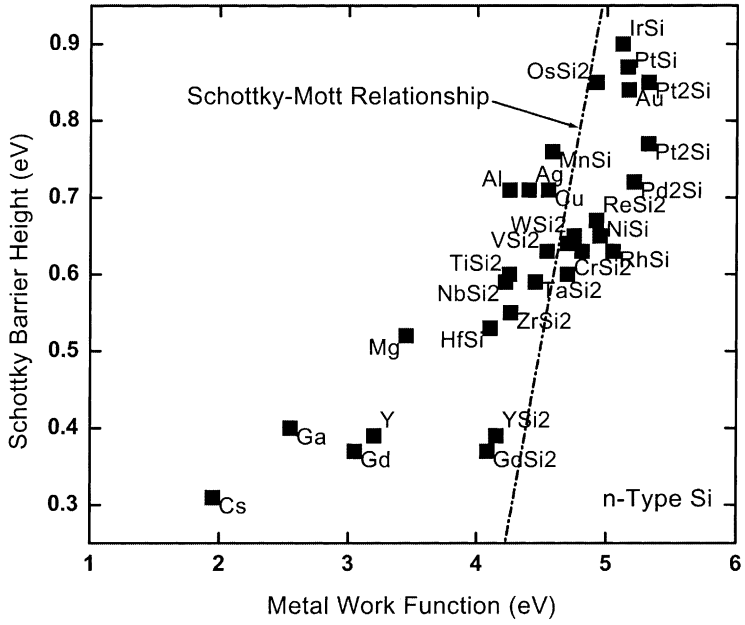

Fig. 64. Experimental Schottky-barrier height on n-type Si, plotted against the Miedema electronegativity. The straight marks the prediction of the Schottky–Mott relationship (from Tung [481]).

hand, SBH studies on wide-gap semiconductors such as GaN and SiC usually find a wider range of available SBH, as reflected in experimental S_Φ of over 0.4. So, it appears that the FL in these other semiconductors is only ''weakly pinned''. One was naturally interested in the distinguishing character of the semiconductor, which determined the degree of FL-pinning. For a long while, a widely held opinion was that that defining character was the ionicity of the semiconductor [66]. Kurtin et al. observed a sharp transition of the degree of FL-pinning as a function of the ionicity of the semiconductor [66]. The ionicity of a semiconductor here was defined as the difference in the Pauling electronegativities between the cation and the anion of the semiconductor. As shown in Fig. 65, the interface behavior parameter $S_\chi(=\partial\Phi^0_{\mathrm{B,n}}/\partial\chi_{\mathrm{M}})$ was small for covalently bonded semiconductors (<0.2, meaning that the FL is strongly pinned), but it exhibited a rather sudden increase as the ionicity of the semiconductor was increased to above 0.5 and it saturated at a value of 1 eV. Both the abruptness of the ''transition'' and the saturation value (of 1) were very surprising and had no good explanation. Fig. 65 was viewed as a mystery which held the secret to understanding the SBH formation mechanism. A partial explanation of the overall trend of Fig. 65, that of an increase in S_χ with ionicity, was offered by a pseudopotential study of the SBH at jellium–semiconductor interfaces [20], which showed that the penetration of MIGS was deeper into covalent semiconductors than ionic semiconductors and, hence, MIGS could more effectively screen out changes in the metal work function in a covalently bonded semiconductor. An explanation on the abruptness of the transition was also offered [20], although this particular aspect was later criticized as having been the result of some unrealistic estimates [67]. As it turned out, the excitement, commotion and debate generated by Fig. 65 all went for naught, because the experimental data on which Fig. 65 was based were later reanalyzed by Schluter [68] and shown to lead to neither an abrupt transition nor a saturation. One notes that there is no fundamental reason for the S_χ parameter to saturate at 1, since it has the unit of energy and is related to the S_Φ by

$$S_\chi = S_\Phi A_\Phi, \tag{10.2.1}$$

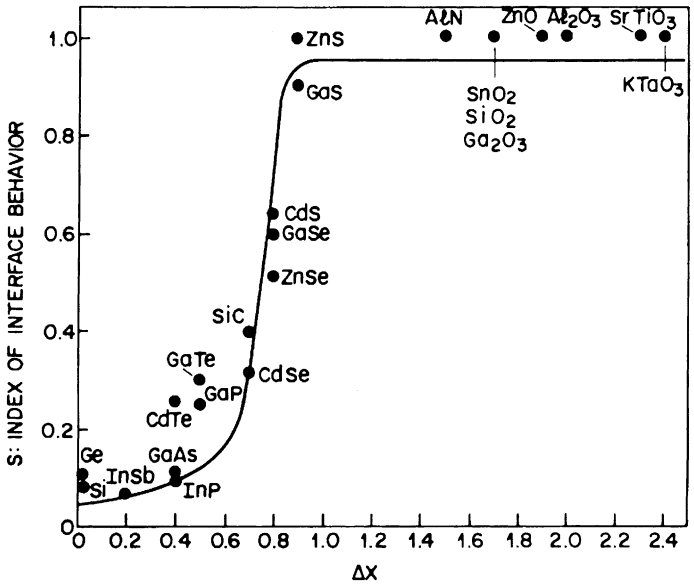

Fig. 65. Index of interface behavior, S_χ, plotted as a function of lattice electronegativity difference (ionicity) of the semiconductor (from Kurtin et al. [66]).

where A_Φ is a constant between 2 and 3 eV. An often used conversion factor is $A_\Phi = 2.27$ eV, which would be the true saturation value of S_χ in the Schottky–Mott limit. Schluter pointed out that a correlation of S_χ (or S_Φ) with the polarizability of the semiconductor would be more in line with the spirit of a linear potential theory [68]. Some reasonable fit was indeed found. Later, a correlation between S_Φ and the polarizability was argued based on the density of MIGS in the one-dimensional complex band structure of the semiconductor. A good agreement was indeed found, as already shown in Fig. 26. As explained in Section 4, the spirit of the MIGS model is essentially based on the bond-polarization concept. The bond-polarization theory has demonstrated an even better fit of the experimentally observed S_Φ with the band gap of the semiconductor, as shown in Fig. 32. So the systematic trend of the Fermi-level pinning effect is in good agreement with the bond-polarization view of the interface dipole.

8.3. Empirical models of Fermi-level pinning

Two empirical SBH models largely intended to account for the SBHs observed at silicide–Si interfaces are well known and are well deserving of some comments. Perhaps inspired by the experimental observation that different silicide phases of the same metal, e.g. Ni_2Si, NiSi, $NiSi_2$, often had similar SBHs on Si [203], Ottaviani et al. postulated the presence of an interfacial layer at reactive interfaces such as silicide–Si interfaces, which tended to dominate the SBH [321]. A layer of interstitials [322] and an amorphous layer were given as possible examples of such an interfacial layer. A correlation of the silicide SBH with the eutectic temperature of the metal–Si system was found, as shown in Fig. 66, which was interpreted as evidence for an interfacial layer and was suggestive of the vital role played by the interface in determining the SBH. While its emphasis on the role played by the interface can hardly be faulted, this model tends to be too vague to be useful and expandable. The basic notion of this model that the same mechanism determines the SBH of a silicide–Si interface, independent of the actual silicide phase, is also the basis of another proposal to

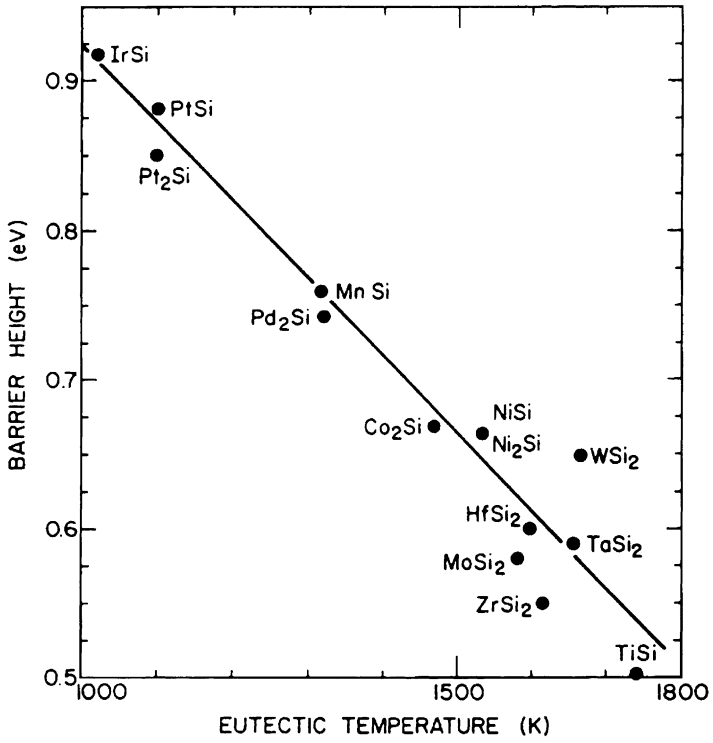

Fig. 66. A plot of Schottky-barrier height against eutectic temperature for transition metal–silicide–Si systems. The eutectic temperature selected is the closest eutectic temperature on the metal (Si) side of the silicide, for silicides whose growth is dominated by metal (Si) diffusion (from Ottaviani et al. [321]).

explain SBHs of silicides. Freeouf assumed that the effective stoichiometry of a silicide–Si interface is always MSi_4 regardless of the actual phase observed by experiment [323]. The work function of the MSi_4 phase was then modeled as a geometric mean of the work functions of the individual constituents, i.e. $\phi(MSi_4) = (\phi_{Si}^4 \phi_M)^{1/5}$, and compared with the experimentally observed silicide SBHs, as shown in Fig. 67. A roughly linear relationship was observed, which was used to suggest the validity of the Schottky–Mott relationship, once the correct work function was chosen. This model is in spirit very similar to the effective work function model from the same author [318]. Experimentally measured work functions of silicides [320] were found to correspond, although only marginally, with the work functions calculated using the geometric averaging method assumed in Freeouf's work [323]. But, the assumption of an interfacial MSi_4 stoichiometry has been shown to run afoul of the actual structures found for the silicide–Si interfaces which have been experimentally studied. The non-interacting picture assumed in this model, i.e. the Schottky–Mott relationship, is hard to reconcile with the strong bonds known to be present at silicide–Si interfaces.

Since the initial motivation for defect pinning models was the photoemission results of semiconductor surfaces with (sub)monolayer coverage of metal, point defects consistent with those results were initially looked for. Spicer et al. proposed a grand unified theory of defect pinning which involved arsenic antisite As_{Ga}, which is a double donor [299,324]. Energy levels of different charge states of the arsenic antisite defect were used to explain the different pinning positions on n- and p-type GaAs surface [324]. The effect of antisite defects on the SBH has also been demonstrated in first principles electronic structure calculations [325]. Daw and Smith used the "common anion rule" and the similar dependencies of both the anion vacancy level and the SBH on the AlGaAs

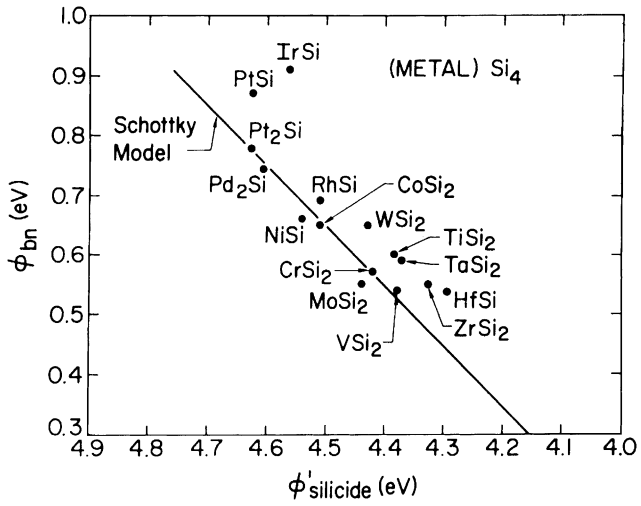

Fig. 67. Barrier height between silicide and n-silicon plotted against calculated silicide work function, based on MSi_4 stoichiometry (from Freeouf [323]).

composition to argue for a mechanism based on anion vacancies [326,327]. Si dangling bond state, sheltered by a neighbor vacancy, was speculated to provide the electronic states which pin the FL at silicide–Si interfaces [328,329]. This view was also shared by Schmid in a systematic analysis of the SBHs of silicide–Si and metal–Si interfaces [30]. Ludeke et al. pointed out that the discrete energy levels for bulk defects, when present at the MS interface, should evolve into resonance as a result of their interaction with the metallic states [330]. Interaction with neighboring defects should also lead to delocalization of the states and broadening into bands. Woodall and Freeouf pointed out that the bulk crystals of compound semiconductors were usually grown under anion-rich conditions, which seemed to suggest that anion precipitates at the MS interface could be responsible for FL-pinning [331]. Hasegawa and Ohno proposed that disorder at the interface could lead to unsaturated s–p bonds and a distribution of gap states independent of the metal, which would be consistent with the observed FL-pinning phenomenon [332]. The energy of the sp^3 hybrid orbitals of the semiconductor was identified as the characteristic reference level [332].

The effectiveness of a high density of defects in rendering the SBH independent of the metal work function is beyond doubt. The issue has always been how to prove the presence and the relevance of defects on the actual SBH. This issue is one of real concern, especially since the results of surface band bending studies involving monolayers of metal have subsequently been shown to be consistent with results from thick-film MS interfaces, as discussed above. Since the magnitude of the SBH was by and large the only criterion used in most studies to speculate on SBH mechanisms, attempts were frequently made to discern defect mechanisms from systematic plots of SBH, as demonstrated in Fig. 16. Because of the flexibility of the analysis model, any complicated dependencies of the SBH on metal work function, surface preparation, annealing condition, etc. can usually be accounted for by the presence of a small number of defects [333,334]. Such a deduction process is, of course, non-unique and very subjective. It has been pointed out that the temperature dependence and the pressure dependence of the SBH could be used to distinguish various SBH mechanisms [335,336]. This is in principle true, but only when the SBH under study results from a single mechanism. As pointed out above, the SBH of most MS interfaces is only a statistical average of a spectrum of inhomogeneous SBHs. So the temperature dependence of SBH offers little insight in this respect. The pressure dependence of SBH has been used to lend support to the pinning

mechanism by antisite defects [336] although this dependence has been shown to be fully accounted for by the calculated deformation potential of band edges, i.e. a bulk band structure effect [43,337].

When defects are present near an interface, it has been customary to model the interface dipole by placing the defects at a distance away from the metal [70,338], in a fixed-separation model (Fig. 15). It is of interest to ponder whether defects should be placed within the ISR, or outside the ISR. When placed inside an ISR, structural defects and imperfections are rather ill-defined since the entire ISR can be viewed as one large defect. After all, the thermodynamically preferred atomic structure of the ISR may differ significantly from that formed by slapping two perfect crystals together. Any energy reference a structural imperfection might have had in a bulk crystal is lost inside the ISR. Instead, the charge distribution of the entire ISR is responsible for the formation of the dipole [21,77,81], with no discrimination for the energetic positions of the electronic states making up the interface charge. The narrow range of the influence line defects have on the local SBH is a good example of the extreme local nature of such irregularity [13,234]. When defects are placed in the interior of a semiconductor, their characteristic energy positions become meaningful. It is apparent that if defects are present near the interface but outside the ISR, they will provide an additional dipole as per Figs. 13 and 15. However, it is also apparent that the interface dipole due to chemical bonds in the ISR is always present and is the proper baseline to which other effects, such as defects, should be added. How much defects can influence the final SBH magnitude depends on the density, energy, and location of the defects. Experimental results described above suggest that defects are not of wide importance to the observed Fermi-level pinning phenomenon observed at MS interfaces, since the observed systematic trend has already been successfully accounted for by the ''baseline'' condition (Fig. 32). However, they (defects) may still be important for some specific MS interfaces.

8.4. Dependence on surface preparation and film processing

Fermi-level pinning is undoubtedly the most prominent picture painted by all the SBH studies of polycrystalline MS interfaces. But there are finer details within these studies which are interesting in their own rights and which may even seem inconsistent with the overall FL-pinning picture. One such example is the sensitivity of the measured SBH on the preparation of the semiconductor surface. It is well known that most semiconductor surfaces are easily oxidized when left in air for extended periods of time. A layer of surface oxide or some other contaminant may be present at most semiconductor surfaces, and can significantly affect the SBH of MS interfaces formed on such a surface. Prior to the introduction of MBE techniques to the fabrication of SB diodes, two surface preparation techniques were very common: chemical etching and cleaving. Cleaving in vacuum should lead to atomically clean and stoichiometric semiconductor surfaces, although the cleaving process is limited to only one crystallographic plane for a given semiconductor and the process is also known to lead to surface defects. Chemical etching, on the other hand, still leaves some contaminants on the surface. In the early days of SBH studies, it was usually assumed that the native oxide layer on etched surfaces was typically a few monolayers thick (0.5–1.0 nm). Modern views would put that number, certainly for a hydrogen terminated Si surface, at less than a monolayer. The SBHs formed on the etched surface and cleaved surface were sometimes found to differ significantly (by $\sim$0.2 eV), although more frequently they were found to be reasonably close (within 0.05 eV). However, an aging phenomenon was sometimes observed at etched semiconductor surfaces [339–341]. The measured SBH was found to change with time, on the scale of tens of hours. The net result of the aging process was usually a decrease in the discrepancy between the SBHs measured on etched and cleaved surfaces. The reason for aging has been speculated to be a reaction or interdiffusion between

the metal and the (oxide) contamination layer, leading to more intimate contact between the metal and the semiconductor.

Various surface treatment procedures have been found to affect the SBH measured subsequently on the semiconductor surface. These procedures include deliberate oxidation [342–345], change in clean-surface composition [346], prolonged chemical solution reaction [347–350], exposure to plasma of various gases [351–356], ion implantation [357–361], ion etching [362–366], vacuum annealing [367], and the growth of a (homo)epitaxial buffer layer [368–371]. Generally speaking, any modification of the surface condition leads to changes in the structure of the ISR and, possibly, changes in the metallic phase. So, it is not surprising that the SBH should be affected by surface treatments. Some of the surface treatments, such as surface doping, introduces known modifications to the electrical nature of the semiconductor, so the SBH modification is predictable and can be accounted for without invoking a change in the ISR dipole. The creation of a thin surface layer, heavily doped to the opposite type (e.g. p^+ on n^- substrate), is known to lead to an apparent increase in the experimentally measured SBH. Ion implantation of shallow dopants [357,372,373], dopant in-diffusion [374], and the growth of a heavily doped epi-layer [369,370,375] have all been used to create the shallow surface p–n junction and accompanying band bending as schematically shown in Fig. 68. Note that in this diagram, the effective barrier height is not determined by the Fermi-level position at the MS interface but by the maximum amount of band bending inside the space–charge region. Experimentally, it is found that the insertion of a heavily doped surface layer of the same type as the substrate (e.g. n^+ on n^- substrate) leads to a decrease in the apparent SBH. The usual explanations of this phenomenon include increased tunneling, increased image-force lowering, and increased lowering by interface states; although, as discussed, such a reduction in the apparent SBH is also consistent with inhomogeneous SBH. Inadvertent doping of the near surface region by common contaminants has been known to happen and has led to some experimental artifacts. A very spectacular example of this is the boron contamination of Si surface after high temperature annealing

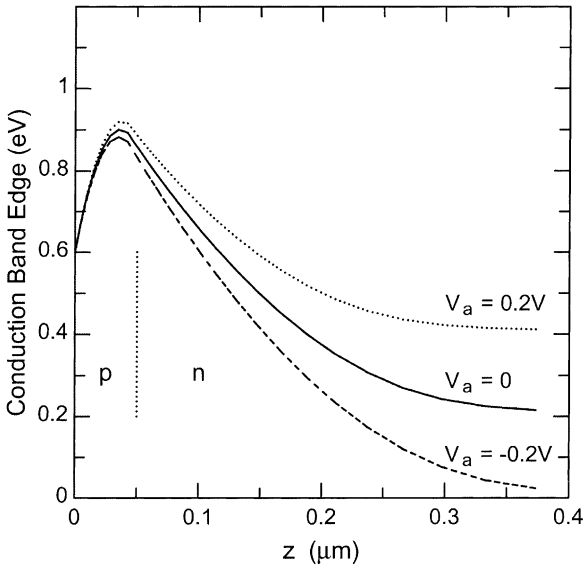

Fig. 68. The effect of surface doping layer on the Schottky-barrier height. Numerically calculated band diagram, under different bias conditions, of a nominally 0.6 eV Schottky barrier formed on 1×10^{16} cm^{-3} doped n-type Si, but with a thin (50 nm), 3×10^{17} cm^{-3} p-type doped, layer at the interface. The effective SBH is increased to ~0.9 eV and varies slightly with the applied bias (Tung, unpublished).

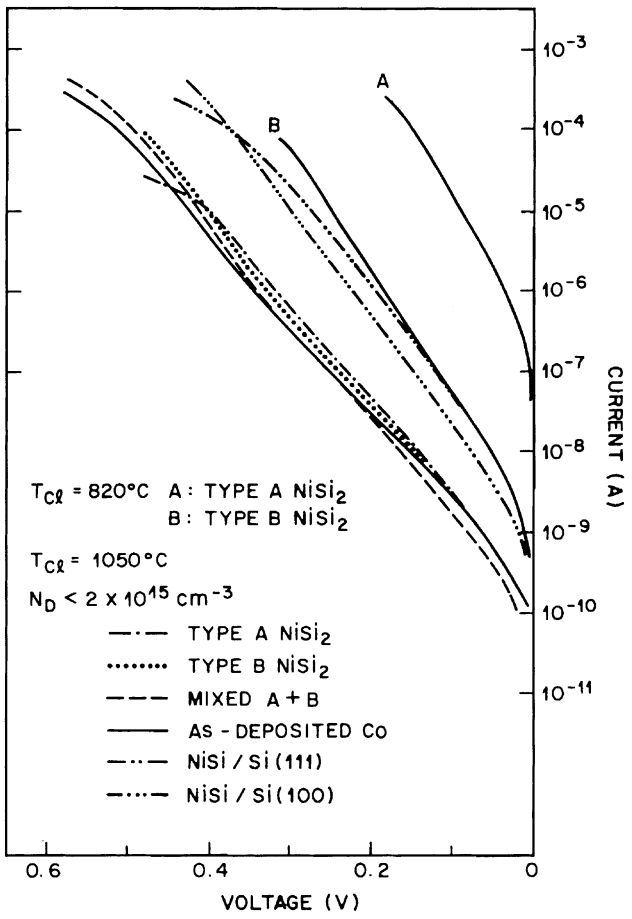

Fig. 69. The *I–V* traces of an assortment of silicide–silicon junctions. All diodes have the same area, 2×10^{-3} cm^2. T_{Cl} is the cleaning temperature of the lightly doped ($N_D < 2 \times 10^{15}$ cm^{-3}) Si substrates in UHV. The two solid curves are for epitaxial type A and type B $NiSi_2$ layers fabricated on Si(1 1 1) substrate cleaned at a low T_{Cl} of 820 °C. The rest of the curves are from various diodes fabricated on substrates which have been annealed at a T_{Cl} of 1050 °C. Boron contamination on the surface of Si diffuses into the Si at this temperature, causing the formation of a p-type surface layer. An increase in the apparent n-type SBH and an increase in the ideality factor are observed from these diodes (from Tung et al. [197]).

in UHV [197,376,377], as shown in Fig. 69. High temperature annealing of compound semiconductors (GaAs, InP, etc.) is also known to lead to a loss of anion and the creation of donor defects [367]. In addition, defects generated by energetic particles during implantation or sputtering are often found to possess donor type activities and they affect the apparent SBH accordingly [358]. Other surface preparation procedures which have been used to deliberately modify the SBH will be discussed in Section 10.5.

Beside surface preparation, other conditions of the processing of the SB diodes were also found to have a strong effect on the experimental SBH. The deposition of metal layer under cryogenic temperature has been shown to lead to very different SBH results than RT depositions. On some strongly pinned compound semiconductors, e.g. InP and InGaAs, the fabrication of high SBH n-type diode has been difficult at room temperature. However, it was discovered that deposition of metal at cryogenic temperatures (<100 K) led to a significant increase (up to 0.4–0.5 eV) in the SBH of some metals [378–383], as the example of Fig. 70 illustrates. Metal layers deposited at low temperatures were found to be more uniform and their interfaces more abrupt than those deposited at RT, likely

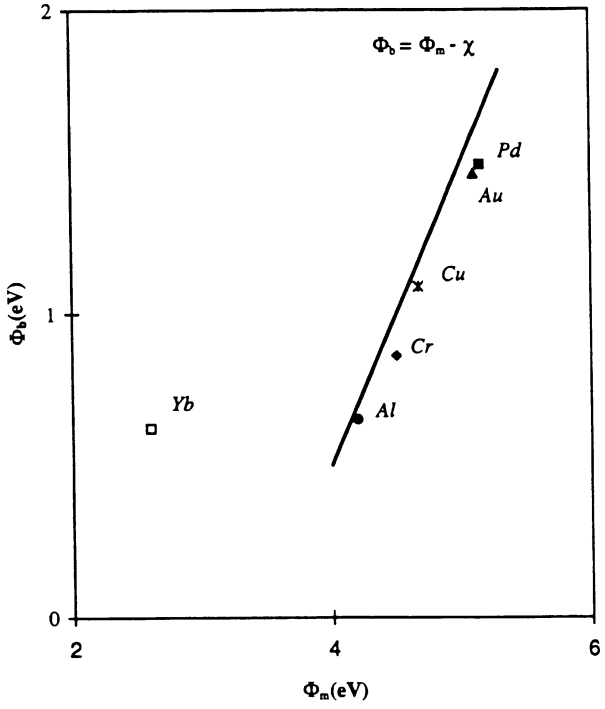

Fig. 70. Dependence of barrier height on metal work function for Schottky diodes fabricated at 77 K on n-type $ZnS_{0.07}Se_{0.93}$. The solid line is the prediction from the Schottky–Mott relationship. The point due to Yb is an exception which may be due to its reactivity (from Wang and Anderson [486]).

because of reduced interfacial reaction [384]. But the exact reason why a morphology change should lead to a different SBH is not clear. It was also thought that the damage to the surface from the low-temperature deposition process might be less. Electrochemical deposition of metal has some obvious advantages in terms of processing SBH diodes. The ability to etch the surface in the same electrolyte bath, the reduced damage to the semiconductor surface, the preservation of hydrogen termination throughout the deposition process, the wide range of processing parameters, the altered surface/interface energies of the deposited metal in the presence of the electrolyte, and the uniformity of the deposition may all offer some advantages. Some metals electrochemically deposited were found to display diode characteristics which are highly ideal and whose SBH magnitudes are quite different from that of sputtered or evaporated diodes [385–389]. The most spectacular effect has been observed for electrochemically deposited Pt on compound semiconductors, where very high values of the SBH were realized [386,390], as shown in Fig. 71. The FL at these interfaces was thought to be unpinned [391]. However, not all metals showed the same effect [388,392]. Whether the FL is pinned (at its usual position) has been correlated with the mechanical stress introduced in the deposition process [388]. The SBH of electrochemically deposited diodes was also known to depend on the etching and the electrodeposition conditions [393,394], and some electrochemically deposited diodes also displayed aging effect [393,395]. There were also reports of nanometer size effect of the SBH of the electrochemically deposited diodes [396,397]. Electrochemical deposition is obviously a more gentle deposition process than sputtering or vacuum deposition, and it also has strong technological implications. The metal cluster deposition method described above using condensed Xe buffer layer at cryogenic temperature [307], and the picking up of a soft metal layer off of the surface of a liquid [398] are examples of perhaps even more gentle ways of metallization. There are

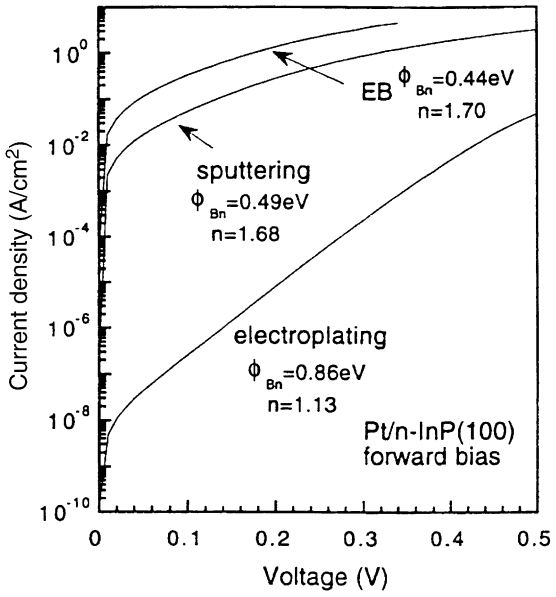

Fig. 71. The measured forward *I–V* characteristics of a Pt–n-InP Schottky diode produced by an electrochemical process, compared with that produced by the conventional e-beam evaporation (EB) and sputtering techniques (from Hasegawa et al. [388]).

other metal deposition schemes, such as chemical vapor deposition, ion beam deposition, ionized cluster beam deposition, which potentially could also lead to variations in the SBH of the diode. But work is scarce in those areas. Along the same vein of the influence of the metal deposition method on the SBH should be included the comment that wafer bonding technologies which have been used to create numerous semiconductor heterojunctions with interesting properties may hold promise for the fabrication of novel MS interfaces in the future.

The annealing behavior of the Schottky-barrier height is of wide interest for scientific as well as technological reasons [346,399]. With annealing, many kinetic processes can take place at an MS interface. Driven by thermodynamics, inter-diffusion, contamination, chemical reaction, compound formation, interface roughening, defect generation, defect annealing, dopant migration, etc. can all occur during annealing. In general, annealing tends to bring the system more toward thermal equilibrium and lead to more reproducible structure. So, unusual SBH resulting from metastable structures tend to fade as a result of annealing. For Si, a major interface effect is the formation of various binary silicide phases. Metal reaction with compound semiconductors could be much more complex and non-uniform [400]. In fact, ''balling up'' has been a very common problem for sintered Ohmic contact on compound semiconductors [401]. A surprising discovery which had supported the general concept of Fermi-level pinning has been the observation of rather minor changes in the SBH when interface reactions take place. In the case of silicide reactions, it has been noticed that different silicide phases of the same metal tend to have similar SBHs and, furthermore, SBHs of silicides are similar to that of the as-deposited metal [203,402,403]. However, some minor variations in the magnitude of the SBH and in other junction characteristics, such as the ideality factor, the difference between *I–V* and *C–V* measurements, the reverse currents, etc. are almost always present. Silicide reaction consumes silicon, which could lead to a change in the doping profile. Dopants have been observed to be rejected (snow-ploughed) from silicides such as PtSi [404] and they are also known to be driven into silicides like $TiSi_2$ and $TaSi_2$ to take part in the formation of inter-metallic compounds [405]. Aluminum was a very common contact to Si at the early days of integrated

circuits. It was well known that the SBH of Al on n-type Si increases upon high temperature annealing, due to the dissolution of Si in Al at high temperature and the subsequent precipitation of heavily Al doped Si (p-type) at the interface. Some compound semiconductors become defective upon high temperature anneals and/or reaction with metal.

Hydrogen, to which samples are commonly exposed in standard semiconductor processing, is known to induce a variety of effects in metals and semiconductors. It is also known to lead to changes in the SBH of some MS interfaces [406–410]. The ability of hydrogen to passivate the electrical activity of many dopants is well documented, and this effect alone has lead to changes in apparent SBH [411,412]. For example, it has been shown that chemical etching of boron doped Si often leads to spurious effects in SBH measurement because of this effect [413]. Hydrogen termination is known to dramatically reduce the density of states of some semiconductor surfaces, which presumably should affect the SBH of interfaces subsequently formed [414]. A very spectacular example of this is the observation of unusually large SBH and highly ideal electrical characteristic from Hg liquid probes on H-terminated p-type Si. It was thought that the elimination of surface states freed the surface from Fermi-level pinning. The introduction of hydrogen after the formation of the MS interface was also found to affect the SBH [415–417]. As a matter of fact, the decrease of the n-type SBH with hydrogen exposure at Pd- and Pt-based MIS Schottky diodes has potential application as hydrogen gas sensor [415,418–420]. Here the effect has largely been attributed to the catalytic effect of Pd and the hydrogen-induced changes in the metal work function [418,421]. Interestingly, the dependence of the SBH on hydrogen partial pressure is very strong on ionic semiconductors, with $S_\Phi \approx 1$, as shown in Fig. 72. This dependence is much weaker for covalent semiconductors [415]. The introduction of hydrogen by annealing and plasma exposure has

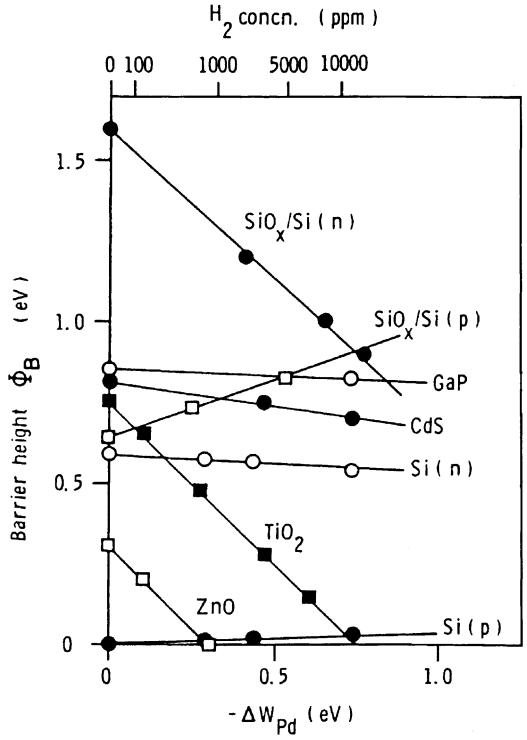

Fig. 72. Relationship between the barrier height at Pd–semiconductor interfaces obtained from *I–V* curves and the change in work function of Pd film against various hydrogen partial pressures in air (from Yamamoto et al. [415]).

also been shown to change the apparent SBH. An intriguing "biased annealing" phenomenon has been observed, where the electrical bias applied to a SB diode during hydrogen anneal is found to affect the change in the SBH [422–425].

8.5. Deliberate Modification of SBH

In addition to the dependence of the SBH on the various treatments of the MS interface just described, our ability to intentionally change the SBH has been demonstrated in some technologically important systems [426]. The most successful scheme to change the magnitude of the SBH has been to insert a very thin layer of material between the metal and the semiconductor. Such a step is sometimes speculated to change the surface property, such as by reducing the surface state density, and the subsequent modification of the SBH is then regarded as a result of this change in the original surface condition. At other times, it is clear that the property of the inserted interface layer is itself the critical feature in the observed change of the SBH. For III–V compound semiconductor surfaces, it has been found that pre-treating the surface with a monolayer of chalcogen (S, Se, . . .) or Sb could lead to a significant change in the SBH of some metals [427–435]. For example, the SBH of Au and Pt on n-type InP increased by about 0.3 eV as a result of sulfur passivation [436] and the SBH of Al on n-type GaAs decreased by about 0.4 eV because of Se treatment [435], as shown in Fig. 73. The most common explanation of the effect of chalcogen treatment is surface-passivation [437–440], i.e. a reduction in the density of surface states. The growth on the semiconductor surface of a thin layer of insulator prior to the deposition of metal has

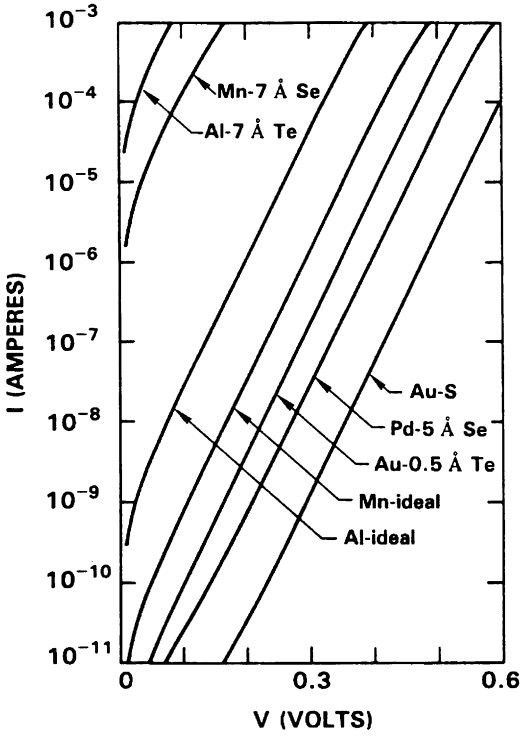

Fig. 73. Representative *I–V* characteristics for vacuum evaporated metal films on n-type GaAs(1 0 0). All diodes have an area of 5×10^{-4} cm^2. Prior to metal deposition, the GaAs surface was exposed to a chalcogen beam, as indicated. "Ideal" interfaces are those formed without exposure to chalcogen (from Waldrop [429]).

also been pursued as a method to modify the SBH. Deposited oxide and nitride layers, and direct oxidation of III–V semiconductor surfaces led to SBHs which are very different from that measured on clean semiconductor surfaces [342,344,345,436,441]. However, a common observation from such thin metal–insulator–semiconductor structure is that the SBH determined from Richardson plot deviates considerably from that determined from *I–V* traces taken at any single temperature. For example, a thin layer of deposited PO_x layer was shown to increase the Au SBH on n-type InP from typically ∼0.4 eV to as high as 0.88 eV, according to *I–V* determination at a fixed temperature [442]. However, activation energy study of the forward-bias current yielded a SBH of 0.41 eV, almost identical to that found without the oxide layer. Similar effects have been seen for other MIS systems [355,443–445].

The insertion of a thin layer of a (different kind of) semiconducting material between a metal and a semiconductor substrate led to changes in the SBH, which have been more consistently measured by different techniques [85,446–448]. The thickness of the interface semiconductor layer, sometimes referred to as the interface control layer (ICL), varies from a few monolayers, in which case the entire ICL may be considered to reside inside the ISR and its effect would be inseparable from the behavior of the entire MS interface, to tens and hundreds of angstroms, in which case the property of the heterojunction can be separated out from that of the MS interface. In the latter case, the effective barrier height for the entire layered structure obviously depends on the heterojunction band offset between the ICL and the semiconductor and the SBH between the metal and the ICL. In addition, the band bending within the ICL, associated with doping and/or interface charge, may become important in rendering the effective barrier height [375,449–452]. The use of a narrow-gap ICL layer is a well-known and effective way to lower the overall SBH and make better Ohmic contact to wide bond gap semiconductors. The reduction in the effective barrier height through the structure is accomplished largely through the breakdown of one large (Schottky) barrier height into two smaller ones (an SBH and a heterojunction band-offset). Most of the experimental results involving thick ICL layers can be explained simply by considering the band diagram of the system. More intriguing is the mechanism by which ultra-thin ICL layers, ∼2 ML, modify the effective SBH [86,453–457], as shown in Fig. 74. Monolayers of Si ICL have been shown to lead to very significant changes in the SBH on GaAs and InP. For a while, it was speculated that the efficacy of the ICL,

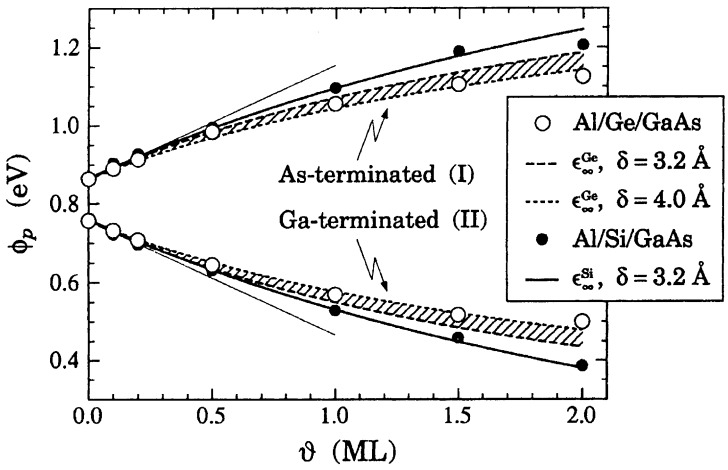

Fig. 74. Comparison of the Schottky-barrier heights in Al–Ge–GaAs(1 0 0) and Al–Si–GaAs(1 0 0) junctions as a function of interlayer atomic coverage. The circles are the results of a self-consistent calculations and the curves are the predictions of a simple interface capacitor model (from Berthod et al. [87]).

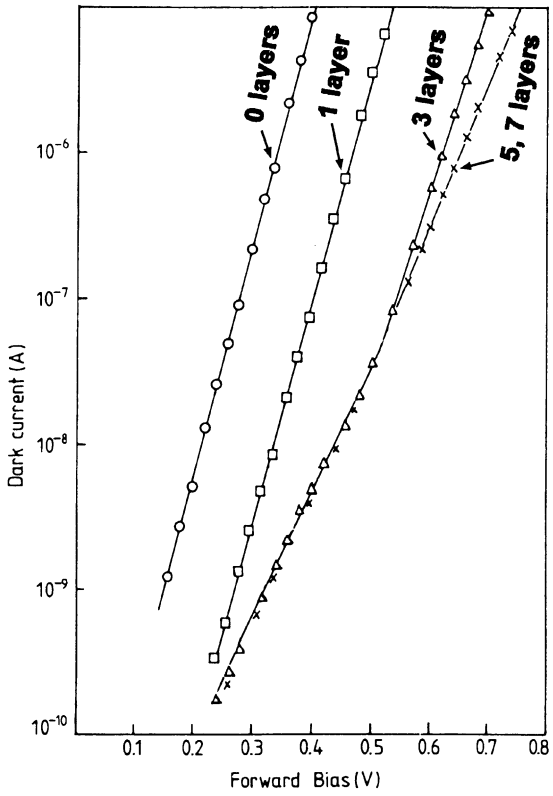

Fig. 75. Dark current vs. forward bias characteristics for GaAs having $10^{16}\,cm^{-3}$ free carriers and various numbers of stearic acid layers between the semiconductor and the Au top electrode (from Tredgold and El-Badawy [459]).

even in the thickness range of <1 nm, was also due to effects associated with doping [86]. But more extensive experimental and theoretical investigations have suggested the important role played by charge distribution resulted from interface bonding.

The well-known uniformity, the ease of application, and the selectable dipole moment of Langmuir–Blodgett films have made them obvious choices to insert at a MS interface to change the SBH [458,459]. Indeed, the inserted molecular layer affected the interface band lineup in the expected way, as shown in Fig. 75. The SBH was roughly described by the Schottky–Mott relationship, with the modification that the semiconductor electron affinity used, χ'_S, is that after the molecular layer has been applied, namely,

$$\Phi^0_{B,n} = \phi_M - \chi'_S = \phi_M - \chi_S + \frac{e^2 D_{dip} N_{dip} \cos\theta}{\varepsilon_{it}} \tag{10.5.1}$$

where D_{dip} is the dipole moment of the molecule, N_{dip} the number of molecules per area, and θ is the average angle the molecule makes with the surface normal. Other methods of grafting a monolayer of self-assembled organic molecules, either on the semiconductor or on the metal surface, prior to the formation of the MS interface also produced very significant change ($\sim$1 eV) in the SBH [398,460,461]. The controllability of the SBH offered by monolayer(s) of organic molecules and inorganic material [462,463] at some organic semiconductor–metal interface is deemed crucial in the development of efficient contacts to electro-luminescence devices. Metal–molecule interfaces have also displayed some intriguing transport properties [464,465].

8.6. The relationship between "pinning" and "bonding"

Even though the overall picture displayed by the SBH of polycrystalline MS system is the Fermi-level pinning phenomenon, the various dependencies of specific SBH on processing condition suggest a more active role played by the interface condition. The Fermi-level pinning phenomenon and also, in particular, the finer SBH dependencies described above are consistent with the bond-polarization picture. After all, any change in the interface structure changes the bonding configuration, and therefore, the interface dipole. These dependencies are more difficult to rationalize with the rigid assumption of a MIGS distribution which depends only on the semiconductor. A recurring theme in the experimental results described above, is the seemingly valid view of the effect the passivation of surface/interface states has on freeing the Fermi-level from being pinned. For instance, the use of chalcogen to passivate the surface of III–V compound semiconductors is known to lead to a genuine reduction in the surface state density, as reflected by a dramatically increased minority carrier lifetime on these surfaces [437]. The much weaker pinning observed for the SBH on MS interfaces subsequent formed on these passivated surface is certainly in good agreement with the prediction of the fixed-separation model of interface/surface gap states. However, it should be apparent that the explanation of such an unpinning phenomenon is also trivial within the bond-polarization picture. The density of surface/interface states, after all, is an indication of the chemical reactivity of the surface. The higher the density of surface states, the more reactive is the surface, and, therefore, the more readily the surface will form chemical bonds with adsorbed species. When a surface is passivated, all the bonds in the surface region are saturated and the surface is chemically inert. When a metal comes into contact with a chemically inert surface, it requires more energy to break old bonds and form new bonds. So, the number of bonds at such interfaces is much smaller than at a chemically active surface. A reduced bond density naturally leads to a weaker pinning phenomenon, in good agreement with experimental results on sulfur- and selenium-passivated III–V semiconductor surfaces. From this example, it seems appropriate to think in equal weight the terms ''pinning'' and ''bonding'', namely, strongly pinned interfaces are usually strongly bonded, and vice versa.

To further explore the analogy between pinning and bonding, one may ponder what the ideal condition might be for non-bonded interface. One certainly expects to find the Schottky–Mott relationship to prevail in those situations. One way to achieve non-bonding may be to maintain a very small gap between a flat facet of a metal and a flat plateau of a semiconductor. This may seem difficult experimentally but, with the advent in STM and MEMS technologies, may some day be achieved. Interface bonding may also be avoided by introducing metal to a passivated or inert semiconductor surface. Most metal deposition methods cannot be used because they disrupt the semiconductor bonds and introduce new bonds. However, the pressing of a mercury droplet [466,467] against a hydrogen-passivated Si [468] does not lead to strong bonding between the Hg and the surface, because the Hg can be retracted afterward without leaving a surface residue. It is interesting to note that the SBH measured from actual experiment was in very good agreement with the Schottky–Mott prediction [468]. Clearly, the electron affinity for a H-terminated Si surface should be the one used in the Schottky–Mott equation.

A wealth of literature exists concerning the electron transfer rate at the interface between electrolytes and semiconductor electrodes [469–471]. Silicon electrodes have been found to be chemically stable in a number of solvents [469]. Redox agents in the electrolyte can exchange charge with the semiconductor electrode via the majority carrier band of the semiconductor, without involving the semiconductor surface atoms in chemical reactions. The redox potential of the solution, which is equivalent to the electrochemical potential of the solution, can be varied by the choice of the additive agents [472,473]. The barrier height at the electrolyte–semiconductor

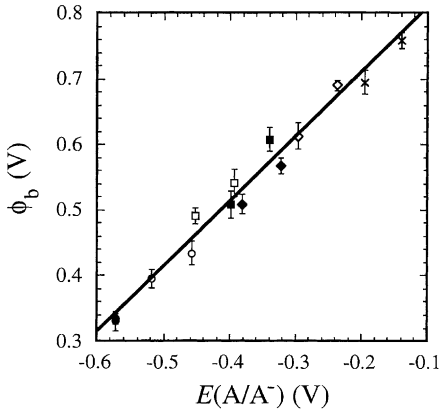

Fig. 76. Plot of the barrier height vs. the Nernstian solution potential for Si–CH_3OH–viologen$^{2+/+}$ junctions. Different symbols represent different redox agents. The linear regression slope is 0.984 and the correlation coefficient is 0.988 (from Fajardo and Lewis [469]).

interface, defined as the difference between the conduction band of the semiconductor and the redox potential, can be measured by *I–V* and *C–V* methods in essentially the same fashion SBHs are measured at MS interfaces. Since the semiconductor electrode surface, in contact with the solvent, should have a structure that is independent of the redox agents, the barrier height dependence on the Nernstian potential is expected to be sharp. As a matter of fact, the dependence of the barrier height on the redox potential of the electrolyte should yield an equivalent "Schottky–Mott" relationship since the liquid molecules are not "bonded" to the semiconductor electrode. A systematic study of eight different redox systems at the methanol–Si interface [469] as shown in Fig. 76, yielded results in excellent agreement with the prediction of the Schottky–Mott theory (extended to the semiconductor–electrolyte interface). A word of caution, however, the semiconductor–liquid interface may have a structure (a Helmholz layer) that is dependent on the solvent. This brings a correction to the semiconductor electron affinity in the Schottky–Mott equation, but does not affect the relative dependence of the barrier height on the redox potential. If, however, the structure of the Helmholz layer depends on the redox agent, then an apparent pinning phenomenon may still be observed. The electrochemical potential of some conducting polymers can be manipulated by doping [474,475]. These polymer systems, are thus, equivalent to non-aqueous electrolytic systems with controllable redox potentials, and their junction characteristics with semiconductors have been studied. The macromolecular structure of these conjugated polymers suggests the absence of surface dangling bonds, and therefore, some degree of chemical inertness against interfacial reaction. The dependence of the equivalent SBH on the work function in these polymer-semiconductor systems has been found to be much stronger than that observed at ordinary metal–semiconductor interfaces [475]. This is another example which suggests the validity of the Schottky–Mott theory whenever interface bonding can be avoided. This is in excellent agreement with the bond-polarization view of the formation of the SBH.

9. Concluding remarks

9.1. The physics of SBH formation

In this article, existing theories and models on the formation of the SBH have been discussed and their strengths and weaknesses analyzed. Most of the theories contain some valuable and valid

views on the underlying physics that governs the formation of the electric dipole at MS interfaces. All of the models contain approximations, which is necessary in view of the complexity of the electronic structure inside the ISR. The magnitude of the SBH contains a bulk contribution and an interface contribution (cf. Eq. (1.3.6a)). It is convenient to view the bulk contribution, i.e. the Schottky–Mott condition, as a condition required by the continuity of the electrostatic potential (the Poisson equation), and the interface contribution as a condition demanded by the thermodynamic forces of the interface, i.e. a minimization of the total interface energy. The bulk contribution is fixed. How the theoretical models differ is in their view on how to minimize the interface energy. Since the interface energy is of vital importance to the formation of the SBH, the important role played by interface atomic structure is naturally exposed. Knowledge on the atomic structure of the ISR is usually lacking for ordinary metal–semiconductor systems. From the limited number of epitaxial MS interfaces of which the atomic structure has been experimentally determined, theoretical calculations showed that the distribution of electronic states inside the ISR is complicated and system-specific. Without knowledge on the atomic structure of ordinary MS interfaces and without simple guidelines concerning the formation of electronic structure from known interface structure, the rigorous way to predict the interface dipole simply will not work for MS interfaces. Some approximations and assumptions have to be used to simplify the SBH problem to a manageable form.

Fortunately, the only electronic property of the ISR that has any bearing on the SBH is the total potential drop across the ISR. The energetic distribution of states is immaterial. So, the focus of the SBH models is how to model the charge rearrangement that has to take place to minimize the interface energy. Both the bond-polarization theory and the MIGS theory have proposals that are either explicitly or loosely based on the electrochemical potential equalization potential concept. These models are successful in predicting the general trend of SBH behavior, but are of course not very accurate when the SBHs of specific MS interfaces are concerned. For a long while to come at least, such simple analysis models are probably the best we can hope for. To go any further, one likely needs to bring the atomic structure of the interface into the theory and employ tedious numerical calculations. It does seem that all the physics one needs to know to view the formation of the SBH properly is already embodied in these simple models one presently has. Even though the two models give roughly similar predictions on the systematic trends of the SBH, their basic assumptions are quite different. Between the two models, the bond-polarization model should be favored because its connection to the chemical potential equalization concept is more direct and it does not make, or rely on, unrealistic assumptions on the distribution of the actual gap states. Also, the notion that interface states are a result of interaction at the interface is expressed fluently in the chemical bonding picture, and it is completely lost in existing MIGS models. But one should remember that these models are just convenient ways to view the physics of SBH formation, which, of course, is the main theme of all theoretical SBH work. There is just one important message that the present review wishes to deliver, namely, the rules of SBH formation are not any different from general physical laws that are obeyed everywhere else. These are, simply, Maxwell's equations and thermodynamic laws. These rules can explain a wide spectrum of seemingly conflicting results observed in SBH studies, without any additional, specific, assumptions. The search for a satisfactory model on the formation of the SBH has been a long and arduous struggle. At present, it looks as though we finally have at hand a coherent explanation of all the experimental data. Furthermore, the bond-polarization theory is a necessary consequence of firmly established physical laws. No special features need to be proposed or unduly assumed. In time, this simple theory on SBH formation is expected to gain wide acceptance, not for its prowess in predicting SBHs with great precision but for its most transparent identification and interpretation of the basic driving forces for interface charge transfer.

9.2. Implications for semiconductor heterojunction band offsets

The basic rules governing the formation of band offsets at semiconductor heterojunctions are obviously identical to that described above for the SBH. There are, however, several important differences. Heterojunction interfaces are usually of high epitaxial quality, with extremely low densities of "missed" bonds. Thus, there are good reasons to believe that BOs are laterally homogeneous. From earlier discussions, one notices that the prevalent view is that the formation of the BO is predominantly a bulk effect. There is some influence due to the interfaces, but the interface effect seems secondary. The concept of bond-polarization [14] can be applied to semiconductor HJs by assuming a density, N_{bond}, and a length, d_{AB}, of interface bonds between two semiconductors A and B. Ignoring the band-gap-related problem, one can apply the electrochemical potential equalization method to obtain a valence band offset, $e\Delta_{\text{VBO}}^{\text{A-B}}$, of

$$e\Delta_{\text{VBO}}^{\text{A-B}} = \gamma_{\text{HJ}}(I_{\text{B}} - I_{\text{A}}) + (1 - \gamma_{\text{HJ}})[\phi_{\text{CNL}}^{\text{S(B)}} - \phi_{\text{CNL}}^{\text{S(A)}}], \tag{11.2.1}$$

where

$$\gamma_{\text{HJ}} = \left[1 + \frac{e^2 N_{\text{bond}} d_{\text{AB}}}{\varepsilon_{\text{it}} E_{\text{g}}(\text{A}) + \varepsilon_{\text{it}} E_{\text{g}}(\text{B})}\right]^{-1}. \tag{11.2.2}$$

These equations predict the expected dependencies of the BO on both the bulk contribution and the interface chemistry. However, they are not very useful because this approach is too crude and cannot deliver the kind of accuracy, $\sim$0.2 eV, expected from BO theories. For epitaxial heterojunction interfaces, the interface structure is known and the electric dipole can be modeled more accurately. The bond-polarization theory [14] for SBH is in spirit close to the approach used by Frensley and Kroemer [42] and the interface-bond-polarity (IBF) model of Lambrecht and Segall [44]. A central step of these approaches is the division of the total charge density of a bulk compound semiconductor into charges belonging to the anion and the cation sites, respectively. This was done by either using an electronegativity scale [42] or, more accurately, parametrizing the calculated bulk wave functions with a short-range basis set [44]. There is some ambiguity involved in either case. A similar ambiguity exists in molecular chemistry when the net charge on each atom in a molecule needs to be determined [99,105]. There the most logical approach seems to be a division method based solely on the charge density of the molecule [476,477]. Such a scheme may be borrowed to bulk crystals to give more coherent analyses of the ionicities of semiconductors and to improve the estimates on charge transfer at heterojunction interfaces [478].

9.3. Implications for applications

In various applications involving the MS interface, the ability to tune the SBH is always desirable. In the old frame of mind, captivated by the Fermi-level pinning effect, such modification of the SBH seemed unfeasible. However, the bond-polarization picture of the SBH formation shows clearly that controlling the SBH is possible, and that the trick is to create some dipole layer at the interface. Various schemes discussed earlier all demonstrated considerable tunability of the SBH. A main issue to some of the schemes is the metastability of the structures created at the interface. However, as the trend of present technologies continues to march toward lower temperature processing, more and more schemes to modify the SBH will be at our disposal. Here, we mention two possible applications for SBH, which may benefit most significantly from a control of its barrier

height. One is the implementation of metal gates in MOSFET or MISFET devices. The ability to control the barrier height at the insulator–metal interface is vital to the operation of such a device. An adjustment of the effective SBH to beyond the band gap of the semiconductor, in principle feasible in these structures, could alleviate problems associated with the short channels presently looming over extremely small FETs. Secondly, the fabrication of low resistance contact to some wide band gap semiconductors is quite problematic at the present. A change in the SBH can certainly improve the Ohmic contact performance. Actually, the use of dipole layers in the control of heterojunction BOs may also be quite valuable in some Ohmic contact strategies.

9.4. Future directions of SBH research

There is plenty of room for refinement and further development of the bond-polarization theory, which might improve its ability to predict SBHs. Some simple rules based on thermodynamic consideration may be established on the type of bonds and the geometry of bonds, which may help the design of a better structural model of common MS interfaces. A better library on the charge density distribution in bulk semiconductors and the tabulation of pure bulk contribution of the electron affinities or ionization potentials will more accurately set the initial matching condition. As for experiments, the areas mentioned above with potential for applications are worth pursuing. Increased activities in related areas, which share the same issues as the MS interface, are also good indications that these are both scientifically challenging and technologically important. These areas include the metal–insulator interface, the metal–organic material interface, and the semiconductor–liquid interface. Better control in metal deposition condition is also thought to be important for future research and application. For instance, the use of electrolyte, clusters, or even wafer bonding, to create metal–semiconductor interfaces may be interesting topics with handsome rewards. As for unfinished issues and standing mysteries, one can perhaps points to the role played by minority carriers and tunneling at MS interfaces as areas which still need some work.

Acknowledgements

I would like to thank many colleagues who have educated me, at different times in my career, on many different facets of the Schottky-barrier height problem, through discussions, writings, and collaborations: Drs. John Sullivan, Kwok Ng, Jurgen Werner, John Freeouf, Hideaki Fujitani, Tony Levi, Walter Brown, Walter Harrison, Robin Williams and Mark Lonergan. My gratitude is also extended to various authors who have generously granted me permission to share some of their results: Drs. M. Aboelfotoh, W. Anderson, A. Baldereschi, L. Brillson, A. Continenza, C. Duke, H. Hasegawa, A. Kahn, N. Lewis, S. Louie, T. McGill, W. Monch, I. Ohdomari, T. Okumura, A. Olbrich, G. Ottaviani, C. Palmstrom, J. Phillips, M. Schulz, W. Spicer, R. Tredgold, H. Tsubomura, H. von Kaenel, J. Waldrop, H. Weitering, and P. Werner.

References

[1] L.J. Brillson, Surf. Sci. Rep. 2 (1982) 123.
[2] W. Monch, Festkorperprobleme 26 (1986) 67.
[3] E.H. Rhoderick, R.H. Williams, Metal–Semiconductor Contacts, 2nd Edition, Clarendon Press, Oxford, 1988.
[4] L.J. Brillson, Contacts to Semiconductors, Noyes Publishers, New Jersey, 1993.
[5] W. Schottky, Z. Physik 113 (1939) 367.

[6] N.F. Mott, Proc. Roy. Soc. (London) 171 (1939) 27.
[7] R.T. Tung, Phys. Rev. Lett. 52 (1984) 461.
[8] C.J. Palmstrom, T.L. Cheeks, H.L. Gilchrist, J.G. Zhu, C.B. Carter, B.J. Wilkens, R. Martin, J. Vac. Sci. Technol. A 10 (1992) 1946.
[9] R.T. Tung, in: D. Wolf, S. Yip (Eds.), Materials Interfaces: Atomic-level Structure and Properties, Chapman and Hall, London, 1992.
[10] R.T. Tung, Phys. Rev. B 45 (1992) 13509.
[11] W.J. Kaiser, L.D. Bell, Phys. Rev. Lett. 60 (1988) 1406.
[12] H. Palm, M. Arbes, M. Schulz, Phys. Rev. Lett. 71 (1993) 2224.
[13] H. Sirringhaus, T. Meyer, E.Y. Lee, H. von Kanel, Phys. Rev. B 53 (1996) 15944.
[14] R.T. Tung, Phys. Rev. Lett. 84 (2000) 6078.
[15] N.W. Ashcroft, N.D. Mermin, Solid State Physics, Holt, Rinehart and Winston, New York, 1976.
[16] C.G. Van de Walle, R.M. Martin, Phys. Rev. B 35 (1987) 8154.
[17] A. Baldereschi, S. Baroni, R. Resta, Phys. Rev. Lett. 61 (1988) 734.
[18] N.D. Lang, Solid State Phys. 28 (1973) 225.
[19] W.F. Egelhoff Jr., Surf. Sci. Rep. 6 (1986) 253.
[20] S.G. Louie, J.R. Chelikowsky, M.L. Cohen, Phys. Rev. B 15 (1977) 2154.
[21] M. van Schilfgaarde, N. Newman, Phys. Rev. Lett. 65 (1990) 2728.
[22] M. Peressi, N. Binggeli, A. Baldereschi, J. Phys. D 31 (1998) 1273.
[23] J.L. Freeouf, T.N. Jackson, S.E. Laux, J.M. Woodall, Appl. Phys. Lett. 40 (1982) 634.
[24] R.T. Tung, Appl. Phys. Lett. 58 (1991) 2821.
[25] J.P. Sullivan, R.T. Tung, M.R. Pinto, W.R. Graham, J. Appl. Phys. 70 (1991) 7403.
[26] S.M. Sze, Physics of Semiconductor Devices, 2nd Edition, Wiley, New York, 1981.
[27] R.L. Anderson, Solid-State Electron. 5 (1962) 341.
[28] H.H. Wieder, J. Vac. Sci. Technol. 15 (1978) 1498.
[29] R.H. Williams, R.R. Varma, V. Montgomery, J. Vac. Sci. Technol. 16 (1979) 1418.
[30] P.E. Schmid, Helv. Phys. Acta 58 (1985) 371.
[31] J.D. Levine, J. Appl. Phys. 42 (1971) 3991.
[32] J.M. Borrego, R.J. Gutmann, S. Ashok, Solid-State Electron. 20 (1977) 125.
[33] K. Maeda, Appl. Surf. Sci. 159/160 (2000) 154.
[34] E.T. Yu, J.O. McCaldin, T.C. McGill, Solid State Physics 46 (1992) 1.
[35] A. Franciosi, C.G. Van de Walle, Surf. Sci. Rep. 25 (1996) 1.
[36] L. Sorba, G. Bratina, G. Ceccone, A. Antonini, J.F. Walker, M. Micovic, A. Franciosi, Phys. Rev. B 43 (1991) 2450.
[37] F. Gozzo, H. Berger, I.R. Collins, G. Margaritondo, W. Ng, A.K. Ray-Chaudhuri, S. Liang, S. Singh, F. Cerrina, Phys. Rev. B 51 (1995) 5024.
[38] W.A. Harrison, J. Vac. Sci. Technol. 14 (1977) 1016.
[39] W.A. Harrison, Phys. Rev. B 24 (1981) 5833.
[40] E.A. Kraut, J. Vac. Sci. Technol. B 2 (1984) 486.
[41] W.R. Frensley, H. Kroemer, J. Vac. Sci. Technol. 13 (1976) 810.
[42] W.R. Frensley, H. Kroemer, Phys. Rev. B 16 (1977) 2642.
[43] C.G. Van de Walle, Phys. Rev. B 39 (1989) 1871.
[44] W.R.L. Lambrecht, B. Segall, Phys. Rev. B 41 (1990) 2832.
[45] R. Resta, S. Baroni, A. Baldereschi, Superlatt. Microstr. 6 (1989) 31.
[46] C. Tejedor, F. Flores, E. Louis, J. Phys. C 10 (1977) 2163.
[47] F. Flores, C. Tejedor, J. Phys. C 12 (1979) 731.
[48] J. Tersoff, Phys. Rev. Lett. 52 (1984) 465.
[49] J. Tersoff, Phys. Rev. B 30 (1984) 4874.
[50] W.A. Harrison, J. Tersoff, J. Vac. Sci. Technol. B 4 (1986) 1068.
[51] I. Lefebvre, M. Lannoo, C. Priester, G. Allan, C. Delerue, Phys. Rev. B 36 (1987) 1336.
[52] J.M. Langer, H. Heinrich, Phys. Rev. Lett. 55 (1985) 1414.
[53] A. Zunger, Annu. Rev. Mater. Sci. 15 (1985) 411.
[54] J. Tersoff, W.A. Harrison, Phys. Rev. Lett. 58 (1987) 2367.
[55] A.D. Katnani, G. Margaritondo, J. Appl. Phys. 54 (1983) 2522.
[56] J. Tersoff, Phys. Rev. Lett. 56 (1986) 2755.
[57] J.N. Andersen, E. Lundgren, R. Nyholm, J. Elec. Spec. Rel. Phen. 75 (1995) 225.
[58] J.A. Rodriguez, R.A. Campbell, D.W. Goodman, Surf. Sci. 307–309 (1994) 377.
[59] M. Alden, H.L. Skriver, B. Johansson, Phys. Rev. B 50 (1994) 12118.
[60] J.B. Mann, Atomic Structure Calculations. Part 1. Hatree–Fock Energy Results for Elements Hydrogen to Lawrencium, Clearinghouse for Technical Informations, Springfield, VA, 1967.
[61] J.M. Andrews, J.C. Phillips, Phys. Rev. Lett. 35 (1975) 56.
[62] S. Hara, I. Ohdomari, Phys. Rev. B 38 (1988) 7554.

[63] K. Hirose, I. Ohdomari, M. Uda, Phys. Rev. B 37 (1988) 6929.
[64] L.J. Brillson, Phys. Rev. Lett. 40 (1978) 260.
[65] P.A. Tove, Surf. Sci. 132 (1983) 336.
[66] S. Kurtin, T.C. McGill, C.A. Mead, Phys. Rev. Lett. 22 (1970) 1433.
[67] F. Flores, C. Tejedor, E. Louis, Phys. Rev. B 16 (1977) 4695.
[68] M. Schluter, Phys. Rev. B 17 (1978) 5044.
[69] M. Cardona, N.E. Christensen, Phys. Rev. B 35 (1987) 6182.
[70] W. Monch, Phys. Rev. Lett. 58 (1987) 1260.
[71] G.H. Parker, T.C. McGill, C.A. Mead, D. Hoffmann, Solid-State Electron. 11 (1968) 201.
[72] J.M. Andrews, M.P. Lepselter, Solid-State Electron. 13 (1970) 1011.
[73] C.R. Crowell, J. Vac. Sci. Technol. 11 (1974) 951.
[74] V. Heine, Phys. Rev. 138 (1965) A1689.
[75] R.T. Tung, A.F.J. Levi, J.P. Sullivan, F. Schrey, Phys. Rev. Lett. 66 (1991) 72.
[76] G.P. Das, P. Blochl, O.K. Andersen, N.E. Christensen, O. Gunnarsson, Phys. Rev. Lett. 63 (1989) 1168.
[77] H. Fujitani, S. Asano, Phys. Rev. B 42 (1990) 1696.
[78] N.V. Rees, C.C. Matthai, J. Phys. C 21 (1988) L981.
[79] H. Fujitani, S. Asano, Appl. Surf. Sci. 41/42 (1989) 164.
[80] R. Stadler, R. Podloucky, Phys. Rev. B 62 (2000) 2209.
[81] R.G. Dandrea, C.B. Duke, J. Vac. Sci. Technol. B 11 (1993) 1553.
[82] R.J. Needs, J.P.A. Charlesworth, R.W. Godby, Europhys. Lett. 25 (1994) 31.
[83] J. Bardi, N. Binggeli, A. Baldereschi, Phys. Rev. B 59 (1999) 8054.
[84] W.R.L. Lambrecht, A.G. Petukhov, B.T. Hemmelman, Solid-State Commun. 108 (1998) 361.
[85] J.R. Waldrop, Appl. Phys. Lett. 53 (1988) 1518.
[86] J.C. Costa, T.J. Miller, F. Williamson, M.I. Nathan, J. Appl. Phys. 70 (1991) 2173.
[87] C. Berthod, N. Binggeli, A. Baldereschi, J. Vac. Sci. Technol. B 18 (2000) 2114.
[88] S.C. Erwin, W.E. Pickett, Solid-State Commun. 81 (1992) 891.
[89] W.R.L. Lambrecht, Physica B 185 (1993) 512.
[90] J. Hoekstra, M. Kohyama, Phys. Rev. B 57 (1998) 2334.
[91] M. Kohyama, J. Hoekstra, Phys. Rev. B 61 (2000) 2672.
[92] S. Picozzi, A. Continenza, G. Satta, S. Massidda, A.J. Freeman, Phys. Rev. B 61 (2000) 16736.
[93] A.P. Sutton, Electronic Structure of Materials, Oxford University Press, Oxford, 1993.
[94] D. Pettifor, Bonding and Structure of Molecules and Solids, Oxford University Press, Oxford, 1995.
[95] R.T. Tung, Phys. Rev. B 64 (2001) 0000.
[96] R.P. Iczkowsky, J.L. Margrave, J. Am. Chem. Soc. 83 (1961) 3547.
[97] W.J. Mortier, S.K. Ghosh, S. Shankar, J. Am. Chem. Soc. 108 (1986) 4315.
[98] A.K. Rappe, W.A. Goddard III, J. Phys. Chem. 95 (1991) 3358.
[99] J. Cioslowski, B.B. Stefanov, J. Chem. Phys. 99 (1993) 5151.
[100] D.M. York, Y. Yang, J. Chem. Phys. 104 (1996) 159.
[101] J.P. Perdew, R.G. Parr, M. Levy, J.L. Balduz Jr., Phys. Rev. Lett. 49 (1982) 1691.
[102] F. De Proft, S. Liu, R.G. Parr, J. Chem. Phys. 107 (1997) 3000.
[103] R.G. Parr, R.G. Pearson, J. Am. Chem. Soc. 105 (1983) 7512.
[104] A.E. Reed, F. Weinhold, J. Chem. Phys. 84 (1986) 2428.
[105] K.B. Wiberg, P.R. Rablen, J. Comp. Chem. 14 (1993) 1504.
[106] J. Tersoff, Phys. Rev. B 32 (1985) 6968.
[107] F. Cyrot-Lackmann, Adv. Phys. 16 (1967) 393.
[108] J.R. Lince, D.J. Carre, P.D. Fleischauer, Phys. Rev. B 36 (1987) 1647.
[109] G. Baccarani, J. Appl. Phys. 47 (1976) 4122.
[110] F. Berz, Solid-State Electron. 28 (1985) 1007.
[111] H.A. Bethe, MIT Radiation Lab. Rep. 43 (1942) 12.
[112] J.P.A. Charlesworth, R.W. Godby, R.J. Needs, Phys. Rev. Lett. 70 (1993) 1685.
[113] F.A. Padovani, R. Stratton, Solid-State Electron. 9 (1966) 695.
[114] C.R. Crowell, V.L. Rideout, Solid-State Electron. 12 (1969) 89.
[115] D.L. Scharfetter, Solid-State Electron. 8 (1965) 299.
[116] M.A. Green, J. Shewchun, Solid-State Electron. 16 (1973) 1141.
[117] M.M.S. Hassan, Solid-State Electron. 44 (2000) 1111.
[118] B. Elfsten, P.A. Tove, Solid-State Electron. 28 (1985) 721.
[119] D. Sands, C.G. Scott, J. Appl. Phys. 77 (1995) 3295.
[120] J. Werner, A.F.J. Levi, R.T. Tung, M. Anzlowar, M. Pinto, Phys. Rev. Lett. 60 (1988) 53.
[121] M. Missous, E.H. Rhoderick, Electron. Lett. 22 (1986) 477.
[122] H. Norde, J. Appl. Phys. 50 (1979) 5052.
[123] K. Sato, Y. Yasumura, J. Appl. Phys. 58 (1985) 3655.

[124] J.H. Werner, Appl. Phys. A A47 (1988) 291.
[125] C. Barret, P. Muret, Appl. Phys. Lett. 42 (1983) 890.
[126] A.N. Saxena, Surf. Sci. 13 (1969) 151.
[127] C. Canali, F. Catellani, S. Mantovani, M. Prudenziati, J. Phys. D 10 (1977) 2481.
[128] I. Ohdomari, K.N. Tu, J. Appl. Phys. 51 (1980) 3735.
[129] I. Ohdomari, T.S. Kuan, K.N. Tu, J. Appl. Phys. 50 (1979) 7020.
[130] D. Dasculu, G. Brezeanu, P.A. Dan, C. Dima, Solid-State Electron. 24 (1981) 897.
[131] M.V. Schneider, A.Y. Cho, E. Kollberg, H. Zirath, Appl. Phys. Lett. 43 (1983) 558.
[132] T.Q. Tuy, I. Mojzes, Appl. Phys. Lett. 56 (1990) 1652.
[133] V.B. Bikbaev, S.C. Karpinskas, J.J. Vaitkus, Phys. Stat. Sol. A 75 (1983) 583.
[134] Y.P. Song, R.L. Van Meirhaeghe, W.H. Laflere, F. Cardon, Solid-State Electron. 29 (1986) 633.
[135] J.H. Werner, H.H. Guttler, J. Appl. Phys. 69 (1991) 1522.
[136] J.L. Freeouf, T.N. Jackson, S.E. Laux, J.M. Woodall, J. Vac. Sci. Technol. 21 (1982) 570.
[137] A.I. Bastys, V.B. Bikbaev, J.J. Vaitkus, S.C. Karpinskas, Lit. Fiz. Sbor. 28 (1988) 191.
[138] Y. Nakato, K. Ueda, H. Yano, H. Tsubomura, J. Phys. Chem. 92 (1988) 2316.
[139] R.H. Cox, H. Strack, Solid-State Electron. 10 (1967) 1213.
[140] J. Osvald, J. Appl. Phys. 85 (1999) 1935.
[141] R.T. Tung, J. Appl. Phys. 88 (2000) 7366.
[142] F.A. Padovani, J. Appl. Phys. 38 (1967) 891.
[143] B. Pellegrini, G. Salardi, Solid-State Electron. 21 (1978) 465.
[144] P.K. Vasudev, B.L. Mattes, E. Pietras, R.H. Bube, Solid-State Electron. 19 (1976) 557.
[145] F.J. Bryant, J.M. Majid, C.G. Scott, D. Shaw, Solid-State Commun. 63 (1987) 9.
[146] C.W. Kao, C.L. Anderson, C.R. Crowell, Surf. Sci. 95 (1980) 321.
[147] T. Okumura, K.N. Tu, J. Appl. Phys. 61 (1987) 2955.
[148] T. Okumura, K.N. Tu, J. Appl. Phys. 54 (1983) 922.
[149] A. Tanabe, K. Konuma, N. Teranishi, S. Tohyama, K. Masubuchi, J. Appl. Phys. 69 (1991) 850.
[150] J.Y.F. Tang, J.L. Freeouf, J. Vac. Sci. Technol. B 2 (1984) 459.
[151] R. Ludeke, Surf. Sci. 168 (1986) 290.
[152] M.H. Hecht, Phys. Rev. B 41 (1990) 7918.
[153] T. Okumura, K. Shiojima, Jpn. J. Appl. Phys. Part 2 28 (1989) L1108.
[154] K. Shiojima, T. Okumura, Japan. J. Appl. Phys. 30 (1991) 2127.
[155] S. Miyazaki, T. Okumura, Y. Miura, K. Hirose, Inst. Phys. Conf. Ser. 149 (1996) 307.
[156] F. Gozzo, M. Marsi, H. Berger, G. Margaritondo, A. Ottolenghi, A.K. Ray-Chaudhuri, W. Ng, S. Liang, S. Singh, J.T. Welnak, J.P. Wallace, C. Capasso, F. Cerrina, Phys. Rev. B 48 (1993) 17163.
[157] S. Heun, T. Schmidt, J. Slezak, J. Diaz, K.C. Prince, B.H. Muller, A. Franciosi, J. Cryst. Growth 202 (1999) 795.
[158] M. Giesen, R.J. Phaneuf, E.D. Williams, T.L. Einstein, Surf. Sci. 396 (1998) 411.
[159] J.M. Gibson, R.T. Tung, C.A. Pimentel, D.C. Joy, Inst. Phys. Conf. Ser. 76 (1985) 173.
[160] H.C.W. Huang, C.F. Aliotta, P.S. Ho, Appl. Phys. Lett. 41 (1982) 54.
[161] W.D. Rau, P. Schwander, F.H. Baumann, W. Hoppner, A. Ourmazd, Phys. Rev. Lett. 82 (1999) 2614.
[162] F. Schaffler, G. Abstreiter, J. Vac. Sci. Technol. B 3 (1985) 1184.
[163] L.D. Bell, W.J. Kaiser, Phys. Rev. Lett. 61 (1988) 2368.
[164] M.D. Stiles, D.R. Hamann, J. Vac. Sci. Technol. B 9 (1991) 2394.
[165] L.J. Schowalter, E.Y. Lee, Phys. Rev. B 43 (1991) 9308.
[166] R. Ludeke, A. Bauer, Phys. Rev. Lett. 71 (1993) 1760.
[167] A.M. Milliken, S.J. Manion, W.J. Kaiser, L.D. Bell, M.H. Hecht, Phys. Rev. B 46 (1992) 12826.
[168] H. Sirringhaus, E.Y. Lee, H. von Kanel, Phys. Rev. Lett. 74 (1995) 3999.
[169] K. Reuter, P.L. de Andres, F.J. Garcia-Vidal, D. Sestovic, F. Flores, K. Heinz, Phys. Rev. B 58 (1998) 14036.
[170] K. Reuter, F.J. Garcia-Vidal, P.L. de Andres, F. Flores, K. Heinz, Phys. Rev. Lett. 81 (1998) 4963.
[171] T. Meyer, D. Migas, L. Miglio, H. Von Kanel, Phys. Rev. Lett. 85 (2000) 1520.
[172] J. Heil, M. Primke, A. Bohm, P. Wyder, B. Wolf, J. Major, P. Keppler, Phys. Rev. B 54 (1996) R2280.
[173] Y. Khang, K.M. Mang, K.H. Booh, Y. Kuk, J. Vac. Sci. Technol. B 14 (1996) 1221.
[174] H.C. Card, E.H. Rhoderick, J. Phys. D 4 (1971) 1589.
[175] S.J. Fonash, J. Appl. Phys. 54 (1983) 1966.
[176] A.M. Goodman, J. Appl. Phys. 34 (1963) 329.
[177] A.M. Cowley, J. Appl. Phys. 37 (1966) 3024.
[178] C.R. Crowell, G.I. Roberts, J. Appl. Phys. 40 (1969) 3726.
[179] P. Muret, J. Appl. Phys. 53 (1982) 6300.
[180] C. Barret, F. Chekir, A. Vapaille, J. Phys. C 16 (1983) 2421.
[181] P.S. Ho, E.S. Yang, H.L. Evans, W. Xu, Phys. Rev. Lett. 56 (1986) 177.
[182] P. Muret, D. Elguennouni, M. Missous, E.H. Rhoderick, Appl. Phys. Lett. 58 (1991) 155.
[183] J.H. Werner, in: I.P. Batra (Ed.), Metallization and Metal–Semiconductor Interfaces, Plenum Press, New York, 1989.

[184] B. Bati, C. Nuhoglu, M. Saglam, E. Ayyildiz, A. Turut, Phys. Scr. 61 (2000) 209.
[185] C.H. Champness, W.R. Clark, Appl. Phys. Lett. 56 (1990) 1104.
[186] M. Matsumura, Y. Hirose, Jpn. J. Appl. Phys. Part 2 39 (2000) L123.
[187] R.T. Tung, J.M. Gibson, J.M. Poate, Phys. Rev. Lett. 50 (1983) 429.
[188] R.T. Tung, J.M. Gibson, J.M. Poate, Appl. Phys. Lett. 42 (1983) 888.
[189] D. Cherns, G.R. Anstis, J.L. Hutchison, J.C.H. Spence, Phil. Mag. A 46 (1982) 849.
[190] H. Foll, Phys. Stat. Sol. A 69 (1982) 779.
[191] E. Vlieg, A.E.M.J. Fischer, J.F. Van Der Veen, B.N. Dev, G. Materlik, Surf. Sci. 178 (1986) 36.
[192] I.K. Robinson, R.T. Tung, R. Feidenhans'l, Phys. Rev. B 38 (1988) 3632.
[193] M. Liehr, P.E. Schmid, F.K. LeGoues, P.S. Ho, Phys. Rev. Lett. 54 (1985) 2139.
[194] R.J. Hauenstein, T.E. Schlesinger, T.C. McGill, B.D. Hunt, L.J. Schowalter, Appl. Phys. Lett. 47 (1985) 853.
[195] M. Ospelt, J. Henz, L. Flepp, H. von Kanel, Appl. Phys. Lett. 52 (1988) 227.
[196] J. Vrijmoeth, J.F. van der Veen, D.R. Heslinga, T.M. Klapwijk, Phys. Rev. B 42 (1990) 9598.
[197] R.T. Tung, K.K. Ng, J.M. Gibson, A.F.J. Levi, Phys. Rev. B 33 (1986) 7077.
[198] J.L. Batstone, J.M. Gibson, R.T. Tung, A.F.J. Levi, Appl. Phys. Lett. 52 (1988) 828.
[199] J.P. Sullivan, R.T. Tung, F. Schrey, J. Appl. Phys. 72 (1992) 478.
[200] D. Cherns, C.J.D. Hetherington, C.J. Humphreys, Phil. Mag. A 49 (1984) 165.
[201] H. Fujitani, S. Asano, J. Phys. Soc. Jpn. 60 (1991) 2526.
[202] C.C. Matthai, N.V. Rees, T.H. Shen, Appl. Surf. Sci. 56–58 (1992) 525.
[203] G. Ottaviani, K.N. Tu, J.W. Mayer, Phys. Rev. B 24 (1981) 3354.
[204] J.P. Sullivan, R.T. Tung, D.J. Eaglesham, F. Schrey, W.R. Graham, J. Vac. Sci. Technol. B 11 (1993) 1564.
[205] D. Loretto, J.M. Gibson, S.M. Yalisove, Phys. Rev. Lett. 63 (1989) 298.
[206] C.W.T. Bulle-Lieuwma, A.F. De Jong, D.E.W. Vandenhoudt, Phil. Mag. A 64 (1991) 255.
[207] P. Werner, W. Jager, A. Schuppen, J. Appl. Phys. 74 (1993) 3846.
[208] P. Werner, W. Jager, A. Schuppen, MRS Symp. Proc. 320 (1994) 227.
[209] D.R. Heslinga, H.H. Weitering, D.P. van der Werf, T.M. Klapwijk, T. Hibma, Phys. Rev. Lett. 64 (1990) 1589.
[210] G. Le Lay, K. Hricovini, J.E. Bonnet, Appl. Surf. Sci. 41/42 (1989) 25.
[211] G. Le Lay, K. Hricovini, Phys. Rev. Lett. 65 (1990) 807.
[212] H.H. Weitering, D.R. Heslinga, T. Hibma, T.M. Kalpwijk, Phys. Rev. Lett. 65 (1990) 808.
[213] A.Y. Cho, P.D. Dernier, J. Appl. Phys. 49 (1978) 3328.
[214] R. Ludeke, L.L. Chang, L. Esaki, Appl. Phys. Lett. 23 (1973) 201.
[215] S.K. Donner, K.P. Caffey, N. Winograd, J. Vac. Sci. Technol. B 7 (1989) 742.
[216] W.C. Marra, P. Eisenberger, A.Y. Cho, J. Appl. Phys. 50 (1979) 6927.
[217] D.J. Eaglesham, C.J. Kiely, D. Cherns, M. Missous, Philos. Mag. A 60 (1989) 161.
[218] J. Mizuki, K. Akimoto, I. Horosawa, K. Hirose, T. Mizutani, J. Matsui, J. Vac. Sci. Technol. B 6 (1988) 31.
[219] W.I. Wang, J. Vac. Sci. Technol. B 1 (1983) 574.
[220] C. Barret, J. Massies, J. Vac. Sci. Technol. B 1 (1983) 819.
[221] M. Missous, E.H. Rhoderick, K.E. Singer, J. Appl. Phys. 60 (1986) 2439.
[222] K. Hirose, K. Akimoto, I. Hirosawa, J. Mizuki, T. Mizutani, J. Matsui, Phys. Rev. B 43 (1991) 4538.
[223] T. Sands, Appl. Phys. Lett. 52 (1988) 197.
[224] J.P. Harbison, T. Sands, N. Tabatabaie, W.K. Chan, L.T. Florez, V.G. Keramidas, Appl. Phys. Lett. 53 (1988) 1717.
[225] C.J. Palmstrom, B.O. Fimland, T. Sands, K.C. Garrison, R.A. Bartynski, J. Appl. Phys. 65 (1989) 4753.
[226] C.J. Palmstrom, N. Tabatabaie, S.J. Allen Jr., Appl. Phys. Lett. 53 (1988) 2608.
[227] N. Tabatabaie, T. Sands, J.P. Harbison, H.L. Gilchrist, V.G. Keramidas, Appl. Phys. Lett. 53 (1988) 2528.
[228] J.G. Zhu, C.B. Carter, C.J. Palmstrom, K.C. Garrison, Appl. Phys. Lett. 55 (1989) 39.
[229] T.L. Cheeks, T. Sands, R.E. Nahory, J. Harbison, N. Tabatabaie, H.L. Gilchrist, B.J. Wilkens, V.G. Keramidas, Appl. Phys. Lett. 56 (1990) 1043.
[230] T. Sands, C.J. Palmstrom, J.P. Harbison, V.G. Keramidas, N. Tabatabaie, T.L. Cheeks, R. Ramesh, Y. Silberberg, Mater. Sci. Rep. 5 (1990) 99.
[231] C.J. Palmstrom, T.L. Cheeks, H.L. Gilchrist, J.G. Zhu, C.B. Carter, R.E. Nahory, Mat. Res. Soc. Ext. Abs. 21 (1990) 63.
[232] Y. Hasegawa, Y. Kuk, R.T. Tung, P.J. Silverman, T. Sakurai, J. Vac. Sci. Technol. B 9 (1991) 578.
[233] H. Sirringhaus, E.Y. Lee, U. Kafader, H. von Kanel, J. Vac. Sci. Technol. B 13 (1995) 1848.
[234] H. Sirringhaus, E.Y. Lee, H. von Kanel, Phys. Rev. Lett. 73 (1994) 577.
[235] O. Engstrom, H. Pettersson, B. Sernelius, Phys. Stat. Sol. A 95 (1986) 691.
[236] A.E. Fowell, R.H. Williams, B.E. Richardson, A.A. Cafolla, D.I. Westwood, D.A. Woolf, J. Vac. Sci. Technol. B 9 (1991) 581.
[237] M.H. Hecht, L.D. Bell, W.J. Kaiser, F.J. Grunthaner, Appl. Phys. Lett. 55 (1989) 780.
[238] A.A. Talin, R.S. Williams, B.A. Morgan, K.M. Ring, K.L. Kavanagh, Phys. Rev. B 49 (1994) 16474.
[239] S. Zhu, R.L. Van Meirhaeghe, C. Detavernier, G.P. Ru, B.Z. Li, F. Cardon, Solid-State Commun. 112 (1999) 611.
[240] A. Olbrich, J. Vancea, F. Kreupl, H. Hoffmann, Appl. Phys. Lett. 70 (1997) 2559.

[241] A. Olbrich, J. Vancea, F. Kreupl, H. Hoffmann, J. Appl. Phys. 83 (1998) 358.
[242] S. Yae, R. Tsuda, T. Kai, K. Kukuchi, M. Uetsuji, T. Fujii, M. Fujitani, Y. Nakato, J. Electrochem. Soc. 141 (1994) 3090.
[243] R.C. Rossi, M.X. Tan, N.S. Lewis, Appl. Phys. Lett. 77 (2000) 2698.
[244] M.O. Aboelfotoh, J. Appl. Phys. 64 (1988) 4046.
[245] A.Y.C. Yu, E.H. Snow, J. Appl. Phys. 39 (1968) 3008.
[246] M.P. Lepselter, S.M. Sze, Bell. Syst. Tech. J. 47 (1968) 195.
[247] Z. Liliental-Weber, R. Gronsky, J. Washburn, N. Newman, W.E. Spicer, E.R. Weber, J. Vac. Sci. Technol. B 4 (1986) 912.
[248] J.P. Sullivan, R.T. Tung, F. Schrey, W.R. Graham, J. Vac. Sci. Technol. A 10 (1992) 1959.
[249] F. La Via, P. Lanza, O. Viscuso, G. Ferla, E. Rimini, Thin Solid Films 161 (1988) 13.
[250] M. Wittmer, Phys. Rev. B 42 (1990) 5249.
[251] S.M. Sze, C.R. Crowell, D. Kahng, J. Appl. Phys. 35 (1964) 2534.
[252] V.L. Rideout, C.R. Crowell, Solid-State Electron. 13 (1970) 993.
[253] J.L. Freeouf, Appl. Phys. Lett. 41 (1982) 285.
[254] H.H. Hosack, Appl. Phys. Lett. 21 (1972) 256.
[255] N. Toyama, T. Takahashi, H. Murakami, H. Koriyama, Appl. Phys. Lett. 46 (1985) 557.
[256] T.U. Kampen, W. Monch, Appl. Surf. Sci. 117/118 (1997) 388.
[257] W. Monch, J. Vac. Sci. Technol. B 17 (1999) 1867.
[258] L.F. Wagner, R.W. Young, A. Sugerman, IEEE Elec. Dev. Lett. EDL-4 (1983) 320.
[259] V.W.L. Chin, M.A. Green, J.W.V. Storey, J. Appl. Phys. 68 (1990) 3470.
[260] M.O. Aboelfotoh, J. Appl. Phys. 69 (1991) 3351.
[261] F.A. Padovani, G.G. Sumner, J. Appl. Phys. 36 (1965) 3744.
[262] S. Ashok, J.M. Borrego, R.J. Gutmann, Solid-State Electron. 22 (1979) 621.
[263] M.O. Aboelfotoh, A. Cros, B.G. Svensson, K.N. Tu, Phys. Rev. B 41 (1990) 9819.
[264] B. Tuck, G. Eftekhari, D.M. de Cogan, J. Phys. D 15 (1982) 457.
[265] F.A. Padovani, in: R.K. Willardson, A.C. Beer (Eds.), Semiconductors and Semimetals, Academic Press, New York, 1971.
[266] G.S. Visweswaran, R. Sharan, Proc. IEEE 67 (1979) 436.
[267] C.R. Crowell, Solid-State Electron. 20 (1977) 171.
[268] J. Basterfield, J.M. Shannon, A. Gill, Solid-State Electron. 18 (1975) 290.
[269] B. Studer, Solid-State Electron. 23 (1980) 1181.
[270] M.O. Aboelfotoh, J. Appl. Phys. 66 (1989) 262.
[271] M.O. Aboelfotoh, K.N. Tu, Phys. Rev. B 34 (1986) 2311.
[272] Z.J. Horvath, V. Van Tuyen, Appl. Phys. Lett. 66 (1995) 3068.
[273] B.Y. Tsaur, D.J. Silversmith, R.W. Mountain, L.S. Hung, S.S. Lau, T.T. Sheng, J. Appl. Phys. 52 (1981) 5243.
[274] C.-A. Chang, J. Appl. Phys. 59 (1986) 3116.
[275] A.Y.C. Yu, C.A. Mead, Solid-State Electron. 13 (1970) 97.
[276] T. Arizumi, M. Hirose, Jpn. J. Appl. Phys. 8 (1969) 749.
[277] V.W.L. Chin, J.W.V. Storey, M.A. Green, J. Appl. Phys. 68 (1990) 4127.
[278] C.J. Kircher, Solid-State Electron. 14 (1971) 507.
[279] M. Wittmer, W. Luthy, B. Studer, H. Melchior, Solid-State Electron. 24 (1981) 141.
[280] V.F. Drobny, J. Elec. Mater. 14 (1985) 283.
[281] J.M. Andrews, F.B. Koch, Solid-State Electron. 14 (1971) 901.
[282] A.M. Cowley, Solid-State Electron. 13 (1970) 403.
[283] A. Thanailakis, A. Rasul, J. Phys. C 9 (1976) 337.
[284] N. Newman, M. van Schilfgaarde, T. Kendelwicz, M.D. Williams, W.E. Spicer, Phys. Rev. B 33 (1986) 1146.
[285] A.B. McLean, R.H. Williams, J. Phys. C 21 (1988) 783.
[286] D. Khang, Solid-State Electron. 6 (1963) 281.
[287] R.J. Archer, T.O. Yep, J. Appl. Phys. 41 (1970) 303.
[288] R.F. Broom, Solid-State Electron. 14 (1971) 1087.
[289] H.H. Guttler, J.H. Werner, Appl. Phys. Lett. 56 (1990) 1113.
[290] J.A. Copeland, IEEE Trans. Elec. Dev. ED17 (1970) 404.
[291] H. Grinolds, G.Y. Robinson, J. Vac. Sci. Technol. 14 (1977) 75.
[292] J.D. Wiley, G.L. Miller, IEEE Trans. Elec. Dev. ED-22 (1975) 265.
[293] L.J. Brillson, C.F. Brucker, N.G. Stoffel, A.D. Katnani, G. Margaritondo, Phys. Rev. Lett. 46 (1981) 838.
[294] W.E. Spicer, I. Lindau, P. Skeath, C.Y. Su, P. Chye, Phys. Rev. Lett. 44 (1980) 420.
[295] R.H. Williams, Contemp. Phys. 23 (1982) 329.
[296] J.E. Rowe, S.B. Christman, G. Margaritondo, Phys. Rev. Lett. 35 (1975) 1471.
[297] R. Ludeke, T.C. Chiang, T. Miller, J. Vac. Sci. Technol. B 1 (1983) 581.
[298] M. del Giudice, J.J. Joyce, M.W. Ruckman, J.H. Weaver, Phys. Rev. B 32 (1985) 5149.

[299] W.E. Spicer, P.W. Chye, P.R. Skeath, C.Y. Su, I. Lindau, J. Vac. Sci. Technol. 16 (1979) 1422.
[300] L.J. Brillson, R.E. Viturro, M.L. Slade, P. Chiaradia, D. Kilday, M.K. Kelly, G. Margaritondo, Appl. Phys. Lett. 50 (1987) 1379.
[301] W. Chen, A. Kahn, P. Soukiassian, P.S. Mangat, J. Gaines, C. Ponzoni, D. Olego, Phys. Rev. B 51 (1995) 14265.
[302] K. Stiles, S.F. Horng, A. Kahn, J. McKinley, D.G. Kilday, G. Margaritondo, J. Vac. Sci. Technol. B 6 (1988) 1392.
[303] R. Cao, K. Miyano, I. Lindau, W.E. Spicer, Solid-State Commun. 70 (1989) 7.
[304] D.R.T. Zahn, W. Richter, A.B. McLean, R.H. Williams, C. Stephens, I.T. McGovern, R. Cimino, W. Braun, N. Esser, Appl. Surf. Sci. 41/42 (1989) 179.
[305] S. Chang, J.L. Shaw, R.E. Viturro, L.J. Brillson, P.D. Kirchner, J.M. Woodall, J. Vac. Sci. Technol. A 8 (1990) 3803.
[306] L.J. Brillson, M.L. Slade, R.E. Viturro, M.K. Kelly, N. Tache, G. Margaritondo, J.M. Woodall, P.D. Kirchner, G.D. Pettit, S.L. Wright, Appl. Phys. Lett. 48 (1986) 1458.
[307] G.D. Waddill, C.M. Aldao, I.M. Vitomirov, S.G. Anderson, C. Capasso, J.H. Weaver, J. Vac. Sci. Technol. B 7 (1989) 950.
[308] D. Mao, K. Young, K. Stiles, A. Kahn, J. Appl. Phys. 64 (1988) 4777.
[309] W.E. Spicer, R. Cao, K. Stiles, A. Kahn, P. Prietsch, M. Domke, C. Laubschat, G. Kaindl, Phys. Rev. Lett. 62 (1989) 605.
[310] L. Kronik, Y. Shapira, Surf. Sci. Rep. 37 (1999) 5.
[311] M. Alonso, R. Cimino, K. Horn, Phys. Rev. Lett. 64 (1990) 1947.
[312] I.T. McGovern, C. Stephens, K. Fives, R. Whittle, R. Cimino, D.R.T. Zahn, W. Braun, Surf. Sci. 251/252 (1991) 447.
[313] S.P. Wilks, J.I. Morris, D.A. Woolf, R.H. Williams, J. Vac. Sci. Technol. B 9 (1991) 2118.
[314] W.G. Spitzer, C.A. Mead, J. Appl. Phys. 34 (1963) 3061.
[315] C.A. Mead, W.G. Spitzer, Phys. Rev. 134 (1964) A713.
[316] R.K. Swank, Phys. Rev. 153 (1967) 844.
[317] J.O. McCaldin, T.C. McGill, C.A. Mead, Phys. Rev. Lett. 36 (1976) 56.
[318] J.L. Freeouf, J.M. Woodall, Appl. Phys. Lett. 39 (1981) 727.
[319] R.H. Williams, V. Montgomery, R.R. Varma, J. Phys. C 11 (1978) L735.
[320] E. Bucher, S. Schulz, M.C. Lux-Steiner, P. Munz, U. Gubler, F. Greuter, Appl. Phys. A 40 (1986) 71.
[321] G. Ottaviani, K.N. Tu, J.W. Mayer, Phys. Rev. Lett. 44 (1980) 284.
[322] K.N. Tu, Appl. Phys. Lett. 27 (1975) 221.
[323] J.L. Freeouf, Solid-State Commun. 33 (1980) 1059.
[324] W.E. Spicer, Z. Liliental-Weber, E. Weber, N. Newman, T. Kendelewicz, R. Cao, C. McCants, P. Mahowald, K. Miyano, I. Lindau, J. Vac. Sci. Technol. B 6 (1988) 1245.
[325] M. van Schilfgaarde, N. Newman, J. Vac. Sci. Technol. B 9 (1991) 2140.
[326] M.S. Daw, D.L. Smith, Appl. Phys. Lett. 36 (1980) 690.
[327] M.S. Daw, D.L. Smith, Solid-State Commun. 37 (1981) 205.
[328] O.F. Sankey, R.E. Allen, J.D. Dow, Solid-State Commun. 49 (1984) 1.
[329] R.E. Allen, T.J. Humphreys, J.D. Dow, O.F. Sankey, J. Vac. Sci. Technol. B 2 (1984) 449.
[330] R. Ludeke, A. Taleb-Ibrahimi, G. Jezequel, Appl. Surf. Sci. 41/42 (1989) 151.
[331] J.M. Woodall, J.L. Freeouf, J. Vac. Sci. Technol. 21 (1982) 574.
[332] H. Hasegawa, H. Ohno, J. Vac. Sci. Technol. B 4 (1986) 1130.
[333] S. Chang, L.J. Brillson, Y.J. Kime, D.S. Rioux, P.D. Kirchner, G.D. Pettit, J.M. Woodall, Phys. Rev. Lett. 64 (1990) 2551.
[334] T.J. Drummond, Phys. Rev. B 59 (1999) 8182.
[335] W. Shan, M.F. Li, P.Y. Yu, W.L. Hansen, W. Walukiewicz, Appl. Phys. Lett. 53 (1988) 974.
[336] M. van Schilfgaarde, E. Weber, N. Newman, Phys. Rev. Lett. 73 (1994) 581.
[337] J. Bardi, N. Binggeli, A. Baldereschi, Phys. Rev. B 54 (1996) R11102.
[338] A. Zur, T.C. McGill, D.L. Smith, Phys. Rev. B 28 (1983) 2060.
[339] M.J. Turner, E.H. Rhoderick, Solid-State Electron. 11 (1968) 291.
[340] J.D. Mottram, D.C. Northrop, C.M. Reed, A. Thanailakis, J. Phys. D 12 (1979) 773.
[341] R.R. Varma, A. McKinley, R.H. Williams, I.G. Higginbotham, J. Phys. D 10 (1977) L171.
[342] R.H. Williams, V. Montgomery, R.R. Varma, A. McKinley, J. Phys. D 10 (1977) L253.
[343] O. Wada, A. Majerfeld, Electron. Lett. 14 (1978) 125.
[344] F. Hasegawa, M. Onomura, C. Mogi, Y. Nannichi, Solid-State Electron. 31 (1988) 223.
[345] J. Nakamura, H. Niu, S. Kishino, Jpn. J. Appl. Phys. Part 1 32 (1993) 699.
[346] Y.H. Wang, M.P. Houng, P.W. Sze, J.F. Chen, A.Y. Cho, J. Appl. Phys. 71 (1992) 2760.
[347] G.A. Adegboyega, Phys. Stat. Sol. A 111 (1989) K31.
[348] T. Teraji, S. Hara, H. Okushi, K. Kajimura, Appl. Phys. Lett. 71 (1997) 689.
[349] J.-S. Jang, T.-Y. Seong, J. Appl. Phys. 88 (2000) 3064.
[350] T. Tsuzuku, T. Sugimura, Y. Kasai, T. Inokuma, K. Iiyama, S. Takamiya, Jpn. J. Appl. Phys. Part 1 39 (2000) 5788.
[351] H. Iwakuro, T. Inoue, T. Kuroda, Jpn. J. Appl. Phys. Part 2 30 (1991) L255.

[352] H. Iwakuro, M. Tokonami, T. Kuroda, S. Tamaki, Y. Kitatsuji, Jpn. J. Appl. Phys. Part 1 32 (1993) 5487.
[353] A. Paccagnella, A. Callegari, Solid-State Electron. 34 (1991) 1409.
[354] A.Y. Polyakov, M. Stam, A.G. Milnes, A.E. Bochkarev, S.J. Pearton, J. Appl. Phys. 71 (1992) 4411.
[355] Y. Sakamoto, T. Sugino, T. Miyazaki, J. Shirafuji, Electron. Lett. 31 (1995) 1104.
[356] T. Sugino, Y. Sakamoto, T. Sumiguchi, K. Nomoto, J. Shirafuji, Jpn. J. Appl. Phys. Part 2 32 (1993) L1196.
[357] J.M. Shannon, Solid-State Electron. 19 (1976) 537.
[358] S. Ashok, H. Krautle, H. Beneking, Appl. Phys. Lett. 45 (1984) 431.
[359] R. Tyagi, T.P. Chow, J.M. Borrego, K.A. Pisarczyk, Appl. Phys. Lett. 63 (1993) 651.
[360] P.C. Srivastava, C. Colluza, S. Chandra, U.P. Singh, Solid-State Electron. 37 (1994) 520.
[361] A. Fricke, G. Stareev, T. Kummetz, D. Sowada, J. Mahnss, W. Kowalsky, K.J. Ebeling, Appl. Phys. Lett. 65 (1994) 755.
[362] E. Grusell, S. Berg, L.P. Andersson, J. Electrochem. Soc. 127 (1980) 1573.
[363] S. Ashok, T.P. Chow, B.J. Baliga, Appl. Phys. Lett. 42 (1983) 687.
[364] X.C. Mu, S.J. Fonash, IEEE Elec. Dev. Lett. EDL-6 (1985) 410.
[365] Y.G. Wang, S. Ashok, Physica B 170 (1991) 513.
[366] H. Thomas, J.K. Luo, Solid-State Electron. 35 (1992) 1401.
[367] M. Yamada, C.J. Spindt, K.E. Miyano, P.L. Meissner, A. Herrera-Gomez, T. Kendelewicz, W.E. Spicer, J. Appl. Phys. 71 (1992) 314.
[368] P.M. White, D.M. Brookbanks, Appl. Phys. Lett. 30 (1977) 348.
[369] S.J. Eglash, P. Shihong, M. Dang, W.E. Spicer, D.M. Collins, Jpn. J. Appl. Phys. (Suppl.) (1982) 431.
[370] J.H. Kim, S.S. Li, L. Figueroa, Electron. Lett. 24 (1988) 687.
[371] K. Zhang, D.L. Miller, MRS Symp. Proc. 262 (1992) 899.
[372] C.-Y. Wu, J. Appl. Phys. 54 (1983) 971.
[373] R. Tyagi, T.P. Chow, J. Electron. Mater. 22 (1993) 221.
[374] G. Lubberts, B.C. Burkey, H.K. Bucher, E.L. Wolf, J. Appl. Phys. 45 (1974) 2180.
[375] P. Kordos, M. Marso, R. Meyer, H. Luth, J. Appl. Phys. 72 (1992) 2347.
[376] J.D. Mottram, A. Thanailakis, D.C. Northrop, J. Phys. D 8 (1975) 1316.
[377] L.N. Aleksandrov, R.N. Lovyagin, P.A. Simonov, I.S. Bzinkovskaya, Phys. Stat. Sol. A 45 (1978) 521.
[378] Z.Q. Shi, W.A. Anderson, Solid-State Electron. 35 (1992) 1427.
[379] Z.Q. Shi, W.A. Anderson, J. Appl. Phys. 72 (1992) 3803.
[380] H.J. Lee, W.A. Anderson, H. Hardtdegen, H. Luth, Appl. Phys. Lett. 63 (1993) 1939.
[381] S.A. Clark, S.P. Wilks, A. Kestle, D.I. Westwood, M. Elliott, Surf. Sci. 352 (1996) 850.
[382] L. He, Solid-State Electron. 41 (1997) 1881.
[383] D.S. Cammack, S.M. McGregor, J.J. McChesney, S.A. Clark, P.R. Dunstan, S.R. Burgess, S.P. Wilks, F. Peiro, J.C. Ferrer, A. Cornet, J.R. Morante, A. Kestle, D.I. Westwood, M. Elliott, Appl. Surf. Sci. 123 (1998) 501.
[384] J.W. Palmer, W.A. Anderson, D.T. Hoelzer, M. Thomas, J. Electron. Mater. 25 (1996) 1645.
[385] T. Okumura, S. Yamamoto, M. Shimura, Jpn. J. Appl. Phys. Part 1 32 (1993) 2626.
[386] T. Hashizume, G. Schweeger, N.J. Wu, H. Hasegawa, J. Vac. Sci. Technol. B 12 (1994) 2660.
[387] D.C. Dumka, R. Riemenschneider, J.M. Miao, H.L. Hartnagel, J. Electrochem. Soc. 143 (1996) 1945.
[388] H. Hasegawa, T. Sato, T. Hashizume, J. Vac. Sci. Technol. B 15 (1997) 1227.
[389] J.M. DeLucca, H.S. Venugopalan, S.E. Mohney, R.F. Karlicek, Appl. Phys. Lett. 73 (1998) 3402.
[390] S. Uno, T. Hashizume, S. Kasai, N.J. Wu, H. Hasegawa, Jpn. J. Appl. Phys. Part 1 35 (1996) 1258.
[391] H. Hasegawa, Y. Koyama, T. Hashizume, Jpn. J. Appl. Phys. Part 1 38 (1999) 2634.
[392] T. Okumura, C. Kaneshiro, Trans. Inst. Elec. Inf. Commun. Eng. J81C-II (1998) 690.
[393] P.M. Vereecken, G.M. Vanalme, R.L. VanMeirhaeghe, F. Cardon, W.P. Gomes, J. Chem. Soc., Faraday Trans. 92 (1996) 4069.
[394] P.M. Vereecken, P.C. Searson, Appl. Phys. Lett. 75 (1999) 3135.
[395] K. Strubbe, P.M. Vereecken, W.P. Gomes, J. Electrochem. Soc. 146 (1999) 1412.
[396] T. Sato, C. Kaneshiro, H. Okada, H. Hasegawa, Jpn. J. Appl. Phys. Part 1 38 (1999) 2448.
[397] H. Hasegawa, T. Sato, S. Kasai, Appl. Surf. Sci. 166 (2000) 92.
[398] A. Vilan, A. Shanzer, D. Cahen, Nature 404 (2000) 166.
[399] L.C. Chen, D.A. Caldwell, T.A. Muller, T.G. Finstad, W. Schildgen, C.J. Palmstrom, J. Cryst. Growth 201/202 (1999) 146.
[400] C.J. Palmstrom, C.C. Chang, A. Yu, G.J. Galvin, J.W. Mayer, J. Appl. Phys. 62 (1987) 3755.
[401] A. Iliadis, K.E. Singer, Solid-State Electron. 26 (1983) 7.
[402] K.N. Tu, R.D. Thompson, B.Y. Tsaur, Appl. Phys. Lett. 38 (1981) 626.
[403] R. Purtell, G. Hollinger, G.W. Rubloff, P.S. Ho, J. Vac. Sci. Technol. A 1 (1983) 566.
[404] I. Ohdomari, K.N. Tu, K. Suguro, M. Akiyama, I. Kimura, K. Yoneda, Appl. Phys. Lett. 38 (1981) 1015.
[405] V. Probst, H. Schaber, A. Mitwalsky, H. Kabza, B. Hoffmann, K. Maex, L. Van den Hove, J. Appl. Phys. 70 (1991) 693.
[406] Y.Q. Jia, G.G. Qin, Appl. Phys. Lett. 56 (1990) 641.

[407] P.P. Sahay, M. Shamsuddin, R.S. Srivastava, Solid-State Electron. 34 (1991) 727.
[408] E.K. Kim, Y.J. Park, S.-K. Min, J.-G. Lee, W.C. Choi, Ungyong Mulli 8 (1995) 132.
[409] Z.M. Wang, Y.X. Zhang, K. Wu, M.H. Yuan, W.X. Chen, G.G. Qin, Phys. Rev. B 51 (1995) 7878.
[410] V.G. Bozhkov, V.A. Kagadei, N.A. Torkhov, Izv. Vyssh. Uchebn. Zaved., Fiz. 40 (1997) 115.
[411] R.L. van Meirhaeghe, W.H. Laflere, F. Cardon, J. Appl. Phys. 76 (1994) 403.
[412] S.A. Ding, Z. Xu, Chin. J. Semicond. 15 (1994) 367.
[413] J.P. Sullivan, W.R. Graham, R.T. Tung, F. Schrey, Appl. Phys. Lett. 62 (1993) 2804.
[414] L. Jun, C.R. Ortiz, Z. Ying, H. Bakhru, J.W. Corbett, Phys. Rev. B 44 (1991) 8918.
[415] N. Yamamoto, S. Tonomura, T. Matsuoka, H. Tsubomura, J. Appl. Phys. 52 (1981) 6227.
[416] B.Y. Tsaur, J.P. Mattia, C.K. Chen, Appl. Phys. Lett. 57 (1990) 1111.
[417] M.O. Aboelfotoh, A.D. Marwick, J.L. Freeouf, Phys. Rev. B 49 (1994) 10753.
[418] K.I. Lundstrom, M.S. Shivaraman, C.M. Svensson, J. Appl. Phys. 46 (1975) 3876.
[419] H.Y. Nie, Y. Nannichi, Jpn. J. Appl. Phys. Part 1 30 (1991) 906.
[420] C.-K. Kim, J.-H. Lee, N.-I. Cho, C.-S. Hong, Trans. Korean IEE C 49 (2000) 388.
[421] G.G. Kovalevskaya, M.M. Meredov, E.V. Russu, M.K. Salikhov, S.V. Slobodchikov, V.M. Fetisova, Fiz. Tek. Polup. 26 (1992) 1750.
[422] M.H. Yuan, H.Z. Song, S.X. Jin, H.P. Wang, Y.P. Qiao, G.G. Qin, Phys. Rev. B 48 (1993) 17986.
[423] S.X. Jin, H.P. Wang, M.H. Yuan, H.Z. Song, H. Wang, W.L. Mao, G.G. Qin, Z.-Y. Ren, B.-C. Li, X.-W. Hu, G.-S. Sun, Appl. Phys. Lett. 62 (1993) 2719.
[424] S.X. Jin, L.P. Wang, M.H. Yuan, J.J. Chen, Y.Q. Jia, G.G. Qin, J. Appl. Phys. 71 (1992) 536.
[425] H.-Y. Nie, Y. Nannichi, Jpn. J. Appl. Phys. Part 2 32 (1993) L890.
[426] H. Hasegawa, Jpn. J. Appl. Phys. Part 1 — Regul. Pap. Short Notes Rev. Pap. 38 (1999) 1098.
[427] J.J. Coleman, Appl. Phys. Lett. 31 (1977) 283.
[428] V. Montgomery, R.H. Williams, G.P. Srivastava, J. Phys. C 14 (1981) L191.
[429] J.R. Waldrop, Appl. Phys. Lett. 47 (1985) 1301.
[430] M. Yamada, A.K. Wahi, T. Kendelewicz, W.E. Spicer, Phys. Rev. B 45 (1992) 3600.
[431] H. Nobusawa, H. Ikoma, Jpan. J. Appl. Phys. Part 1 32 (1993) 3713.
[432] T.S. Huang, R.S. Fang, Solid-State Electron. 37 (1994) 1461.
[433] E.K. Kim, M.H. Son, Y.J. Park, J.-G. Lee, S.-K. Min, J. Appl. Phys. 78 (1995) 4276.
[434] S. Hohenecker, T.U. Kampen, W. Braun, D.R.T. Zahn, Surf. Sci. 433–435 (1999) 347.
[435] S. Meskinis, K. Slapikas, V. Grigaliunas, J. Matukas, S. Smetona, Phys. Stat. Sol. A 180 (2000) 499.
[436] J. Her, H. Lim, C.H. Kim, I.K. Han, J.I. Lee, K.N. Kang, J. Korean Inst. Tel. Elec. 31A (1994) 56.
[437] E. Yablonovitch, B.J. Skromme, R. Bhat, J.P. Harbison, T.J. Gmitter, Appl. Phys. Lett. 54 (1989) 555.
[438] R.S. Besser, C.R. Helms, J. Appl. Phys. 65 (1989) 4306.
[439] Y.T. Oh, S.C. Byun, B.R. Lee, T.W. Kang, C.Y. Hong, S.B. Park, H.K. Lee, T.W. Kim, J. Appl. Phys. 76 (1994) 1959.
[440] V.N. Bessolov, M.V. Lebedev, Fiz. Tek. Polup. 32 (1998) 1281.
[441] H. Sawatari, O. Oda, J. Appl. Phys. 72 (1992) 5004.
[442] K. Hattori, Y. Torii, Solid-State Electron. 34 (1991) 527.
[443] D.T. Quan, H. Hbib, Solid-State Electron. 36 (1993) 339.
[444] T. Sugino, Y. Sakamoto, J. Shirafuji, Jpn. J. Appl. Phys. Part 2 32 (1993) L239.
[445] S. Kasai, H. Hasegawa, in: Proceedings of the IEEE International Conference on InP, 1994, 220 p.
[446] H. Hasegawa, H. Ishii, K. Koyanagi, Appl. Surf. Sci. 56–58 (1992) 317.
[447] J.C. Costa, F. Williamson, T.J. Miller, K. Beyzavi, M.I. Nathan, D.S.L. Mui, S. Strite, H. Morkoc, Appl. Phys. Lett. 58 (1991) 382.
[448] M. Cantile, L. Sorba, S. Yildirim, P. Faraci, G. Biasiol, A. Franciosi, T.J. Miller, M.I. Nathan, Appl. Phys. Lett. 64 (1994) 988.
[449] C. Gaonach, S. Cassette, M.A. Di Forte-Poisson, C. Brylinski, M. Champagne, A. Tardella, Semicond. Sci. Technol. 5 (1990) 322.
[450] S.A. Chambers, J. Vac. Sci. Technol. A 11 (1993) 860.
[451] Y. Bing, J.C. Chen, F.S. Choa, MRS Symp. Proc. 340 (1994) 259.
[452] K. Shiojima, K. Nishimura, T. Aoki, F. Hyuga, J. Appl. Phys. 77 (1995) 390.
[453] M. Akazawa, H. Ishii, H. Hasegawa, Jpn. J. Appl. Phys. Part 1 30 (1991) 3744.
[454] T.L. Cheeks, T. Sands, R.E. Nahory, J.P. Harbison, H.L. Gilchrist, V.G. Keramidas, J. Electron. Mater. 20 (1991) 881.
[455] K. Koyanagi, S. Kasai, H. Hasegawa, Ext. Abs. SSDM 548 (1992).
[456] T. dell'Orto, J. Almeida, A. Terrasi, M. Marsi, C. Coluzza, G. Margaritondo, P. Perfetti, Phys. Rev. B 50 (1994) 18189.
[457] J. Ivanco, H. Kobayashi, J. Almeida, G. Margaritondo, J. Appl. Phys. 87 (2000) 795.
[458] J.E. Pattison, M.F. Daniel, D.A. Anderson, P.R. Tapster, N. Apsley, M.J. Slater, Ext. Abs. ESSDERC 64 (1981).
[459] R.H. Tredgold, Z.I. El-Badawy, J. Phys. D 18 (1985) 103.

[460] I.H. Campbell, S. Rubin, T.A. Zawodzinski, J.D. Kress, R.L. Martin, D.L. Smith, N.N. Baraskkov, J.P. Ferraris, Phys. Rev. B 54 (1996) R14321.
[461] L. Zuppiroli, L. Si-Ahmed, K. Kamaras, F. Nuesch, M.N. Bussac, D. Ades, A. Siove, E. Moons, M. Gratzel, Euro. Phys. J. B 11 (1999) 505.
[462] L.S. Hung, C.W. Tang, M.G. Mason, Appl. Phys. Lett. 70 (1997) 152.
[463] E.I. Haskel, A. Curioni, P.F. Seidler, W. Andreoni, Appl. Phys. Lett. 71 (1997) 1151.
[464] C. Zhou, M.R. Deshpande, M.A. Reed, L. Jones II, J.M. Tour, Appl. Phys. Lett. 71 (1997) 611.
[465] J. Chen, M.A. Reed, A.M. Rawlett, J.M. Tour, Science 286 (1999) 1550.
[466] R.S. Nakhmanson, S.B. Sevastianov, Solid-State Electron. 27 (1984) 881.
[467] E. Suzuki, Y. Hayashi, Appl. Surf. Sci. 63 (1993) 218.
[468] M. Wittmer, J.L. Freeouf, Phys. Rev. Lett. 69 (1992) 2701.
[469] A.M. Fajardo, N.S. Lewis, J. Phys. Chem. B 101 (1997) 11136.
[470] A.J. Nozik, R. Memming, J. Phys. Chem. 100 (1996) 13061.
[471] B.B. Smith, A.J. Nozik, Chem. Phys. 205 (1996) 47.
[472] H. Gerischer, W. Ekardt, Appl. Phys. Lett. 43 (1983) 393.
[473] H. Reiss, J. Phys. Chem. 89 (1985) 3783.
[474] D. Ofer, R.M. Crooks, M.S. Wrighton, J. Am. Chem. Soc. 112 (1990) 7869.
[475] M.C. Lonergan, Science 278 (1997) 2103.
[476] R.F.W. Bader, A. Larouche, C. Gatti, M.T. Carroll, P.J. MacDougall, K.B. Wiberg, J. Chem. Phys. 87 (1987) 1142.
[477] R.F.W. Bader, Atoms in Molecules: A Quantum Theory, Clarendon Press, Oxford, 1994.
[478] R.T. Tung, 2001, submitted for publication.
[479] W.A. Harrison, J. Vac. Sci. Technol. B 3 (1985) 1231.
[480] S.G. Louie, M.L. Cohen, Phys. Rev. Lett. 35 (1975) 866.
[481] R.T. Tung, J. Vac. Sci. Technol. B 11 (1993) 1546.
[482] T. Meyer, H. von Kaenel, Phys. Rev. Lett. 78 (1997) 3133.
[483] R.F. Schmitsdorf, T.U. Kampen, W. Monch, Surf. Sci. 324 (1995) 249.
[484] W.E. Spicer, I. Lindau, P. Skeath, C.Y. Su, J. Vac. Sci. Technol. 17 (1980) 1019.
[485] K. Stiles, A. Kahn, Phys. Rev. Lett. 60 (1988) 440.
[486] A. Wang, W.A. Anderson, J. Electron. Mater. 25 (1996) 201.